Activity-dependent changes in neuronal architecture dendrites, axon and the axon initial segment

Mukanowa, Janina

Awarding institution:
King's College London

Activity-dependent changes in neuronal architecture: dendrites, axon and the axon initial segment

Janina Mukanowa

Thesis submitted for the degree of
Doctor of Philosophy
October, 2013

MRC Centre for Developmental Neurobiology,
King's College London

Abstract

The assembly of the brain during embryonic development was thought to be largely independent of its electrical activity. It was believed that activity, broadly defined as spontaneous or evoked changes in membrane potential, is important only in later stages of development, after a basic template of the nervous system has already been established. Recent data, however, suggests that activity plays a crucial role in all stages of neural development, from cell proliferation and migration to establishment and maturation of synaptic connections.

In this thesis, I explore the role of activity on early development of axons, dendrites and the axon initial segments of hippocampal neurons *in vitro*. Activity was modulated by either elevated levels of KCl or optogenetic stimulation of ChR2-expressing neurons. Elevated activity had only a modest effect on the morphology of dendritic and axonal compartments, however it strongly affected the structure of the axon initial segment (AIS).

Chronic depolarisation of developing hippocampal neurons led to reversible, cell-death independent, AIS disassembly in a subset of susceptible neurons. This effect required Ca^{2+} influx though L-type voltage-gated Ca^{2+} channels and was observed mostly in young (4-7 DIV) neurons, suggesting the existence of a developmental window for this type of activity-induced change. Electrophysiological recordings and Ca^{2+} imaging experiments showed that cells without an AIS have markedly decreased Na^{+} currents and are unable to initiate repetitive firing.

The AISs that were not disassembled in response to elevated activity had significantly altered structural properties, in terms of their length and position along the axon. The exact nature of these changes depended on the specific developmental stage at which the neurons were depolarised. The susceptibility of the AIS to alterations in neuronal activity may suggest the existence of a novel form of plasticity in immature neurons, which may be important for stabilisation of neuronal activity in developing hippocampal circuits.

Acknowledgements

First of all, I would like to thank to my supervisor Prof. Juan Burrone for his help, expertise and contagious enthusiasm. He never failed to excite me about science. I am also incredibly grateful to my PhD advisors, Prof. Ian Thompson and Dr Esther Bell, for their support and guidance throughout the PhD; and to my second supervisor, Dr Robert Hindges, for teaching me molecular biology and *in vivo* electroporation techniques.

I would also like to thank the following people: Dr Winnie Wefelmeyer, for her patience in explaining intricate scientific ideas; Dr Andrew Lowe, for his encouragement, statistical advice and help with optogenetics; Mideia Kotsogianni, for her help with cell cultures; Martin Crossley, for teaching me patching; and Tom Ryan for his help with Matlab. In addition, big thanks go to all the members of the unofficial MRC baking and book club, for making my time at the Centre so much more enjoyable.

I am also incredibly grateful to Werner Valentin for his enormous support during the tough times, to Dane Miller for all the fun and home-cooked dinners, and to all my friends for being there when I needed them most.

Last, but not least, I would like to thank Medical Research Council for funding my PhD and allowing me undertake this fascinating project.

Table of contents

List of figures

Chapter 1 Introduction

Chapter 2 Materials and methods

Chapter 3 The role of activity on dendritic and axonal morphology

Chapter 4 The role of activity on the structure of the axon initial segment

Chapter 5 The consequences of AIS disassembly on neuronal excitability

List of abbreviations

AIS – Axon initial segment

AMPA - α-Amino-3-hydroxy-5-methyl-4-isoxazolepropionic acid

AnkG – Ankyrin G

ANOVA – Analysis of variance

AP – Action potential

APV – DL-2-amino-5-phosphonovaleric acid

CA1 – Cornu ammonis area 1

CA3 - Cornu ammonis area 3

CaN – Calcineurin

cGMP - Cyclic guanosine monophosphate

Cdk5 - Cyclin-dependent kinase 5

ChR2 - Channelrhodopsin-2

C_m – Membrane capacitance

CK2 - Casein kinase 2

CNQX - 6-cyano-7-nitroquinoxaline-2,3-dione

CSPG - Chondroitin sulfate proteoglycan

DABCO - 1,4-diazabicyclo[2.2.2]octane

DIV – Day in vitro

DMSO - Dimethyl sulfoxide

ECM – Extracellular matrix

EGTA - Ethylene glycol tetraacetic acid

EPSP - Excitatory postsynaptic potential

ΔF – Change in fluorescence

F_0 – Basal fluorescence

GABA - Gamma-aminobutyric acid

GSK3 - Glycogen synthase kinase 3

HBS - HEPES buffered saline

HDAC6 - Histone deacetylase 6

HEPES - 4-(2-hydroxyethyl)-1-piperazineethanesulfonic acid

I_{Na} – Sodium current

LED - Light-emitting diode

LSD test - least significant difference test

MAP2 - Microtubule-associated protein 2

MDL 18130 - N-[N-[(Phenylmethoxy)carbonyl]-L-va-phenylalaninal]

NF-186 – Neurofascin-186

NFAT - Nuclear factor of activated T-cells

NL – Nucleus laminaris

NM - Nucleus magnocellularis

NrCAM - Neuronal cell adhesion molecule

OGB – Oregon green BAPTA

PI – Propidium iodide

PKG - cGMP-dependent protein kinase

R_m – Membrane resistance

ROI – Region of interest

SGC - Soluble guanylate cyclase

SPA – Synchronised plateau assembly

TTL – Transistor-transistor logic

TTX - Tetrodotoxin

V_m – Membrane voltage

V_{max} – Maximal membrane voltage

V_{rest} - Resting membrane voltage

V_{thresh} Threshold voltage

vGLUT - Vesicular glutamate transporter

VGCC – Voltage-gated calcium channel

WAVE-1 - Wiskott-Aldrich syndrome protein family member 1

Chapter 1

Introduction

One of the most fundamental properties of the brain is its ability to generate electric activity. Neural activity forms the basis for signal transduction in mature neural circuits; however it also plays a vital role in shaping the development of the nervous system. Conventionally, activity is divided into spontaneous and evoked. Evoked activity requires an external trigger, which *in situ* is delivered through extensive network of synaptic contacts converging onto each neuron. This type of activity is mediated by all-or-nothing action potentials and is predominant in late development, when the majority of neurons have already formed synaptic connections. Spontaneous activity, on the other hand, occurs in the absence of explicit external stimuli and is typically associated with early development, before the formation of synapses.

Traditionally it was believed that the early phase of brain development is independent of neuronal activity but it is exclusively controlled by genetic programmes, which establish a coarse framework of neuronal connections in an activity-independent manner. Activity was thought to be important only later, when the coarse neuronal networks are fine-tuned to give rise to adult patterns of connectivity (Goodman and Shatz, 1993, Katz and Shatz, 1996, Sengpiel and Kind, 2002). This traditional model is being updated to accommodate growing evidence that activity is also important in earlier stages of development. An accumulating number of studies show that neural activity and genetic programmes interact to instruct the composition and organisation of neural networks at all stages of development (Spitzer, 2006, Yamamoto and Lopez-Bendito, 2012).

Both spontaneous and evoked forms of neural activity are implicated in a wide range of developmental processes, from neuronal proliferation and migration to formation and stabilisation of synaptic connections (Spitzer, 2006). In the next section, I briefly review the role of activity in development of axonal and dendritic arborisations, especially its influence on neurite elongation and branching, together with its modulatory role on the behaviour of axonal growth cones.

1.1 Activity-dependent development of dendritic and axonal arborisations

1.1.1 The role of activity on axonal outgrowth, branching and pathfinding

It has long been established that electrical activity is involved in refinement of coarse axonal projections into mature patterns of connectivity (Hubel and Wiesel, 1970, Hubel et al., 1977). Yet only recently it has been fully recognized that neuronal activity can also regulate the initial targeting of axons during the formation of neural circuits. Modulatory effects of neural activity have been observed in a variety of model systems, both *in vivo* and *in vitro*. For example, spontaneous bursts of neuronal activity are vital for the proper development of thalamocortical connectivity. In mice, thalamocortical axons (TCAs) reach the cortex around embryonic day (E) 15 and establish functional transient connections with subplate neurons before they reach their final target in the cortical plate (Lopez-Bendito and Molnar, 2003). Silencing spontaneous activity by *in utero* electroporation of *Kcnj2* (a gene encoding a human inwardly rectifying potassium channel Kir2.1) into a mouse embryo at the peak of TCA extension (between E12.5 and E15.5), slows down the elongation of the axons *in vivo* (Mire et al., 2012). Conversely, increasing activity with high levels of extracellular KCl accelerates axonal outgrowth in the thalamic explants. Interestingly, membrane depolarisation increases axon outgrowth only in young neurons; old neurons are not affected by elevation of membrane voltage, suggesting a developmental regulation of activity-dependent axon outgrowth. Activity also modulates axon outgrowth in motor neurons of developing spine cord and colossal neurons of visual and somatosensory cortex. In developing chick spinal cord, modest alterations to the normal frequency of neural activity perturbs pathfinding decisions of elongating motor neurons (Hanson and Landmesser, 2004; Kastanenka and Landmesser, 2010), whereas blocking activity in mouse visual and somatosensory cortex leads to a disrupted growth of axons and their arbours in colossal projection neurons (Mizuno et al., 2007, Wang et al., 2007).

How does neuronal activity affect the axonal growth? Several studies *in vitro* showed that electrical activity and associated membrane depolarisation regulates the expression of axon guidance receptors in the elongating growth cones. For example, membrane depolarisation with high extracellular KCl recruited DCC to the growth cones of embryonic rat cortical neurons, which considerably potentiated axon outgrowth in netrin-1 gradients (Bouchard et al., 2008). Similarly, intermittent

stimulation with KCl enhanced responsiveness of retinal ganglion cells (RGCs) to BDNF and other trophic factors (Goldberg et al., 2002). Interestingly, the stimulation pattern that elicited the largest growth displayed the characteristics of spontaneous activity normally present in developing retina *in vivo* (Wong et al., 1998), further emphasising the role of early activity on axonal outgrowth. In either cortical or retinal cultures, membrane depolarisation on its own had no effect on the rate of axon outgrowth. Guidance cues, on the other hand, could stimulate axon growth on their own, but did so inefficiently. Therefore a combined effect of activity and various trophic factors seems to be necessary for efficient axon elongation in the development of neural circuits.

Membrane depolarisation can not only potentiate axonal growth in response to molecular guidance cues but also actively inhibit the growth of neighbouring unstimulated axon collaterals. Studies performed in compartmented cultures of rat sympathetic cultures showed that neuronal activity and neurotrophins can interact to select one axon over the other. For example, Singh and Miller (2005) demonstrated that the axons of KCl-depolarised neurons had a competitive growth advantage over unstimulated axon collaterals when both were grown in the presence of NGF. The axons that were locally depolarised exhibited NGF-mediated axonal growth and branching, at the cost of the unstimulated axons, which were actively inhibited from growing. Thus neuronal activity can regulate both positive and negative neurotropin-mediated signals to selectively enhance the growth of one axon over another, providing an additional, activity-dependent mechanism for axonal outgrowth and branching.

Not all neuronal types display activity-induced axon growth. In dorsal root ganglion (DRG) cells of mice (Fields et al., 1990) and chick (Diefenbach et al., 2000), as well in molluscan sensory neurons (Mattson and Kater, 1987), electrical activity and subsequent Ca^{2+} influx were shown to suppress axonal growth. Similarly, in hippocampal neurons in culture, transient global activation of ionotropic AMPA/kainate receptors with glutamate or kainate resulted in axon retraction and growth cone stalling (Chang and De Camilli, 2001; Tashiro et al., 2003; Ibarretxe et al., 2007). This neurotransmitter-induced effect was dependent on membrane depolarisation and could be mimicked by transient discharges of action potentials by intracellular current injections with patch clamp electrodes (Ibarretxe, et al., 2007). Interestingly, local application of glutamate to axons of 4 days in vitro (DIV) dentate granule cell had no effect on axon behaviour, but it effectively collapsed axonal

growth cones leading to axon retraction when applied to somatodendritic areas (Yamada et al., 2008). Thus activity-mediated axon retraction does not necessarily require local depolarisations at the axonal growth cone, but can be modulated through long-range intracellular signals arising in the somatodendritic compartment. These signals consist of a long-range Ca^{2+} wave (termed 'axonal Ca^{2+} sweep') that propagates from the soma to the axon terminal following the perisomatic application of glutamate. The molecular mechanism that leads from Ca^{2+} signal to axon retraction is not known, however it is postulated that the initial Ca^{2+} transient might induce phosphorylation of microtubule associated protein 1b and tau through Ca^{2+}/calmodulin-dependent protein kinase. This, in turn, destabilises microtubules, which are then completely depolymerised by the second Ca^{2+} wave (Yamada et al., 2008).

Apart from the action of neurotransmitters, a change in membrane potential can also be induced by molecular guidance cues. Electrophysiological recordings from growth cones showed that attractive cues, such as BDNF and Netrin-1 (mediated via the DCC homomeric receptor complex) cause membrane depolarisation of approximately 15mV in cultured spinal neurons of Xenopus embryo. On the contrary, repellents such as Slit2, Sema3A and Netrin-1 (mediated by the DCC/UNC5 receptor complex) lead to hyperpolarisation of a similar magnitude (Henley et al., 2004; Nishiyama et al., 2008; Wang and Poo, 2005). Interestingly, manipulating membrane potential with electrophysiology or various concentrations of KCl can change the direction of growth cone turning, regardless of the presence of specific guidance cues (Ming et al., 2001; Nishiyama et al., 2008). For example, inducing depolarisation while exposing the growth cones to Sema3A or myelin-associated glycoprotein (MAG) leads to attraction rather than repulsion, whereas clamping the voltage at the resting level induces no preferential turning. Therefore, polarity of the change in membrane potential appears to have an important role in growth cone turning, at least in response to Sema3A or MAG, whereby depolarisation leads to attraction and hyperpolarisation to repulsion of axonal growth cones.

The molecular mechanism that leads to a change in membrane potential involves a network of second messenges, such as Ca^{2+} and cyclic nucleotides (Tojima et al., 2011). For example, growth cone turning triggered by Sema3A in Xenopus spinal neurons involves an interplay between the intracellular levels of cGMPs (cyclic guanosine monophosphates), Cl^- and Ca^{2+} ions (Nishiyama et al. 2008). cGMPs are

produced by soluble guanylate cyclase (SGC) in response to Sema3A binding to its receptor, neutropilin-1. The intracellular levels of cGMP determine whether the growth cones will be repelled or attracted towards the Sema3A gradient. Low levels of cGMP have been found to induce growth cone repulsion, whereas high levels lead to growth cone attraction (Song et al., 1998). Increase in cGMP activates Cl^- channels, triggering Cl^- influx and subsequent membrane hyperpolarisation. Membrane hyperpolarisation leads, through an unknown mechanism, to opening of Ca^{2+} channels, reorganisation of cytoskeleton and repulsive growth cone turning. In attractive Sema3A signalling, increased levels of SGC-generated cGMPs result in activation of cGMP-dependent protein kinase (PKG), leading to opening of Na^+ channels, Na^+ influx and membrane depolarisation. Memebrane depolarisation, in turn, opens voltage-gated Ca^{2+} channels (VGCCs) and triggers attractive growth cone turning (Nishiyama et al., 2008).

The exact pathway leading from the change of membrane potential to Ca^{2+} influx is not known, however, it has been postulated that non-VGCCs are more likely to mediate hyperpolarisation-triggered membrane repulsion, whereas VGCCs, due to their higher Ca^{2+} influx, mediate depolarisation-triggered growth cone attraction. Differential spatial patterns of Ca^{2+} at the growth cone can trigger different sets of downstream effectors leading to bidirectional turning responses (Nishiyama et al., 2003, 2008; Tokima et al., 2011). The direction of growth cone turning is thus determined by the polarity of the growth cone potential shift and the resulting magnitude of growth cone Ca^{2+}.

1.1.2 The role of activity on dendritic outgrowth and branching

Neural activity also plays a key role in dendritic growth and branching (Wong and Ghosh, 2002). Dendritic development occurs concurrently with synapse formation, suggesting that afferent terminals might stimulate dendritic growth. Indeed, it has long been recognised that afferent activity can shape dendritic arbours, whereby decreasing or blocking activity often leads to a stunted development of dendritic trees. For example, monocular deprivation causes atrophy and stunted growth of dendritic trees in the lateral geniculate nucleus (LGN) of kittens (Wiesel and Hubel, 1963), whereas visual deprivation induced by dark rearing results in decreased length and number of dendrites in mice stellate neurons (Coleman and Riesen, 1968). Conversely, enhanced levels of afferent activity can promote dendritic growth and branching. For example, in Xenopus laevis tadpoles, visual activity

driven by a light stimulus increases the growth of developing dendritic arbours and stabilises existing ones in tectal neurons (Sin et al., 2002). Similarly, hippocampal neurons from mice housed in enriched environments had larger dendritic trees compared to littermates raised in standard cages (Faherty et al., 2003).

Increased levels of activity do not always lead to larger dendritic trees, just like activity blockage does not necessarily cause stunted dendritic growth. In some cases decreased levels of activity can lead to paradoxical increase in dendritic size, whereas high levels of activity have the opposite, growth-stunting, effect. For instance, inhibiting neural activity by blocking glutamate receptors or L-type Ca^{2+} channels increased dendritic growth in cultured visual cortex of a ferret (McAllister et al., 1996). Conversely, enhanced levels of activity mediated by increased Ca^{2+} flux in mutant mice expressing defective alleles of AMPA receptor GLUR-B subunit, resulted in stunted dendritic growth in pyramidal neurons in hippocampal CA3 area (Feldmeyer et al., 1999). Neural activity can also cause both increases and decreases in the size of dendritic arbours, in a cell-specific manner. In the nucleus laminaris of a chick, for example, monoaural auditory deprivation caused systematic changes in dendritic size depending on which frequency the neurons are responsive to. In high frequency areas, the dendrites receiving the inputs from the deprived ear were shorter than the dendrites from the normal ear. In low frequency areas, on the other hand, auditory deprivation had the opposite effect, where the dendrites receiving the inputs from the deprived ear were longer compared to those from the nondeprived ear (Smith et al., 1983).

In vitro, neuronal activity has been shown to predominantly enhance the growth of dendritic arbours. For example, membrane depolarisation induced with high levels of extracellular KCl enhances the growth of dendritic arbours in rat cortical (Redmond et al., 2002), sympathetic (Vaillant et al., 2002), cerebellar (Gaudilliere et al., 2004) and hippocampal cultures (Yu and Malenka, 2003; Wayman et al., 2006; Tan et al., 2010; Ma et al., 2011). Mattson et al., (1988), however, showed an opposite effect, whereby chronic membrane depolarisation with elevated levels of KCl or global application of glutamate, led to dose-dependent reduction in the length of dendritic trees in pyramidal-like neurons in low-density hippocampal cultures (Mattson et al., 1988). The reasons for this apparent discrepancy are not clear. An obvious explanation, apart from cell- and culture-type-related differences, is that KCl may have distinct effects depending on the developmental stage at which the treatment is applied. Thus very young neurons (<4 DIV) may respond differently

than the older, more mature cells (>7 DIV) In agreement with this, activity-dependent dendrite growth was observed mostly in older neurons (7-8 DIV cells harvested at P0; Yu and Malenka, 2003; Tan et al., 2010) but not in 1-4 DIV neurons (harvested from E18 rat embryos and P0 pups; Mattson et al., 1988; Tan et al., 2010). This, however is not consistent with the finding from Ma et al., (2011) where KCl-treatment induced dendritic outgrowth in 3 DIV neurons (harvested from E18 rat embryos). The reasons for this disparity are not immediately clear and may be due to combinatorial effect of culture density, culturing protocol and growth conditions, as well as the duration of the treatment and the concentration of KCl used in each study.

These often contrasting effects of activity on axonal and dendritic development demonstrate the complexity of cellular and molecular mechanisms that underlie activity-dependent neurite growth and maturation. As the majority of activity-induced changes are mediated by cytosolic Ca^{2+} rises, diverse features of Ca^{2+} signalling has been proposed to account for distinct effects of neural activity on axonal and dendritic growth and guidance. Different spatiotemporal characteristics of the Ca^{2+} signal have been shown to evoke distinct behavioural effects in the stimulated cells. For example, the direction of growth cone turning seems to have a U-shaped dependence on the magnitude of the Ca^{2+} increase, where moderate increase in Ca^{2+} favours attraction, whereas low or very high Ca^{2+} increase favours repulsion (Zheng, 2000; Gomez and Zheng, 2006), suggesting there is an optimal range for intracellular [Ca^{2+}] that supports maximal growth. Ca^{2+} signals of distinct spatiotemporal characteristics can in turn activate distinct intracellular pathways, which can differentially regulate dendritic and axonal growth through either cytoplasmic or nuclear targets. By recruiting local and global calcium signalling to regulate dendritic development, neuronal activity plays an important role in shaping the architecture of the developing brain.

Because electrical activity regulates the development of dendritic and axonal compartments, this leads to the question of what is the source of that activity during development. In the next section, I describe different forms of activity found in embryonic mouse hippocampus.

1.2 Early forms of electrical activity in developing hippocampus

Even before synapse formation, neurons exhibit spontaneous electrical and chemical activity (Blankenship and Feller, 2010). In the developing hippocampus this activity is mediated by Ca^{2+} ions and can be correlated across a large number of neurons. Crepel et al., (2007) used multibeam two-photon Ca^{2+} microscopy combined with targeted electrophysiological recordings to characterise different activity patterns in embryonic and early postnatal hippocampus. On the basis of these recordings, the authors distinguished three distinct forms of spontaneous activity: uncorrelated Ca^{2+} spikes, synchronous plateau assemblies and giant depolarising potentials (Figure 1.1).

Uncorrelated Ca^{2+} spikes were detected in E16-19 embryos, where they most likely constitute the first form of electrical activity in immature hippocampus. These sporadic events were present in around 20% of neurons and consisted of brief (~3s), poorly correlated, spontaneous Ca^{2+} discharges occurring on average every 30 seconds. Treating the slices with blockers of voltage-gated L-type Ca^{2+} channels and voltage-gated Na^{+} channels reduced the incidence of these events, suggesting that they require Na^{+} and Ca^{2+} voltage-gated conductances for their generation. In contrast, they were not abolished by treatment with NMDA/AMPA/$GABA_A$ receptor antagonists, indicating that neurotransmitter-gated channels are not involved in generating these events.

Around birth, between postnatal P0-P2, a larger proportion of cells generated Ca^{2+} spikes but also another activity pattern was present in around 20% of cells, termed synchronous plateau assemblies (SPAs) due to its spatiotemporal dynamics. SPAs consist of long-lasting (~9s) Ca^{2+} plateaus, which recur with an interval of around 8 seconds and are considered to be the earliest coherent pattern of electrical activity in the developing hippocampus. In contrast to Ca^{2+} spikes, SPAs are correlated between 3-7 neurons, which are electrically coupled through gap junctions. SPAs are strongly voltage-dependent and they occur only within a specific membrane voltage window (between -40mV and -80mV), suggesting they are mediated by voltage-gated conductances. Indeed, pharmacological assays revealed that SPAs are generated by high threshold Ca^{2+} channels with a contribution of an immature form of a Na^{+} conductance. In contrast to Ca^{2+} spikes, SPAs require the activation of hyperpolarisation-activated ionic current (I_h), however, similarly to Ca^{2+} spikes, they are not blocked by antagonists of NMDA/AMPA/$GABA_A$ receptors, ruling out

any fast synaptic signalling. SPAs are progressively inhibited by synapse-driven events that begin to predominate in the postnatal period.

Between P6 and P10, neurons start to exhibit correlated synapse-driven spikes that are commonly known as giant depolarising potentials (GDPs). The existence of GDPs has been well-documented in both *in vitro* and *in vivo* systems. They have been first described in rat hippocapampal slices between P0-P10 (Ben-Ari et al., 1989) but have also been detected in intact hippocampus *in vitro* (Leinekugel et al., 1998; Khalilov et al., 1997) and *in vivo* (Leinekugel et al., 2002). GDPs progressively replace SPAs, but the two forms of spontaneous activity coexist during the first postnatal week in a spatially-exclusive manner. GDPs constitute synapse-driven slow depolarisations occurring every 3-10 seconds and correlate across large populations of cells. GDPs require activation of $GABA_A$ and glutamate receptors (Khasipov et al, 1997) and I_h currents conducted by HCN channels (Bender et al., 2005). GDPs are preferentially generated in CA3 and propagate to CA1 but around 20% of GDPs originate in CA1 and propagate backwards to CA3, which appears to have the highest pacemaker activity. GDPs are also observed in granule cells, but with less frequent incidence (Memendez de la Prida, et al., 1998). Both SPAs and GDPs disappear by the second week after birth.

1.3 A hub of neuronal activity: the axon initial segment

As development progresses, the levels of spontaneous activity diminish and the cell progressively gains the ability to initiate mature forms of electrical signals. This transition from immature to mature form of excitability coincides with the formation of a specialised structure at the beginning of the axon, known as the axon initial segment (AIS). The AIS is responsible for the generation of mature types of neural activity, taking the form of self-propagating action potentials (Foust et al., 2010, Meeks and Mannerick, 2007, Schmidt-Hieber et al., 2008). At the AIS, graded electrical potentials arriving from the soma and dendrites are integrated into all-or-nothing neuronal spikes, which propagate along the axon and trigger the release of neurotransmitters at presynaptic terminals. In addition to its role in initiation of action potentials, the AIS also acts as a boundary between somatodendritic and axonal compartments, restricting the free diffusion of dendritic proteins into axon. As a result of this, the AIS preserves axonal identity and is a key player in the maintenance of neuronal polarity (Sobotzik et al., 2009, Rasband, 2010). The two

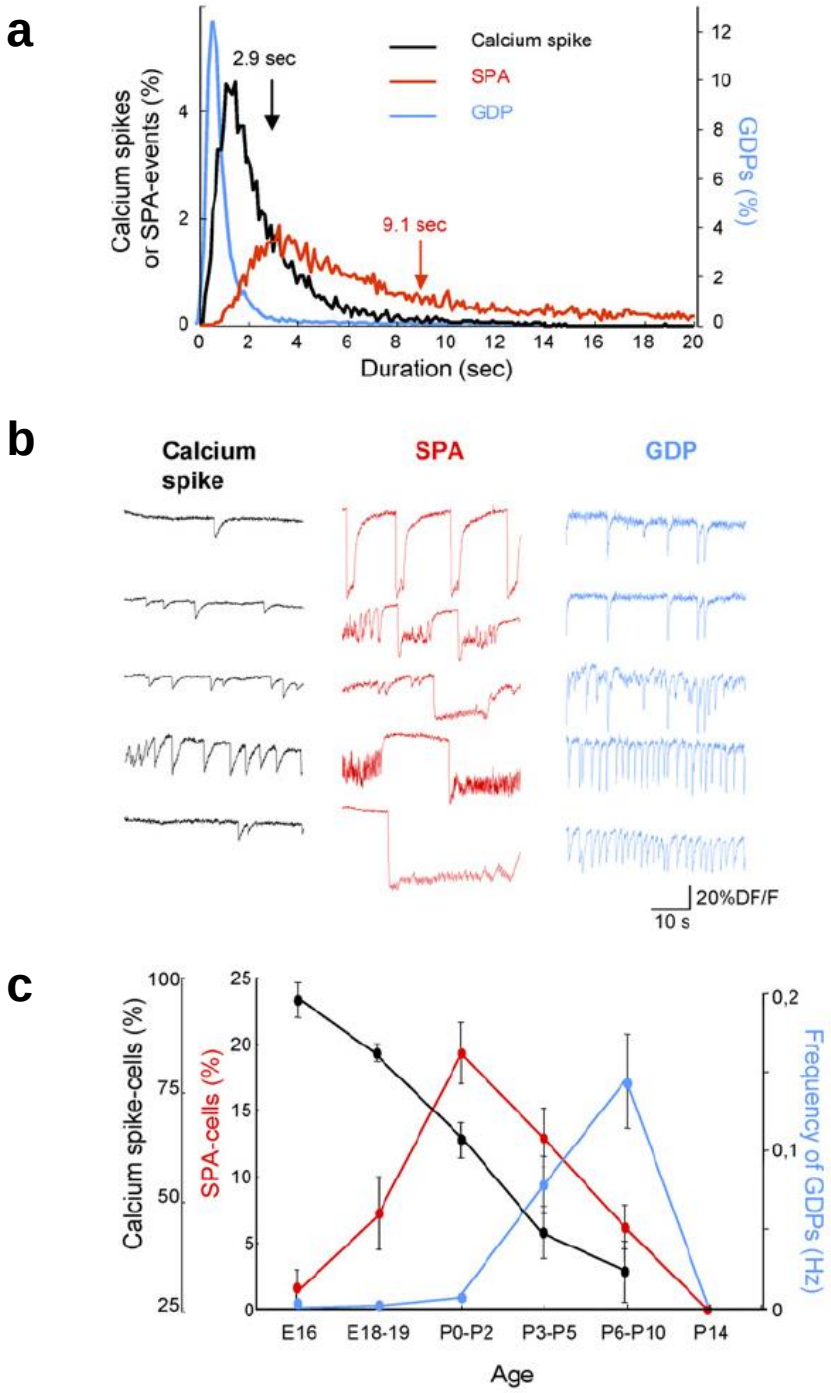

Figure 1.1 Early forms of activity recorded from a CA1 region of a mouse hippocampus. (a-b) Temporal characteristics of Ca^{2+} transients (a) and example Ca^{2+} fluorescence traces (b) of uncorrelated Ca^{2+} spikes (black), SPAs (red) and GDPs (blue) (c) Proportion of cells exhibiting Ca^{2+} spikes (black line), SPAs (red line) and GDPs (blue line) for different age groups. The graph also shows the frequencies of GDP. Uncorrelated Ca^{2+} spikes dominate at embryonic stages (E16-E19), after which they are progressively replaced by SPAs and GDPs. Both SPAs and GDPs disappear by the second postnatal week. Error bars, SEM. (adapted from Crepel et al., 2007).

key roles of the AIS arise from its strategic localisation in the neuron and from its unique, highly specialised, molecular organisation. In this section I describe the structural components of the AIS, their unique functions and their assembly in development. In addition, I will briefly review recently-discovered plastic properties of the AIS, which allow the cell to fine-tune its excitability to ongoing levels of neuronal activity.

1.3.1 Molecular composition of the AIS determines its functional properties

Historically, the axon initial segment was defined as the initial unmyelinated portion of the axon, between the axon hillock and the beginning of myelination (Palay et al., 1968). At the electron microscopic level the AIS is characterised by an electron-dense granular material that coats the inner surface of the plasma membrane not found at the soma and is thought to represent high density clusters of AIS proteins (Figure 1.2a; Peters et al., 1968). Indeed, later anatomical and physiological studies revealed that the AIS consists of a large number of transmembrane and cytoplasmic proteins, including ion channels, cell adhesion molecules and cytoskeletal and membrane scaffold proteins.

Ion channels

A unique feature of the AIS is its enrichment in voltage gated Na^+, K^+ and Ca^{2+} channels. The biophysical characteristics of these channels dictate the threshold, shape and amplitude of the spike as well as the pattern of repetitive firing (Lorincz and Nusser, 2008). The diversity of ion channels expressed at the AIS thus determines how different cell types transform synaptic inputs into an output (Kole et al., 2012). Different classes of neurons express unique complements of these channels which allows them to fine-tune AIS excitability to their specific needs.

Na^+ channels

Voltage-gated Na^+ channels are responsible for the main transient current in the rapid depolarising phase of the action potential and thus are of key importance of the initiation of neuronal spikes (Hodgkin and Huxley, 1952). A large number of immunocytochemical, anatomical and electrophysiological studies showed that the AIS contains a significantly higher density of Na_v channels than the soma. The first evidence for this was obtained by immunocytochemistry (Wollner and Catterall, 1986) and later confirmed with electrophysiological recordings (Kole et al., 2008; Hu et al., 2009) and Na^+ imaging (Fleidervish et al., 2010, Palmer and Stuart, 2006;

Bender and Trussell, 2009). While the general consensus is that the density of Na^+ channels at the AIS is high, the relative number of channels to the soma is still an area of intense debate. Estimates range widely, suggesting anywhere from 3-fold higher at the AIS versus the soma (Fleidervish et al., 2010) to ~40-fold (Lorincz and Nusser, 2010). The density of the channels, however, is likely to vary between different types of neurons, depending on their electrophysiological requirements. Large cortical neurons may require ~50-fold difference (Kole et al., 2008), whereas electrically compact dentate granule cells may need only ~5-fold enrichment (Schmidt-Hieber and Bischofberger, 2010).

Out of the four Na^+ channel alpha subunits ($Na_v1.1$, $Na_v1.2$, $Na_v1.3$ and $Na_v1.6$), three are expressed in the AIS ($Na_v1.1$, $Na_v1.2$ and $Na_v1.6$). The distribution of these channels varies with cell type, age and the presence of myelination. $Na_v1.1$ is dominant at the AIS of GABAergic neurons (Ogiwara et al., 2007) but is also found in retinal ganglion cells (Van Wart et al., 2007) and spinal cord motorneurons (Duflocq et al., 2008). $Na_v1.2$ is primarily expressed in the AIS in early development and in adult unmyelinated axons (Boiko et al., 2003). $Na_v1.6$ is found in the majority of axons, and it is the only Na_v isotype present in cerebellar Purkinje neurons and the auditory neurons of chick (Kuba et al., 2010), but is coexpressed with 1.1 or 1.2 subtypes in most other cell types. Interestingly, there is a switch in Na_v subtype expression during development. In RGCs, $Na_v1.2$ is first expressed early in development, for it to be gradually replaced by $Na_v1.6$ as the axons become myelinated, which also marks the onset of repetitive firing in these cells (Boiko et al., 2001, 2003).

In dentate granule cells and hippocampal pyramidal neurons (Royeck et al., 2008; Kress et al., 2010), $Na_v1.6$ is coexpressed with $Na_v1.2$ in a specific spatiotemporal manner. $Na_v1.2$ is predominant in the proximal region of the AIS, whereas $Na_v1.6$ is more prevalent in the distal part of the AIS. It is thought that the subcellular specification (Hu et al., 2009; Lorincz and Nusser, 2008, 2010; Zhou and Goldin, 2004; Schmidt-Hieber and Bischofberger, 2010) and voltage-dependence of these channels can explain some of the unique properties of the AIS in these cells (Rush et al., 2005). Distally located $Na_v1.6$, has a lower voltage threshold (hyperpolarised by ~10mV compared to Na_v channels in the soma; Colbert and Pan, 2002; Kole et al., 2008; Hu et al., 2009), creating favourable conditions for action potential initiation. Proximally located $Na_v1.2$, on the other hand, has a higher activation voltage and is thought to mediate the backpropagation of the action potential to the

soma (Hu et al., 2009; Dulla and Huguenard, 2009). The high concentration of Nav1.6 at the AIS, coupled to its hyperpolarized activation voltage and its distal location all contribute to the low threshold for action potential firing measured at the AIS. In fact, simultaneous patch-clamp studies of the soma and the AIS have shown that current threshold at the AIS is indeed lower (Kole et al., 2008).

K^+ channels

K^+ channels mediate the repolarisation phase of the action potential and modulate action potential amplitude, duration and frequency of firing. In addition, they can also regulate neuronal excitability through setting the resting membrane potential of the cell. In most neuronal types, the predominant K_v channels are the low-threshold K_v1 subtype together with auxiliary β-subunits ($K_v1.1$ and $K_v1.2$; Inda et al., 2006, Lorincz and Nusser, 2008, Ogawa et al., 2008, Van Wart et al., 2007). Both types are frequently found at the AIS of excitatory and inhibitory hippocampal neurons and tend to be located at the very distal end of the AIS, showing some overlap with $Na_v1.6$. Distal parts of pyramidal neurons also contain a high density of K_v7 channels (7.2 and 7.3, also called KCNQ channels; Devaux et al., 2004; Pan et al, 2006). These channels carry a slowly activating and inactivating M-type current (Brown and Passmore, 2009) and are essential for the regulating action potential firing in hippocampal cells, by controlling the resting membrane potential of the cell and the threshold for generating an action potential (Shah et al., 2002, 2008). By regulating the waveform of the action potential, K_v1 channels can also modify the levels of depolarization sensed by presynaptic terminals and thus indirectly affect neurotransmitter release (Kole et al., 2007).

Ca^{2+} channels

The presence and function of Ca_v channels at the AIS is the least explored, compared to the well-characterised Na_v and K_v channels. Nonetheless, several types of Ca_v channels have been identified at the AIS. These include voltage-gated Ca_v channels of T- and R-type expressed at the AIS of brain stem cartwheel cells (Bender and Trussell, 2009; Yu et al, 2010; Bender et al., 2012), P/Q type in the AIS of cerebellar Purkinje cells (Callewaert et al, 1996) and P/Q and N-type in neocortical pyramidal cells (Yu et al., 2010). Ca_v channels, just like Na_v and K_v channels, can regulate the firing properties of the neuron, such as spike timing, burst firing and action potential threshold. For example, blocking P/Q and N-type channels in neocortical pyramidal cells increases neuronal excitability and results in slower action potential repolarisation phase (Yu et al., 2010). These changes are

thought to be mediated, at least in part, through a reduction in Ca^{2+}-dependent K^+ currents, which normally contribute to the repolarisation of action potentials and mediate the fast phase of afterhyperpolarisation following an action potential (Berkefeld et al., 2010). Blocking T- and R- type channels in brain stem cartwheel cells, on the other hand, decreases neuronal excitability by elevating spike threshold and inhibiting generation of spike bursts (Bender and Trussel, 2008). Therefore, these channels may act by enhancing depolarising sub-threshold events to reach spike threshold. These contrasting roles of the AIS Ca_v channels reflect the complexity of neuronal processing at the AIS and underscore their importance in shaping the properties of neuronal spikes.

Apart from high density of voltage-gated ion channels, the AIS is the preferred site of action potential initiation for a couple of other reasons. First, it is strategically located at the beginning of the axon, positioning itself close enough to the soma to 'sense' the activity inputs arriving from the somatodendritic compartment. Secondly, through its small diameter and electrical isolation (especially the more distal segments) the AIS has a smaller local capacitance and therefore requires less current (and lower density of Na_v channels) to generate an action potential compared to larger somatodendritic compartment. The smaller capacitance of the axon also facilitates rapid changes in membrane potential during the rising phase of the action potential. Therefore, the local milieu of the AIS is energetically more favourable for spike initiation than other neuronal compartments, making the AIS an ideal location for the generation of neuronal spikes.

Neurotrasmitter receptors

Ionotropic GABA receptors

As mentioned above, the strategic location of the AIS renders it an optimal site for the generation of neuronal activity, which also makes it an ideal target for rapid and efficient modulation of neuronal firing. Indeed, it has been long recognised that the AIS of neocortical and hippocampal pyramidal neurons receives inhibitory synaptic inputs from a specific set of axo-axonic GABAergic interneurons called chandelier cells (Somogyi et al., 1998). The presynaptic terminals of these cells align with the α2 variant of the $GABA_A$ receptor enriched at the AIS (Brunig et al., 2002). Given the proximity to the spike initiation site, these synapses can greatly influence neuronal output, providing direct control of neuronal firing properties.

In the mature nervous system, GABA is predominantly inhibitory, however, some evidence exists that suggests that the GABAergic inputs onto the AIS may in fact be depolarising (Szabadics et al., 2006). This is thought to be due to a high axonal concentration of Cl^-, brought about by the local expression of a Na-K-Cl cotransporter, NKCC1, that serves to keep intracellular Cl^- concentration high and the low expression of a K-Cl symporter, KCC2, that is responsible for pumping the Cl^- out of the cell. High intracellular Cl^- establishes a relatively depolarised $GABA_A$ reversal potential, leading to Cl^- extrusion from the cell upon opening of $GABA_A$ channels and subsequent depolarisation of the cell. This depolarising action of GABA has been observed in a number of cell types, including cortical pyramidal cells (Szabadics et al., 2006), basolateral amygdala (Woodruff et al., 2006) and in hippocampal granule cells (Khirug et al., 2008). Other reports, however, point towards a hyperpolarising effect of axo-axonic synapses (Glickfeld et al., 2009; Canepari et al., 2010). Overall, this is an area of intense debate, with many opposing views that require further investigation to resolve the many currently outstanding discrepancies.

Metabotropic dopamine receptors

In addition to $GABA_A$ receptors, the AIS also contains G-protein-coupled type 3 dopamine receptors (D3R). These receptors are expressed in the AIS of cartwheel interneurons where they regulate the function of T-type Ca_v channels (Bender et al., 2012). Interestingly, dopaminergic cells do not synapse onto the AIS of cartwheel cells, instead, dopamine regulates the Ca_v channel function in a paracrine manner. Even though a release of dopamine from a single axon terminal could potentially impact several cells, dopamine has been found to affect T-type Ca^{2+} channels exclusively at the AIS, without affecting dendritic T-type Ca^{2+} channels and AIS Na^+ channels (Bender et al., 2010). Dopaminergic modulation of Ca^{2+} channels has a profound effect on neuronal excitability. Blocking D3R reduces spike-evoked Ca^{2+} influx through these channels, which results in the 50% loss of evoked spikes in these cells (Bender et al., 2010). Moreover, it greatly affects spontaneous activity, changing their spontaneous firing pattern from bursting to tonic (Bender et al., 2012).

Protein matrix

Apart from ion channels and neurotransmitter receptors, the AIS is also highly enriched in a variety of cell adhesion molecules (CAMs), extracellular matrix molecules and cytoskeletal and scaffolding proteins, which collectively form a

membrane diffusion barrier between somatodendritic and axonal compartments (Winckler et al., 1999; Nakada et al., 2003) and result in preferential segregation of proteins (Song et al., 2009) that plays a fundamental role in the maintenance of neuronal polarity.

Cell adhesion molecules

Cell adhesion molecules (CAMs) that are enriched at the AIS include two members of the L1 family of CAMs, neurofascin (NF-186) and NrCAM (neuronal cell adhesion molecule), and a heterodimer composed of TAG-1 and Caspr2 (contactin-associated protein 2) protein. Mutations in Caspr2 were linked to epilepsy and susceptibility to autism spectrum disorders (Alarcon et al., 2008; Friedman et al., 2008; Wimmer et al., 2010). NF-186, on the other hand, is required for targeting NrCAM to the AIS (Zonta et al., 2011) and for the assembly of a specialised, brevican-based ECM around the AIS (Hedstrom et al., 2007). NF-186 has also been suggested to play a key role in regulating the assembly of GABAergic synapses. For example, pinceau synapse formation at the cerebellar Purkinje neurons requires a NF-186 gradient along the AIS (Ango et al., 2004). Similarly, loss of NF-186 gradient in hippocampal pyramidal cells disrupts the localisation of gephyrin, a scaffolding protein found at inhibitory synapses, which prevents GABA receptor clustering in the postsynaptic membrane in the axon hillock (Burkarth et al., 2007). In cerebellar Purkinje cells, NF-186 is not essential for AIS assembly during development but is critical for AIS stabilisation in adult neurons, as its absence causes AIS disintegration and loss of key structural components of the AIS, including Na_v channels, βIV-spectrin and AnkG (Zonta et al., 2011). Studies in hippocampal neurons *in vitro*, however, demonstrated that NF-186 is dispensable for formation and stabilisation of the AIS (Hedstrom et al., 2007, 2008).

Extracellular matrix molecules

Neurons are sheathed by perineural nets composed of extracellular matrix (ECM) proteins. The ECM surrounding the AIS has a unique composition and it is enriched in brevican, aggrecan and tenascin-R (Bruckner et al., 2006, John et al., 2006). The function of the ECM proteins at the AIS are currently unknown, however they have been suggested to play a role in recruitment and clustering of other AIS proteins, ionic buffering and synaptic stabilisation (Ogawa et al., 2008). The knockouts of brevican, aggrecan and tenascin-R display very subtle phenotypes on the composition and formation of perineuronal nets, indicating a possible redundancy in

the function of these proteins (Bruckner et al., 2000; Brakebusch et al., 2002; Giamanco et al., 2010).

Scaffolding proteins

The structure of the AIS is held together by scaffolding proteins, including ankyrin G, β-spectrin, and PSD-93, of which ankyrin G is the most important. Ankyrin G (AnkG, ANK3) is a member of adaptor proteins that link the spectrin-based membrane cytoskeleton to other membrane proteins (Kordeli et al., 1995). AnkG plays a critical role at the AIS, as it anchors other components of the AIS and for this reason it is known as 'the master organiser of the AIS' (Garrido et al. 2003, Pan et al. 2006; Dzhashiashvili et al., 2007; Hedstrom et al., 2007; Yang et al., 2007; Zhou et al., 1998; Jenkings and Van Bennett, 2001). AnkG recruits and stabilised proteins containing an AnkG-targeting motif, which include βIV-spectrin, Na_v channels, K_v7 channels, NF-186 and NrCAM (Garrido et al., 2003; Hedstrom et al., 2007; Pan et al., 2006).

Consistent with its role as the master organiser, loss of AnkG disrupts the AIS structure and molecular function (Zhou et al., 1998; Jenkins and Van Bennett, 2001; Hedstrom 2007, 2008). Mice lacking cerebellar AnkG fail to cluster key components of the AIS, including Na_v channels and L1 CAMs (Zhou et al., 1998; Jenkins and Van Bennett, 2001). This lack of AnkG severely affects neuronal function resulting in an impaired ability to fire action potentials (Zhou et al., 1998). Purkinje cells from knock-out mice display a higher threshold for action potential initiation, a lower probability of firing and an impaired ability to fire multiple action potentials in response to long current injections (Figure 1.3a). In addition, the absence of AnkG results in the loss of neuronal polarity. AnkG-depleted axons appear to lose their axonal identity and develop features characteristic of dendrites. Specifically, they develop protrusions closely resembling dendritic spines, which are enriched with postsynaptic proteins and ionotropic and metabotropic glutamate receptors, and are contacted by presynaptic glutamatergic boutons (Figure 1.3b). The accumulation of axonal marker tau was also reduced in the spine-rich portions of the axon(Sobotzik et al., 2009). Interestigly, in these AnkG-deficient Purkinje neurons the putative axon-turned-dendrite was still identifiable as a single process opposite the large dendritic tree, suggesting that AnkG is not required to for axon specification.

Similar observations were made in hippocampal neurons *in vitro*. When the expression of AnkG was reduced with a short hairpin RNA (shRNA), it resulted in

the dismantling of the AIS and loss of the major components of the AIS, such as NF-186, NrCAM, Na_v channels and βIV spectrin. The former axons acquired the molecular characteristics of dendrites, including the formation of spines with postsynaptic densities, and were invaded by proteins that are typically restricted to the somatodendritic domains, such as MAP2 and the K^+/Cl^- cotransporter KCC2 (Figure 13c). Therefore, even though the AIS is not required for axon specification, it appears to be essential for the maintenance of axonal identity and polarity (Hedstrom et al., 2008; Sobotzik et al., 2009; Song et al., 2009).

Cytoskeletal proteins

The underlying AIS cytoskeleton is composed of actin filaments and a specialised microtubule network. Both of these cytoskeletal proteins have been implicated in the formation of a diffusion barrier between somatodendritic and axonal compartments which is crucial for the function of many polarised cells. This AIS barrier restricts the diffusion of membrane proteins and lipids and hinders the passage of dendritic cargoes into the axon (Kobayashi et al., 1992; Winckler et al., 1999; Nakada et al., 2003; Song et al., 2009). It is not clear how axonal cargos are able to pass through the AIS barrier. According to Song et al. (2009), this is dependent on the higher transport efficacy of motor complexes carrying axonal proteins rather than dendritic proteins. For example, kinesins carrying axonal proteins (KIF5-VAMP2 complex) were shown to be more efficient in crossing the AIS barrier than the kinesins carrying vesicles with dendritic proteins (KIF17-NR2B complex; Song et al., 2009). The entry of axonal proteins may also be facilited by distinct posttranslational modification of axonal microtubules, which are mostly acetylated, in contrast to tyrosinated dendritic microtubules (Gomis-Ruth et al., 2008). Microtubule acetylation has been shown to increase the binding efficiency of kinesins, such as kif5, complexed with axonal proteins (Konishi and Setou, 2009). Therefore the binding of motor proteins to microtubules will vary dramatically depending on the biochemical properties of axonal or dendritic microtubules. Specific cargos may also influence the affinity of the kinesin-cargo complexes by changing the conformation of the microtubule-binding tail domain and affecting transport efficiency.

Despite clear demonstrations of the existence of the diffusion barrier at the AIS, little is known about how it contributes to selective filtering. One possibility is that the distinct molecular organisation of actin at the AIS may be responsible for the formation of the barrier. Recent electron microscope studies of cultured hippocampal neurons show that actin filaments along an axon are arranged in periodically-distributed rings wrapped around the circumference of axons, a feature not observed in dendrites (Xu et al., 2013). This cytoskeletal arrangement forms at around 7DIV and coincides with the beginning of formation of the AIS barrier is in cultured hippocampal neurons (Winkler et al., 1999; Nakada et al., 2003; Song et al., 2009). Furthermore, using rat cortical cultures as a model, Watanabe et al. (2013) demonstrated a very different kind of actin arrangement at the AIS. They described the presence of specialised actin 'patches' within the AIS that were proposed to act as a semipermeable vesicle filters. Actin patches were shown to coincide with areas of very low mobility, and even stalling, of vesicles carrying dendritic proteins, indicating that these actin networks may act as a barrier that prevents dendritic proteins from reaching the distal axon.

In addition to actin filaments, the AIS is enriched with a specialised microtubule network (Palay et al., 1968). Within the AIS, microtubules are highly polarised with their fast growing 'plus end' oriented away from the cell body. This orientation is important for polarised trafficking that depend on a number of motor proteins (kinesins and dyneins), their distinct cargo and the posttranslational modifications of microtubules along which they travel (Rasband, 2010). Microtubules in the proximal axon are tyrosinated and less stable than the microtubules in the distal axon, which are preferentially acetylated. In mature hippocampal neurons, pharmacological stabilisation of microtubules induces the transformation of a dendrite into an axon (Gomis-Ruth et al., 2008). Therefore this distinct modification of tubulin may be essential for the establishment of neural polarity through polarised trafficking of cargo-bound motor proteins.

1.3.2 The assembly of the AIS

As shown in the previous section, the molecular organisation of the AIS is incredibly complex. How is this protein complex assembled? The general consensus is that AIS development is dependent on AnkG (Zhou et al., 1998; Jenkins and Van Bennett, 2001; Dzhashiashvili et al., 2007; Hedstrom et al., 2007; Rassmussen et al., 2007; Yang et al., 2007; Gasser et al., 2012). Transgenic mice lacking AnkG

also lack the AIS (Zhou et al., 1998) and in cultures where AnkG has been knocked down, the AIS never forms (Hedstrom et al., 2007). AnkG is one of the first proteins concentrated at the proximal axon, where it recruits other AIS components through its multiple akyrin repeats (Figure 1.4a). The proteins containing AnkG-targeting motifs include Na_v and K_v channels, βIV-spectrin and L1 CAMs (Davies and Bennett, 1994; Garrido et al., 2003; Boiko et al., 2007; Rasmussen et al., 2007; Gasser et al., 2012). Interestingly, the AnkG-binding motif of Na_v channels is not specific for AnkG as it can also bind to ankyrin-B, another scaffolding protein which is expressed throughout the length of the axon (Bennett and Lambert, 1999). Specific targeting of Na_v channels is achieved by phosphorylation of the AnkG-binding motif by casein kinase II (CK2), an enzyme enriched at the AIS, which facilitates the interaction between Na_v channels and AnkG (Brechet et al., 2008). Similarly, the protein kinase Cdk5 (cyclin-dependent kinase 5) promotes targeting of K_v channels to the axonal membrane (Vacher et al., 2011), suggesting that clustering and stabilisation of other AIS proteins may also require posttranslational modification.

Relatively late in development, the AIS begins to be enveloped in a dense net of extracellular matrix (ECM) proteins, preferentially enriched in the chondroitin sulphate proteoglycan brevican (John et al., 2006). The formation of this brevican-rich ECM is directed by NF-186, which is necessary for its targeting to the AIS (Hedstrom et al., 2007). Interestingly, in the nodes of Ranvier, which have a similar structural and molecular organisation to the AIS, NF-186 also recruits AnkG, which then clusters nodal ion channels. The NF-186 itself is localised to the nodes by signals from neighbouring glial cells during myelination (Dhashiashvili et al., 2007; Feinberg et al., 2010). AnkG clustering at the AIS, however, is an intrinsic property of neurons and does not require glial signals or NF-186 (Hedstrom et al., 2007; Zonta et al., 2011). How is AnkG recruited to the AIS?

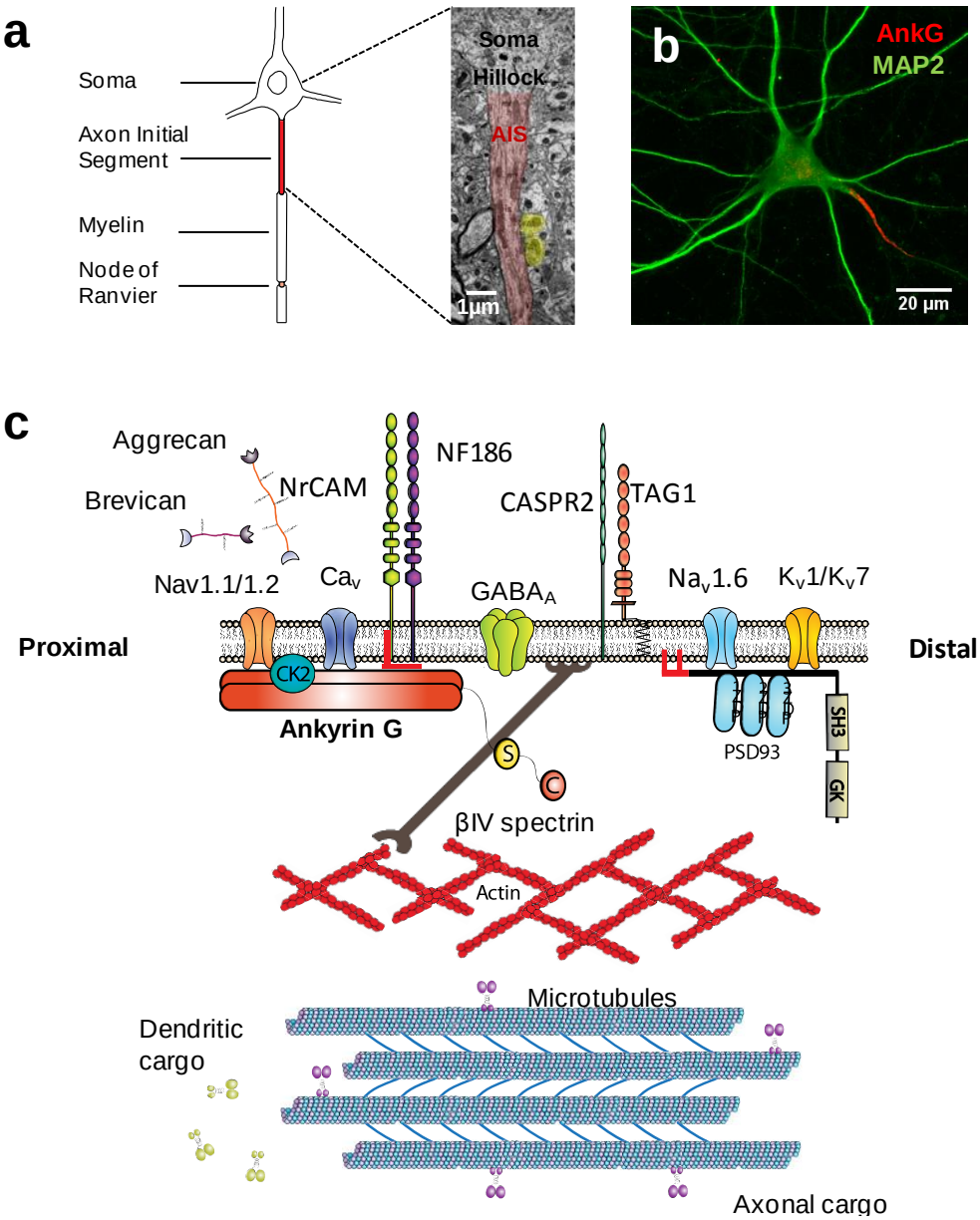

Figure 1.2 The structure of the axon initial segment (a) Schematic diagram of a neuron showing the location of the axon initial segment (AIS; red) and electron micrograph of the AIS of a cortical pyramidal neuron (adapted from Peters et al., 1968). Soma, axon hillock and the AIS (red) are indicated. Yellow shading indicates presynaptic terminals onto the AIS. (b) A cultured hippocampal neuron at 14 DIV stained for Ankyrin G (AnkG) and MAP2. (c) Major molecular components of the AIS. AIS is composed of extracellular matrix molecules, (only brevican and aggrecan are shown), ion channels ($Na_v1.1/1.2/1.6$, $K_v1.1/1.2/7.2/7.3$ and Ca_v), cell adhesion molecules (neuronal cell adhesion molecule (NrCAM), neurofascin 186 (NF186) and a heterodimer consisting of transient axonal glycoprotein 1 (TAG1) and CASPR2), cytoskeletal scaffolds (AnkG, βIV-spectrin and postsynaptic density protein93 (PSD93) and casein kinase II (CK2). Actin filaments are linked to membrane proteins via the interaction with βIV-spectrin. Microtubule fascicles with unique cross bridges allow axonal but not dendritic cargos enter the AIS. GK, guanylate kinase; PDZ, PSD95/discs large/zonula occludens; SH3, SRC homology 3 (modified from Rasband, 2010).

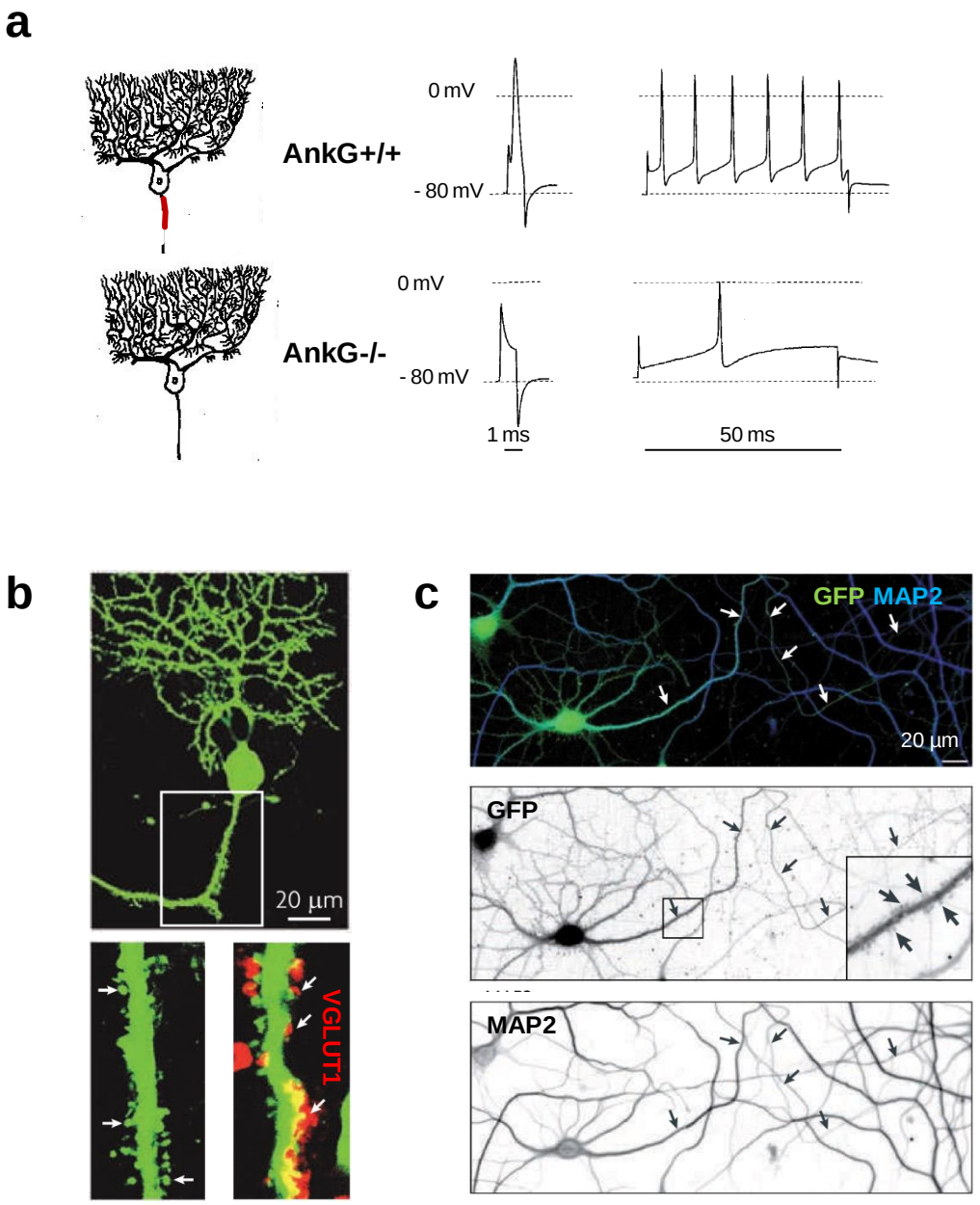

Figure 1.3 AIS is essential for action potential firing and the maintenance of neuronal polarity (a) Whole-cell current clamp recordings of Purkinje cells in cerebellar slices from a normal mouse (AnkG+/+ ; top) and a mutant mouse with cerebellar knockout of AnkG (AnkG-/-; bottom). AnkG-deficient neurons have impaired ability fire single and multiple action potentials, in response to short (1ms) and long (50ms) current injections (Adapted from Zhou et al., 1998; the drawings of Purkinje neurons were taken from http://www.gutenberg.org/files/31382/31382-h/31382-h.htm). (b) Purkinje neurons from AnkG-deficient mice develop an axon with spine–like protrusions (indicated by arrows), which are contacted by axonal terminals expressing vesicular glutamate transporter 1 (VGLUT1; red; adapted from Sobotzik et al., 2009). (c) A micrograph showing cultured hippocampal neurons infected with an adenoviral vector expressing GFP and a short hairpin RNA (shRNA) sequence for ankyrinG. GFP immunofluorescence shows the axon (arrows) and the presence of dendritic spines along the axon near the cell body (inset). MAP2 immunoreactivity illustrates high levels of this protein along the former axon (adapted from Hedstrom et al., 2008)

Galiano et al., (2012) examined early events in axogenesis that could contribute to AnkG clustering. Interestingly, AnkG accumulation at the proximal axon of cortical pyramidal neurons was found to be a consequence of an extrusion mechanism rather than an active recruitment. This extrusion mechanism is achieved though assembly of a distal axonal cytoskeleton composed of ankyrin B, αII-spectrin and βII-spectrin. These proteins are originally enriched at the growth cones and then progressively fill in the distal region of developing axon, establishing an intra-axonal boundary (Figure 1.4b). This boundary serves as a nucleating point for the AnkG accumulation and limits its distribution to the proximal axon. Because AnkG is also found at nodes of Ranvier, the boundary cannot be a strict barrier that excludes all AnkG trafficking but rather it prevents its incorporation into distal sites. Experimentally moving this boundary by overexpressing AnkB, αII-spectrin or βII-spectrin, early on in development shortens the length of the AnkG-based AIS, whereas overexpression of AnkG causes a distal shift in the AIS boundary. Disruption of the boundary through the knock-down of the distal-cytoskeletal proteins disrupts AnkG clustering and redistributes it to the distal axon. Consistent with this, αII-spectrin and βII-spectrin deficient mice have disrupted AIS (Galiano et al., 2012).

1.3.3 Activity-dependent AIS plasticity

Highly complex organization of the AIS and its extensive cross-linking with the cytoskeletal and ECM proteins may suggest that it is a rather static structure. A number of recent observations, however, challenge this view and demonstrate that the structure of the AIS is, in fact, surprisingly plastic and can undergo activity-dependent changes in its length and position (Grubb and Burrone, 2010; Kuba et al., 2010; Grubb et al., 2011). The existence of these plastic changes has been demonstrated in the avian auditory system *in vivo* and in rat hippocampal neurons *in vitro*.

AIS plasticity in the avian auditory system

In the avian auditory system the length and position of the AIS along the axon varies with the tuning frequency of neurons and depends on the specific excitability requirements of the cell. These requirements differ according to the location of the neurons within the auditory nuclei and the configuration of their synaptic inputs. In chick auditory nuclei, neurons are arranged in a tonotopic manner according to their

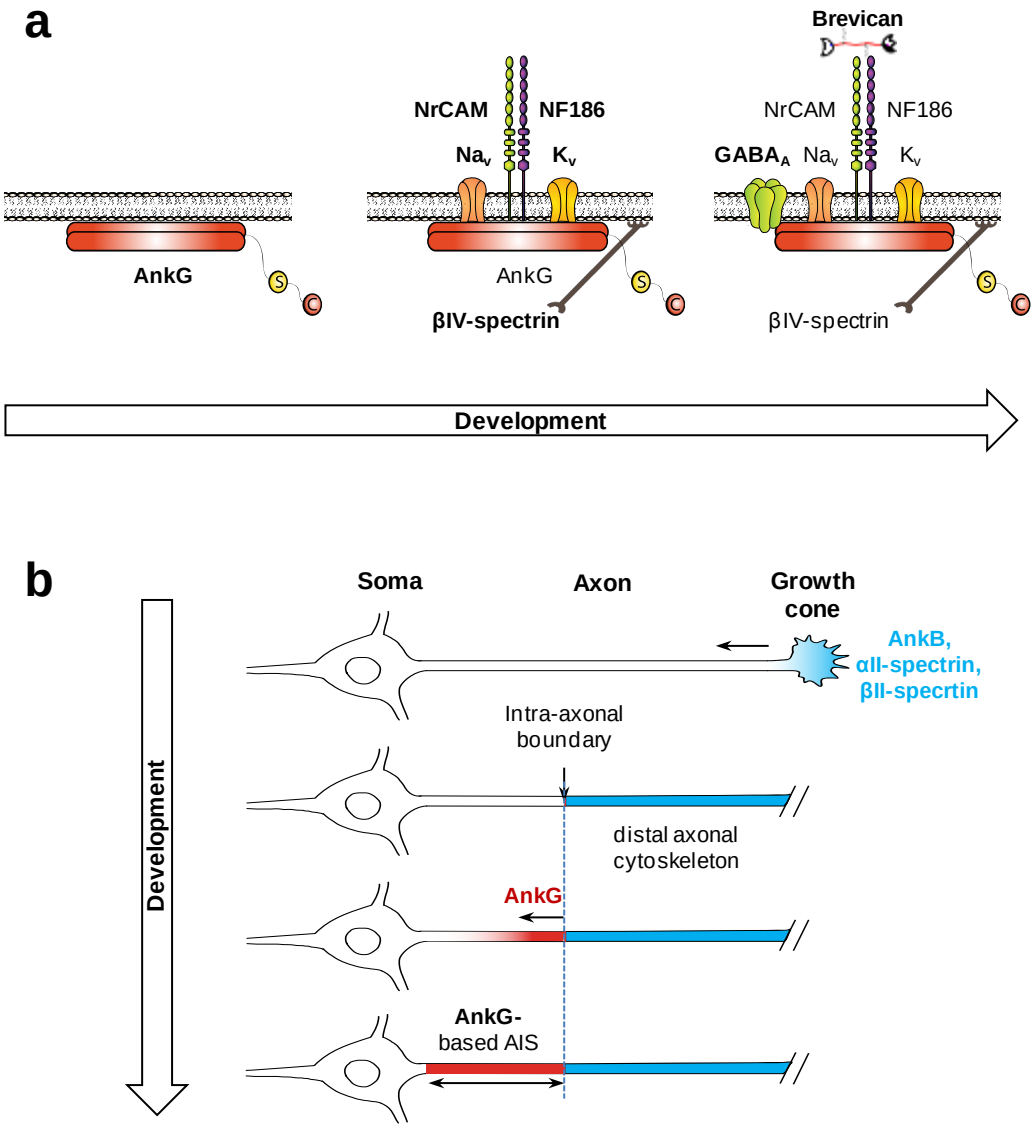

Figure 1.4 AIS development (a) Simplified stages of AIS development. AnkG is one of the first proteins localised to the proximal axon. AnkG recruits other AIS proteins, including βIV-spectrin, Na_v and K_v channels and cell adhesion molecules NF-186 and NrCAM. Later in development NF-186 directs the formation of brevican-rich extracellular matrix and regulates the development of GABAergic synapses at the AIS. (b) A model of AnkG clustering at the proximal axons in developing cortical pyramidal neurons. AnkB, αII-spectrin, βII-spectrin (blue) are enriched in the growth cones and gradually fill in the distal part of the axon forming an intra-axonal boundary. This boundary serves as a nucleating point for accumulation of AnkG (red) which gradually fills in the proximal axon.

characteristic frequency: from high-frequency inputs in the rostro-medial region (~4Hz) to low-frequency inputs (~0.2Hz) in the caudo-lateral region (Kuba et al., 2012).

In nucleus magnocellularis (NM), which is a second order auditory nucleus, low-frequency neurons receive a larger number of synaptic inputs than high frequency cells, which helps to prevent timing fluctuations in the activity of the auditory nerve. The convergence of many small synaptic inputs, however, results in decreased firing probability of the cells due to inactivation of its voltage-gated Na^+ channels during the slow rise of summating EPSPs. To compensate for lower excitability differences, the low-frequency neurons contain longer AISs than the high-frequency cells. The location of the AIS from the soma, however, is similar in both types of neurons (Figure 1.5a). Longer AIS clusters more Na_v channels, which allow for effective compensation of Na^+ current inactivation during slow depolarisation of summed synaptic inputs and efficient firing of action potentials (Kuba and Ohmori, 2009).

The outputs from nucleus magnocellularis are conveyed to nucleus laminaris (NL), a third order nucleus in chick auditory system. The neurons in NL are also tonotopically arranged, the precise location of which determines the properties of the AIS. This time however, the structural properties of the AIS depend on the frequency, rather than a number of synaptic inputs along the tonotopic axis. The higher the frequency of inputs, the shorter the AIS and the further it is from the soma. Thus the neurons receiving low frequency inputs have long AISs (25µm) that are located close to the soma (10µm), whereas the cells receiving high frequency inputs have short (10µm), distally-located (up to 80µm) AISs (Figure 1.5a). Similarly to what is observed in the NM, this arrangement is optimal for effective firing in the NL (Kuba et al., 2006). The distal location of the AIS enhances the sensitivity of the neuron to synaptic inputs because of the electrical isolation of the initiation site from the somatodendritic compartment, whereby less depolarisation is required to trigger an action potential. In addition, this arrangement minimises Na^+ channel inactivation in response to sustained depolarisation resulting from high frequency activity. The observations in these two nuclei show that AIS position and length in the auditory nuclei of chick appear to be fine-tuned to the frequency and magnitude of synaptic inputs to the cell.

Would the properties of the AIS change if the synaptic input to these nuclei was altered? Kuba et al., (2010) answered this question by silencing the activity in one of the auditory nuclei, the nucleus magnocellularis (NM). Silencing auditory inputs to the NM through removal of the cochlea resulted in marked changes occurring within 7 days of deprivation. Lack of activity abolished the tonotopic variation in the length of the AIS normally observed in the NM (Figure 1.5b, left panel), suggesting that synaptic activity is crucial for structural tuning of the AIS. On average, the AIS of activity-deprived cells were 50% longer than control cells but displayed no change in location. Structural changes of the AIS were accompanied by an increase in the amplitude of Na^+ currents, however their electrophysiological properties were unchanged, suggesting that the elongation of the AIS involves insertion of Na^+ channels of the same type. In addition to higher Na^+ currents, activity deprivation resulted in reduced spike threshold and enhanced spontaneous firing of the activity-deprived neurons. Thus, the neurons of chick NM respond to lower levels of activity by lengthening their AISs, which in turn leads to compensatory increase in neuronal excitability.

Hippocampal neurons

Activity-dependent changes in the structure of the AIS were also observed in hippocampal neurons *in vitro*. Grubb and Burrone, (2010) showed that chronic (48hr) increases in activity led to a distal shift in AIS position without a change in length. The activity was increased by either global cell depolarisation with high levels of KCl or by evoking action potentials in a spatiotemporally controlled manner with optogenetic photostimulation. The shift was observed in multiple components of the AIS, i.e. AnkG, βIV-spectrin and Na^+ channels, suggesting that the whole structure was moved to a more distal location. The distribution of Na_v channels also remained the same, as $Na_v1.6$, $K_v1.1$ and $K_v1.2$ were still preferentially located in the distal AIS (Evans and Grubb, 2011). More importantly, the distal shift in AIS position was coupled to profound changes in neuronal excitability. The neurons with distally-located AIS had a higher threshold for action potential initiation than cells with an AIS located close to the soma. Interestingly, this type of plasticity is bidirectional, as the AIS returns to its proximal position upon removal of the source of activity. In addition, it is cell-type specific, as it seems to be present only in excitatory cell types (pyramidal cells of CA1 and CA3 regions and dentate granule cells) but not in GABAergic interneurons (Evans et al., 2013).

What is the mechanism of this shift? Surprisingly, it is independent of action-potential-mediated activity, as blocking voltage-gated Na^+ channels with tetrodotoxin (TTX) did not prevent the AIS shift (Grubb and Burrone, 2010). Neither did the treatment with antagonists of AMPA and NMDA receptors, suggesting this form of plasticity is not dependent on enhanced synaptic transmission (Evans et al., 2013). Blocking L-type Ca^{2+} channels, on the other hand, abolished the effect, suggesting that Ca^{2+} signalling may play a key role in the activity-dependent AIS shift. Evans et al. (2013) investigated signalling pathways downstream of Ca^{2+} entry and showed that subsequent signalling requires calcium-calmodulin-activated phosphatase calcineurin (CaN), inhibition of which was sufficient to block both KCl and optogenetically-induced AIS relocation. Intriguingly, neither CaN nor L-type Ca^{2+} channels are detected at the AIS (Bender and Trussel, 2009; Yu et al., 2010). CaN is localised mainly in the nucleus (with diffuse concentration in the neurites), whereas L-type Ca^{2+} channels are known to preferentially distribute in the soma and proximal dendrites of hippocampal neurons (Obermair et al., 2004), thus suggesting the signals for AIS relocation may arise in the somatodendritic compartment. CaN is known to phosphorylate and activate a transcription factor called NFAT (nuclear factor of activated T cell), which translocates to the nucleus and triggers transcription of relevant genes, which may be required for AIS relocation. However, the precise cascade of intracellular events that is activated in response to CaN activation have yet to be fully determined.

Apart from controlling gene expression, calcineurin signalling can also directly affect the cytoskelon. CaN has been shown to dephosphorylate various cytoskeletal organising proteins, including Tau, MAP2, coffilin, WAVE-1 and synaptopodin (Goto et al. 1985, Ferreira ea al., 1993, Gong et al., 1994, Wen et al., 2003, Faul et al. 2008, Ceglia et al., 2010). Mice lacking neuronal CaN α subunit have an abnormal phosphorylation of microtubules, decreased density of neurofilaments and abnormal organisation of the cytoskeleton (Kayyali et al. 1997). Because the AIS is highly enriched in distinct cytoskeleton, including fasciculated microtubules (Palay et al., 1968) and F-actin (Nakada et al., 2003), it is possible that AIS relocation may require cytoskeletal remodelling. In such case , CaN/NFAT signalling may provide the link between membrane depolarisation and the subsequent reorganisation of the neuronal cytoskeleton.

AIS as the new site for homeostatic regulation

The studies in chick auditory system and cultured hippocampal neurons show that the AIS can be dynamically regulated by ongoing levels of activity. The changes in the length or location of the AIS have profound consequences on neuronal excitability. The longer AISs resulting from auditory deprivation lead to higher excitability of the NM neurons, while the more distal AISs in chronically depolarised hippocampal neurons are coupled with lower neuronal excitability. The activity-dependent changes in the structure of the AIS described to date may thus act as a homeostatic mechanism, where excessive or insufficient excitation is counterbalanced to maintain the excitatory input within its physiological boundaries (Nelson and Turrigiano, 2004). Such homeostatic fine-tuning of neuronal activity may be particularly important for optimising the function of neuronal networks in the developing brain (Grubb et al., 2011).

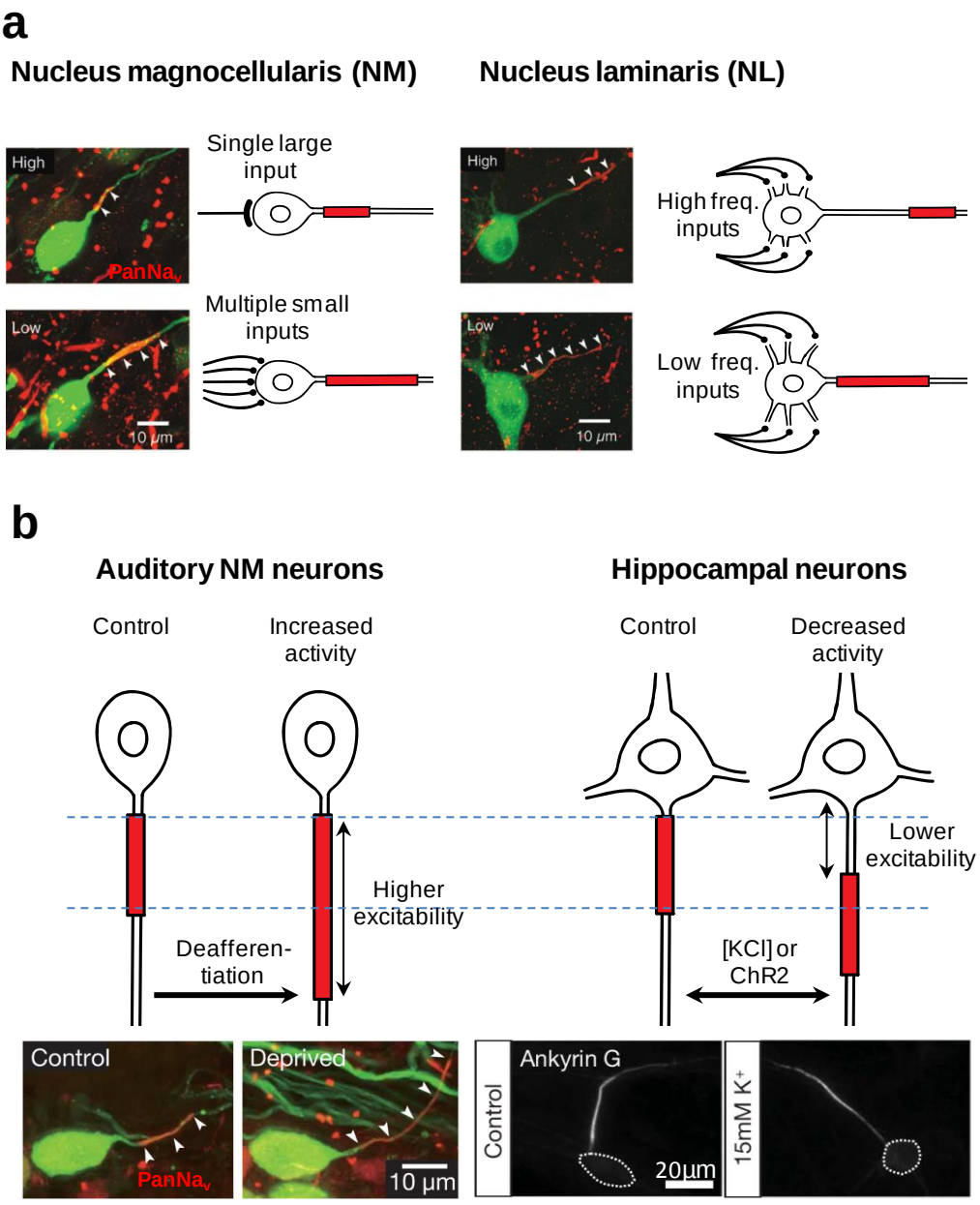

Figure 1.5 Activity-dependent structural plasticity (a) Structural tuning of the AIS to synaptic inputs in nucleus magnocellularis (NM; left) and nucleus laminaris (NL; right). In the NM, neurons differ in terms of the length of their AIS, depending on the number and size of synaptic inputs they receive. Neurons receiving a single large synaptic inputs (top) have short AISs, in contrast to neurons receiving multiple small inputs, (bottom) which contain an almost two-fold longer AIS . In the NL, the cells differ in terms of both the length and the position of the AIS, depending on the frequency of their synaptic inputs. Neurons receiving high frequency inputs (top) have short distally-located AIS, whereas neurons receiving low frequency inputs (bottom) have long AIS located close to the cell body (Adapted from Kuba et al., 2006 and Kuba and Ohmori, 2009). (b) Activity-dependent plasticity of NM neurons (left) and cultured hippocampal neurons (right). Silencing afferent activity in the NM elongates the AIS of deafferentiated neurons, which results in enhanced excitability of these cells. Increasing the activity in dissociated hippocampal neurons, with either high levels of extracellular KCl or optogenetic stimulation of ChR2-transfected neurons, causes a distal shift in the AIS position, leading to lower excitability of chronically active cells (Adapted from Kuba et al., 2010 and Grubb and Burrone, 2010)

1.4 Aims of the thesis

The aim of this thesis was to explore the role of neural activity on the development of hippocampal neurons *in vitro*. In **chapter 3**, I investigate how modulating the membrane potential of young, 4 DIV, cells affects neuronal morphology. Specifically, I measure the length, shape and complexity of axonal and dendritic arborisations following chronic (16hr) membrane depolarisation. In **chapter 4**, I shift my focus to the axon initial segment (AIS), the site of action potential initiation in neurons. First, I characterise the emergence of the AIS in our culture system in order to establish when the AIS first appears in excitatory neurons of the hippocampus *in vitro* and to describe the basic structural properties of the AIS, such as its length and position, during development. Subsequently, I investigate how chronic (16hr) membrane depolarisation affects the proportion of cells containing the AIS at different time points in development, and characterise any changes in the structural properties of the AIS. I briefly investigate the immediate downstream sensors of this membrane depolarisation phenotype, such as L-type voltage-gated Ca^{2+} channels, and examine possible roles of the Ca^{2+}-dependent protease calpain. Finally, I describe the temporal characteristics of this activity-dependent form of AIS plasticity and examine its reversibility. In **chapter 5**, I investigate the relationship between the presence of an AIS and neuronal excitability. Specifically, I explore how the emergence of the AIS affects the physiology of neurons and enables them to fire action potentials. Finally, I examine the functional consequences of losing the AIS in response to membrane depolarisation and propose possible mechanism that might help explain the data.

Chapter 2

Materials and methods

2.1 Dissociated hippocampal cultures

Hippocampal neurons were grown on glass coverslips (18mm and 13mm diameter, Menzel Glaser, Germany). The coverslips were prepared by 30-minute wash in 70% ethanol, followed by another 30-minute wash in 96% ethanol. Ethanol-washed coverslips were rinsed in distilled H_2O and air-dried. Dry coverslips were sterilised at 220°C for 2 hrs and kept in a sterile glass Petri dish until required. Prior to culturing, the coverslips were coated with poly-L-lysine (50 µg/ml in PBS) and laminin (20 µg/ml PBS).

Cultures were prepared from E18 Sprague-Dawley rat embryos of either sex (Charles River Laboratory). Hippocampi were dissected out in HBSS, digested in trypsin (0.5 mg/ml in HBSS; Worthington) for 15 min at 37°C, washed three times in HBSS and triturated through fire-polished Pasteur pipettes of increasingly narrower diameter. The cell suspension was added to culture media and the cells were plated at 50,000 cells per 18mm coveslip (12-well plate; 1ml medium) and at 40,000 per 13mm coverslip (4 well-plate; 0.5 ml medium). Culture media were based on Neurobasal, supplemented with 1% fetal calf serum, 1% glutamax, 1% B27 and 0.5% Pen/Strep (Sigma). The cultures were kept at 37°C in 6% CO_2. At 3 DIV the media were replaced with fresh (serum-free for limited glial growth) neurobasal media supplemented with 2% B27 and 1% glutaMAX. All culture reagents, unless specified otherwise, were purchased from Invitrogen.

2.2 Plasmids and transfections

ChR2–YFP construct was pLenti-Synapsin-hChR2(H134R)-EYFP-WPRE, a gift from K. Deisseroth. Vector sequence and map can be viewed at: http://www.everyvector.com/sequences/show_public/2506

The cells were transfected using Effectene (Qiagen) at 1 DIV using a modified protocol available at http://www.qiagen.com/Products/Catalog/Assay-Technologies/Transfection-Reagents/Effectene-Transfection-Reagent. For

transfection of a single coverslip, 0.1 µg (13mm coverslip) or 0.2 µg (18mm coverslip) of plasmid was mixed with 30 µl of buffer and 0.8 µl (4-well plates) or 1.6 µl (12-well plates) enhancer. The mixture was briefly vortexed and incubated for 2-5 minutes at room temperature. The DNA-enhancer mixture was supplemented with 5 µl of Effectene, briefly vortexed and incubated for 5-10 minutes. The prepared effectene solution was added drop-wise to the coverslips, followed by the incubation at 37°C for 30-45 minutes. After this time, the Effectene was removed and replaced with fresh pre-warmed culture media.

2.3 Optogenetics

2.3.1 LED stimulation system

Optogenetic experiments based on ChR2 protein required a steady source of blue light to control cell behaviour. For this purpose an LED stimulation system was built according to a design by Dr Andrew Lowe (King's College London). The system consisted of 12 LED stimulation units, an LED driver box, a PC running stimulation paradigms and a power supply (Figure 2.1a). Each LED unit was made of 4 individual LEDs attached to a heat sink and the spacing between the LEDs was adjusted to the dimension of a 4-well plate. LED lights require constant current at a given voltage to produce luminosity. The required voltage was delivered from the power supply and the level of delivered current was controlled by the LED drivers. LED drivers also allowed turning the LEDs on and off, as well as to change the degree of luminance. Light power required to activate ChR2 is approximately 5-12mW/mm^2 (Boyden *et al*. 2005; Ishizuka *et al*. 2006). Although light intensity of our LED stimulation system has not been measured, it was sufficiently bright to open the ChR2 channel (see Figure 3.2).The frequency and duration of light signals was controlled by TTL pulses supplied by a computer program written by Dr Andrew Lowe. This system allowed manipulation of light signal on the millisecond scale similar to that underlying neural excitability *in vivo*.

The assembly of LED stimulation was completed in several steps. First, blue (447.5 nm) LEDs (Luxeon Star ®LEDs; Part No. LXML-PR01-0425) were attached to 75 mm aluminium heat sinks (Fisher Electronik; SK 100/75 SA) with thermal adhesive tape (Luxeon Star ®LED; Part No. LXT-S-12). The LEDs were then connected to each other in a series circuit. Plastic 20 mm hexagonal collimator holders (Luxeon Star ®LED; Part No. 10434) were glued on top of the LED bases and 35 deg

circular collimators (RS components; Part No. 10196) were fitted in. The constructed LED units were connected to DC/DC LED drivers (RS components; Part No. 706-3238), arranged in three 12-way rectangular junction boxes (RS components; Part No. 262-7893), and the power supply (Mascot; Part No. 8921 24V). The cables and cable plugs were ordered from RS components (Part No. 129-6460 and 469-125).

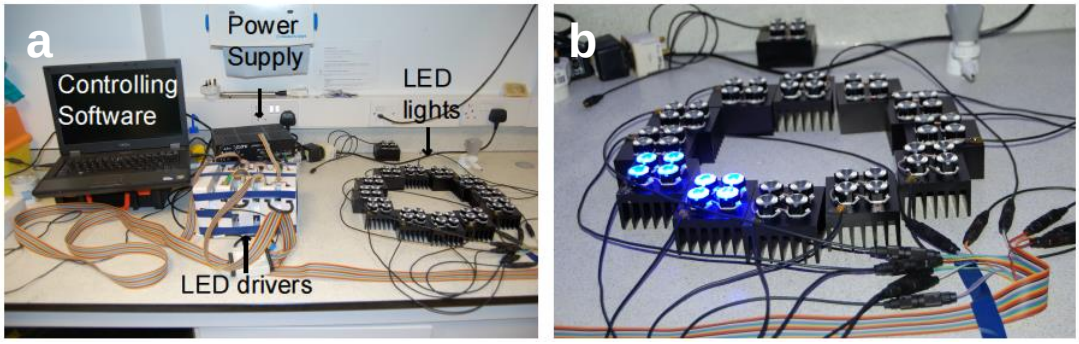

Figure 2.1 The LED stimulation system (a) The system consisted of a PC with custom-written controlling software, LED driver box, power supply and 12 LED units. (b) Each LED unit was made of four individual LEDs attached to a heat sink. The arrangement of the LEDs on the heat sink was adjusted to fit under the 4-well plate containing neurons plated on 13 mm glass coverslips.

2.3.2 ChR2 photostimulation

Two hours prior to photostimulation, cultures transfected with ChR2-YFP had their growth media supplemented with a number of additional antioxidants (110 µM vitamin C, 100 µM Trolox, 77 nM superoxide dismutase, 3.2 µM glutathione and 2.3 µM vitamin E; all from Sigma apart from glutathione ordered from Fisher Scientific). For long-term photostimulation, 12-well culture plates were placed directly onto a bed of collimator-topped blue LEDs and kept at 37°C, 5% CO_2 conditions. All coverslips in a given plate received the same pattern of photostimulation.

2.4 Immunocytochemistry

Coverslips were fixed with pre-warmed to 37°C 4% or 1% formaldehyde (TAAB Laboratories; in 3% sucrose, 60mM PIPES, 25mM HEPES, 5mM EGTA, 1mM $MgCl_2$; pH7.4) for 20 minutes at room temperature. Cells were permeabilised for 5 minutes with 0.25% Triton X-100 (Sigma), rinsed in PBS (Phosphate Buffered

Saline; 0.1M phosphate buffer, 0.15M NaCl) three times and blocked in 3% BSA solution (in PBS) for 45-60 minutes. The blocking step was followed by addition of the primary antibody diluted in the blocking solution. The antibodies used, together with their working dilutions, host and the company from which they were purchased are shown in table 2.1. Cells were incubated with primary antibody for 12-48 hours at 4°C, which was followed by a wash (3x) in PBS and subsequent incubation in the secondary antibody (1:500) for 30 minutes at room temperature. Antibody-stained coverslips were incubated with Hoechst solution (1:2000 in H_2O) to label for cell nuclei (3 minutes at room temperature, light-protected) and mounted in moviol (Moviol 4-88, Calbiochem; 5g moviol + 20 ml PBS + 10 ml glycerine + DABCO (Sigma, antifade).

Table 2.1 Antibodies used in the thesis

Antibody	Supplier	Dilution	Host and isotype
anti-ankyrin G	NeuronMab	1:500	Mouse $IgG_{2a,}$ IgG_1
anti-αCaMKII	Millipore	1:1500	Mouse IgG_1
anti-CTIP2	Abcam	1:1000	Rat
anti-prox1	Sigma	1:500	Rabbit
Anti-tau	Daco	1:2000	Rabbit
anti-Pan-neurofascin-186	NeuroMab	1:500 (fixed) or 1:100 (live)	Mouse IgG_{2a}
Anti-PanNav	Alomone	1:250	Rabbit
Anti-mouse IgG1	Molecular Probes	1:500	Alexa Fluor 488
Anti-mouse Ig2a	Molecular Probes	1:500	Alexa Fluor 568
Anti-mouse Ig2b	Molecular Probes	1:500	Alexa Fluor 568
Anti-rabbit	Molecular Probes	1:500	Alexa Fluor 488
Anti-rabbit	Molecular Probes	1:500	Alexa Fluor 568
Anti-rabbit	Molecular Probes	1:500	Alexa Fluor 633
Anti-rat	Molecular Probes	1:500	Alexa Fluor 488

2.5 Image acquisition and analysis

2.5.1 Neuronal morphology

Images of immunostained ChR2YFP-transfected neurons (chapter 3) were acquired using an Olympus FluoView 1000 laser scanning confocal microscope equipped

with a 40x/0.8 NA water immersion objective (Olympus). YFP and Alexa Fluor 568 fluorophores were imaged sequentially using 488 nm and 543 nm lasers, respectively, along with appropriate excitation and emission filters. To avoid bias, all transfected cells of a given coverslip were imaged, unless: (1) neurites were cut off/damaged or overlapping with other transfected cells or (2) the whole dendritic tree did not fit into a single imaging frame. Image sequences were exported as 16-bit TIFF files and then converted into single maximum intensity z-axis projections with ImageJ. To measure neuronal morphology, the z-projections were converted to 8-bit and imported into an imageJ plug-in, the NeuronJ (ImageScience.org, Meijering et al., 2004). Using NeuronJ, fluorescently labelled neurons were manually traced, with separate traces for axons and dendrites. Such traced images were saved as NDF files and imported into Matlab (Mathworks) for analysis using custom-written routines.

Table 2.2 Definitions of morphometric parameters

Total dendritic length (µm)	Total extension of the dendritic arborisation
Total axonal length (µm)	Total extension of the axonal arborisation
Total length (µm)	Total extension of the dendritic and axonal arborisation
Number of soma branches	Number of dendritic branches around the soma
Number of tips	Number of tree terminals per neuron
Straightness	A ratio of a straightline distance of the dendritic tip from the soma over the tip path distance
Tip path distance (µm)	Distance along the dendrite between the soma and the furthest terminal tip
Max Scholl distance	Euclidean distance of a compartment from the soma
Bifurcations per mm	Number of bifurcations per mm per cell
Branch order	Maximal number of bifurcations between soma and terminal tips
Tree asymmetry index	Average partition over all bifurcations. Partition is computed at every bifurcation, and it is defined as (r - l)/(r + l -2), where *r* and *l* are the number of terminations of the two daughter trees (Van Pelt et al., 1992)

2.5.2 AIS

Images of axon initial segments (chapter 4 and 5) were taken on Olympus IX71 inverted microscope with a 40x oil immersion objective and a CCD camera (Coolsnap HQ, Photometrics) coupled to Slidebooke software (Intelligent Imaging Innovations). The excitation light source was a Xenon-arc lamp (Lambda-LS, Sutter Instruments) with appropriate excitation and emission filters (Chroma Tech. Corp.) regulated by a fast shutter (SmartShutter; Sutter Instruments). The cells were imaged blind with respect to experimental condition and the type of neuron imaged. To avoid biased capture of certain cell types, neurons were located using the Hoechst stain rather than a specific cell type marker. Approximately 60 random frames were captured per coverslip.

Image stacks were exported as raw 16-bit TIFF files, and imported into Matlab for analysis of AIS properties (length and distance from the soma) using custom-written codes. To measure AIS properties, a line profile was drawn along the AIS, starting at the beginning of the axon (chosen by eye; defined as the intersection between the axon and the outer edge of the soma) and extended down through (and past) the AIS (Figure 2.2a-b). For each pixel (1 pixel = 0.129 µm) along this line, the values of fluorescence intensity (Figure 2.2c) were averaged over a 3 x 3 pixel square centred on the pixel through which the line was drawn (Figure 2.2d). The average profiles were then smoothed using a 40-point (~5 µm) sliding mean, and normalised between 1 (maximum smoothed fluorescence) and 0 (minimum smoothed fluorescence; (Figure 2.2e). AIS start and end positions were defined as the positions where the normalised and smoothed profile declined to 33% of the maximum fluorescence. Previous work have shown that these positions strongly correlate (Spearman r>0.8) with AIS start and end points measured by eye. Varying the threshold value between 0.1 and 0.9 did not affect the reported pattern of results (Grubb and Burrone, 2010). Peak fluorescence was taken as the maximum value of each profile, whereas integrated AIS fluorescence was calculated as the area underneath the profile, inbetween the AIS start and end positions.

2.6 Cell viability assay

Cell viability was estimated blind to the experimental condition, by staining the cells with propidium iodide. PI is a highly stable, polar fluorescent dye that only penetrates the membranes of damaged, and/or potentially dying cells, thereby

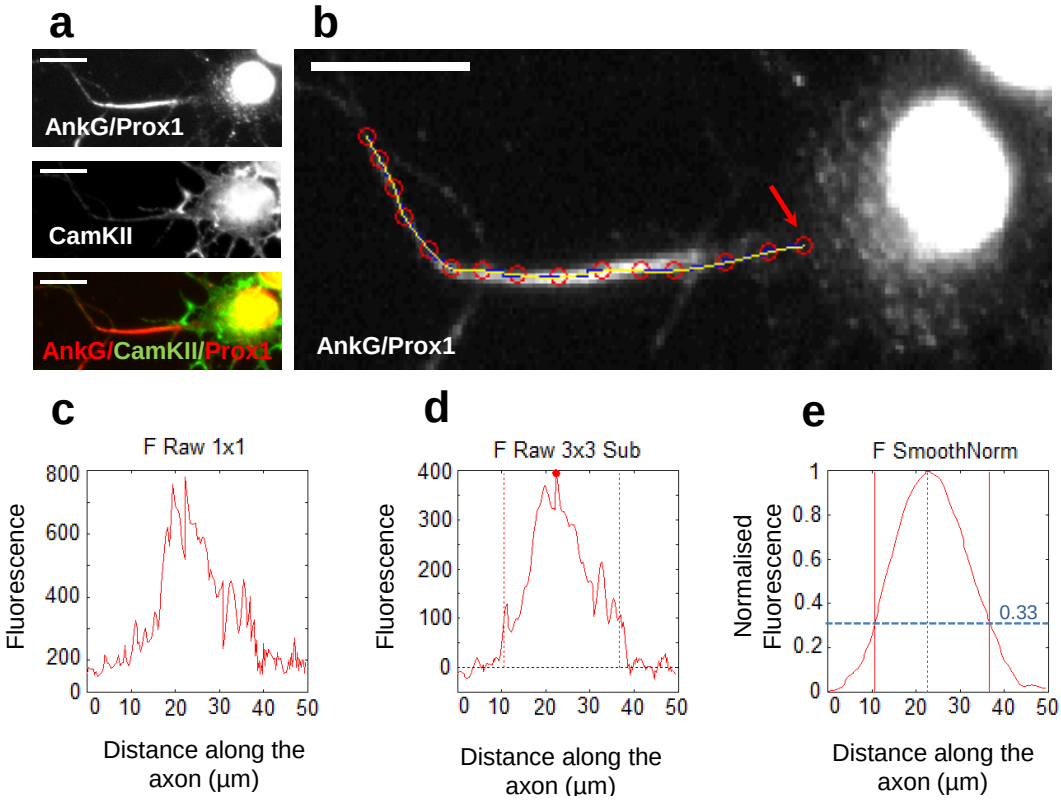

Figure 2.2. Measurement of the AIS properties. (a) An example 7 DIV hippocamapal cell stained for Prox1 (a marker for granule neurons), AnkG (a marker for the AIS) and CamKII (a marker for excitatory cells). (b) The cell from (a) traced along the axon using a custom-written MATLAB program. The beginning of the axon (red arrow) was chosen by eye. Red circles correspond to individual mouse clicks, whereas the yellow line represents an interpolated trace joining the individual points (created by MATLAB). (c) A raw (unbinned) fluorescence profile of the region traced in (b). (d) An average fluorescence profile where the values of fluorescence intensity from (c) were averaged over a 3 x 3 pixel square centred on the pixel through which the tracing was drawn (e) A smoothed fluorescence profile, normalised between 1 (maximum smoothed fluorescence) and 0 (minimum smoothed fluorescence).Dotted red lines indicate the cutoff points where the fluorescence intensity declines to 0.33 (blue dotted line). AIS start and end positions were taken as the positions where the normalised and smoothed profile declined to 33% of the maximum fluorescence (solid red lines). Peak fluorescence was defined as the maximum value of each profile (dotted red line), whereas integrated AIS fluorescence was calculated as the area underneath the profile, inbetween the AIS start and end positions. Scale bar, 10 µm.

binding nucleic acids and emitting a bright red fluorescence upon excitation. To label dead/dying cells, the cultures were incubated with PI-containing culture media (0.6 µg/ml) for 3 minutes at 37°C, followed by a quick rinse in HBS and immediate imaging of PI-stained cultures. Ten consecutive but not overlapping frames were taken along the central axis of the coverslip using 20x air objective on inverted fluorescence microscope (Olympus IX71; 1392 x 1040pixels; 4x4 binning; 1.288µm/pixel). Fluorescence intensity of PI was detected at an excitation of 535 nm and emission of 617 nm. The cells displaying PI fluorescence were counted and compared across the conditions (3 coverslips per condition).

2.7 Calcium imaging of live-labelled neurons

To perform live-labelling of the AIS in hippocampal neurons, 7 DIV coverslips were incubated with neurofascin-186 (NF-186) antibody diluted in cell culture medium (1:100). Following 15-60-minute incubation period, the cells were rinsed in fresh culture media (pre-warmed to 37°C) and briefly (30-60s) incubated in the secondary antibody (Alexa Fluor 568) diluted in culture medium (1:500). Such immunostained neurons were loaded with the Oregon Green BAPTA-1 488 dye (OGB, Invitrogen). To make a working solution of the dye, 2mM of OGB stock (prepared by dissolving 50 µg vial of the dye in 20 µl DMSO) was dissolved in HBS (1:200) together with pluronic F-127 acid (1:200; 20% solution in DMSO, Invitrogen). To stain the cells, coverslips were incubated in the OGB solution for 15-20 minutes at room temperature, light-protected, and rinsed in HBS prior to mounting. Immunostained and OGB-loaded coverslips were mounted in a custom-made chamber equipped with a pair of parallel platinum electrodes placed approximately 5mm apart (Figure 2.2). The cells were maintained in HBS containing 25 µM DL-2-amino-5-phosphonovaleric acid (APV, Sigma), 10 µM 2,3-Dioxo-6-nitro-1,2,3,4-tetrahydrobenzo[*f*]quinoxaline-7-sulfonamide (NBQX, Sigma) and 10 µM SR-95531 (gabazine, Sigma), which block NMDA, AMPA/kainate and $GABA_A$ receptors, respectively (Grubb and Burrone, 2010). All experiments were performed at room temperature (~23°C).

To evoke action potentials, neurons were stimulated with 1 ms, 25-mA current pulses using an SD9 stimulator (Grass Instruments), whose timing was controlled by a TTL signal from the imaging software (Slidebook). Image sequences were captured using an inverted microscope (Olympus IX71) with a CCD camera controlled by Slidebook software. The light source was a xenon-arc lamp (Lambda

LS, Sutter), in which light exposure was regulated by a rapid shutter (Sutter SmartShutter) controlled by a Sutter Instruments lambda 10-3 controller, fitted with a 470 ± 20-nm bandpass excitation filter (Chroma Tech) and suitable neutral density filters. Images were exported as TIFF files and analysed using custom-written MATLAB program. Fluorescence intensity was calculated from square regions of interest (ROIs) drawn across cell bodies.

2.8 Electrophysiology

Whole-cell patch-clamp recordings were obtained from 7 DIV cultures. Cells were maintained in HBS extracellular solution (pH7.4, ~280mOsm, ~23°C) that contained 136mM NaCl, 2.5mM KCl, 10mM HEPES, 10mM D-glucose, 2mM $CaCl_2$, 1.3mM $MgCl_2$, supplemented with 10µM gabazine (Sigma), 10µM NBQX

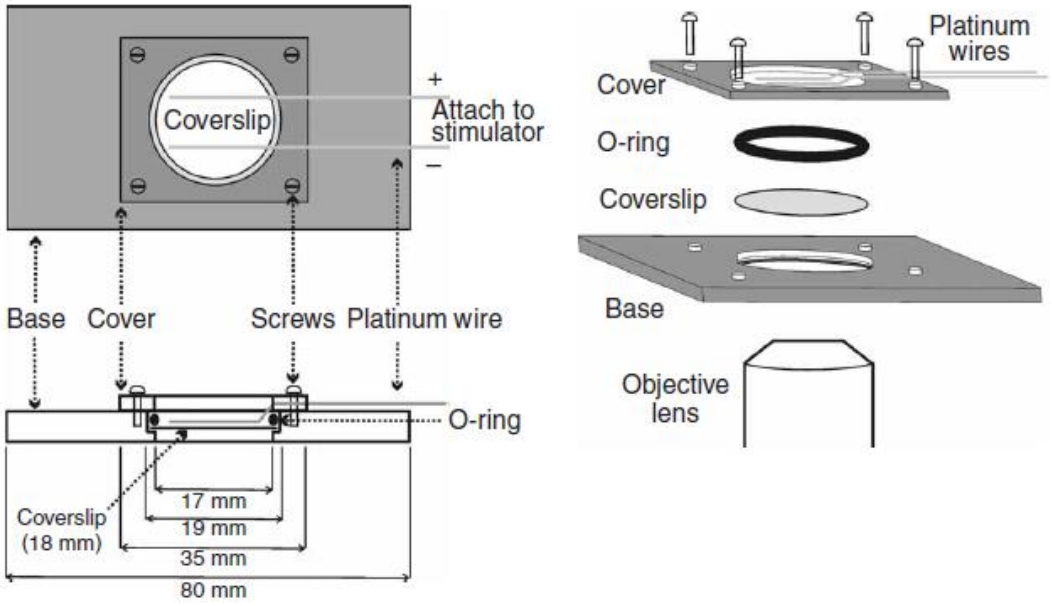

Figure 2.3 Schematic drawing of the stimulating chamber used for calcium imaging (adapted from Burrone and Murthy, 2006).

(Sigma) and 25µM APV (Sigma). Pipettes were pulled from borosilicate glass (outer diameter 1.5mm, inner diameter 1.17mm, Harvard Apparatus) with a tip resistance of 3–7MΩ, and were filled with an internal solution containing: 130mM K-gluconate, 10mM NaCl, 1mM EGTA, 0.133mM $CaCl_2$, 2mM $MgCl_2$, 10mM HEPES, 3.5mM NaATP and 1mM NaGTP. Recordings were made using HEKA EPC10 amplifier coupled to Pulse acquisition software, MPC-200 multi-manipulator controller and

ROE-200 manipulator (Sutter Instrument Company). Fast capacitance was compensated in the on-cell configuration.

Electrophysiological parameters were measured using MATLAB custom-written codes. The resting membrane potential (V_{rest}) was estimated in current clamp mode with zero holding current (I = 0) without adjusting for an estimated liquid junction potential of ~+15 mV. Membrane resistance (R_m) and membrane capacitance (C_m) was estimated from 10 mV hyperpolarisation step. Voltage changes in response to 10 and 500 ms somatic current injections were recorded in current-clamp mode with a holding voltage of around −60 mV, using the basic HBS external and K-gluconate-based internal solutions described above. Action potentials were defined as transient depolarisations crossing the 0 mV line. Current threshold (I_{thresh}) was measured from the lowest current input that reliably evoked at least one spike, and voltage threshold (V_{thresh}) was measured as the voltage at which the first derivative of the recording (dV/dt) exceeded 10x the standard deviation of its baseline.

2.9 Statistical analysis

Statistical analysis was carried out in SPSS (SPSS Inc.) Prior to analysis, data distributions were assessed for normality using Kolmogorov-Smirnov (small sample sizes, n < 50) or Shapiro-Wilk test (larger sample sizes, n > 50). If the samples had a Gaussian distribution, parametric tests (one-way ANOVA, t test, Pearson's r test) were used. If the data set did not follow a normal distribution and had a significant heterogeneity of variance, non-parametric tests (Kruskal-Wallis ANOVA and Mann-Whitney U-test) were used. All tests were two-tailed. Levels of significance were set at 0.05. Bonferroni correction was used when multiple comparisons were made. The variability (SD and SEM) in % of AIS-positive cells in different conditions (chapter 4) was assessed using bootstrapping procedure in MATLAB. Descriptive statistics are reported as mean ± SEM unless specified otherwise.

Chapter 3

The role of activity on dendritic and axonal morphology

3.1 Introduction

Electrical activity plays a key role in regulation of neural development (Spitzer, 2006). One of the many developmental processes influenced by electrical activity is the formation of dendritic and axonal domains, the unique arrangement of which ultimately determines the morphological features of the cell. Numerous studies have been published that illustrate the effects of neuronal activity on axonal and dendritic size and shape. The overall effect of activity on neuronal morphology is far from straightforward as it is neurite-specific and strongly dependent on the model system, developmental time point, brain region and the type of activity manipulation. For example, electrical stimulation restricts the axon growth in sensory neurons (Cohan and Kater, 1987; Fields et al., 1990; Diefenbach et al., 2000; Enes et al., 2010) but it has no effect on the outgrowth of spinal neurons (Ming et al., 2001). In hippocampal neurons, increased levels activity have been shown to induce growth cone stalling and reduction in axonal length (Mattson et al., 1988, Chang and DeCamilli, 2001; Tashiro et al., 2003; Ibarretxe et al. 2007), but also promote dendritic outgrowth and branching (Yu and Malenka, 2003; Wayman et al., 2006; Tan et al., 2010; Ma et al., 2011).

Morphological characteristics of axons and dendrites determine not only the connectivity of cells within the neural circuit, but also profoundly influence their electrophysiological properties. The geometry of dendritic trees have been shown to affect neuronal firing patterns, such that altering dendritic size or topology in model neurons leads to change in firing patterns from tonic to bursting (Krichmar et al, 2002; Van Ooyen et al., 2002). Therefore, understanding how activity affects neuronal morphology may ultimately help to elucidate how complex neuronal connectivity is established in development and how it shapes neuronal function in the mature brain.

In this chapter I investigate the role of chronic (16-hour) activity on dendritic and axonal morphology of 4 DIV cultured hippocampal neurons. Activity was induced with either high levels of extracellular KCl, to globally depolarise the neurons, or with optogenetic photostimulation that allowed for delivery of neuron-specific, temporally regulated depolarising stimuli. To assess depolarisation-induced effect, I measured a number of metric and topological variables characterising neuronal morphology. I begin by briefly describing neuronal types in our culture system, followed by an assessment of effectiveness of the KCl treatment and optogenetic stimulation with regards to inducing neuronal depolarisation. Subsequently, I examine the morphological properties of the neurons in response to chronic depolarisation induced by the two methods mentioned above.

3.2 Cultured hippocampal neurons

The role of activity on morphology of a neuron was investigated using dissociated hippocampal cultures. Hippocampal cultures have been extensively used to study axonal and dendritic outgrowth and morphology (Smith-Swintosky et al., 2006; Wayman et al., 2006; Nielsen et al., 2009; Yamamoto et al., 2012). Due to the two-dimensional arrangement of the cells and relative ease of transfection with fluorescent markers, cultured hippocampal cells are easy to visualise and manipulate, providing a suitable model system to explore the intricate branching patterns of dendritic and axonal arbours. In hippocampal cultures dendritic and axonal domains are largely established by the end of first week *in vitro* (Goslin et al., 1988). To examine activity-dependent changes in neural morphology, I chose a developmental time point when (1) the majority of cells have already broken the symmetry and established separate dendritic and axonal domains, but (2) before an extensive dendritic outgrowth took place, as it would make the analysis too complex. In our culture system, this occurs around 3-4 DIV.

Our hippocampal cultures consist of a heterogeneous population of neurons, including many classes of excitatory and inhibitory cells. The largest proportion of neurons is excitatory (70-90%) and consists mostly of two cell types: granule cells of the dentate gyrus and pyramidal cells of the CA1 and CA3 areas. Inhibitory neurons, of which basket cells are the most common, are much less widespread and constitute no more than 30% of all the cells. To reduce the variability within the hippocampal population, I have focused on a single cell type, the granule cells. Granule cells can be specifically labelled with an antibody against prox1, a

transcription factor expressed in all granule neurons (Williams et al., 2011). To obtain a more complete picture of the role of activity on cell morphology in hippocampal cultures, I have also analysed neurons immunonegative for prox1. Hence, the analysed population of cells consisted of two pools of neurons: prox1-positive (granule cells) and prox1-negative (mostly pyramidal cells and some GABAergic interneurons).

To visualise neuronal morphology, I transfected the cells with channelrhodopsin-2 fused to YFP protein (ChR2-YFP) driven by a pan-neuronal synapsin promoter (Fletcher et al., 1991). ChR2 is a light-sensitive cation channel and it is one of the most-commonly used tools in optogenetics (Nagel et al., 2003). In this chapter, ChR2-YFP has been used both to control neuronal excitability and as a marker of neuronal morphology. Neuron-specific expression of the ChR2-YFP construct reliably labelled neuronal membranes resulting in a clear outline of dendritic and axonal trees. Axons and dendrites were distinguished primarily by morphological criteria. Axons were the longest processes that were relatively thin and of uniform diameter, whereas dendrites were shorter, thicker and highly tapered. In some cases the distinction was aided by immunostaining for axonal protein tau, however this method was not used routinely as high density of axonal arborisation in the culture did not permit reliable identification of individual axons.

Figure 3.1 illustrates ChR2-YFP-transfected neurons from rat hippocampal cultures at 4 days *in vitro* (DIV). Cells immunopositive for prox1 (a, c) correspond to dentate granule cells, whereas cells lacking prox1 immunofluorescence (b, d) most likely represent pyramidal cells and interneurons. Granule neurons tend to be relatively small with a round or oval soma and long, often conical-shaped, apical dendrites (Amaral et al., 2007). Some immature granule neurons may also transiently display basal dendrites, which disappear as the cell matures (Jones et al., 2003). Pyramidal cells have characteristic triangular somata, a large apical dendrite and multiple highly-branched basal dendrites (Amaral et al., 1978; Figure 3.1b). GABAergic cells, on the other hand, are relatively unbranched and have long thin dendrites radially arranged around the cell body (Benson et al. 1994, Figure 3.1c).

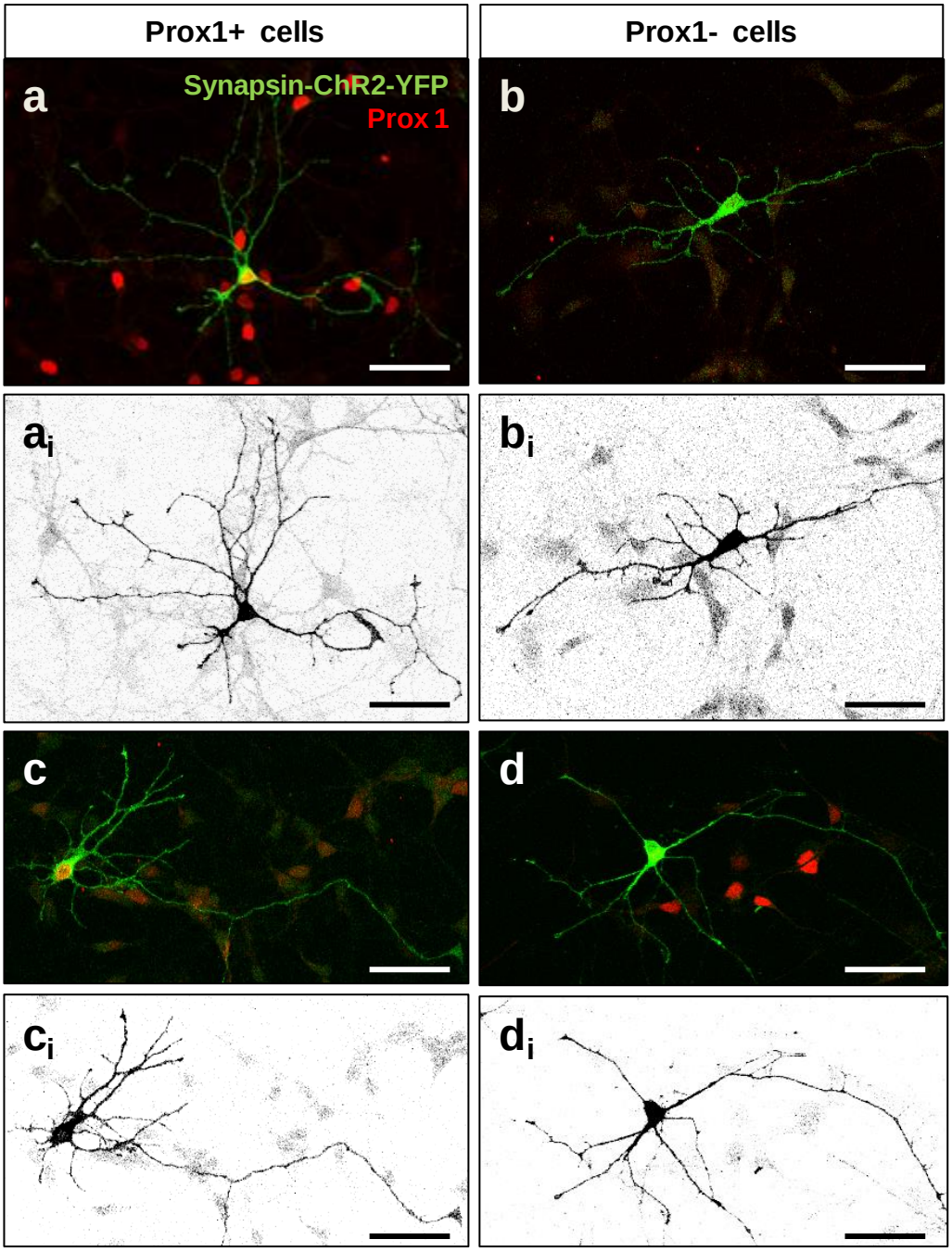

Figure 3.1 Dendritic morphology of prox1-positive and prox1-negative neurons in dissociated hippocampal cultures at 4 DIV (a, b, c, d) Fluorescence images of cells transfected with ChR2-YFP (green) and immunostained for prox1 (red). (a_i, b_i, c_i, d_i) Inverted images of a, b, c and d. Cells a and c are prox1-positive granule neurons, whereas cells b and d are prox1-negative neurons, displaying the morphological characteristic of pyramidal and GABAergic neurons, respectively. Scale bar, 40µm.

3.3 Effectiveness of KCl treatment and optogenetic stimulation

Activity-dependent changes in neuronal morphology were investigated by depolarising the cultures with either (1) high levels of KCl or (2) optogenetic photostimulation of ChR2-transfected cells. To validate that these two techniques were capable of sufficiently depolarising the neurons, I examined the acute effects of these treatments on cellular physiology. Specifically, I monitored Ca^{2+} transients in response to increasing extracellular levels of KCl (20mM and 50mM) with organic Ca^{2+}-sensitive dye and recorded membrane voltage depolarisations in response to photostimulation using electrophysiology. Concentrations of KCl ranging from 10 to 50mM KCl have been previously used to induce activity-dependent dendrite growth in both cortical (Redmont et al. 2002) and hippocampal (Tan et al. 2010; Yu and Malenka, 2003, Ma et al., 2011) neurons *in vitro*.

3.3.1 KCl treatment triggers Ca^{2+} transients

The maturation of neuronal excitability is associated with differential expression of voltage- and ligand-gated ion channels in development. Young immature neurons express a different configuration of these channels than adult mature cells, which correlates with their distinct electrophysiological properties (Moody and Bosma, 2005). This transition between mature and immature electrical states characteristic of *in vivo* systems is also reproduced in hippocampal cells *in vitro* (Liu et al., 1996). At 4 DIV dissociated hippocampal cells do not yet express a full complement of voltage-gated Na^+ and K^+ channels, hence they are unable to fire action potentials. Despite the lack of significant Na^+ and K^+ conductance, immature hippocampal cells contain a large number of voltage gated Ca^{2+} channels, especially of the L-type, which are thought to play a vital role in early development of the hippocampus (Bray and Mynlieff, 2009; Kramer et al., 2012). In immature hippocampal cells, voltage-gated Ca^{2+} channels are the principal channels that open in response to depolarisation (Wayman et al., 2006). Therefore, to investigate the effectiveness of KCl treatment, I monitored intracellular levels of Ca^{2+} while adding increasing concentrations of KCl to 4 DIV cultured hippocampal neurons.

Previous work from our lab showed that the application of high levels of extracellular KCl to neuronal cultures depolarised the resting membrane potential by about 1mV for every 1mM of KCl added (Grubb and Burrone, 2010). To further verify that our KCl solution can produce a detectable change in membrane potential and open voltage-gated Ca^{2+} channels, I loaded the cells with a Ca^{2+}-sensitive dye (Oregon

Green BAPTA-1) and monitored Ca^{2+} influx following the addition of 15 mM KCl to the culture media. Our culture media already contained 5mM KCl and application of an additional 15mM to the bath markedly raised the resting levels of Ca^{2+} in the cells (Fig. 3.2a). Adding a further 30 mM KCl to take it to a final concentration of 50 mM, increased Ca^{2+} levels even further, although to a lesser extent than 20mM KCl, indicating a non-linearity of the effect. Following the initial rise, the fluorescence values of the OGB slowly but progressively decreased, suggesting Ca^{2+} sequestration by intracellular proteins and organelles, in addition to active Ca^{2+} extrusion by plasma membrane Ca^{2+} pumps. Despite this slight buffering, Ca^{2+} levels remained elevated throughout the duration of the imaging experiment. Overall, substantial Ca^{2+} flux in response to high levels of KCl shows that KCl treatment was an effective means to elevate neuronal activity.

3.3.2 Optogenetic photostimulation induces transient membrane depolarisation

Optogenetics controls neuronal activity by expressing light-gated channels in neurons and then using light to control the behaviour of the cell (Hausser and Smith, 2007; Deisseroth, 2011). ChR2 is one such light-gated ion channels, which opens in response to blue light, allowing mono-and bivalent cations (mostly Na^{+} and Ca^{2+}) to enter the cell down their electrochemical gradients and consequently depolarise the neuron.

ChR2-YFP-transfected neurons were patched under the whole-cell configuration. In current-clamp recordings, the membrane potential was measured as the cells were stimulated with brief, 20ms, pulses of blue light (Figure 3.2b). The light stimulus triggered a depolarisation of the membrane potential (V_m), which was mirrored by a simultaneous increase in cell conductance (I) when in voltage clamp configuration. Overall, this indicates that the optogenetic technique applied here was effective and resulted in the depolarisation of neuronal membranes in young neurons, which are yet incapable of firing action potentials As expected, no action potential firing was observed with this photo-stimulation approach.

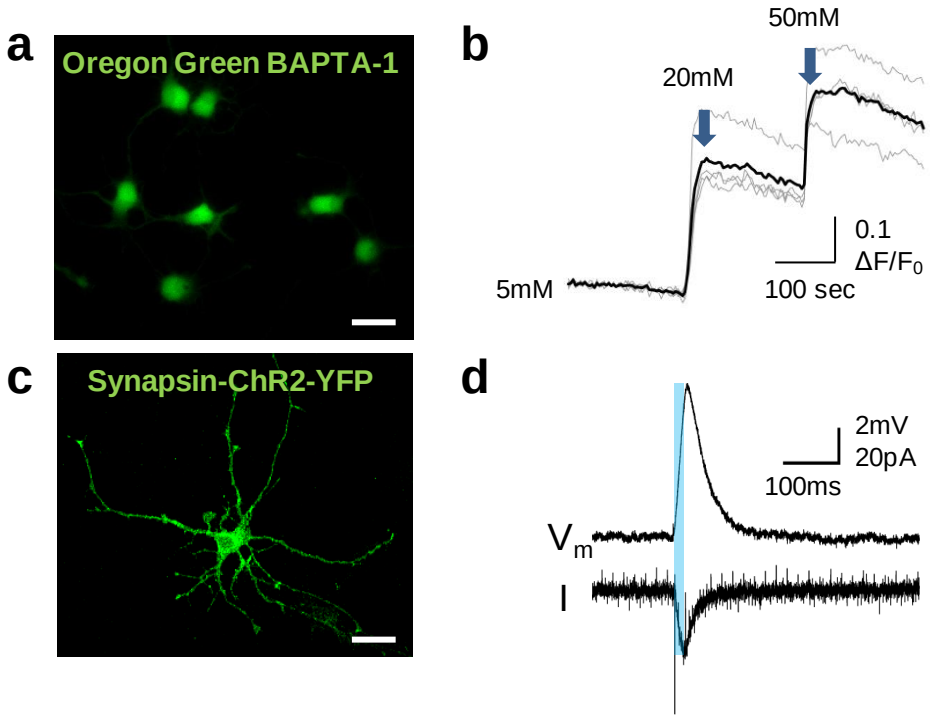

Figure 3.2 Cellular effects of KCl treatment and optogenetic stimulation in dissociated hippocampal neurons at 4 DIV (a) Hippocampal cells loaded with Oregon Green BAPTA-1 (OGB). (b) A trace of fluorescence change ($\Delta F/F_0$) of OGB-loaded cells in response to addition of 20 and 50 mM KCl (arrows). Black trace denotes a mean change, whereas grey traces show responses of individual cells uncorrected for bleaching. Baseline, 5mM KCl. Depolarisation following bath application of KCl rapidly triggered a large increase in the concentration of intracellular [Ca^{2+}] (c) image of a hippocampal neuron expressing ChR2-YFP. (d) Voltage (V_m) and current (I) traces from a ChR2-transfected neuron photo-stimulated with a 20ms flash of blue light (blue bar). Scale bar, 20µm.

3.4 Neuronal morphology after KCl treatment

Having established that KCl treatment and optogenetic stimulation were suitable for modulating activity in our culture system, I proceeded to investigate the role of activity on gross morphology of young hippocampal neurons. First, I examined the role of KCl-induced depolarisation by treating neurons with two concentrations of KCl, 20mM and 50mM, for 16 hours between 3 and 4 DIV (Figure 3.3a). Similar concentrations of KCl have been previously used to induce activity-dependent changes in neuronal morphology in cultured cortical and hippocampal cells (Redmond et al., 2002; Wayman et al., 2006). Following 16 hours of depolarisation, the cells were fixed, immunostained with the antibody against prox1 and imaged. Neurons expressing ChR2-YFP were used to image neuronal morphology, as the channel is localised to all neuronal membranes and labels both dendrites and axons (Figure 3.1 and 3.2b). The imaged cells were traced along their dendritic and axonal compartments and processed to obtain a number of metric and topological measures of neuronal morphology (Figure 3.3b).

3.5.1 Metric measures of dendritic and axonal arborisations

First, I examined whether chronic KCl treatment affected the total size of dendritic and axonal arbours (Figure 3.3). KCl treatment significantly altered the morphology of the neurons, however the effect was process and cell-type specific. In prox1-positive cells KCl treatment significantly decreased total dendritic length ($P = 0.01$, one-way ANOVA with LSD posthoc test, $n_{Control} = 76$, $n_{20mM\ KCl} = 53$, $n_{50mM\ KCl} = 75$; 3 independent experiments) but, interestingly, not axonal length nor the total length of all processes (axons plus dendrites). The absolute length of the dendritic arbor was on average ~ 17% shorter in KCl-treated cultures (342.15 ± 18.57 µm and 341.38 ± 19.84 µm in 20mM KCl-treated and 50mM KCl-treated cultures), than in control cells (414.62 ± 20.64 µm). In prox1-negative neurons, on the other hand, KCl had no effect on dendritic length, however it did significantly reduce axonal length ($P = 0.008$) and the total length of all neurites ($P = 0.019$, one-way ANOVA with the LSD posthoc test, $n_{Control} = 41$ control cells, $n_{20mM\ KCl} = 48$, $n_{50mM\ KCl} = 50$). The axons of high-KCl-treated neurons were on average 36% shorter (466.84 ± 44.48 µm and 511.96 ± 55.13 µm in 20mM KCl and 50mM KCl-treated cells, respectively) than untreated control cells (735.88 ± 88.96 µm).

3.5.2 Topological measures of dendritic arborisations

Next, I measured topological characteristics of dendritic arbours. Topological variables are concerned with the connectivity pattern of dendritic segments and thus help estimate the shape and complexity of the dendritic tree. First, I quantified the number of soma branches, number of terminal tips, tip path distance and the straightness of dendritic branches (Figure 3.4a). Tip path distance denotes path length from dendritic tips to the soma along the dendrite, whereas straightness was defined as the tip path length divided by radial ('straight-line') distance of the dendritic tip from the soma. None of the measures were significantly altered by a KCl treatment in prox1-negative neurons. In prox1-positive cells, on the other hand, 16-hour depolarisation induced significant changes in tip path distance ($P = 0.025$, one-way ANOVA, $n_{Control} = 96$, $n_{20mM\ KCl} = 68$, $n_{50mM\ KCl} = 76$) and in straightness of the dendrites ($P = 0.012$, one-way ANOVA, $n_{Control} = 96$, $n_{20mM\ KCl} = 68$, $n_{50mM\ KCl} = 76$). Tip path distance was reduced from 51.10 ± 1.66 µm in controls to 43.99 ± 1.55 µm and 45.18 ± 2.71 µm in 20mM and 50mM-KCl-treated cells, respectively. This indicates that dendritic tips were on average closer to the cell body in high-KCl-treated cultures, which is consistent with a reduction in the overall dendritic length of these neurons. Apart from decreased tip path length, dendrites of chronically depolarised cells were significantly straighter but only when depolarised with 20mM KCl. The number of terminal tips or number of soma branches appeared to be similar in control and high-KCl-treated cells.

To further analyse the shape of the dendritic arbour, I measured maximal Sholl distance, number of bifurcations per mm, branch order and tree asymmetry index. Sholl distance is a modified version of a Sholl analysis, a commonly used measure of the extent and complexity of a dendritic tree. In Sholl analysis a set of concentric circles is overlayed over the centre of the cell and the number of dendritic intersections is counted at each circle. The number of dendritic intersections is then plotted as a function of a distance from the soma. In this chapter, instead of a full Sholl analysis I specifically measured maximal Sholl distance, which is better suited for statistical analysis due to its scalar properties (Scorcioni et al., 2004). To quantify orientation differences and the complexity of dendritic branching, I measured the asymmetry index (Van Pelt et al., 1992), which is a topological measure of a dendritic tree based on the number or connectivity patterns of the tree segments. According to this measure, 0 indicates a perfectly symmetrical tree and 1 is a perfectly asymmetrical tree.

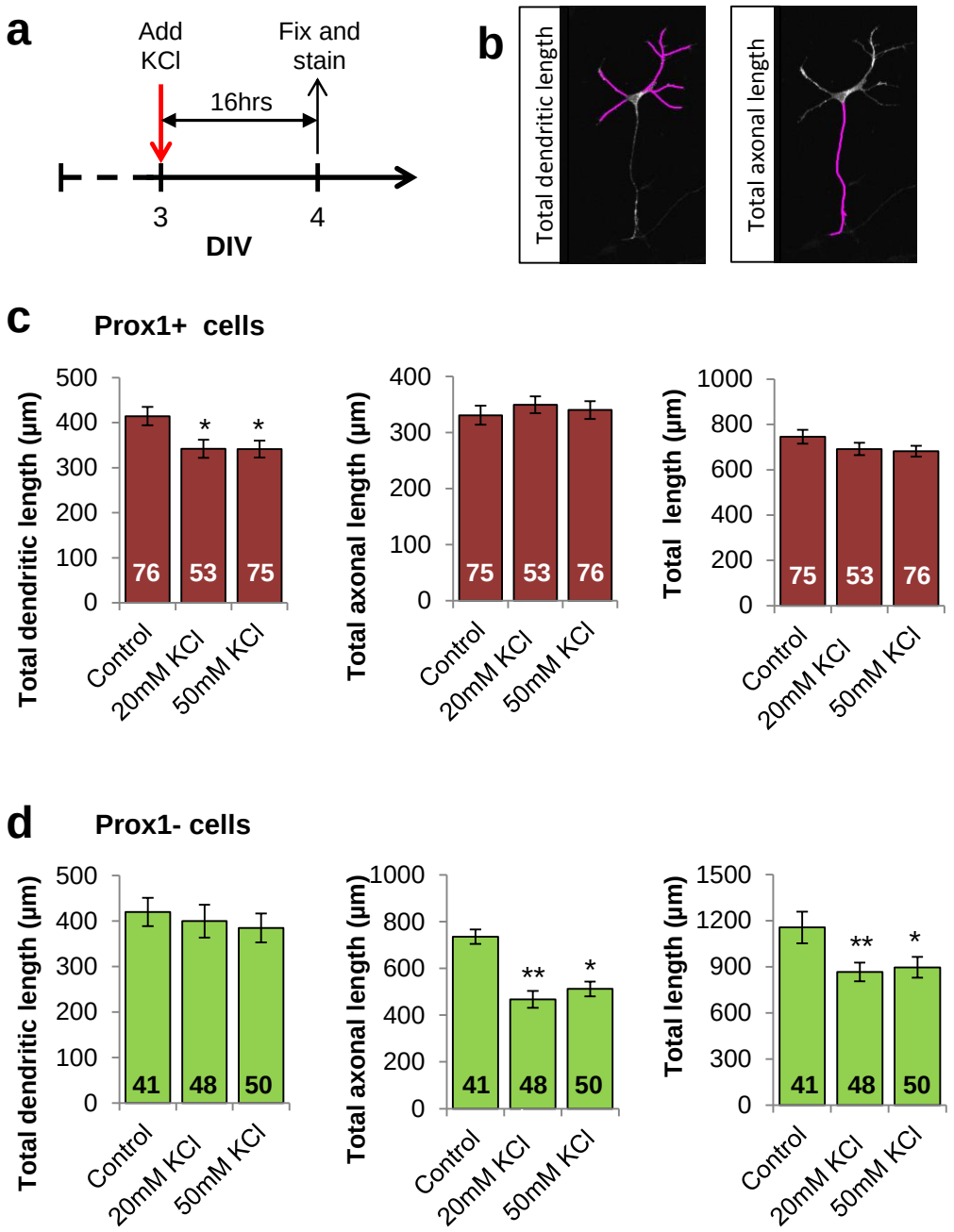

Figure 3.3 Dendritic and axonal lengths after chronic depolarisation with KCl
(a) Schematic of the experiment. KCl (20mM or 50mM) was added to ChR2-YFP-transfected neurons on day 3 and left in the culture media for 16 hrs, following which the cells were fixed and immunostained for prox1. (b) Example images showing dendritic and axonal traces. (c, d) Graphs showing total dendritic length (left), total axonal length (middle) and total length of prox1-positive cells (c, red bars) and prox1-negative cells (d, green bars). Numbers within bars indicate number of cells within each condition. Significance asterisks above the error bars indicate a significant difference relative to control condition: * < 0.05, ** < 0.01, one-way ANOVA followed by LSD test. Error bars, SEM.

Despite trends indicating diminished complexity and greater symmetry of dendritic arbours in KCl-treated cultures, there were no statistically significant differences in tree asymmetry index, bifurcations per mm or max sholl distance. However, mean branch order of prox1-negative cells treated with 50mM KCl was significantly lower than in control cultures ($P = 0.019$, one-way ANOVA followed by LSD test, $n_{Control} = 96$, $n_{20mM\ KCl} = 68$, $n_{50mM\ KCl} = 76$), suggesting lower complexity of the dendritic arbours of chronically depolarised cells. Overall, exposure to KCl for 16-hours, apart from moderately decreasing dendritic length, did not appear to dramatically alter the shape or size of the dendritic tree.

3.6 Neuronal morphology after optogenetic stimulation

KCl treatment is a consistent and straightforward method of depolarising a neuron, however it does not provide a temporal control of the depolarising input. Previous studies have shown that the pattern of membrane depolarisation is important for induction of activity-dependent effects (Sur et al., 1999; Wu et al., 2001, Kastanenka and Landmesser, 2010; Crisp et at., 2011). In addition, KCl treatment does not permit spatial control of the depolarising stimulus and thus it is not clear whether the depolarisation-induced effect is cell-autonomous or relies on signals from the neighbouring cells. To overcome these limitations I used optogenetic stimulation to depolarise the cells. Optogenetics provides a precise temporal control of the stimulus in a targeted population of neurons (Deisseroth, 2011). To use this method, I sparsely transfected 1 DIV hippocampal cultures with a ChR2-YFP plasmid driven by a pan-neuronal synapsin promoter. The transfected cultures were optogenetically stimulated for 16 hrs between 3 and 4 DIV, analogously to the KCl experiment.

I have tested several stimulation paradigms, varying the duration of the light stimulus and the intervals between the stimuli. Stimulation paradigms were created by taking into account activity patterns recorded from *in vivo* and *in vitro* systems (Crépel *et al*. 2007; Leinekugel *et al*., 2002). Initially, I tested 50ms and 250ms light pulses delivered every 0.5, 1, 5 and 10 seconds for 12 hours. These light stimulation patterns appeared to be too harsh for the cells at this stage and negatively affected cell viability. Therefore I decided to shorten the duration of the pulse to 2 and 20 ms, keeping the same intervals between the pulses (every 10, 30 and 60s). After 16 hours of depolarisation, the cells were fixed, immunostained with

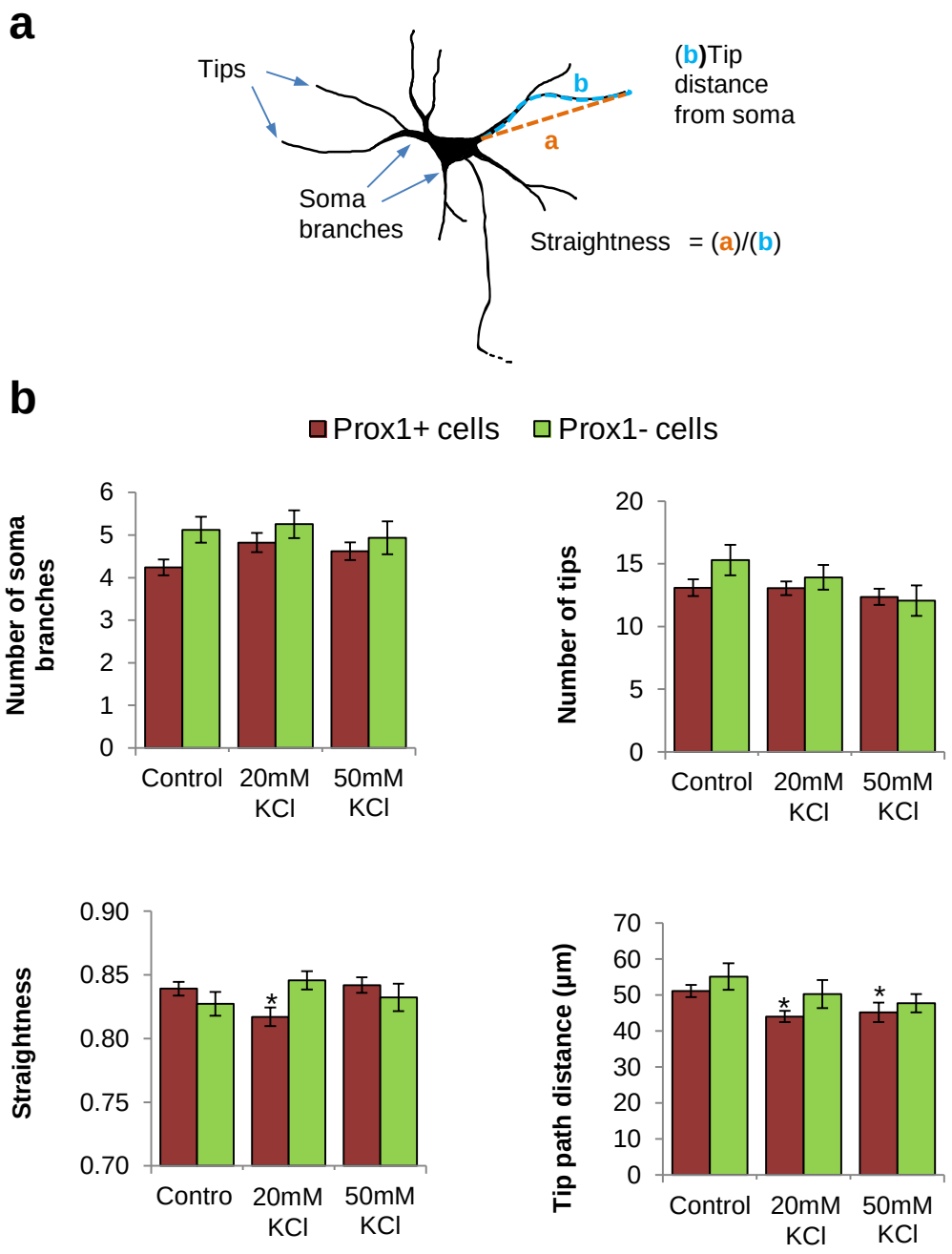

Figure 3.4 Morphometric analysis of dendritic trees of neurons chronically depolarised with KCl (a) A schematic illustrating the measures used in the analysis. (b) Graphs showing number of soma branches, number of tips, straightness and distance to soma in 20mM and 50mM KCl-treated prox1-positive (red) and prox1-negative neurons (green). Error bars, SEM. Prox-positive cells**:** n_C = 71, $n_{20mM\ KCl}$ = 53, $n_{50mM\ KCl}$ = 75; Prox1-negative cells: n_C = 41, $n_{20mM\ KCl}$ = 48, $n_{50mM\ KCl}$ = 50, from three separate cultures.

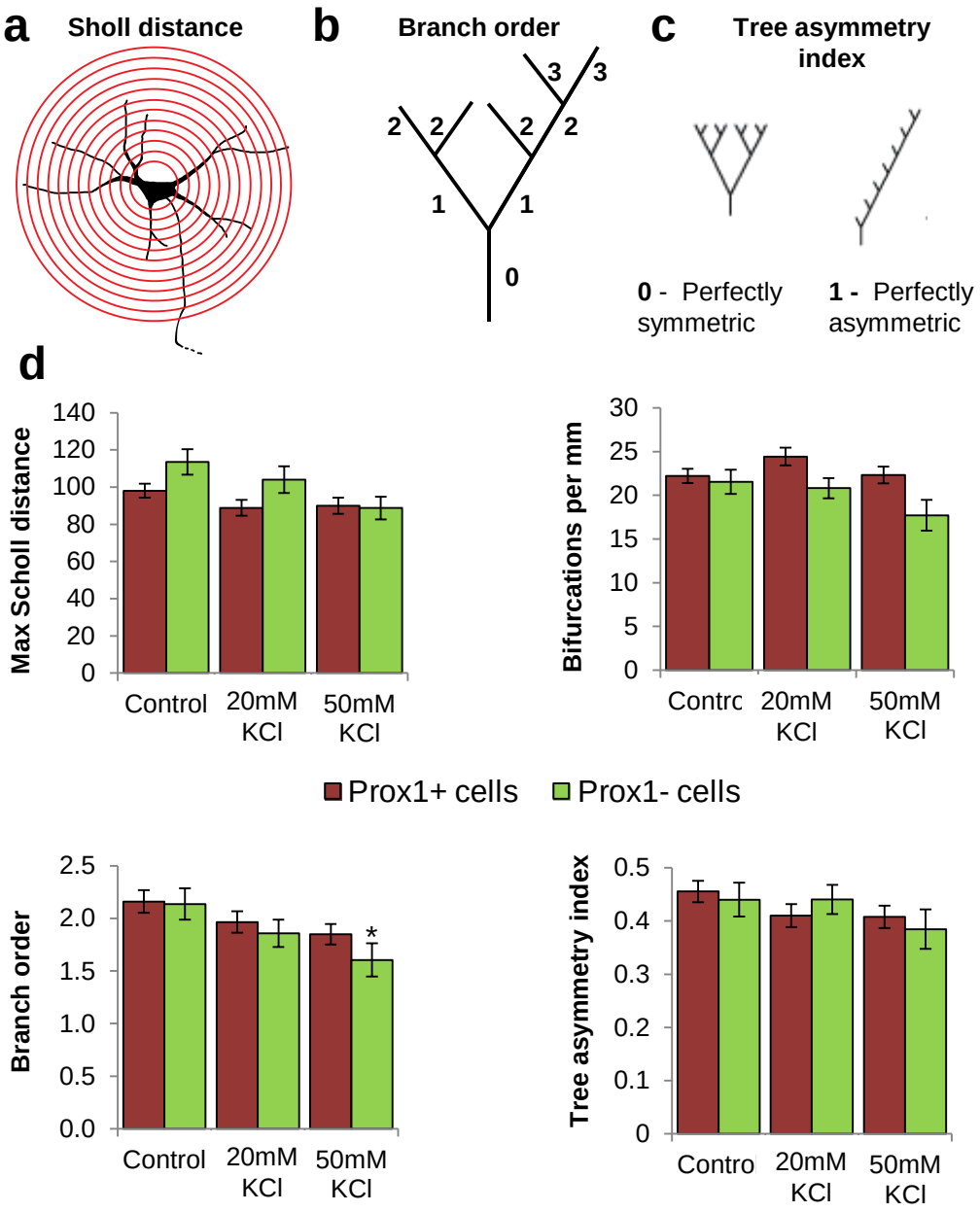

Figure 3.5 Morphometric analysis of dendritic trees of neurons chronically depolarised with KCl, cont. (a) Scholl distance denotes the maximal distance between the soma and the furthest compartment as delineated by a series of concentric circles around the soma (b). Branch order denotes maximal number of bifurcations between the soma and terminal tips. Branches stemming directly from the soma are labelled 0. (c) Tree asymmetry index, based on branching patterns from each bifurcation. 0 is perfectly symmetric, 1 is perfectly asymmetric. (d) Graphs showing max sholl distance, bifurcations per mm, mean branch order and tree asymmetry index of prox1-positive (red) and prox1-negative (green) neurons after they were treated with 20 or 50mM KCl. Error bars, SEM. *, P = 0.019, one-way ANOVA with LSD post hoc test. Error bars, SEM. Cell numbers as in Figure 3.4.

anti-prox1 antibody and imaged. The imaged cells were traced along their dendritic and axonal trees and processed with tracing software (Figure 3.3b). To characterise neuronal morphology I measured the same metric and topological variables as in the KCl experiments.

3.6.1 Total length of dendritic and axonal arborisations

First, I examined whether optogenetic photostimulation alters the total length of dendritic and axonal trees of prox1-positive and prox1-negative neurons. In prox1-positive cells, in agreement with KCl experiments, a 20ms light pulse delivered every 10, 30 or 60 seconds, led to a significant decrease in dendritic length compared to unstimulated neurons ($P = 0.019$, two-way ANOVA, $n_{10s}= 17$, $n_{30s} = 69$, $n_{60s} = 48$). Interestingly, 2ms pulses were not sufficient to induce a change in dendritic length, suggesting they did not provide sufficient amount of depolarisation. There was no significant difference in the total axonal length or the summed length of all processes between control and photostimulated cultures. This result is consistent with the changes seen after KCl treatment and suggests that activity-dependent decrease in dendritic outgrowth in prox1-positve cell is a cell-autonomous process. In prox1-negative neurons, the results were less consistent. In contrast to KCl-treated experiments, the most pronounced effect was seen on dendritic length, where three stimulated conditions (2ms 60s; 20ms 10s; 20ms 30s) had significantly reduced dendritic lengths ($P = 0.01$, two-way ANOVA, $n_{2ms60s}= 41$, $n_{20ms10s} = 24$, $n_{20ms30s} = 61$). Axonal length were significantly reduced only in one condition (the highest stimulation condition, 20ms 10s), where axons shortened by about 42% relative to the control condition, from 735.88 ± 88.96 µm to 424.86 ± 64.32 µm. The change in axonal length also significantly affected the total length of all neurites ($P = 0.024$, two-way ANOVA).

Overall, chronic patterned stimulation delivered with optogenetics differentially affected prox1-positive and prox1-negative neurons in a stimulation-pattern-dependent manner. Stimulation patterns employing longer, 20ms, light stimulus led to a significant decrease in overall dendritic length in prox1-positive cells, without affecting axonal length. These results are in agreement with the observations made using KCl, suggesting that membrane depolarization is an important parameter in controlling dendritic arbour size in granule cells. The results for prox1-negative cells are less consistent and do not always logically follow from KCl treatment to photostimulation. Although there are a number of reasons for this (see discussion), it is likely that the heterogeneity in this neuronal population adds noise to the

measurements and therefore complicates the analysis. Next, I examined whether the optogenetic stimulation significantly altered the shape of the dendritic tree.

3.6.2 Topography of dendritic arbours

Measurements of the topology of photostimulated neurons were carried as above (Figure 3.4 and 3.5). For both prox1-positive and prox1-negative cells, I detected no significant difference in the number of tips, number of soma branches, straightness, max sholl distance, bifurcations per mm, branch order or tree asymmetry ($P > 0.05$, one-way ANOVA). The only significant difference between the conditions was observed for the tip path distance (Figure 3.7, bottom right), which was significantly shorter in depolarised neurons when stimulated with 20ms pulses delivered every 10s ($P = 0.003$, one-way ANOVA, $n_{Control} = 49$; $n_{Stim} = 19$). Other stimulation paradigms, however, did not produce a significant change in this variable.

In summary, depolarisation induced with optogenetic methods did not lead to any major alterations in dendritic shape, however it significantly altered the size of dendritic and axonal arbours. Interestingly, the reduction in size of dendritic trees of prox1-positive neurons (granule cells) was observed both after KCl treatment and optogenetic stimulation, whereas in prox1-negative neurons, this reduction was observed only after optogenetic stimulation, suggesting different mechanisms of activity-dependent dendrite growth in these two groups of cells.

3.7 Discussion

In this chapter I investigated the effects of chronic depolarisation on morphology of cultured hippocampal neurons. Depolarisation was induced by either addition of high extracellular concentration of KCl or optogenetic stimulation of ChR2-transfected cells. Chronic depolarisation by either of these techniques led to a significant, cell-autonomous, alteration of the total length of axonal and dendritic trees, however the shape of the dendritic arborisations was largely unaffected. The specific effect of the depolarisation was method-, neuronal-process- and cell-type-specific. In prox1-positive neurons (dentate granule cells), chronic depolarisation with either KCl or optogenetics, led to a reduced size of dendritic but not axonal arbours. In prox1-neurons, on the other hand, the specific effect was dependent on the method used. KCl treatment considerably shortened the

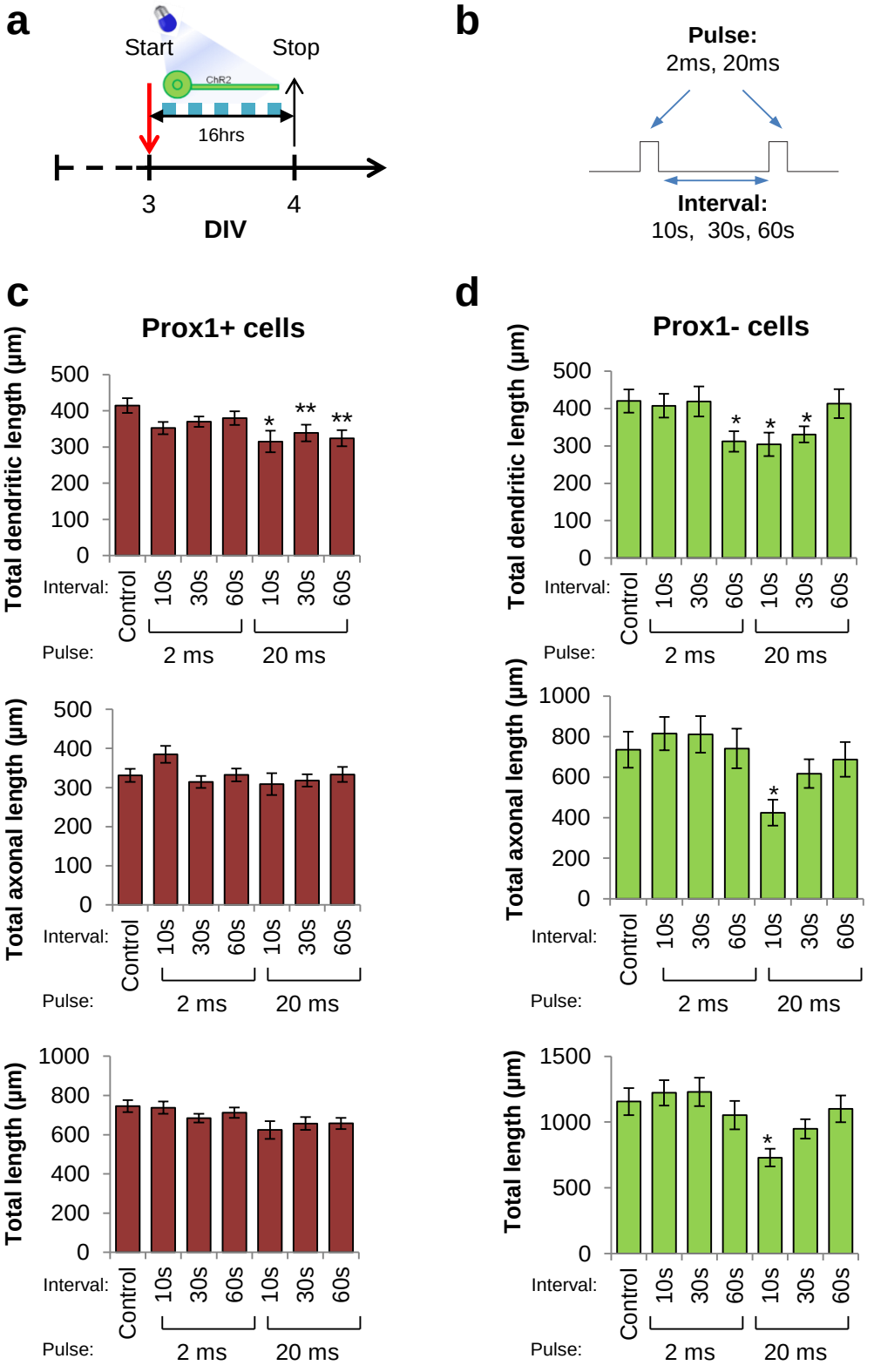

Figure 3.6 Dendritic and axonal lengths of ChR2-transfected neurons stimulated with optogenetics (a) Schematic of the optogenetics experiment. ChR2-transected neurons were photostimulated with blue light (blue rectangles) for 16 hours, from DIV3 (red arrow) to DIV4 (black arrow). (b) Photostimulation paradigms. 2 or 20ms light pulses were delivered every 10, 30 or 60 seconds. Significance: * < 0.05, ** < 0.01, one-way ANOVA followed by the LSD test. Error bars, SEM. Number of neurons as in figure 3.7.

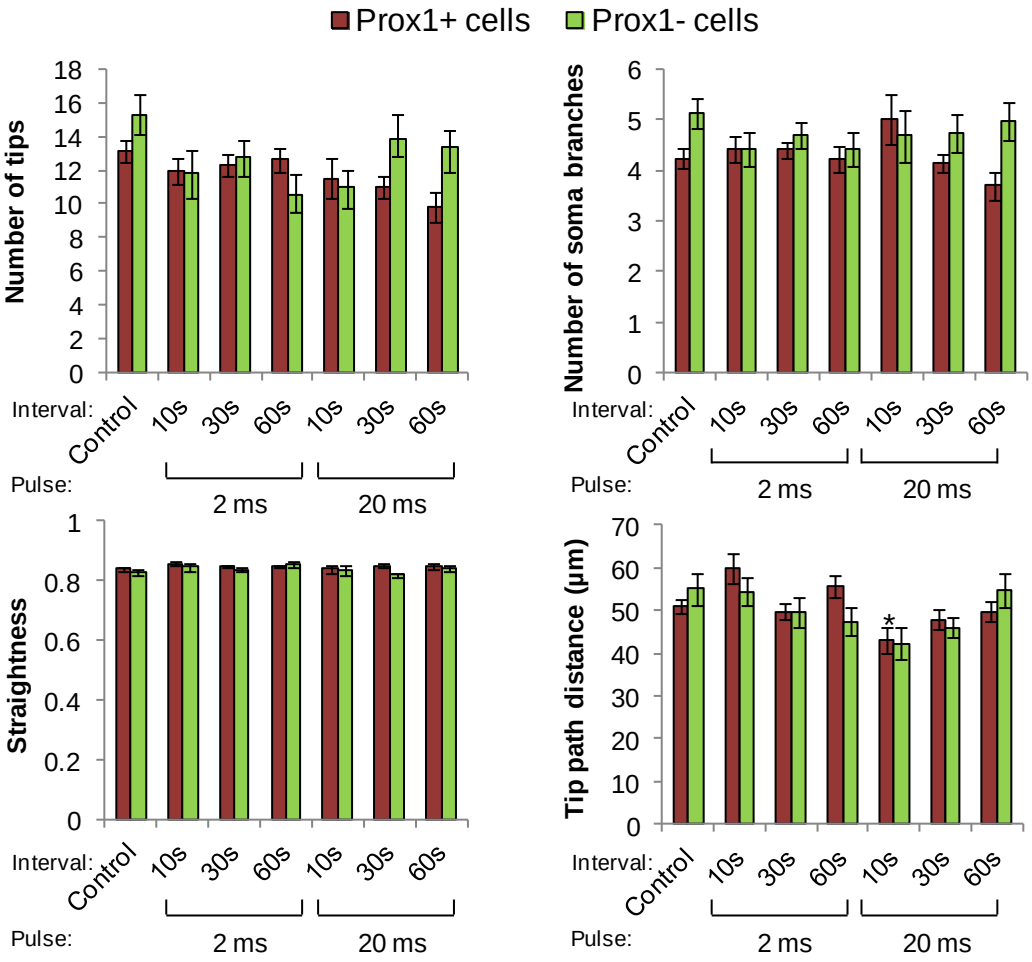

Figure 3.7 Morphometric analysis of dendritic morphology of optogenetically stimulated neurons. Graphs showing number of soma branches, number of tips, straightness and distance to soma in 15mM and 50mM KCl-treated prox1-positive (red) and prox1-negative neurons (green) optogenetically stimulated with different patterns of light pulse. Significance: * < 0.05, one-way ANOVA followed by the LSD test. Prox1-positive neurons: $n_{Control}$ = 97, n_{2ms10s} = 41, n_{2ms30s} = 77; n_{2ms60s} = 65, $n_{20ms10s}$ = 17, $n_{20ms30s}$ = 64, $n_{20ms60s}$ = 39. Prox1-negative neurons: $n_{Control}$ = 49, n_{2ms10s} = 26, n_{2ms30s} = 44; n_{2ms60s} = 36, $n_{20ms10s}$ = 19, $n_{20ms30s}$ = 41, $n_{20ms60s}$ = 35. Error bars, SEM.

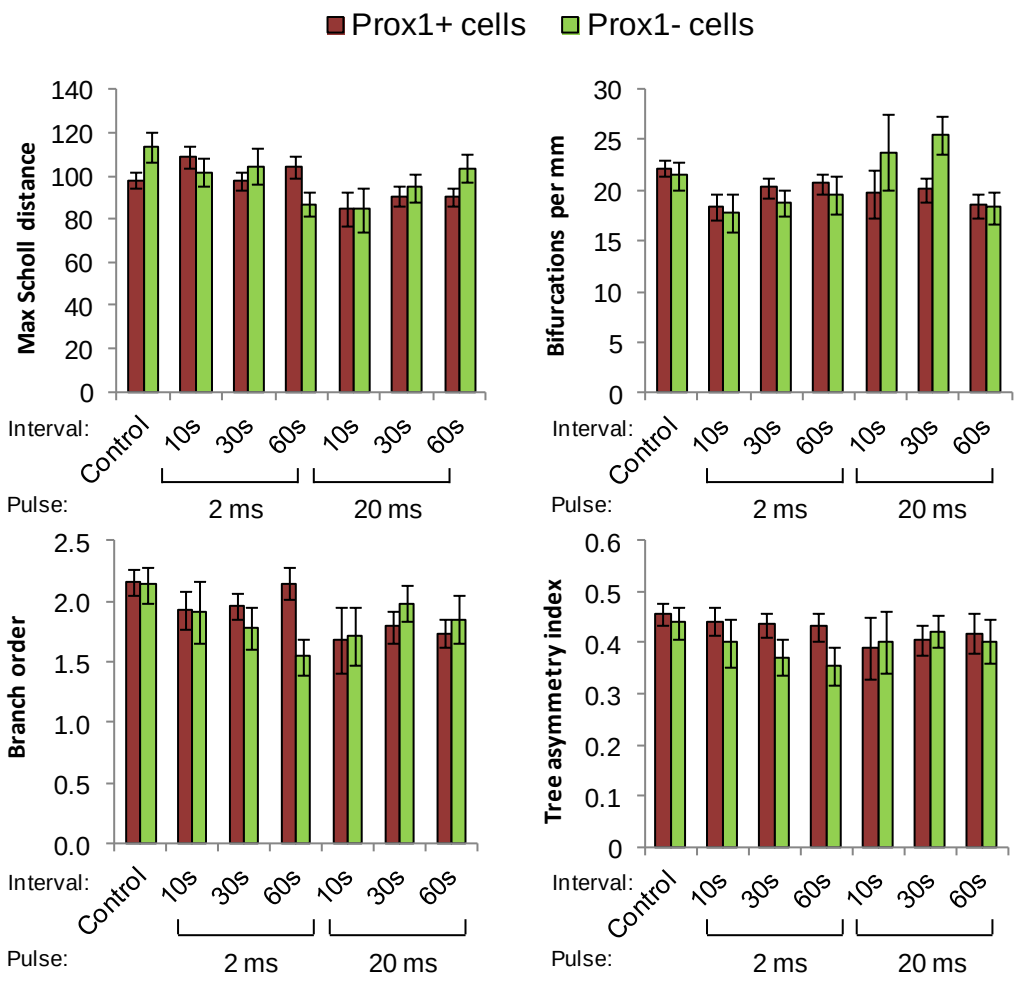

Figure 3.8 Morphometric analysis of dendritic morphology of optogenetically stimulated neurons, cont. Graphs showing max sholl distance, bifurcations per mm, mean branch order and tree asymmetry index of prox1-positive (red) and prox1-negative (green) neurons after 16 hr stimulation with different patterns of light pulse. Error bars, SEM.

axons without affecting dendritic length, whereas optogenetic stimulation reduced the length of both axons and the dendrites, which emphasises the importance of patterned stimulation for induction of dendrite-specific effect in prox1-negative neurons.

The findings presented in this chapter are not consistent with the majority of current studies on activity-dependent dendrite outgrowth. Work performed on cortical and hippocampal cultured neurons showed that elevating neuronal activity with high levels of extracellular KCl leads to accelerated dendritic growth and branching (Redmond et al., 2002; Yu and Malenka, 2003; Wayman et al., 2006; Tan et al., 2010; Ma et al., 2011). Even though I used the same conditions as reported previously (Redmond et al., 2002; Weyman et al., 2006), I failed to observe any increase in dendritic outgrowth and branching in high-KCl-treated neurons. Not all existing studies, however, report an increase in dendritic growth in response to enhanced activity. Mattson et al., (1988) showed an effect consistent with what was observed in this study, namely high-KCl-induced reduction in dendritic arborisations in dissociated hippocampal neurons. The discrepancy between the results seen in different laboratories may be due to a variety of factors, including differences in cell

culture preparations, culture density, media formulations or growth conditions. The direction of the activity effect may also depend on the developmental stage of a stimulated neuron. In addition there may have been some methodological differences in the analysis of dendritic arbours. For example, the border between soma and the origin of the dendrite can be ambiguous in some neurons, requiring an arbitrary decision regarding the origin of the dendrite, which in turn may affect the quantification of dendritic lengths.

The effect of activity on axonal development of prox1-negative was consistent with previous studies in hippocampal neurons (Mattson et al., 1988, Chang and DeCamilli, 2001; Tashiro et al., 2003; Ibarretxe et al. 2007). The majority of the literature on axon outgrowth in dissociated hippocampal cultures show a reduction in axon growth in response to electrical stimulation. This effect is also observed in sensory neurons, in which activity strongly inhibits axonal outgrowth (Fields et al., 1990; Mire et al., 2012). The axons of other neuronal types, however, were shown to behave in a different way in response to elevated levels of activity. For example, in murine thalamocortical axons, membrane depolarisation enhances axonal growth (Mire et al., 2012), whereas in spinal motor neurons it has no effect on neuronal elongation (Ming et al., 2001; Bouchard et al., 2008). In cultured retinal ganglion

cells and cortical neurons activity has no effect on its own but it greatly enhances the rate of trophic factor-stimulated axon growth (Goldberg et al., 2002; Bouchard et al., 2008).

The diverse, neurite-specific, responses of different cell types to membrane depolarisation may be attributed to distinct cellular and molecular mechanisms of neurite outgrowth in different brain regions. Depolarisation-induced neurite outgrowth is typically mediated by intracellular Ca^{2+} signals which then activate specific signalling pathways (Redmond et al., 2002; Yu and Malenka, 2003; Wayman et al., 2006). Principal signalling molecules activated by Ca^{2+} influx in neurons are the calcium/calmodulin-dependent protein kinases (CaM kinase II and CaM kinase IV), mitogen-activated protein kinases (MAPK) and protein kinase (PKA) (Redmont et al., 2003). The exact pathway activated by the Ca^{2+} signal depends on the spatiotemporal characteristics of the Ca^{2+} signal itself, such as its amplitude, frequency, pathway of entry and location (Moody and Bosma, 2005). For example, Wu et al., (2001) showed that large rises in intracellular Ca^{2+} in cultured hippocampal neurons lead to activation of a fast calmodulin kinase (CaMK) pathway followed by a slower, but longer lasting, activation of mitogen-activated protein kinase (MAPK). This, in turn, resulted in long-lasting phosphorylation of the transcription factor CREB. Small increases in Ca^{2+}, on the other hand, triggered only the CaMK pathway, which led to a more transient CREB phosphorylation. Therefore, different spatiotemporal features of Ca^{2+} signal could trigger distinct intracellular signalling cascades that are either conductive or prohibitive of dendritic or axonal growth.

The amplitude of Ca^{2+} rises can also account for cell-type differences in the responsiveness to electrical stimulation. Bouchard et al., (2008) showed that spinal neurons have distinctly lower Ca^{2+} transients than cortical neurons, and as a result they have a reduced capacity to respond to membrane depolarisation. Consequently they are not sensitive to depolarisation-induced enhancement of axon outgrowth observed in cortical neurons. The amplitude and other spatiotemporal characteristic of Ca^{2+} signals is determined by different complements of voltage-gated Ca^{2+} channels and other cell-surface proteins involved in 'sensing' the depolarising stimulus. Differential distribution of these proteins along axon and dendrites in different neuronal subtypes may thus account for different, often opposing, neurite- and cell-type specific responses to neural activity.

Rises in intracellular Ca^{2+} can also be shaped by specific patterns of neuronal activity. In this chapter I showed that a reduction in the dendritic length of prox1-negative cells was observed only after patterned stimulation with optogenetics but not after a sustained KCl treatment, suggesting that the frequency of the Ca^{2+} rise is important in inducing the dendritic phenotype. Previous work on different systems showed that the frequency of neuronal stimulation can differentially regulate dendritic and axon outgrowth. For example, in the visual system, the pattern of afferent activity to ocular dominance columns influence dendritic growth of neurons in the visual cortex (Kossel et al., 1995). Alterations in normal frequency of spontaneous activity can also perturb axon pathfinding in chick spinal motorneurons (Hanson and Landmesser, 2004; Kastanenka and Landmesser, 2010). Different patterns of neuronal activity may trigger different signalling pathways which activate a specific subset of genes (Itoh et al., 1995; Chang and Berg, 2001). Wu et al. (2008) showed that to persistently activate the MAP kinase pathway in hippocampal neurons, a series of strong spaced depolarisaitons are were required, as a single but sustained depolarisation is ineffective (Wu et al., 1001). These observations suggest that neurons have evolved mechanisms to distinguish differences in patterns of neuronal activity and may use this information to trigger specific cellular responses to physiological stimuli.

The ability of neurons to respond to electrical activity before the formation of synapses suggests that developing neurons may receive synaptic inputs at their dendrites and become electrically active while their axons and dendrites are still extending. Alternatively, activity-evoked signals, such as neurotransmitters, can act in a paracrine way, regulating the growth of dendritic and axonal arbours ‘at a distance’. For example, dendritic growth of hippocampal neurons has been shown to be directly and locally regulated by glutamate, whereby local application of glutamate stops growth (Mattson et al., 1988). Paracrine release of neurotransmitters can signal to the elongating axons and dendrites that they have reached their target and may begin formation of synaptic contacts. Thus activity-induced inhibition in axonal and dendritic growth may have physiological significance for formation of synaptic connectivity in developing hippocampal circuits.

Chapter 4

The role of activity on the structure of the axon initial segment

4.1 Introduction

In the previous chapter I investigated the effect of global membrane depolarisation on the gross morphology of the two specialised compartments of a neuron: axons and dendrites. Both axonal and dendritic compartments, however, can be further subdivided into specialised domains that include such structures as proximal and distal dendrites, synapses, nodes of Ranvier and axon initial segments. Each of these domains contains specific sets of proteins and plays a distinct role in neuronal physiology. In this chapter, I focus specifically on one of the axonal domains, the axon initial segment.

The axon initial segment (AIS) is a specialised region at the beginning of the axon that is enriched in cell adhesion molecules, cytoskeletal scaffolding proteins, extracellular matrix molecules and voltage-gated ion channels (Ogawa and Rasband, 2008). This protein-dense structure assembles shortly after the axon has been specified, but before the formation of the majority of synaptic connections. Once fully-formed, the AIS plays two immensely important roles in a cell: (1) it creates a molecular barrier between the somatodendritic and axonal compartments, preventing free diffusion of dendritic proteins into the axon and (2), due to the high density of voltage gated Na^+ and K^+ channels, it is the site where subthreshold somatic inputs summate and the action potential is initiated (Rasband, 2010; Bender and Trussel, 2012). Therefore, not only does it maintain a mature polarised structure of the cell, it also acts as a generator and a gatekeeper of neuronal excitability. These two highly crucial functions of the AIS already make it an exciting structure to investigate. However, what makes the AIS especially relevant for this study is that it has recently been found to be modulated by neuronal activity (Grubb and Burrone, 2010; Kuba et al., 2010).

Two studies have been done that revealed activity-dependence of the AIS structure and function. The first one was carried out in cultured hippocampal neurons, where

a 48-hour depolarisation, either with high levels of KCl or optogenetic photostimulation, resulted in a significant distal shift in the AIS position. The distal relocation of the AIS was reversible upon the removal of the depolarising stimulus and was found to be mediated through L-type Ca^{2+} channels, as blocking them with nifedipine abolished the activity-dependent distal AIS shift. Unsurprisingly, the change in the AIS position had also profound effects on neuronal excitability. Neurons with a proximal AIS were found to be more excitable, whereas neurons with a distal AIS required higher current injections to generate an action potential (Grubb and Burrone, 2010). The second study was performed in the auditory system of the chick, where removing cochlear afferent innervation led to elongation of the AIS in neurons of the nucleus magnocellularis. Electrophysiological recordings revealed a compensatory increase in the intrinsic excitability of the deafferented neurons (Kuba et al., 2010). Taken together, these studies show that the AIS is highly plastic and can alter its length or position to homeostatically compensate for the ongoing activity levels of the cell.

The above studies demonstrate the existence of activity-dependent AIS plasticity in relatively mature hippocampal neurons. Is there any form of AIS plasticity in young hippocampal neurons? The aim of this chapter was to investigate the role of activity on the AIS of very young hippocampal neurons, just after they have already specified their axons but before they are fully integrated into the hippocampal network. I begin by characterising AIS development in our culture system, followed by an in-depth investigation of activity-dependent AIS plasticity in developing hippocampal neurons.

4.2 AIS development in hippocampal excitatory neurones

To understand the role of activity on AIS in early development, I first characterised the emergence of the AIS in our culture system. The aim was to establish when the AIS first appears in excitatory neurons of the hippocampus *in vitro* and to describe the basic structural properties of the AIS, such as its length and position, during development.

4.2.1 Emergence of the AIS in hippocampal excitatory cells

Most studies in dissociated hippocampal neurons do not distinguish between neuronal cell types, treating them mostly as equal. This can be problematic for a number of obvious reasons, but I was specifically concerned about the degree of variability inherent in studying all neurons as one population, irrespective of their

identity. To minimize variability I decided to focus exclusively on hippocampal excitatory cells. This group of neurons was chosen for a number of reasons: (1) I could exploit well-established markers for different excitatory neurons (granule cells versus pyramidal neurons); (2) excitatory neurons comprise the large majority of neurons in our mixed cultures (70-90%; data not shown) and (3) previous findings in the lab suggest that AIS plasticity in mature neurons occurs exclusively in excitatory neurons (Grubb and Burrone, 2010).

Excitatory cells in the hippocampus were identified as the subgroup expressing calcium/calmodulin-dependent protein kinase II (CaMKII). CaMKII is a multifunctional serine/threone kinase (~600 KDa) that is one of the most abundant proteins in the brain (Bennet et al., 1983). In the hippocampus it is selectively expressed by excitatory neurons (Sik et al., 1998), which comprise the pyramidal neurons of the CA1 and CA3 subregions of the hippocampus and the granule cells of the dentate gyrus. To distinguish dentate granule cells from pyramidal neurons, the cultures were co-labelled with prox1, a transcription factor expressed specifically in the nuclei of all dentate granule cells but not in pyramidal neurons (Iwano et al., 2012). In this way it was possible to clearly distinguish between pyramidal neurons and granule cells in our culture system and assess the properties of the AIS in each group of cells independently (Figure 4.1). The AIS itself was labelled using the antibody against Ankyrin G (AnkG). AnkG is one of the first proteins detected at the AIS during development and it functions as a scaffold to which all other AIS proteins are tethered (Boiko et al., 2007; Jenkins and Bennett, 2001). This protein is absolutely essential for the formation and maintenance of the AIS. The absence of AnkG in developing neurons prevents AIS formation (Hedstrom et al., 2007; Zhou et al., 1998), whereas silencing AnkG expression in neurons that already formed an AIS leads to a complete disruption of the AIS structure (Hedstrom et al., 2008).

To characterise AIS development in excitatory neurons, the neuronal cultures were fixed at different time points of development, immunostained as described above and imaged with a fluorescent microscope. The imaging system in our lab permitted successful separation of three channels (green, red and blue). The blue channel was reserved for Hoechst stain, thus leaving an insufficient number of channels for separate labelling of AnkG, prox1 and CamKII. However, because of separate localisation of the prox1 (nucleus) and the AnkG (proximal axon) within a cell, it was possible to use the same fluorophore to stain for both markers on the same neuron. When stained separately, I did not detect any colocalisation of the expression of

prox1 and AnkG. Prox1 was localised exclusively to the nucleus and gave no signal that extended into the axon (data not shown). The CaMKII antibody stained the whole cell and thus it was imaged in a separate channel. Example images of neurons triple-stained with prox1, CamKII and AnkG are shown in figure 4.1. As the CamKII label was equally distributed throughout the cell, it also served as a reliable marker of neuronal morphology. A clearly-distinguishable outline of the neuron was crucial to localise the beginning of the axon, which was essential for the measurement of the AIS position relative to the soma.

In our culture system AISs were first detected at 2 DIV, when 2% of granule cells and 13% of pyramidal neurons showed a clear AnkG labelling along their proximal axons (2 out of 78 granule and 8 out of 60 pyramidal cells were AnkG-positive). Granule cells formed an AIS later than pyramidal cells, with a lag of 3-5 days. By the beginning of the second week *in vitro*, only 50% of the granule cells had an AIS, compared to over 80% of neighbouring pyramidal cells at the same stage. Following the initial lag period, AIS formation in granule cells increased dramatically after 5 DIV and eventually plateaued at 13 DIV, at which stage around 85% of all cells were AIS-positive. On the other hand, AIS formation in pyramidal cells began to plateau much earlier, at around 7 DIV (82% AnkG-positive cells), reaching its peak at 13DIV (85%, see figure 4.2). Despite the clear temporal difference in the emergence of the AIS in granule and pyramidal cells, all neurons in the culture system formed an AIS within the first two weeks *in vitro*, in agreement with previous findings (Yang et al., 2007).

4.2.2 AIS properties change during development

Having characterised the emergence of the AIS in our culture system, I proceeded to examine the structural properties of the AIS throughout development. Specifically, I measured AIS position and its length. AIS position was expressed as the distance of the proximal end of the AIS from the soma, measured along the axon. Hippocampal neurons tend to differ in the location from which an axon emerges. The majority of cells (~95%) in our culture system had axons growing directly out of cell bodies, however a small fraction of cells (2-5%) started their axons from a dendritic shaft that can be a considerable distance away from the cell body. To reduce the heterogeneity of the sample, only soma-derived AISs were included in the analysis as they constituted the majority of cases.

In vivo studies in mouse cortical neurons have shown that the position and the length of the AIS changes throughout early development. Galliano et al. (2012) demonstrated that the AIS initially forms distally from the cell body and then progressively 'fills in' the proximal part of the axon, thus increasing in length whilst simultaneously decreasing its distance to the soma. Interestingly, the distal end of the AIS was proposed to form a border which determines the location of the AIS along the axon. In this section I wanted to determine whether similar changes occurred in excitatory hippocampal neurons *in vitro*.

In agreement with the *in vivo* data, I have observed a significant change in AIS position throughout development in both granule and pyramidal neurons (Kruskal-Wallis ANOVA, $P < 0.0001$, $n_{granule} = 165$, $n_{pyramidal} = 289$) (Figure 4.3). The AIS was significantly closer to the cell body in mature neurons at DIV14 ($n_{granule} = 29$, $n_{pyramidal} = 28$) than in young developing cells at 4 DIV (Mann-Whitney U-test, $P < 0.0001$, $n_{granule} = 5$, $n_{pyramidal} = 43$). This effect occurred in a linear fashion, with the AIS progressively moving closer to the cell body as the cultures matured (Figure 4.3). A greater change in the AIS position between 4 and 14 DIV was observed for granule neurons (12.02 ± 2.53 µm proximal shift) than for pyramidal cells (4.76 ± 4.06 µm proximal shift; mean ± SD), which is interesting considering the slower AIS formation rate in the granule cells.

In Galiano et al. (2012), progressive 'filling in' of the proximal axon by the AIS proteins was accompanied by an increasing length of the AIS. In this study, a similar effect was observed in pyramidal cells but, intriguingly, not in granule neurons. In fact, granule cells displayed the opposite tendency: the progressive proximal shift of the AIS was accompanied by a marked decrease in the AIS length (Kruskal-Wallis ANOVA, $p = 0.001$, $n = 165$). A significant change was seen between 7 and 14 DIV (5.39 ± 4.65 µm, Mann-Whitney U-test; $p = 0.005$; $n_{DIV4} = 22$, $n_{DIV14} = 28$). No significant difference in AIS length was detected between 4 and 14 DIV, presumably due to the low number of AIS-containing granule cells at 4 DIV ($n = 5$). In contrast to the granule cells but in agreement with the data from cortical neurons, the AIS of pyramidal cells was significantly longer in mature neurons at 14 DIV than in young cells at 4 DIV (5.98 ± 5.70 µm, Mann-Whitney U-test, $P < 0.0001$, $n_{DIV4} = 29$, $n_{DIV14} = 43$). Moreover, the AIS of mature pyramidal neurons was also significantly longer than the AIS of mature granule neurons (DIV14; Mann-Whitney U-test, $P < 0.0001$; Granule: 22.95±4.66 µm, Pyramidal: 32.05±4.30 µm, mean ± SD), even though the AISs of both cell types were similar in length when they initially formed (DIV4; Granule cells: 28.34 ± 4.6µm, $n = 5$; Pyramidal cells: 26.07±6.47µm, $n = 43$).

Differences in the AIS length and the time-course of the AIS formation between the two excitatory cell types may reflect the existence of distinct AIS development programmes in these two classes of neurons. Pyramidal cells appear to follow the developmental route of cortical neurons, where the AIS initially forms at the distal part of the axon and gradually lengthens into the proximal part. Granule cells, on the other hand, seem to follow a different route; their AISs get progressively shorter as the cells mature, questioning the validity of the 'distal AIS boundary' hypothesis in this class of excitatory neurons.

Having seen significant changes in AIS length and position during development, I wondered whether the density of the 'master organiser' of the AIS, the AnkG scaffolding protein, is also prone to developmental changes. AnkG serves as a molecular anchor for other AIS proteins, including Na_v and K_v channels and the proteins involved in the formation of the cytoplasmic filter. Therefore any changes in AnkG density at the AIS may reflect overall changes of the molecular composition of the AIS throughout development. To examine whether the levels of AnkG change in development, I used the brightness of AnkG immunostaining as a proxy for AnkG accumulation at the AIS during development. I measured both peak fluorescence and integrated fluorescence of the AnkG stain, both of which significantly changed during development (Kruskal Wallis ANOVA, $P < 0.0001$. Figure 4.3). Peak fluorescence reflects the maximal density of AnkG at the AIS, whereas the integrated fluorescence is indicative of the overall amount of AnkG at the AIS and highly depends on the length of the AIS. Both measures significantly increased between 4 DIV and 14 DIV for both cell types (Mann-Whitney U-test, $P < 0.0001$), however the values of integrated fluorescence increased to a lesser extent for granule cells than for pyramidal neurons. This, may have just been due to the shorter AISs of mature granule cells rather than an absolute lower density of AnkG at the AIS. There was no difference in peak AnkG fluorescence between the cell types. Interestingly, maximal levels of peak/integrated flurescence were reached at DIV7, after which point they remained steady and no further increase in fluorescence was detected. Together, these results show that the levels of AnkG protein at the AIS increase during development, suggesting that there is an ongoing addition of the AnkG components after the initial AnkG 'backbone' has already been formed.

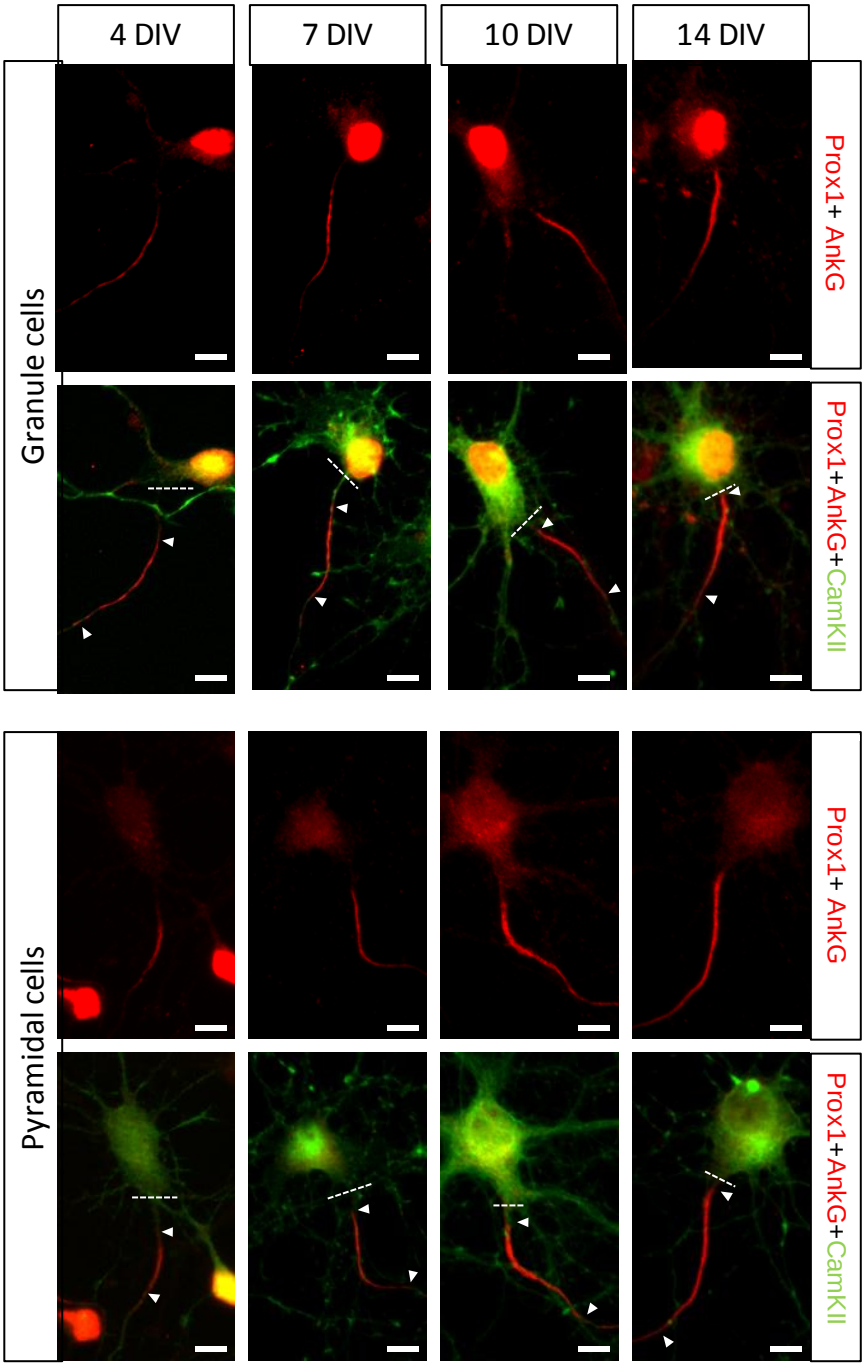

Figure 4.1 AISs of granule and pyramidal cells at different stages of development. AnkyrinG(AnkG, red) was used to label for the AIS, calcium/calmodulin kinase II (CamKII, green) stained all excitatory cells and prox1 (red) labelled the nuclei of dentate granule cells. Arrowheads indicate an approximate beginning and end of the AIS. Note the progressive increase in the size and intensity of the AnkG stain in development. Dotted line demarcates the boundary between the soma and the axon. Scale bar, 10 µm.

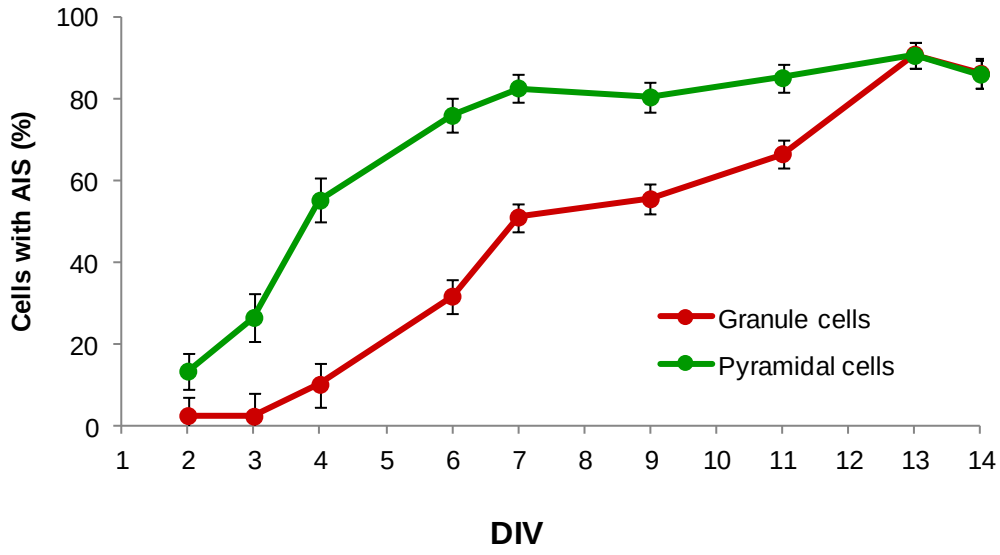

Figure 4.2 Timecourse of AIS formation in cultured granule and pyramidal neurons ($n_{granule}$ = 726 cells, $n_{pyramidal}$ = 832 cells; 43-126 cells of each type per developmental time point). Note the lag period of the AIS formation in granule neurons. Error bars, SD.

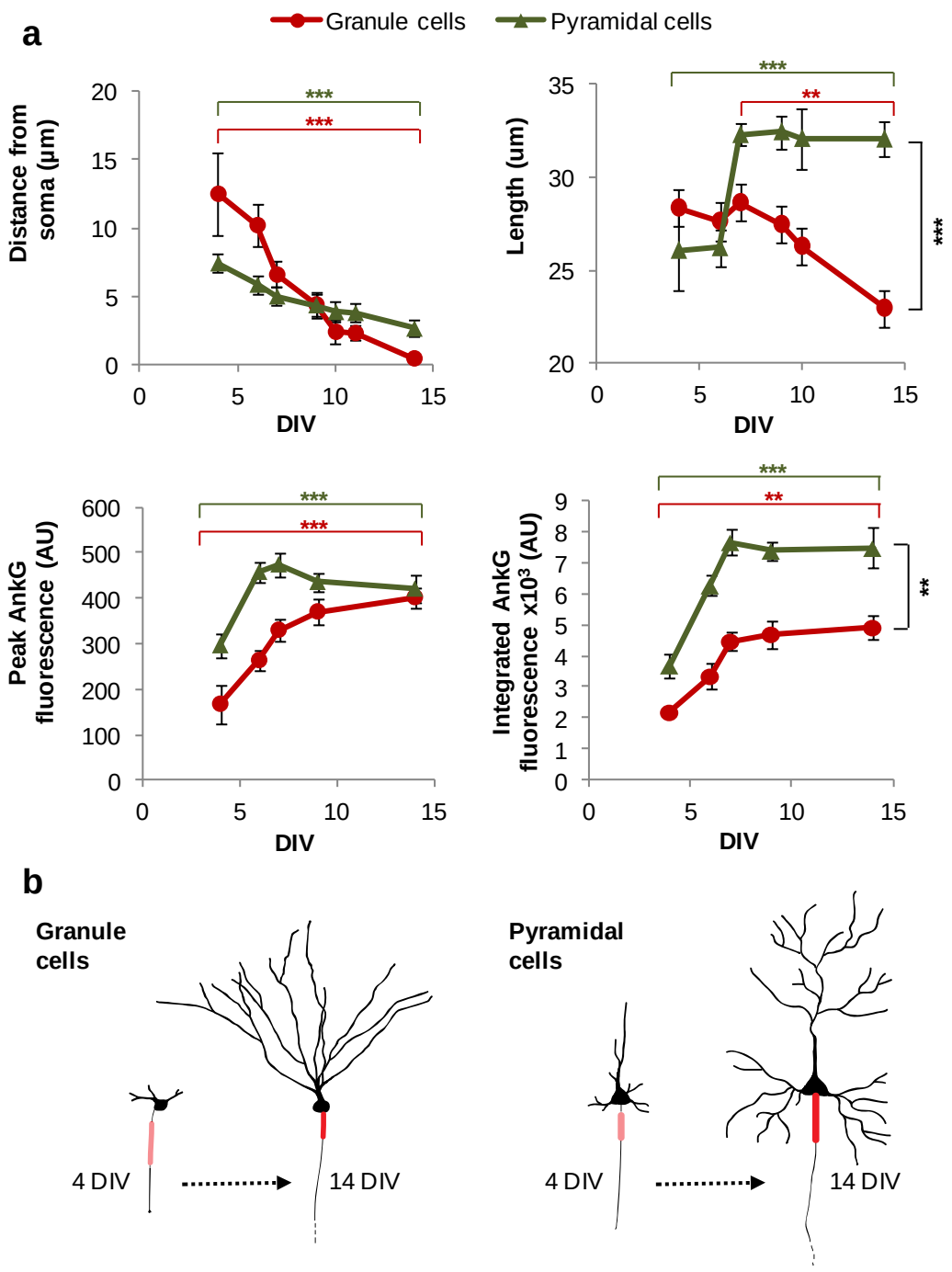

Figure 4.3 The properties of the AIS change in development (a) Graphs showing the distance from the soma, the length, the maximum fluorescence and the total fluorescence of the AIS at different stages of development. Red and green significance brackets refer to granule and pyramidal cells, respectively. * P < 0.05; ** P < 0.01; *** P < 0.001. Error bars, SD. (b) Schematic diagram summarising the changes seen. In both granule and pyramidal cells the AIS gets brighter (as measured by the intensity of the AnkyrinG stain) and moves closer to the cell body as the cells mature. The AIS of granule cells tends to get shorter during development, whereas the opposite effect is seen in pyramidal cells. Mature (14 DIV) pyramidal cells have a longer AIS than granule cells.

4.3 Chronic membrane depolarisation decreases the number of AIS-positive neurons

Having characterised a timeline of AIS development in our culture system, I set out to explore the role of depolarisation on the AIS in early stages of hippocampal development. It has been previously shown that the AIS responds to electrical activity by changing its length and position along the axon (Grubb and Burrone, 2010, Kuba et al., 2010). This effect, however, was investigated primarily in mature systems when the majority of cells have already formed an AIS. Here, I wanted to examine how activity may affect the AIS early in development, at the time when neurons only begin forming the AIS. Does neuronal activity modulate the formation of the AIS?

To answer this question, I measured the effect of chronic changes in activity on AIS formation by estimating the proportion of cells containing an AIS. Electrical activity was modulated by either treating neurons with high levels of KCl or by optogenetic photostimulation of ChR2-expressing cells. All treatments were performed for 16 hrs between 3 and 4 DIV, at a time when the AIS just begins to form (Figure 4.4a).

Previous work in mature hippocampal neurons has found that moderate levels of depolarisation (15mM KCl) were the most effective at inducing the activity-dependent shift in the AIS position (Grubb and Burrone, 2010). To establish the optimal level of depolarisation for the following experiments, I conducted a pilot study with different concentrations of KCl (10,15, 20 and 30mM; Control: 5mM). The aim was to find the optimal stimulus that may alter the proportion of neurons containing an AIS. Interestingly, chronic KCl treatment led to a marked change in percentage of AIS-positive cells in a U-shaped manner. Gradual increases in KCl concentration caused a progressive decline in the number of cells with an AIS, reaching the lowest value at 20mM KCl but then becoming less effective as the KCl concentration was further increased (Figure 4.4b). As the maximal effect was seen with 20mM KCl, this concentration was used throughout the whole thesis.

Repeating the 20mM KCl depolarisation treatment consistently led to a significant decrease in the proportion of AIS-positive cells (Figure 4.4c, Mann-Whitney test, $P < 0.0001$) for both granule (Control: 8.55 ± 1.38%, 4 animals, n = 421 cells; KCl: 1.12 ± 0.65%, 3 animals, n = 269 cells) and pyramidal cells (Control: 63.16 ± 2.63%, 4

animals, n = 324 cells; KCl: 32.96 ± 3.06%, 3 animals, n = 239 cells, mean ± SD). Example images of control and KCl treated cells are shown in Figure 4.5.

KCl treatment is a reliable and straightforward method of depolarising the membrane potential and thus mimicking increased neuronal activity, however it does not provide a temporal control of the depolarising input. Optogenetics, on the other hand, allows a precise temporal control of the stimulus in a targeted population of neurons. To use this method, I sparsely transfected 1 DIV hippocampal cultures with a ChR2-YFP plasmid driven by a pan-neuronal synapsin promoter. The transfected cultures were optogenetically stimulated for 16 hrs between 3 and 4 DIV, akin to the experiment with elevated levels of KCl (Figure 4.4a). Because of the YFP fluorescence of the channelrhodopsin-transfected cells, I could not use the green channel for labelling with CamKII labelling and instead focused on granule cells only, where the effect was the greatest. Granule cells were chosen because of a nuclear localisation of the prox1 stain, which enabled co-labelling with the AnkG antibody in the same fluorescence channel.

I have tested several photostimulation paradigms, either varying the duration of the light stimulus (2 ms and 20 ms) or the intervals between the stimuli (10 s, 30 s and 60 s). The optimal stimulus was found to consist of 20ms light pulses delivered every 30 seconds (Figure 4.4f). Stimuli of higher frequencies compromised cell viability, whereas low-frequency stimuli did not sufficiently depolarise the ChR2-transfected neurons to elicit a significant effect. Application of the optimal stimulus onto ChR2-transfected granule cells for 16 hrs resulted in a significant decrease in neurons with an AIS (Mann-Whitney test, $P < 0.0001$. Control: 9.17 ± 3.59%, n = 67; Photostimulation: 4.62 ± 3.16%. n = 43, mean ± SD). This result is consistent with the changes seen after the KCl treatment and suggests that excitatory hippocampal neurons undergo a radical, cell-autonomous form of AIS plasticity, whereby membrane depolarization causes a total loss of the AIS from developing axons.

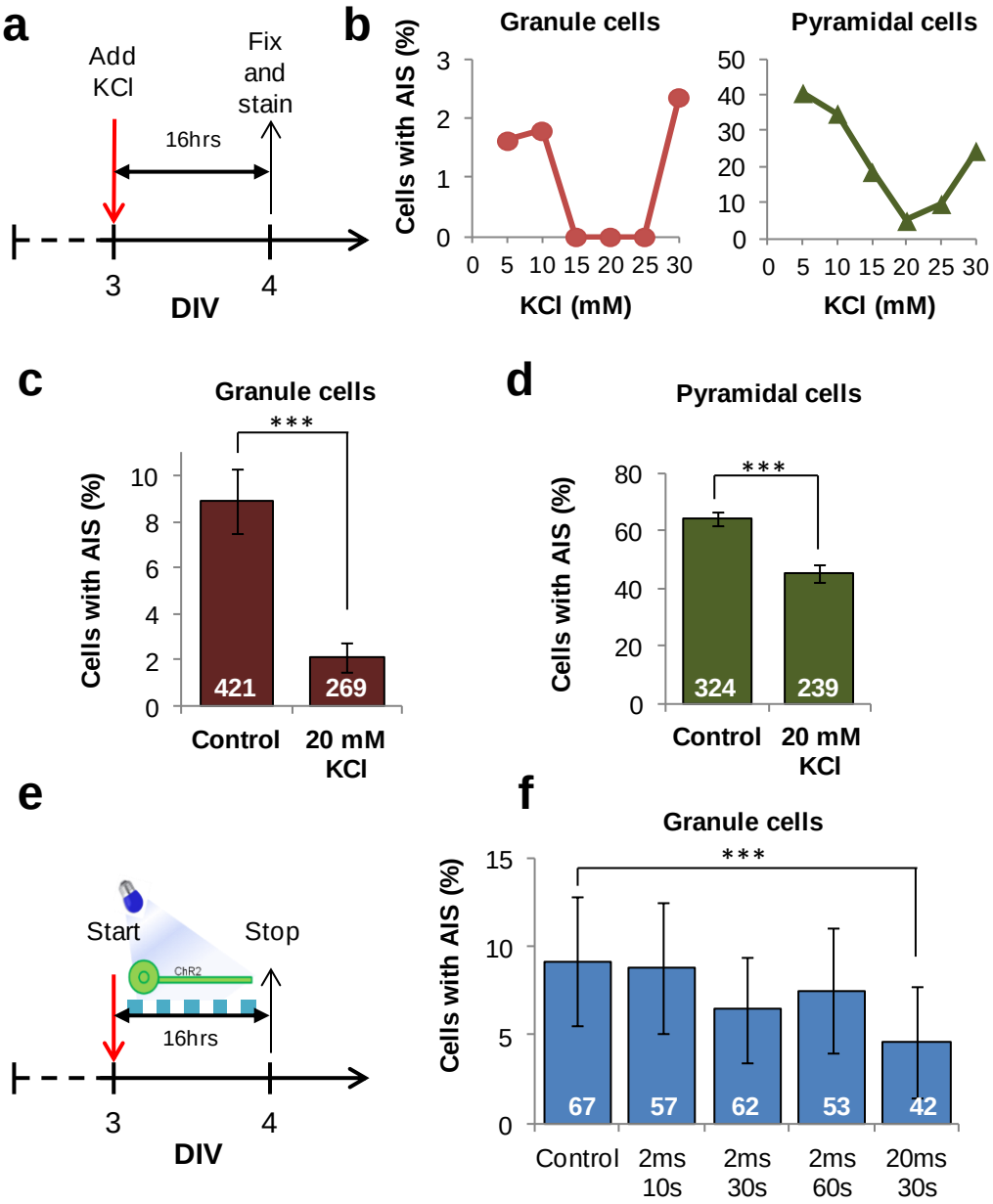

Figure 4.4 Chronic depolarisation with either an elevated concentration of KCl or optogenetics decreases the number of AIS-positive cells. (a) Schematics of the KCl experiment. Different concentrations of KCl were added at 3 DIV (red arrow) and left in the culture media for 16 hours, after which the cells were fixed and immunostained (black arrow) to label for the AIS and specific cell type markers. (b) Pyramidal and granule cells treated with different concentrations of KCl show a dose-dependent decrease in AIS-positive cells. (c, d) Graphs showing the percentage of granule (c) and pyramidal (d) cells with an AIS after 20mM KCl treatment as compared to untreated (control) cells. (e) Schematic of the optogenetics experiment. ChR2-transected neurons were photostimulated with blue light (blue rectangles) for 16 hours, from 3 DIV (red arrow) to 4 DIV (black arrow). Photostimulated cells were then fixed and immunostained for the AIS and granule cells. (f) Graph showing percentage of granule cells with an AIS following a photostimulation with different patterns of blue light. A 2 ms stimulus delivered every 10, 30 or 60 seconds did not elicit any significant change in the percentage of AIS-positive neurons. A significant change, however, was seen with 20 ms pulses delivered every 30 seconds. *** P < 0.0001, Mann-Whitney U-test. Error bars, SD. Numbers within the bars, number of cells in a sample.

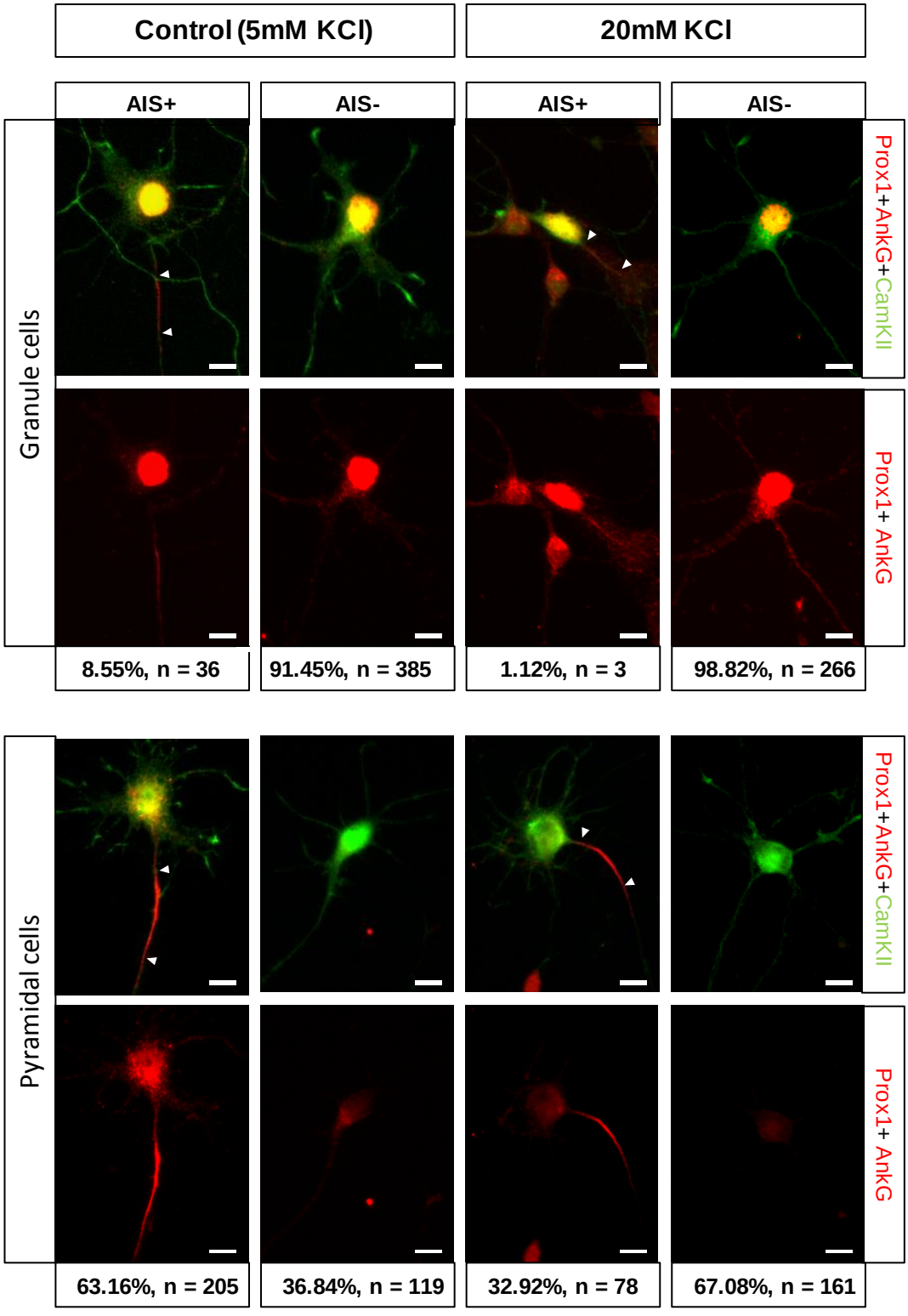

Figure 4.5 Example images of cells in the control and KCl condition. Arrowheads indicate an approximate beginning and an end of the AIS. AnkyrinG (AnkG, red) was used to label for the AIS, calcium/calmodulin kinase II (CamKII, green) stained all excitatory cells and prox1 (red) labelled the nuclei of dentate granule cells. AIS+ and AIS- indicate AIS-positive and AIS-negative cells, respectively. Scale bar, 10 µm.

4.4 Reduction of AIS-positive cells depends on Ca^{2+} influx through L-type Ca^{2+} channels but is not mediated by calpain-dependent proteolysis

A direct consequence of membrane depolarisation with high levels of KCl is an increase in intracellular calcium (Figure 3.1). Previous experiments from our lab showed that L-type voltage-gated calcium channels are necessary for activity-dependent AIS plasticity in mature hippocampal neurons, as pharmacologically blocking L-type calcium channels completely abolishes the activity-dependent AIS movement (Grubb and Burrone, 2010; Evans et al., 2013). In this section I investigate whether the KCl-induced decrease in AIS-positive cells described in the previous section is also dependent on L-type Ca^{2+} channels. To test this I treated the cultures with 20 mM KCl in the presence of 1 µM nifedipine, an L-type Ca^{2+} channel antagonist. In agreement with the previous results, 16-hour KCl treatment between 3 and 4 DIV led to a significant decrease in the number of AIS-positive cells, however simultaneous blockage of L-type Ca^{2+} channels with nifedipine prevented this decrease. Nifedipine itself did not induce any significant changes in the number AIS-positive cells (Figure 4.6 a,b). This effect was seen for both classes of excitatory cells and it indicates that L-type Ca^{2+} channels act as sensors for KCl-induced depolarisation.

An increase in intracellular [Ca^{2+}] triggers various signalling cascades, activating a number of Ca^{2+}-dependent proteins (Burgoyne, 2007). One such protein is the Ca^{2+}-dependent protease calpain. Activated calpain has been shown to cleave cytoskeletal components of the AIS following ischemic injury (Schafer et al., 2009). Here, I examined whether calpain is involved in depolarisation-induced reduction of AIS-positive neurons. To test this I co-treated the cultures with 20 mM KCl and 1 µM of calpain inhibitor MDL 18130 between 3 and 4 DIV, analogously to the previously described nifedipine experiment. As expected, KCl treatment applied on its own caused a marked decrease in the number of AIS-positive cells. However, MDL 18130 treatment did not prevent this decrease from taking place. The number of AIS-positive cells in KCl + MDL 18130 condition was comparable to the cells treated with only KCl. MDL 18130 had no effect when used on its own and both cell types behaved in a similar manner (Figure 4.6 c, d). These results suggest that calpain is not involved in the disappearance of the AIS observed in KCl-treated cultures.

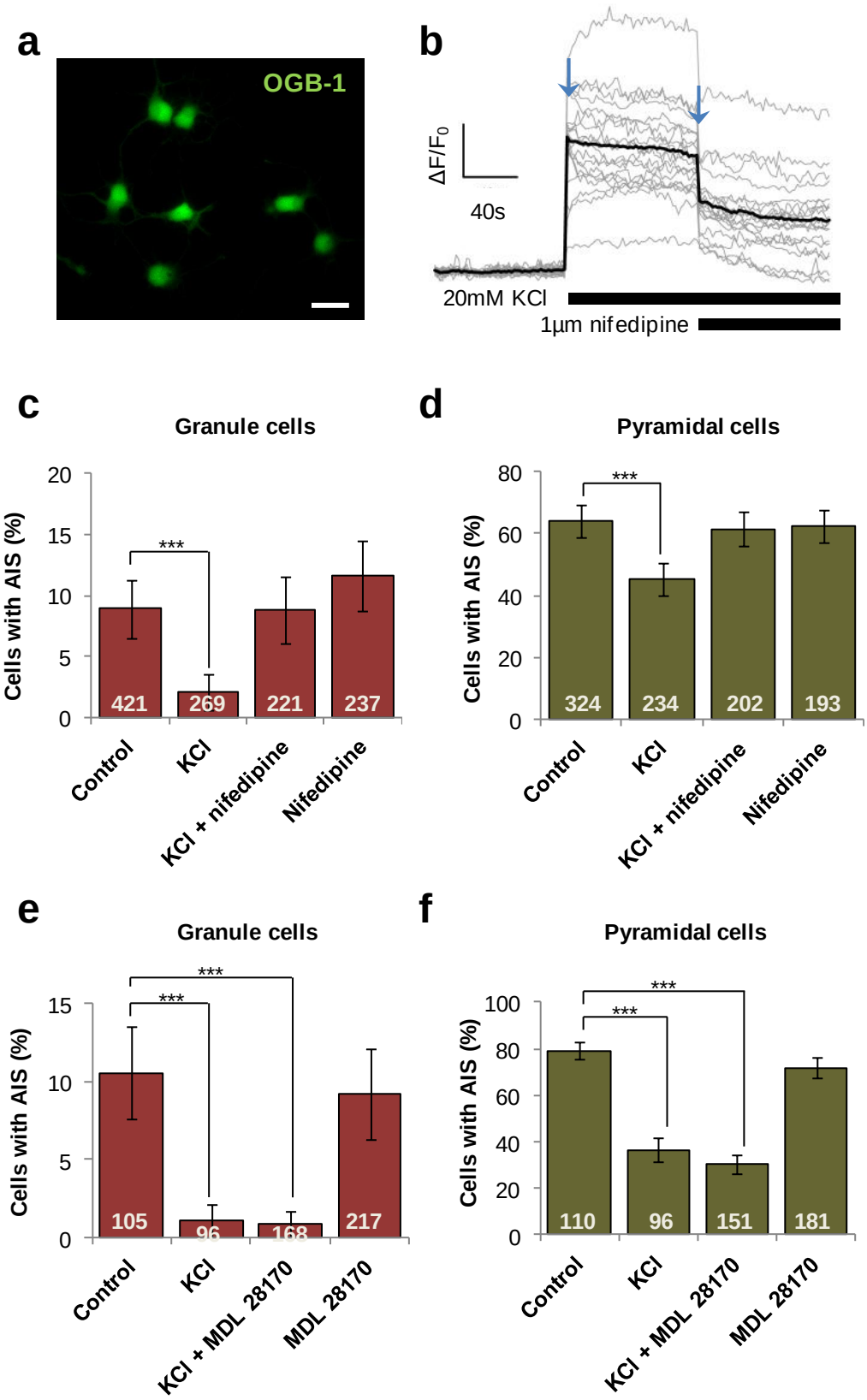
a
OGB-1
b
ΔF/F0
40s
20mM KCl
1µm nifedipine
c
Granule cells
Cells with AIS (%)
***
421
269
221
237
Control
KCl
KCl + nifedipine
Nifedipine
d
Pyramidal cells
Cells with AIS (%)
***
324
234
202
193
Control
KCl
KCl + nifedipine
Nifedipine
e
Granule cells
Cells with AIS (%)
***
***
105
96
168
217
Control
KCl
KCl + MDL 28170
MDL 28170
f
Pyramidal cells
Cells with AIS (%)
***
***
110
96
151
181
Control
KCl
KCl + MDL 28170
MDL 28170

Figure 4.6 The reduction of AIS-positive cells following a 16-hour treatment with KCl depends on Ca^{2+} influx through L-type voltage gated Ca^{2+} channels but is not mediated by calpain-dependent proteolysis (a) 4 DIV hippocampal cells loaded with Oregon Green BAPTA-1 (OGB-1). (b) $\Delta F/F_0$ traces of cultured hippocampal neurons loaded with OGB-1 at 5mM KCl baseline and upon addition of 20mM KCl and 20mM KCl plus 1 µM nifedipine (blue arrows). The thick black line indicates the average trace, whereas thinner grey lines denote responses of individual cells. Note the increase in $\Delta F/F_0$ following the addition of KCl, which reflects an increase in intracellular Ca^{2+}. Addition of nifedipine brings the $\Delta F/F_0$ values down however it does not completely block depolarisation-induced increase in intercellular [Ca^{2+}]. (c, d) Graphs showing the effect of 20 mM KCl, 20 mM KCl with 1 µM nifedipine and 1 µM nifedipine on its own, on the percentage of AIS-positive granule (c, red bars) and pyramidal (d, green bars) neurons. Nifedipine prevents the reduction in AIS-positive neurons following 16-hour KCl treatment. (e, f) Graphs showing the percentage of granule (e) and pyramidal (f) cells with an AIS following a 16-hour treatment with 20 mM KCl, 20 mM KCl with the calpain inhibitor MDL28170 or MDL28170 on its own. MDL28170 did not prevent the KCl-induced decrease in AIS-positive cells. Numbers within bars indicate the total numbers of cells in each condition. ***, $P < 0.0001$, Mann-Whitney U-test. Error bars, SD.

4.5 A critical window for AIS dissassembly

As shown in the previous sections, chronic membrane depolarisation decreases the number of AIS-positive neurons in early development, between 3 and 4 DIV. Next, I investigated whether this new form of plasticity also occurres at other developmental stages or whether it is specific to this very early stage. To test this, I repeated the 16-hour 20mM KCl treatment at three other developmental time points, between 6-7, 9-10 and 14-15 DIV (Figure 4.7a). Although all time points tested showed a significant decrease in AIS-positive neurons after the KCl challenge (Mann-Whitney U test, $P < 0.0001$), this effect was strongest for neurons between 3-4 and 6-7 DIV, and much less so for older neurons. The results are summarised in Table 4.1 and in Figure 4.7b.

To further explore this temporal difference in depolarisation-induced AIS plasticity, I calculated the AIS sensitivity to KCl at each developmental stage tested. Sensitivity to KCl was expressed as a ratio of the percentage of AIS-positive cells in control conditions divided by the percentage of AIS-positive cells after the KCl treatment.

$$\text{Sensitivity to KCl} = \frac{\%\ \text{AIS-positive neurons in control condition}}{\%\ \text{AIS-positive neurons in KCl condition}}$$

In this measure a value of 1 indicates no effect, whereas values larger than 1 denote increasing degrees of sensitivity to KCl. According to this analysis, both classes of excitatory neurons were much more sensitive to KCl treatment between 3 and 4 DIV (4.2-fold change, granule; 1.4-fold, pyramidal) and at 6-7 DIV (4.6-fold, granule; 1.5-fold, pyramidal) than at 9-10 DIV (1.4-fold, granule; 1.1-fold, pyramidal) and 14-15 DIV (1.4-fold, granule; 1.1-fold, pyramidal), suggesting the existence of a developmental time window for this form of AIS plasticity (Figure 4.6c). In addition, granule cells were much more sensitive to KCl-induced depolarisation than pyramidal neurons (maximal 4.6-fold sensitivity versus 1.5-fold at 6-7 DIV).

As the highest sensitivity to the treatment was seen at 6-7 DIV, all further experiments were conducted at this stage. This developmental stage was also advantageous as at 7 DIV a larger proportion of granule neurons have an AIS compared to at 4 DIV (7 DIV: 38.48 ± 4.05%; 4 DIV: 8.55±1.38%, mean ± SD). A larger number of AIS-positive neurons greatly facilitated data collection and analysis required for this thesis.

Table 4.1 The percentage of AIS-positive granule and pyramidal neurons in control and KCl conditions at different stages of development

DIV	Condition	Number of cultures	% AIS+ neurons (Mean ± SD)	
			Granule cells	Pyramidal cells
3-4 DIV	Control	4	8.91 ± 2.44% n = 421	64.18 ± 5.33 n = 324
	KCl	3	2.09 ± 1.44% n = 269	45.34 ± 5.38 n = 239
6-7 DIV	Control	2	38.48 ± 4.05% n =148	69.64 ± 3.66 n=158
	KCl	2	10.59 ± 2.67% n =135	56.80 ± 4.37 n = 128
9-10 DIV	Control	1	87.60 ± 3.94% n = 72	87.23 ± 3.20 n = 59
	KCl	1	60.69 ± 6.09 n = 64,	78.28 ± 5.13 n = 64
14-15 DIV	Control	3	84.65 ± 3.79 n = 85	86.58 ± 2.25 n = 183
	KCl	3	58.57 ± 4.87 n = 104	76.78 ± 3.01 n = 135

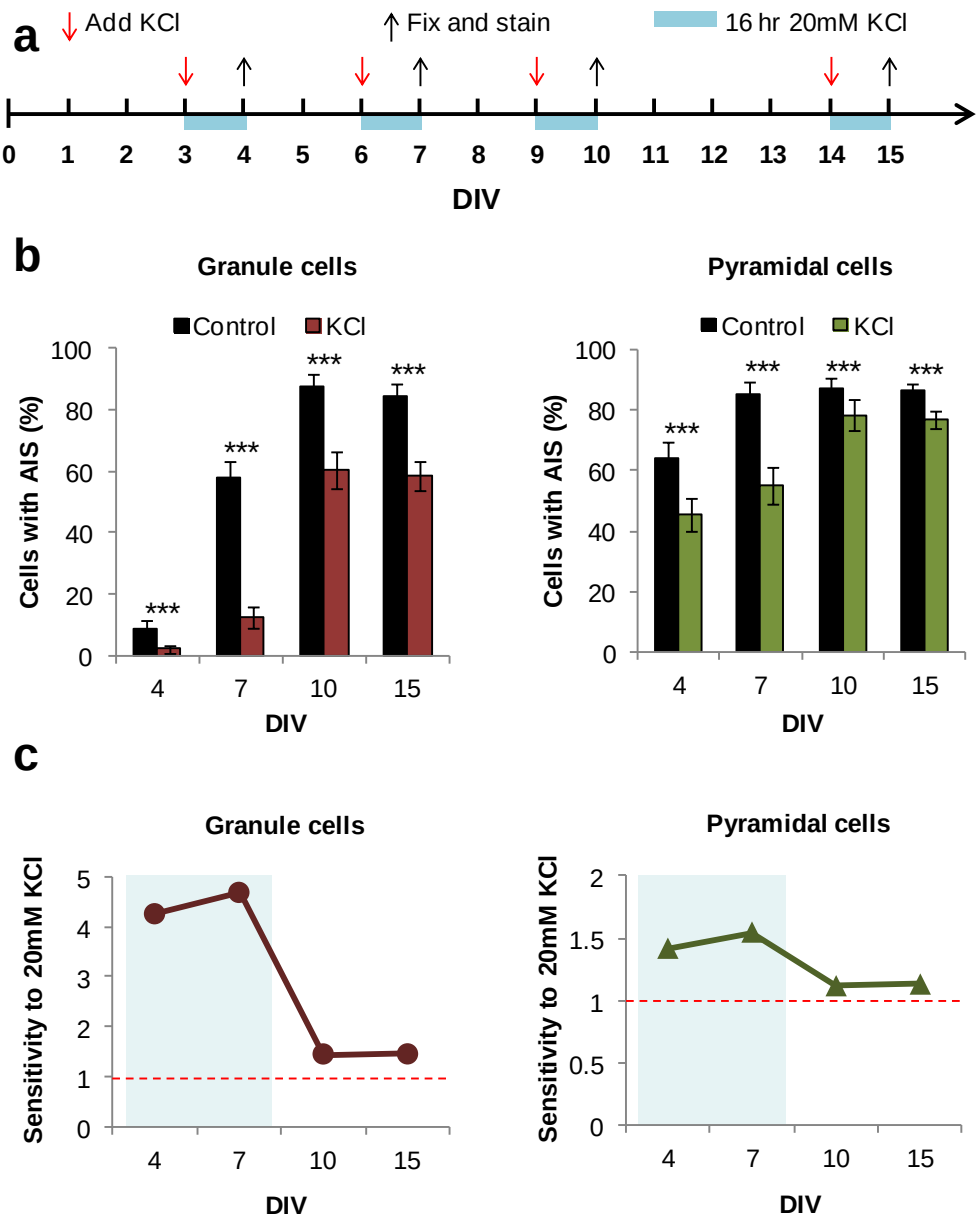

Figure 4.7 Critical window for AIS disappearance. (a) Schematic of the experiment. KCl was added at 3, 6, 9 and 14 DIV (red arrows) and left in the culture media for 16 hours after which the cultures were fixed and stained for the AIS and cell type specific markers (black arrows) (b) Percentage of granule (left) and pyramidal (right) cells with an AIS at 4, 7, 10 and 14 DIV, following a 16-hour KCl treatment. ***, P < 0.0001, Mann-Whitney U-test). Black bars indicate control neurons, whereas red and green bars denote KCl-treated granule and pyramidal cells, respectively. Error bars, SD. (c) Sensitivity to 20 mM KCl as a function of days in vitro (DIV), as calculated by the formula: $\frac{\%\text{-}AIS positive\ neurons\ in\ control\ condition}{\%AIS\text{-}positive\ neurons\ after\ the\ KCl\ treatment}$. Dotted line denotes no sensitivity to the KCl treatment. Blue box indicates the period of highest sensitivity.

4.6 AIS properties change in response to KCl treatment

Chronic depolarisation with KCl or optogenetically reduced the number of cells with an AIS, however a proportion of neurons retained their AIS. What are the properties of the remaining AISs? This is a particularly important question because it has previously been shown that mature hippocampal neurons *in vitro* can change the AIS position in response to high levels of activity (Grubb and Burrone, 2010) and that young neurons in the chick auditory system can alter the length of the AIS in response to sensory deprivation (Kuba et al., 2010). Here I investigated whether the position and length of the AIS changes in response to KCl treatment in developing hippocampal neurons.

As previously shown (Figure 4.3), developing granule and pyramidal neurons change the properties of their AISs as they mature. In both cell types, the AIS begins to form distally from the cell body and then gradually fills in the proximal part of the axon. In pyramidal cells this process is accompanied with an increase in length of the AIS, however the opposite effect is seen in the granule neurons, where the AIS shortens as it grows into the proximal axon. Interestingly, treating the cells with 20mM KCl for 16hrs appears to accelerate this process, resulting in a more proximal position of the AIS in KCl-treated cells as compared to the control cultures (Figure 4.8a, top). The AIS position was defined as the distance of the proximal end of the AIS from the edge of the soma. Using this measure, significant differences between the conditions were observed at 4, 7 and 10 DIV (Mann Whitney U-test. 4 DIV: Granule cells: $p = 0.01$, $n_{Control} = 11$, $n_{KCl} = 3$; Pyramidal cells: $p = 0.0001$, $n_{Control} = 81$, $n_{KCl} = 59$. 7 DIV: Granule cells: $p = 0.001$, $n_{Control} = 72$, $n_{KCl} = 17$; Pyramidal cells: $p = 0.011$, $n_{Control} = 109$, $n_{KCl} = 53$. DIV10: Granule cells: $p = 0.026$, $n_{Control} = 26$, $n_{KCl} = 15$; Pyramidal cells: $p = 0.045$, $n_{Control} = 34$, $n_{KCl} = 28$). No proximal shift in the AIS position was detected at 15 DIV as the AISs of control neurons were already very close to the soma at that developmental time point (15 DIV: Granule cells: $p = 0.11$, $n_{Control} = 71$, $n_{KCl} = 56$; Pyramidal cells: $p = 0.21$, $n_{Control} = 88$, $n_{KCl} = 57$).

Although the effect of the KCl treatment on AIS position was quite strong, its consequence on the AIS length was only moderate (Figure 4.8a bottom). There was a consistent trend toward shortening of the AIS following KCl treatment, however it was statistically significant only at 10 DIV for granule neurons (Mann-Whitney U-test, $P = 0.02$, $n_{Control} = 26$, $n_{KCl} = 15$) and at 4 and 15 DIV for pyramidal cells (Mann-

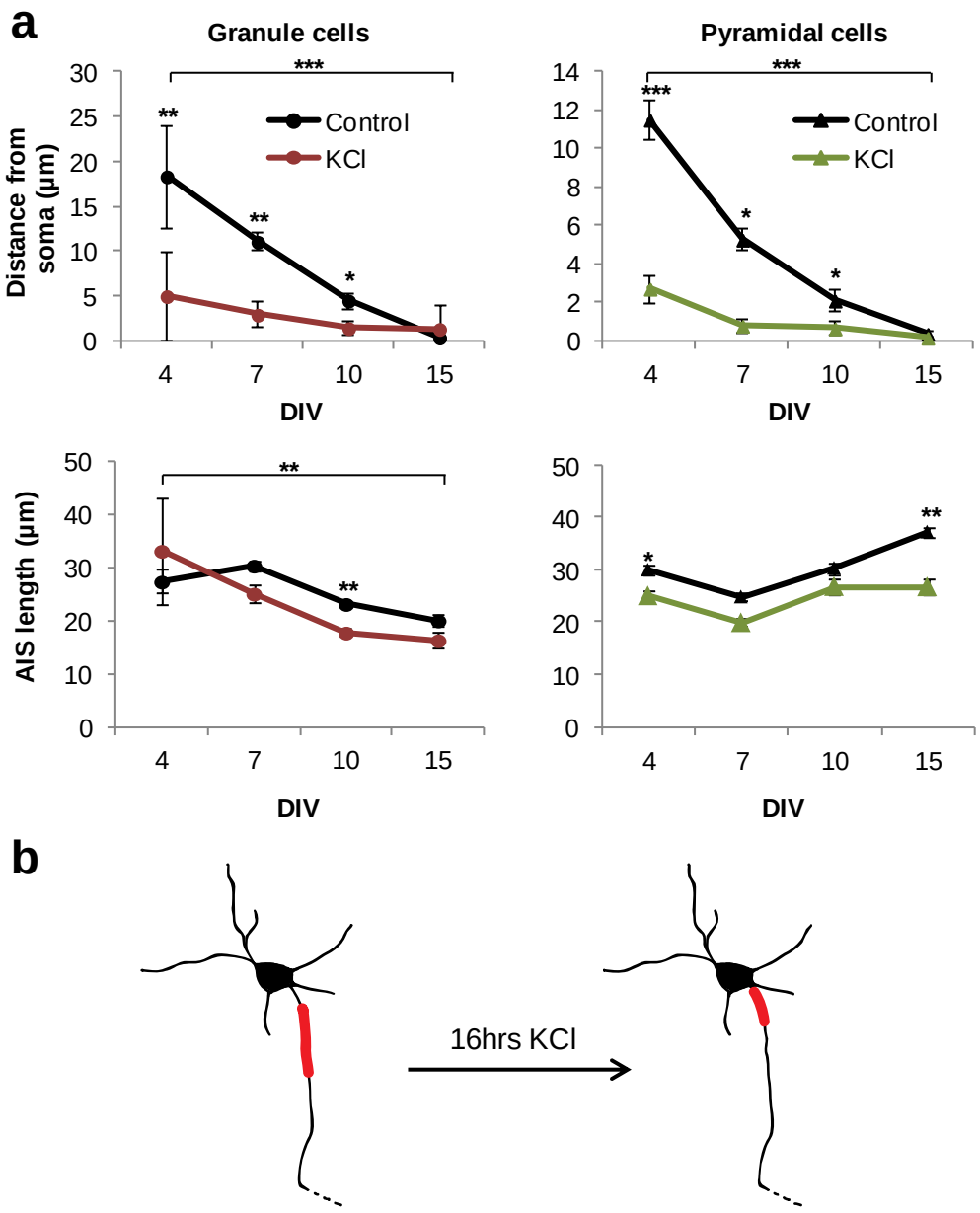

Figure 4.8 AIS properties of neurons change in response to 16-hour depolarisation with 20mM KCl. (a). Graphs showing AIS distance from the soma (top) and AIS length (bottom) at different stages of development for granule and pyramidal cells. *P < 0.05, ** P < 0.01, *** P < 0.001. Error bars, SEM. (b) Schematic representation of the general effect seen. Chronic depolarisation with 20mM KCl for 16 hrs results in shorter and more proximal AISs.

Whitney U test, 4 DIV: P = 0.04, $n_{Control}$ = 81, n_{KCl} = 59; 15 DIV: p = 0.002, $n_{Control}$ = 88, n_{KCl} = 57). It has been postulated that the AIS reduces its length by dismantling its distal end, thus giving rise to a blunted appearance. Hinman et al. (2012) observed such a blunted appearance of the distal end of the AIS together with a significant decrease in the AIS length in mouse motor cortex following focal stroke. Here, no obvious morphological changes accompanied the reduction in the AIS length. All of the AISs investigated tapered off at the distal end, just like in control neurons (see example in Figure 4.1).

Despite any clear morphological signs of disassembly, the AIS may respond to chronic depolarisation by altering its molecular composition throughout its entire length. I have previously shown that the density of the 'master organiser' of the AIS, the AnkG protein, increases in development (Figure 4.3). Here, I investigate whether any changes in AnkG density are seen following a 16-hour KCl treatment. To estimate the density of the AnkG protein at the AIS, I have measured the peak and the integrated fluorescence of the AnkG immunostaining in the control and KCl conditions (see section 4.2.2 for explanation of the measurement). No significant changes were detected in either of the two measures at any of the stages tested, suggesting that the composition of the AIS remained the same after the KCl treatment (Figure 4.9).

4.7 16-hour KCl treatment does not compromise cell viability

Previous experiments showed that chronic depolarisation decreases the proportion of cells containing an AIS, yet it is not clear whether this was due to selective cell death of AIS-containing neurons or whether the KCl treatment affected the AIS without compromising cell viability. To distinguish between these two possibilities and determine whether a decrease in the AIS number is a consequence of cell death or a specific neuronal response to elevated activity levels, I performed viability assays using propidium iodide and the Hoechst dye.

Propidium iodide (PI) is a fluorescent DNA dye that penetrates the membranes of damaged and/or dying cells but is excluded from healthy cells. Once it binds to the nucleus it emits a bright red fluorescence, thus labelling the damaged and dying cells (Figure 4.10a). To examine whether the 16hr-long KCl treatment caused any cell damage, I stained KCl-treated cultures with PI and counted the PI-positive

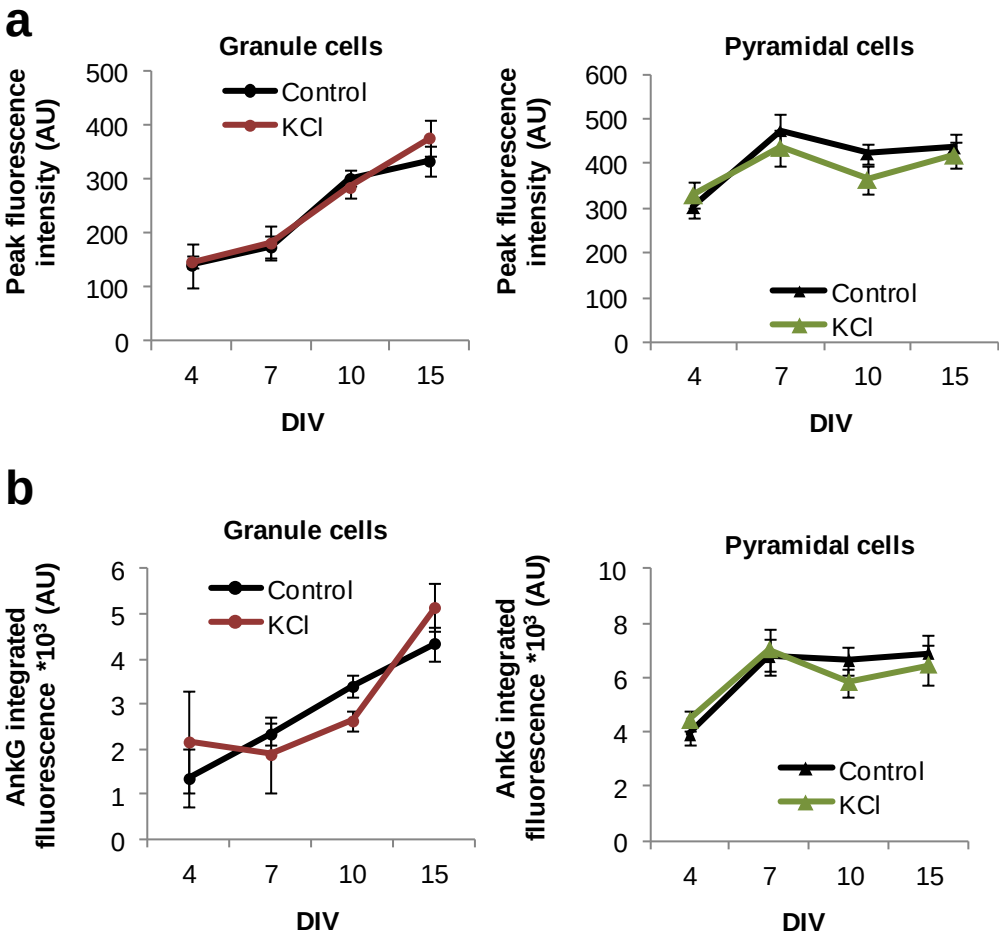

Figure 4.9 The intensity of the AnkG stain was not affected by the 20mM KCl treatment. (a,b) Graphs showing the peak fluorescence intensity (a) and integrated fluorescence (b) of the AnkG stain in granule (left) and pyramidal (right) cells at different stages of development. Black line indicates control cells, whereas red and green lines denote KCl-treated granule and pyramidal neurons, respectively. Error bars, SEM. AU, arbitrary units.

neurons (Figure 4.10b). The assay was performed at each developmental stage tested (4, 7, 10 and 15 DIV). I did not detect any significant differences in PI-positive cells between the two conditions at any of the developmental time points tested (t test, P > 0.3). Interestingly, there were consistently fewer PI-positive cells in KCl-treated cultures, compared to control cells, which is consistent with previous studies showing a protective effect of mild depolarisation on neuronal survival (Iacovitti et al., 1999; Xu et al. 2000; Mennerick and Zorumski, 2001).

The PI stain detects necrotic and apoptotic cells that have lost their membrane integrity. Whereas the loss of membrane integrity occurs quite early in necrosis, it happens very late in the apoptotic process (Darzynkiewicz and Li, 1996). Therefore, relying solely on the PI method may provide an incomplete account of cell viability as this could potentially exclude a proportion of dying cells in early stages of apoptosis. To improve on this and include early-stage apoptotic cells in the assay, I performed a cell viability count based on the Hoechst 33258 stain. Hoechst 33258 is a blue fluorescent dye that is incorporated into the nuclei of both apoptotic and necrotic cells. Dying and viable cells can be distinguished on the basis of nuclear morphology. Viable cells have regularly shaped oval or round nuclei, which are uniformly blue. Dying apoptotic cells, on the other hand, have bright blue nuclei that appear shrunken, condensed or fragmented (Figure 4.10c). To estimate whether the rate of apoptosis in the KCl-treated neurons is different from control cells, I counted the number of condensed/fragmented nuclei in each condition. The values were expressed as the number of apoptotic nuclei per mm^2. Despite a noticeable increase in the number of apoptotic cells during development, there were no significant differences in apoptosis between KCl-treated and control cultures. Similarly to the PI assay, I noticed a distinct trend towards a lower rate of apoptosis in the KCl-treated cells, providing further support for the potential protective role of 20mM KCl on neuronal survival.

The PI and Hoechst stain allow detection of dead cells that have undergone a recent apoptosis or necrosis. However, if KCl treatment induces rapid, early changes in cell viability, they would go undetected in the post-16-hour assay. To overcome this limitation, cell viability was further assessed by comparing the number of viable, 'surviving', cells in each condition. Viable cells were distinguished from dead cells by the morphological appearance of the Hoechst stain, as described previously (Figure 4.10c). The number of viable cells was counted collectively, for all

hippocampal cell types, as well as separately for each excitatory cell type. As our hippocampal cultures are always plated at the same density, any variation in cell number should reflect the effect of the KCl treatment. In agreement with the previous results, there were no significant differences in collective cell counts between the KCl and control conditions (Figure 4.10e). Likewise, individual cell counts of either granule or pyramidal neurons did not reveal any significant differences between the treated and untreated conditions (Figure 4.10 f, g), indicating that KCl-induced depolarisation did not cause extensive cell death at any time between the onset and the end of the treatment.

From the above assays it can be seen that cell death cannot explain the reduction in AIS-positive cells in response to KCl treatment. Previous work in our culture system also showed an absence of ongoing neurogenesis, as culturing the cells in the presence of the thymidine analogue BrdU to label dividing neurons did not detect any cell division (Evans et al., 2013). Therefore, KCl treatment must affect the AIS selectively since a lower proportion of AIS-positive neurons was not a consequence of compromised cell viability or increased density of AIS-negative new-born neurons. In addition, visual examination of the axons of 4 DIV neurons did not detect any instances of increased axon degeneration in the KCl-treated cultures (see chapter 3), thus further emphasising that the loss of AnkG immunofluorescence was not a result of axonal degeneration.

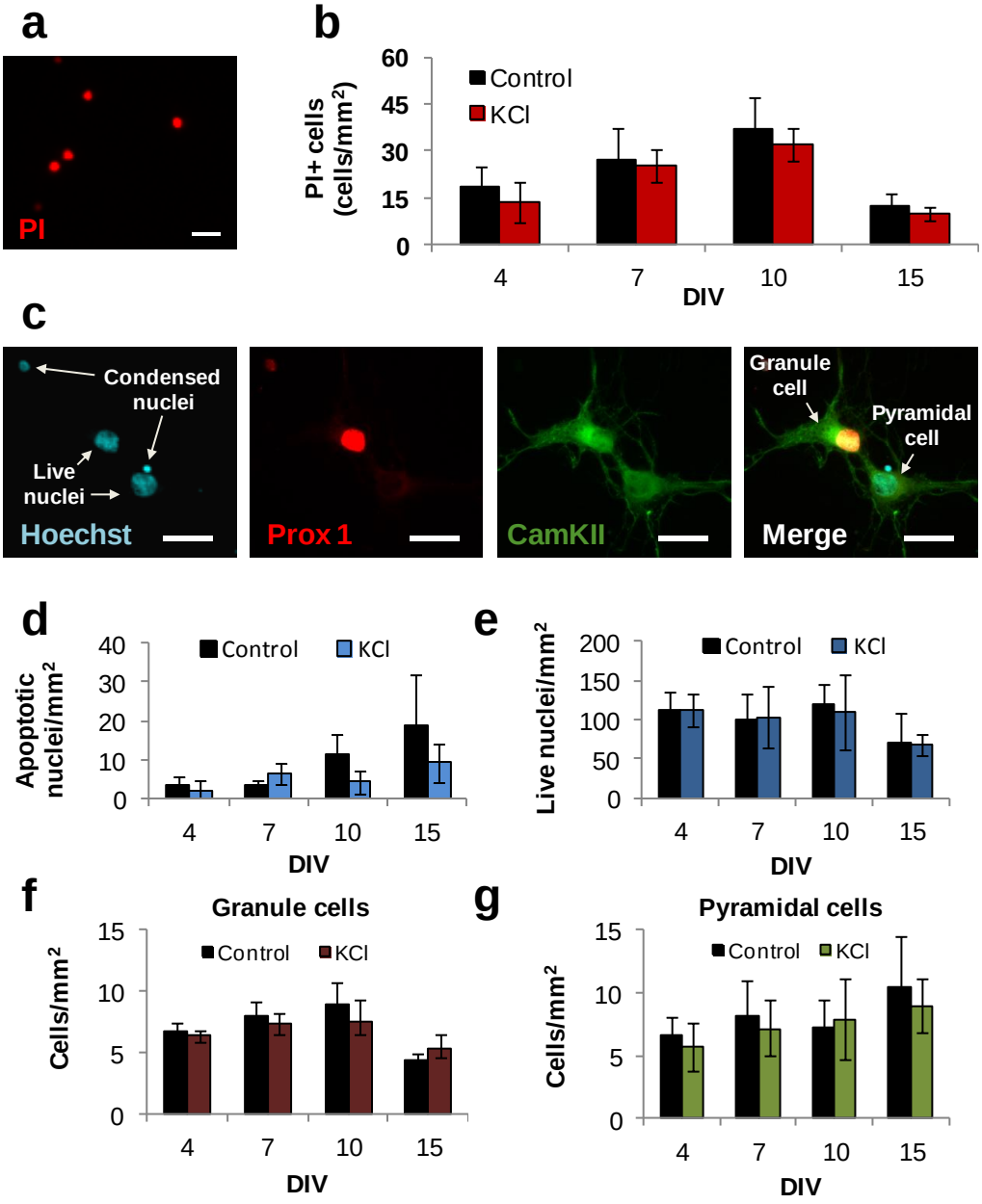

Figure 4.10 16-hour depolarisation with 20mM KCl did not compromise cell viability. (a) Example of cell nuclei stained with propidium iodide (PI). (b) The density of PI-positive (PI+) cells following a 16-hr KCl treatment (red) as compared to the PI+ control neurons (black) at four different stages of development. (c) Example image of a granule and pyramidal cell stained with Hoechst 33258. Condensed nuclei are indicative of dead or dying cells. Live cells have regularly-shaped, round or oval nuclei that are uniform in fluorescence (left). (d, e) Graphs showing the density of apoptotic (d) and live (e) nuclei in control (black) and KCl (blue) conditions. (f, g) Graphs showing the density of granule (f) and pyramidal (g) cells in control (black) and KCl (red, granule; green, pyramidal) conditions. None of the differences observed between the control and KCl conditions were statistically significant. Error bars, SD. Scale bar, 20 µm.

4.8 AIS disassembly in response to depolarisation is relatively rapid

Having established a clear relationship between chronic depolarisation and a cell death-independent decrease in AIS numbers, I now proceed to characterise this effect in greater detail. The aim of this section is to investigate how long it takes for AISs to disappear in response to depolarisation. So far, I have established that a 16-hour treatment has a strong effect, but perhaps shorter treatments would be sufficient to elicit a comparable result.

To test this, I have established a time-course of KCl treatment, where hippocampal cultures were depolarised with 20mM KCl for different amounts of time. In this experiment, KCl was added at 6 DIV and the cells were fixed after 1, 3, 6, 12 or 24 hours of depolarisation (Figure 4.11a). Fixed cells were consequently immunostained for the AIS and specific neuronal markers to label the two excitatory cell types. The results were expressed, as previously, in terms of percentage of cells containing an AIS. Strikingly, in both classes of excitatory neurons, KCl–induced depolarisation led to a rapid loss of AnkG immunofluoresce within the first few hours of the onset of treatment. In granule cells, this effect was seen as early as after 3 hours of depolarisation (Mann-Whitney U test, $P < 0.0001$; figure 4.11b), reaching its maximal level after 6 hours and remaining steady until 24 hours following the addition of KCl. In pyramidal cells, the response to KCl treatment was slower, since a significant difference between the conditions was detected only after 6 hours in KCl (Mann-Whitney U test, $P < 0.0001$). Prolonging the depolarisation to 24 hours did not induce a further decrease in AIS-positive pyramidal neurons.

The results described above suggest that the KCl-induced decrease in AnkG immunofluorescence is a rapid, early-onset event that can be seen within hours of the addition of the depolarising agent. They also provide more information regarding a potential mechanism behind the lower number of AIS-positive neurons in the KCl condition. In the previous section I have shown that a decrease in cells containing an AIS was not due to selective cell death. However, it was still not clear whether the KCl effect was due to active disassembly of the AIS or a reduced rate of AIS formation in the depolarised cultures. All AIS experiments described in this thesis were carried out during a period of on-going AIS assembly, therefore a lower number of AIS-positive cells may reflect the prevention of AIS formation or a delay in this process, rather than an active disruption of the AIS structure itself. The experiments described in this section, however, were performed within a narrower

developmental time window. There was no noticeable increase in AIS numbers within the first 6 hrs in the control conditions (Figure 4.11). Therefore the drop in AIS numbers below the control levels in the KCl treated cultures indicate an active disassembly of the AnkG scaffold rather than just an impeded AIS formation. Thus, on the basis of the current data, it can be concluded that KCl treatment caused a rapid disassembly of the AnkG protein at the AIS, independent of cell death or axonal degeneration.

4.9 The changes in AIS properties have a rapid onset

In the previous section I have shown that depolarisation-induced AIS disassembly is a rapid event, becoming evident after 3 hours of treatment and reaching its maximal level after 6 hours of depolarisation. Not all AISs, however, undergo a complete disassembly in response to KCl treatment, leaving a considerable number of neurons that retain their AISs. I have previously shown that cultures treated with KCl for 16hrs have shorter, more proximally located AISs than the untreated cultures (Figure 4.8). How early can we detect these changes? If 6 hours of depolarisation is sufficient to induce AIS disassembly, is it enough to trigger plastic changes in the remaining AISs?

To test this, I measured the position and length of the AIS after different durations of KCl treatment, between 1 and 24 hours (Figure 4.12a). In agreement with previous results, neurons treated with KCl had an AIS closer to the cell body than neurons left in control medium (Figure 4.12). After 3 hours of depolarisation there was already a noticeable trend towards a more proximal AIS. This rapid early response to depolarisation was seen for both types of excitatory cells, yet it was more pronounced in granule neurons, where the gap between the conditions kept increasing with prolonged levels of depolarisations until it reached its maximal level at 12 hours (Figure 4.12; Mann-Whitney U test, $p = 0.009$; $n_{Control} = 15$, $n_{KCl} = 12$). After 12 hours of depolarisation, the AISs of KCl-treated granule cells were on average 5.97 µm closer to the soma than the AISs of control neurons. In pyramidal cells, this difference was less pronounced. KCl-treated pyramidal neurons had their AISs on average 2.6 µm closer to cell body than control cultures (Mann-Whitney U test $p = 0.049$, $n_{Control} = 61$, $n_{KCl} = 38$). It is interesting to note that in both cases, the change in AIS position starts to become apparent on the same time-scale as the AIS disassembly.

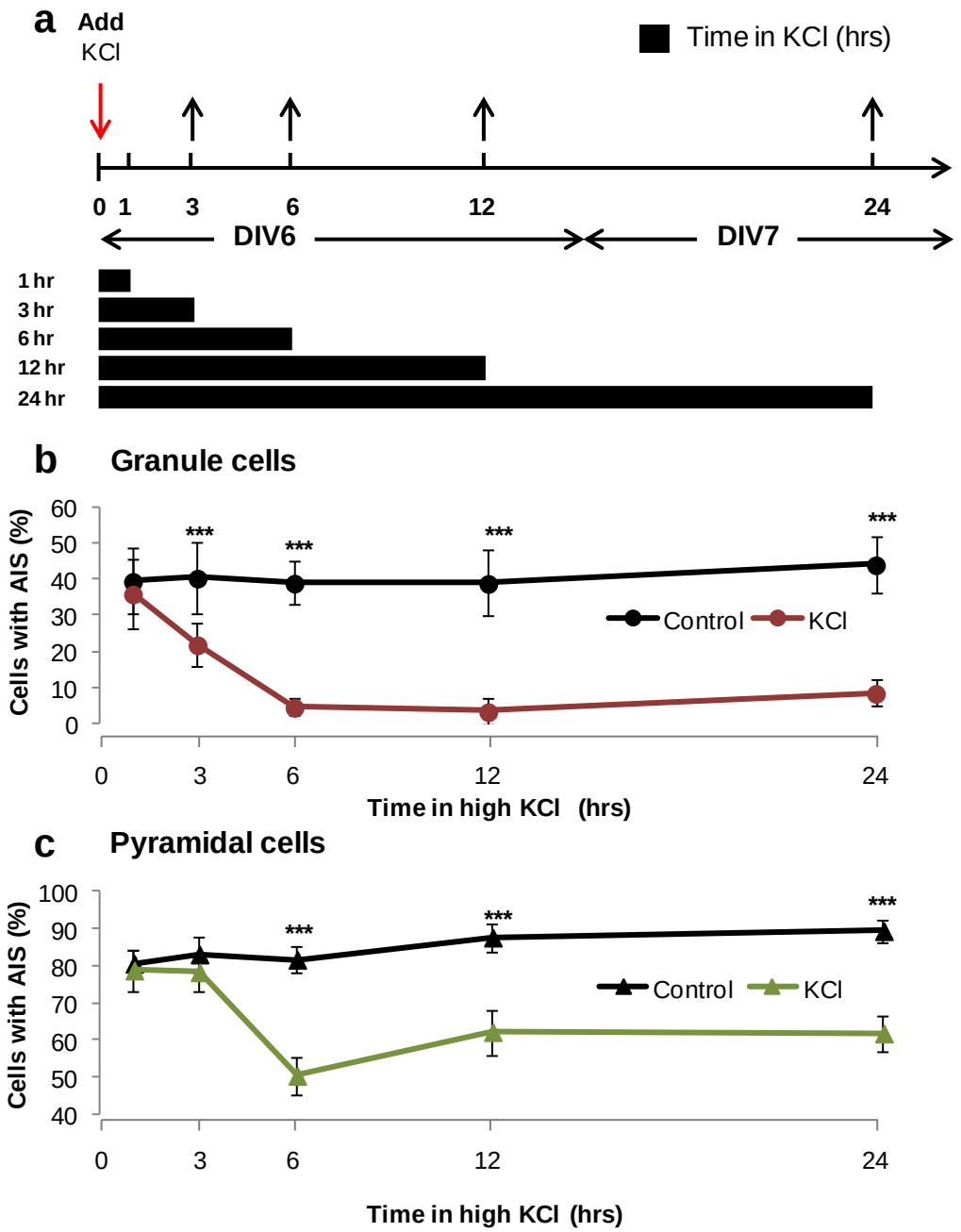

Figure 4.11 KCl treatment induced rapid disassembly of the AIS. (a) A schematic diagram showing the time-line of exposure to KCl. Red arrow indicates the addition of 20mM KCl at time point 0 (6 DIV) Black arrows indicate the time points at which the cells were fixed and analysed. Horizontal arrows show the developmental time points of the treatment, which was carried out between 6 and 7 DIV. Black bars illustrate different durations of depolarising treatment. (b, c) Graphs showing the percentage of granule (b) and pyramidal (c) neurons with detectable AISs as a function of time in KCl. Black lines denote untreated control cells, red and green lines denote KCl treated granule and pyramidal cells, respectively. There was a significant decrease in the percentage of granule neurons after only 3 hours in KCl, which was maximal after 6 hours of the treatment(Mann-Whitney U test, $P < 0.0001$). Pyramidal cells responded more slowly to KCl than granule cells. A significant decrease in the AIS-positive cells was seen only after 6 hours of depolarisation (Mann-Whitney U test, $P < 0.0001$). Prolonging the duration of depolarisation beyond 6 hours did not lead to a further decrease in AIS numbers in either granule or pyramidal neurons. Error bars, SD.

A change in AIS length was also detectable within the first few hours of the treatment. Strikingly, granule neurons had significantly shorter AISs after only 3hrs of depolarisation (Mann-Whitney U test, $p = 0.009$, $n_{Control} = 11$, $n_{KCl} = 11$). After this time, the AISs of KCl-treated granule cells were on average 6.8 µm shorter than the AISs of control neurons. However, this effect was transient and became insignificant beyond the three hour stimulation. In pyramidal cells, a significant difference in AIS length was detected only after 12 hours of KCl treatment, when the AISs of chronically depolarised neurons were on average 3.65 µm shorter than the AISs of control cells (Mann-Whitney U test, $p = 0.001$, $n_{Control} = 66$, $n_{KCl} = 31$), but not at other time points. It thus appears that changes in AIS length may represent an additional form of short-term plasticity in young hippocampal neurons, but this still remains to be confirmed and studied in more detail.

Together these results show that depolarisation-induced changes in AIS properties have a rapid onset, on the same timescale that was shown to be sufficient for AIS disassembly. Excitatory neurons respond rapidly to increased levels of depolarisation by either completely dismantling the AIS or slightly modifying AIS properties. In both cases, these changes are detectable within the first few hours of treatment. Because AIS disassembly occurred in parallel to the change in AIS properties, it was not possible to establish whether the changes seen in AIS location were due to existing AISs moving closer to the cell body or to a selective disassembly of distally-located AISs. This is a critical point that needs to be addressed more closely in the future since it would help illuminate potential mechanisms behind population-wide AIS disassembly.

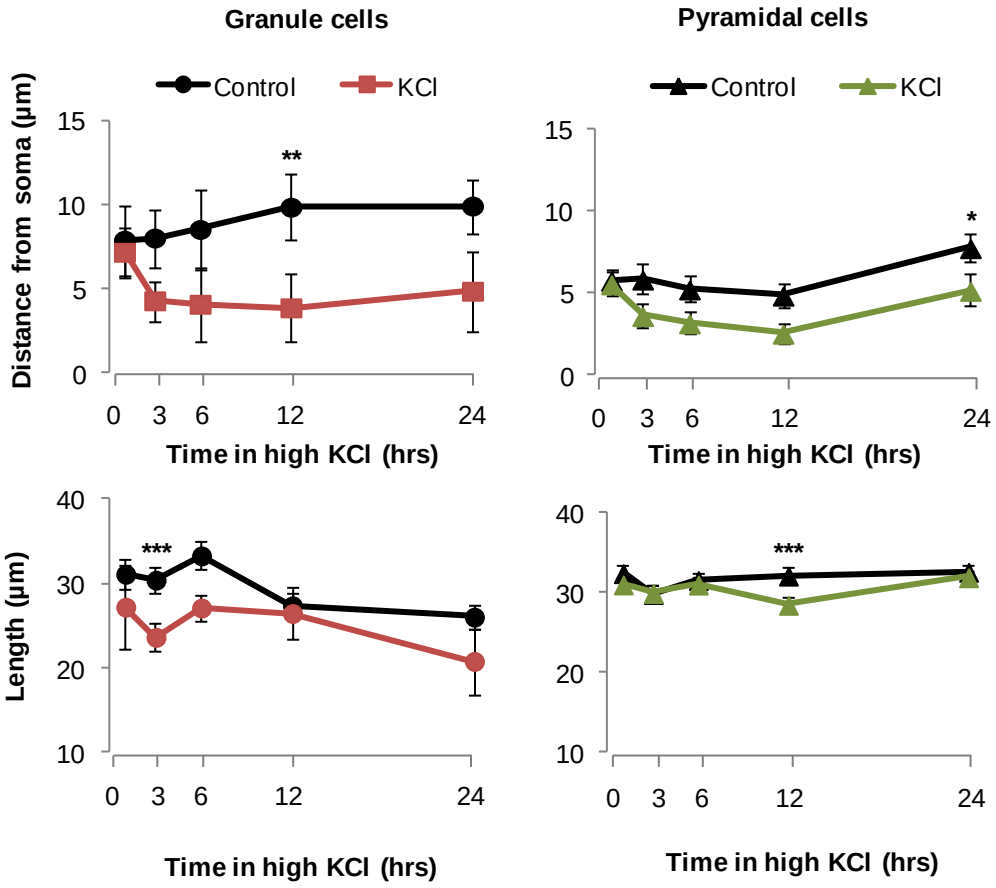

Figure 4.12 KCl treatment induces rapid sustained changes in AIS properties. The graphs showing AIS position (expressed as the distance from the cell body; top) and length (bottom) as a function of time in KCl, for granule (left) and pyramidal (right) neurons. Black lines indicate control cells, whereas red and green lines denote KCl-treated granule and pyramidal cells, respectively. The AISs of KCl treated cells were generally closer to the soma than the AISs of non-treated cells. In granule cells, a noticeable difference in AIS position could be seen after 3hr of KCl treatment, yet a statistically significant effect was detected only after 12 hours of depolarisation ($p = 0.01$; $n_{Control} = 15$, $n_{KCl} = 12$). A similar trend was observed in pyramidal neurons. A trend towards a change in AIS position was already seen after 3 hours in KCl, but a statistically significant difference was detected only after 24 hours of depolarisation ($p = 0.05$, $n_{Control} = 61$, $n_{KCl} = 38$). Significant changes in AIS length were detected after 3hrs of KCl treatment in granule ($P = 0.009$, $n_{Control} = 11$, $n_{KCl} = 11$) and after 12 hours in pyramidal cells ($p = 0.001$, $n_{Control} = 66$, $n_{KCl} = 31$). All significance tests were carried out with the Mann-Whitney U-test. Error bars, SEM.

4.10 Longer depolarisation periods do not lead to large-scale AIS disassembly

Previous experiments showed that chronic depolarisation with high levels of KCl has two distinct effects: a complete disassembly of the AIS in a subset of cells and altered properties of the remaining AISs. Both of these changes occur rapidly, within hours of the addition of the depolarising agent, suggesting they might be in some way related. Therefore it is possible that the change in AIS properties precedes a complete AIS disassembly and all cells eventually lose their AIS, provided the depolarising treatment is sufficiently extended. In previous experiments, I used a maximum of 24 hours of KCl treatment. What are the consequences of extending this treatment? (1) Do more cells disassemble their AIS, or perhaps (2) no further AIS disassembly takes place but AISformation is blocked. Alternatively, (3) do the cells desensitise to the treatment and begin forming new AISs?

To answer the above questions and elucidate the chronology and the scale of the AIS disassembly in response to chronic depolarisation, I extended the KCl treatment from 24 hours to 8 days (Figure 4.13a). The results were expressed in two complementary ways: (1) as a percentage of AIS-containing cells in KCl and control conditions, which takes into account developmental changes in the AIS numbers, and (2) as the magnitude of the AIS disassembly, for better illustration of the extent of the effect. The magnitude of AIS disassembly was expressed as the percent difference between the numbers of AIS-positive cells in control and KCl conditions.

First I investigated the effect of extended depolarisation on the number of AIS-positive cells. For both cell types, 6 to 96 hour depolarisation had a significant effect on the number of AIS-positive cells (Mann-Whitney U-test, $P < 000.1$), however no significant changes were observed when the depolarising treatment was extended from 96 to 168 hours (8 days; Figure 4.13b, top). Interestingly, despite consistently fewer numbers of AIS-positive neurons in KCl-treated cultures, there was a gradual increase in the number of AISs in depolarised neurons, indicating an ongoing AIS formation in the depolarised cultures. The overall magnitude of AIS disassembly was more pronounced in granule than in pyramidal cells, which is consistent with the previous results. The maximal effect was seen after 12 hours for granule cells (Figure 4.12 bottom; 90.86% disassembly, $n_{Control} = 33$, $n_{KCl}= 26$) and after 48 hours for pyramidal cells (46.75% disassembly, $n_{Control} = 174$, $n_{KCl}= 125$). Extending depolarisation beyond these points did not lead to any further increase in the AIS

removal. On the contrary, there was a gradual decline in the magnitude of AIS disassembly until hardly any effect was seen after 8 days in KCl (Granule: 8.34% disassembly, $n_{Control}$ = 48, n_{KCl}= 38; Pyramidal: 5.29 % disassembly, $n_{Control}$ = 128, n_{KCl}= 67). These results show that the depolarising treatment was effective only until a certain point, beyond which the sensitivity of the cells to the treatment gradually declined.

Taken together, these results show that prolonging the duration of the depolarising treatment did not lead to a complete AIS disassembly in all neurons. On the contrary, extending depolarisation beyond a certain point (12 hours for granule and 48 hours for pyramidal cells) resulted in a gradual desensitisation of neurons to the treatment and resumption of AIS formation. It is not clear whether the loss of sensitivity to KCl was due to the extended period of depolarisation or an ongoing 'maturation' of the hippocampal culture. I have previously shown that hippocampal excitatory cells are less sensitive to KCl in later stages of development (section 4.6), suggesting that the effect described here may be linked to a developmental stage of the neuron rather than the duration of the depolarising treatment. There is a possibility that the initial increase in AIS disassembly in pyramidal cells was due to a selective cell death of AIS-positive neurons as no cell viability assays were performed past the 24 hour treatment.

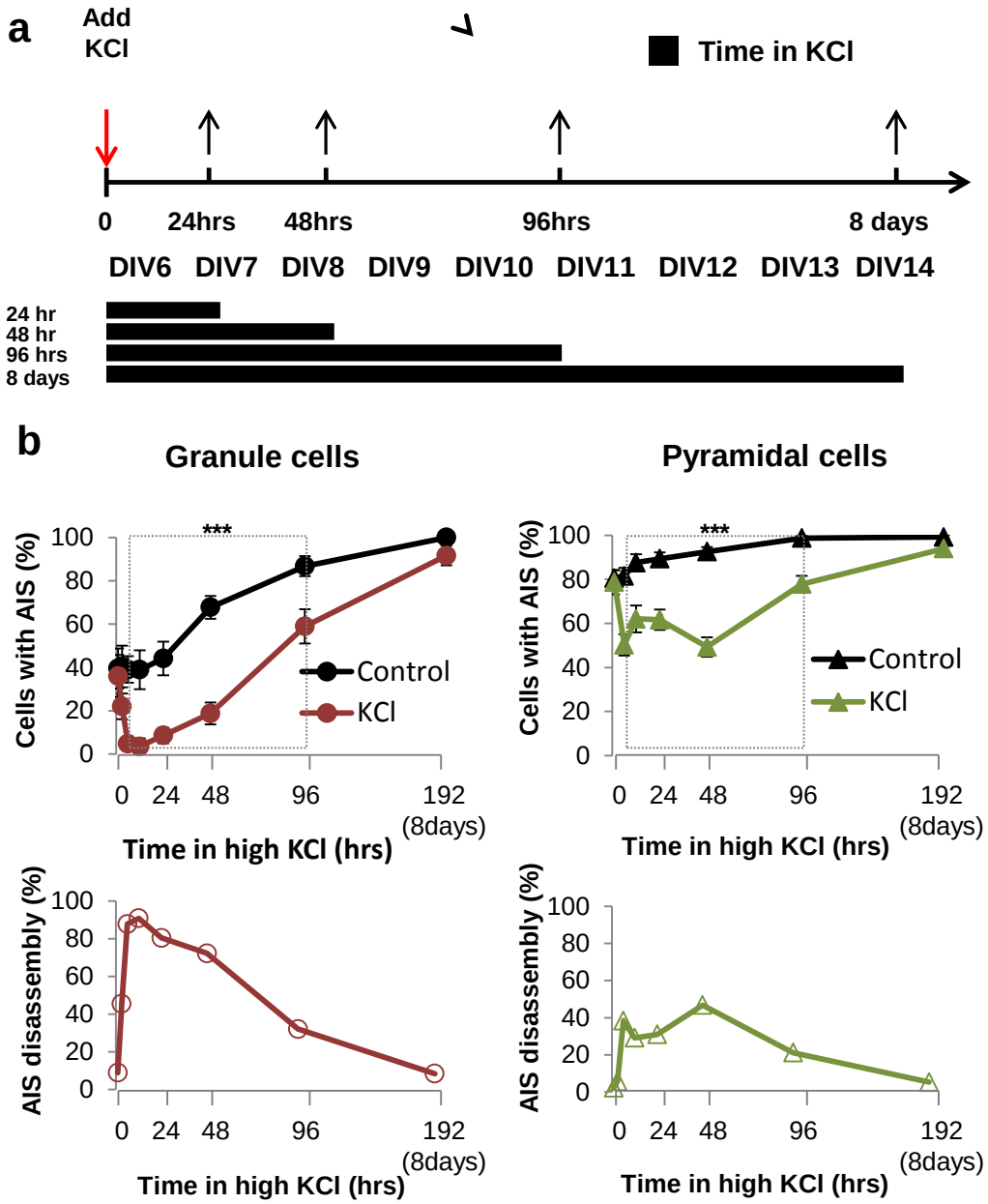

Figure 4.13 Chronically depolarised neurons desensitise to KCl treatment. (a) Schematic of the experiment. KCl was added at time 0 (red arrow). After 3, 6, 12, 24, 48, 72 and 192 hours of depolarisation, the cells were fixed and immunostained for cell type-specific markers (black arrows). Black bars indicate the time in KCl. (b) The graphs at the top show the percentage of AIS-positive cells as a function of time in KCl. The black line indicates control cells, the red and green lines KCl-treated granule and pyramidal cells, respectively. The dotted box indicates the period of significant change in AIS numbers (Mann-Whitney U-test, $P < 0.0001$). The graphs at the bottom show the magnitude of change between the conditions, expressed as the percent difference between the control and KCl conditions. The graph on the left shows the magnitude of change in granule cells, whereas the graph on the right shows it for pyramidal neurons. Note that the magnitude of AIS disassembly peaks after 12-48 hours of depolarisation but then gradually declines until there is no more difference between control and treated cells after 8 days of treatment.

4.11 AIS properties change in response to long-lasting depolarisation

4.11.1 AIS properties after 24-48 hours of the KCl treatment

After 24 hours in KCl, there is ongoing AIS disassembly in pyramidal cells but not in the granule neurons. In granule neurons, the numbers of AISs began to rise again, suggesting that new AISs had began to form despite ongoing depolarisation. What are the properties of newly formed AISs? Do they exhibit developmental characteristics of early AISs, as the ones seen between 2 and 4 DIV or do they match the current developmental stage of the cell (8 DIV)? To answer these questions, I measured the position and length of granule neuron AISs after a 48-hour KCl treatment. I did not detect any changes in the AIS position, however there was a clear (but not significant) trend towards AIS lengthening, suggesting an emergence of a distinct population of very long AISs following a 48-hour KCl treatment (Figure 4.14, left). Long AISs are characteristic of young (4 DIV) granule neurons that have only begun forming an AIS. Therefore, it is likely that newly developed AISs in the depolarised granule neurons begin to form 'from scratch', matching the characteristics of immature AISs seen in the earliest stages of AIS formation. A lack of statistical significance of this effect was most likely due to a higher variability in the AIS properties of the depolarised cultures as compared to the controlled cells. This may reflect a presence of a mixed population of AISs with distinct properties: the 'old' AISs that did not undergo disassembly and the AISs that were just beginning to form.

In contrast to granule cells, pyramidal cells showed no new AIS formation after 48 hours of depolarisation and AIS disassembly was still ongoing. Which AISs are targeted for disassembly? Previously I have shown that neurons have more proximally located AISs after 24 hours of depolarisation. If depolarisation causes a preferential removal of distal AISs, a proximal shift in the AIS position should be even more pronounced after 48 hours of treatment. This, however, was not the case in pyramidal neurons. I did not detect any statistically significant change in either AIS position or length between 24 and 48 hours of depolarisation, even though there was a small, non-significant trend towards AISs lengthening (Figure 4.14, right). Therefore there was no indication that depolarisation-induced AIS disassembly selectively targets only distally-located AISs.

4.11.2 AIS properties after 48-168 hours of depolarisation

Previously I have shown that extending depolarisation beyond 48 hours did not result in any further decrease in the number of AIS-positive cells. On the contrary, the magnitude of AIS disassembly gradually declined until hardly any difference between the conditions was noticeable after 8 days in KCl. What was the reason behind this apparent lack of the KCl effect? Did the cultures become desensitized to high levels of KCl? Or perhaps the neurons remained sensitive to depolarisation, but did not respond to it with the AIS disassembly? If the first possibility is true, then extending the depolarisation treatment beyond 48 hours should not lead to any further changes in the AIS properties. If, however, the treatment was still effective but just not leading to AIS disassembly, I should be able to detect further changes in AIS properties, reminiscent of those previously shown in the lab (Grubb and Burrone, 2010).

Indeed, that is what I observed. In both cell types there was a distinct change in AIS properties following 96 hours of treatment. Interestingly, the changes were of the opposite direction to the ones seen after 24-48 hours of depolarisation. 96- and 168-hour (8-day) treated granule cells had more distally located AISs (Mann-Whitney U-test, $P < 0.0001$. 96 hrs: Control, 5.74 ± 4.85 µm, n = 24; KCl, 10.07 ± 8.58 µm, n = 11. 168 hours: Control, 0.55 ± 1.37 µm, n = 32; KCl, 12.12 ± 11.26 µm, n = 17), which were also significantly longer than the AISs of untreated neurons (Mann-Whitney U-test, $P < 0.0001$. 96 hrs: Control, 22.65 ± 2.76 µm, n = 24; KCl, 34.12 ± 10.51 µm, n = 11. 168 hours: Control, 23.39 ± 5.37 µm, n = 32; KCl, 30.59 ± 7.64 µm, n = 17). In pyramidal cells, no significant change in either length or position was seen between 48 and 96 hours of treatment, however, a significant difference between the conditions was observed after 8 days in KCl (Mann-Whitney U test, $P < 0.0001$, $n_{Control} = 30$, $n_{KCl} = 25$). The AISs of treated neurons were on average shorter (Control: 33.45 ± 5.42 µm; KCl: 26.97 ± 5.59 µm) and located further away from the soma (Control: 0.43 ± 1.31 µm, KCl: 6.54 ± 7.20 µm) than the AISs of untreated cells. Thus, after 8 days of KCl treatment, the AISs of both cell types were closer to the cell body, however the AISs of granule cells were on average longer, whereas the AISs of pyramidal neurons - shorter, than the control cells (Figure 4.14).

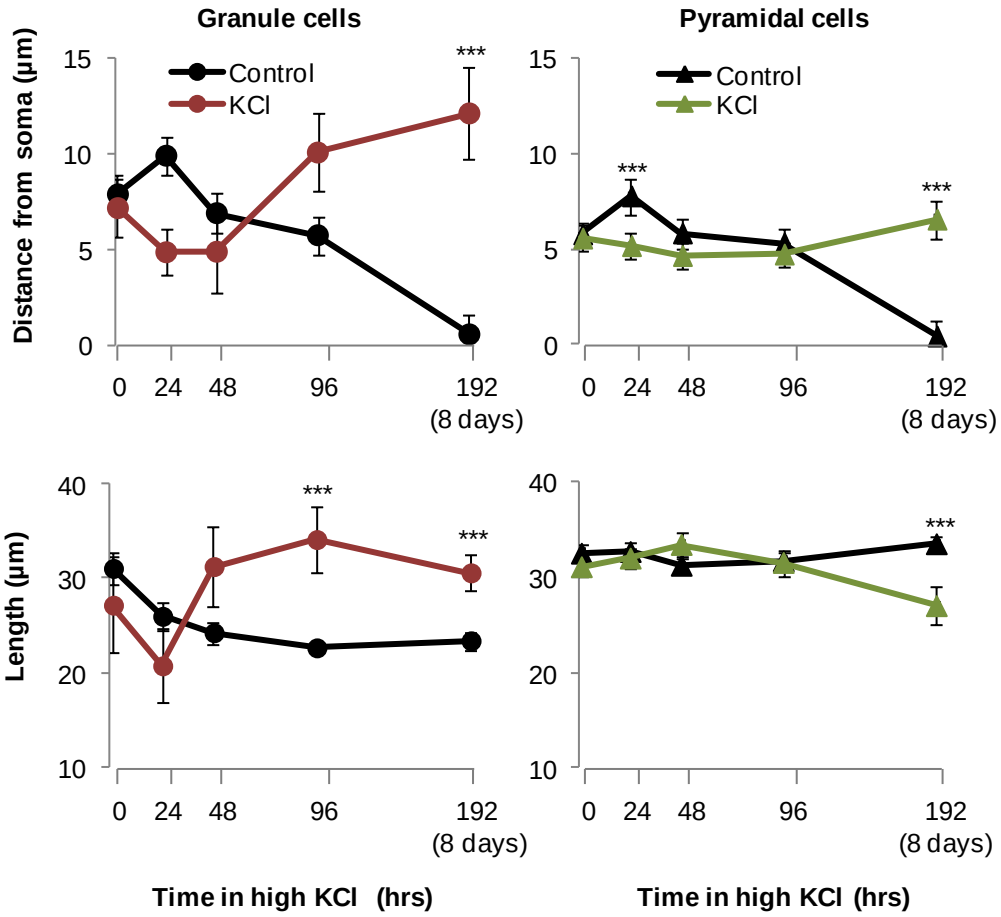

Figure 4.14 Extending the duration of depolarisation resulted in a marked change of AIS properties. Graphs showing position (top) and length (bottom) of the AIS in control neurons (black line) and KCl-treated cells (red line for granule and green line for pyramidal cells). In granule cells, significant differences in AIS position were observed only after 8 days in KCl ($P < 0.0001$ $n_{Control} = 32$, $n_{KCl} = 17$), whereas in pyramidal cells significant differences were detected at two time-points: after 24 ($p = 0.049$, $n_{Control} = 61$, $n_{KCl} = 38$) and 168 hrs ($P = 0.005$, $n_{Control} = 30$, $n_{KCl} = 25$). There was a significant change in AIS length in both cell types after 168 hours of depolarisation ($P < 0.0001$. Granule: $n_{Control} = 32$, $n_{KCl} = 17$, Pyramidal: $n_{Control} = 30$, $n_{KCl} = 25$) and also after 96 hours for granule cells ($P < 0.0001$, $n_{Control} = 24$, $n_{KCl} = 11$). Note that the change in length was in opposite directions for different cell types. Error bars, SEM.

4.12 The AISs of chronically depolarised cells are reminiscent of newly-formed AISs

In this section I investigate the dynamics of AIS properties in more detail. To better visualise the chronology of the change I plotted the differences between treated and untreated cells as a function of time in KCl (Figure 4.15a). The differences were expressed in µm of change, where positive values indicate an increase in length or distance from the soma, whereas negative values show a decrease relative to control values. Overall, this measure should provide more insight into the chronology of the changes in AIS properties, and thus help elucidate the mechanism behind the depolarisation-induced AIS remodelling.

The dynamics of the AIS properties in response to ongoing depolarisation were investigated separately for granule and pyramidal neurons. In granule cells, the initial response to KCl treatment was a rapid decrease in AIS length together with a proximal shift in the position of the AIS, which was detectable after only 6 hours of depolarisation. After 24 hours in KCl (at 7 DIV) however, there was a rapid and sustained increase in the AIS length, which was followed by a gradual distal AIS shift. In pyramidal cells, the dynamics of the change were at first similar to the granule cells, but later followed a different course. Just like granule cells, pyramidal neurons initially responded to KCl treatment by a proximal shift of the AIS and a decrease in the AIS length. After 24 hours of depolarisation, there was a small increase in the AIS length, but no change in the AIS position. After 8 days of depolarisation (14 DIV) there was a dramatic change in the AIS position and length, such that the AISs of KCl-treated pyramidal neurons were significantly more distal and shorter than the AISs of control cells.

Together, these results show that there is a developmental 'switch' in the cell's response to KCl, which occurs earlier for granule (after 24-48hrs, 7-8 DIV) than pyramidal cells (after 96-168 hours, 10-14 DIV). What is more, the depolarisation-induced distal shift in AIS position was always preceded by lengthening of the AIS, an observation that might provide an insight into the mechanism of AIS remodelling in response to high activity. It is not clear, however, whether the changes in AIS properties were due to the increasing length of depolarisation or the developmental stage of the neuron. In any case, the AISs of cells that had been depolarised for 8 days (14 DIV) strikingly resembled the AISs of immature neurons at 4 DIV.

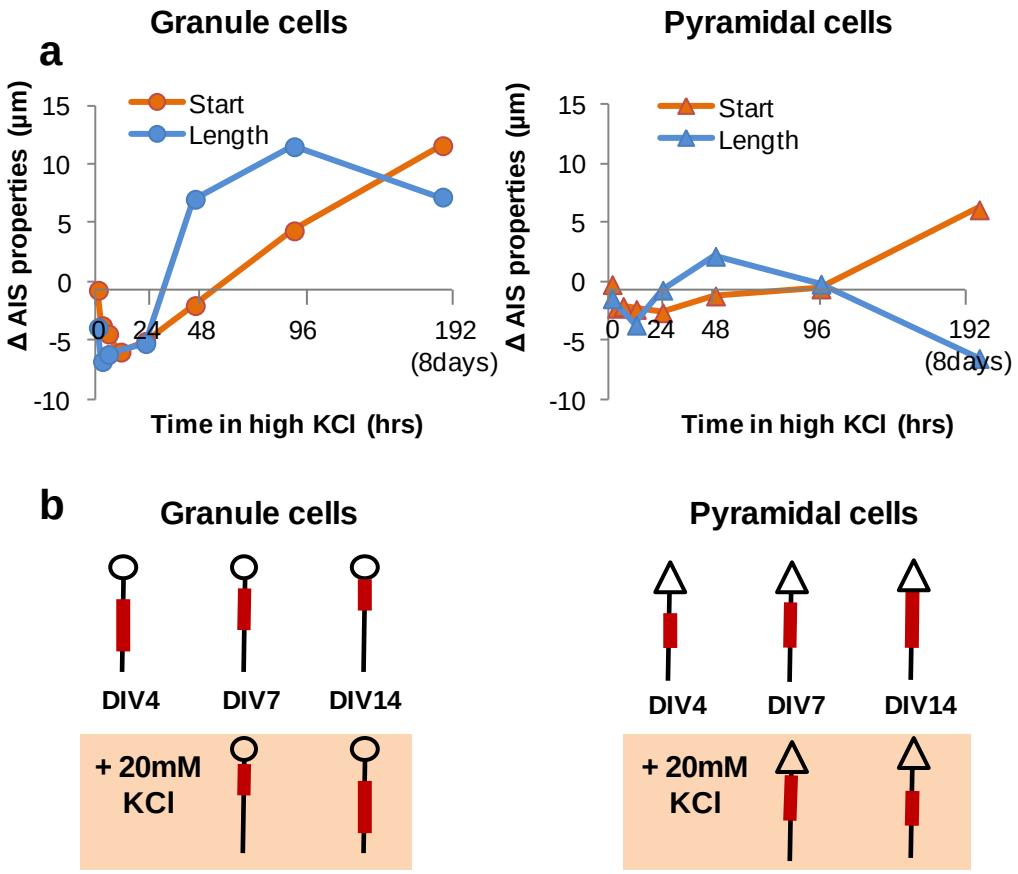

Figure 4.15 The chronology of changes in AIS properties in response to KCl treatment. (a) Graphs showing a relative direction and magnitude of the change in AIS length (blue line) and start position (orange line, expressed as a distance from the soma). The values indicate the relative change observed in KCl-treated cultures normalised to control cells. Positive values indicate an increase, whereas negative values a decrease in the AIS length or distance from soma. Note the shift in the direction of change occurred between 24-48 hours for granule cells and 48-96 hours for pyramidal cells. (b) Schematic representation of the AIS at different stages of development in control condition (top) and after the addition of KCl at DIV6 (bottom, orange box). Note the similarity of the AIS at 4 DIV in control conditions and at 14 DIV after the KCl treatment.

4.13 The neurons recover the AIS upon removal of depolarisation

In the previous sections I have shown that chronic depolarisation results in rapid, cell-death independent AIS disassembly in a subset of excitatory cells. Even though the neurons eventually desensitise to the effect of KCl treatment and cease to disassemble their AISs, this does not fully take place until after 8 days of depolarisation, when the cultures reach 14 DIV. Until 10-11 DIV, the cells are still sensitive to the KCl treatment and there is a significant difference in AIS numbers between treated and control cultures. Can we bring the AIS numbers back to control levels before the cells begin desensitising to KCl if we remove the source of depolarisation?

To answer this question and investigate whether the changes observed after KCl treatment can be reversed, I removed KCl from a subset of cells and let them recover from a 24-hour KCl treatment in normal culture medium. KCl, as in the previous experiment (section 4.10), was added at 6 DIV, left in the culture medium for 24 hours, then removed and replaced with fresh control medium. The prediction was that if the cells do recover their AISs, it would take place rather slowly, as new AISs would have to form. Therefore I have used 24- , 72- and 162-hours (7 days) recovery periods, each starting from the end of the 24-hour treatment (Figure 4.16a). After each recovery period, the cultures were fixed, stained for the AIS and cell-type-specific markers and imaged. I then counted the number of AIS positive cells. As controls I have used untreated cultures of the same developmental stage and the cultures that were treated with KCl continuously. Strikingly, both granule and pyramidal cells recovered their AISs upon removal of KCl. The rate of recovery was quite slow and full recovery was only observed after 72 hours in granule cells and 7 days in pyramidal cells (Figure 4.16b, c).

The slow rate of AIS recovery was probably due to the cells having to start the AIS formation ‘from scratch’. Because of the population-wide nature of this research, it is not clear how quickly a single neuron can assemble an AIS. I have previously shown that AIS disassembly is a rapid event (Figure 4.11), however it seems that the AIS formation requires significantly more time. Moreover, removing KCl brings the AIS numbers back to control levels before the cells begin to desensitise to KCl treatment but when AIS disassembly has already begun to decrease. This suggests that KCl treatment, apart from inducing AIS disassembly, may act as a

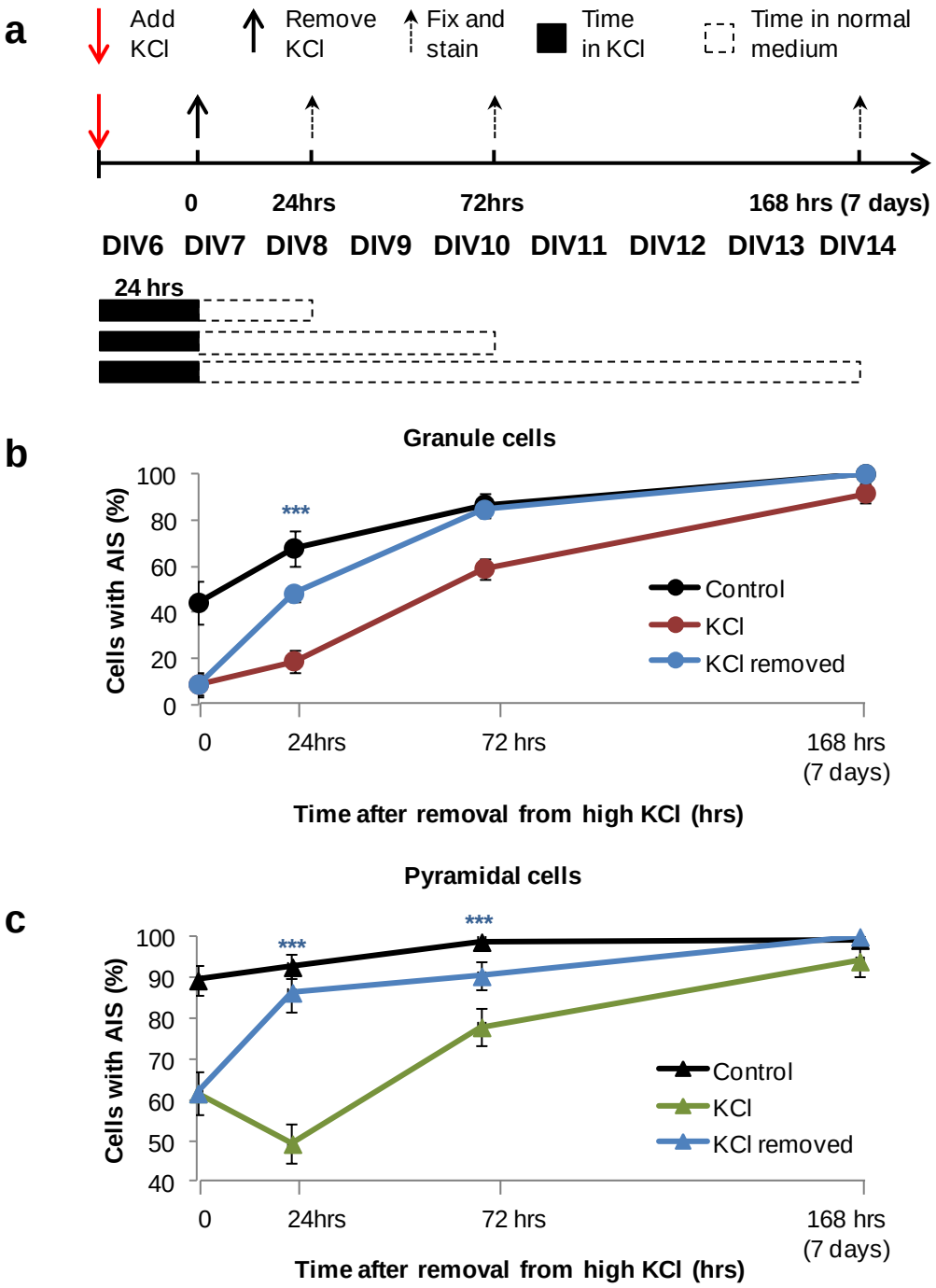

Figure 4.16 The number of AIS-positive cells recovers back to control levels upon removal of KCl. (a) Schematic of the experiment. The cultures were depolarised for 24 hours (red arrow signifies addition of KCl and black arrow the removal of KCl-containing medium and its replacement with the normal medium). The cells were fixed after 24, 72 and 168 hours of recovery in the normal medium (dotted arrows). The black and white bars represent the duration of KCl treatment and the recovery periods, respectively. (b and c) Graphs showing the percentage of granule (b) and pyramidal (c) cells as a function of time in KCl. Black lines indicate control neurons, green and red lines the neurons to which KCl was added at 6 DIV and the blue lines indicate the recovering neurons. Asterisks indicate statistical significance between the control (black line) and recovering (blue line) neurons ($P < 0.0001$, Mann-Whitney U-test).

developmental block' for the formation of new AISs. The results of this experiment also provide further support for intact cell viability of KCl-treated cultures.

4.14 AIS properties recover to control levels upon removal of KCl

In the previous section I showed that removing KCl from depolarised cultures and allowing the cells to recover in normal medium brings the proportion of AIS-positive neurons back to control levels, suggesting that new AISs have formed in the recovering cultures. What are the properties of these AISs? Do they resemble the AISs of young immature neurons at 4 DIV or do they match the AIS characteristics of the current developmental stage (8-14 DIV)? What happens to the properties of the AISs that were modified by KCl treatment? Previous work from our lab showed that removing KCl after 48 hours of depolarisation and letting the cells recover in normal medium for further 48 hours completely reversed the depolarisation-induced distal shift (Grubb and Burrone, 2010). Do the AIS properties in this experiment also recover back to control levels and how long does it take?

To answer these questions, I measured the length and position of the AIS of recovering cells after 24, 72 and 168 hrs (7 days) of recovery. As in the previous section, I used untreated cells of the same developmental age and cells that were treated with KCl continuously as controls. Interestingly, the AIS properties of both granule and pyramidal cells went back to control levels within the 24 hour period of recovery and remained at the control level until the end of the experiment. Both the position and length of the AIS remained statistically undistinguishable from the control cultures throughout the duration of the recovery experiment (Mann-Whitney U-test, ns. 24 hrs: Granule, $n_{Control} = 23$; $n_{KCl} = 6$; $n_{KCl\ removed} = 10$; Pyramidal, $n_{Control} = 75$; $n_{KCl} = 40$; $n_{KCl\ removed} = 43$. 72hrs: Granule, $n_{Control} = 26$; $n_{KCl} = 9$; $n_{KCl\ removed} = 39$; Pyramidal, $n_{Control} = 42$; $n_{KCl} = 27$; $n_{KCl\ removed} = 46$. 168hrs: Granule, $n_{Control} = 32$; $n_{KCl} = 17$; $n_{KCl\ removed} = 35$; Pyramidal, $n_{Control} = 31$; $n_{KCl} = 25$; $n_{KCl\ removed} = 44$). These results suggest that newly formed AISs in the recovering cultures match the developmental stage of the neuron rather than recapitulate the early steps of the AIS formation (Figure 4.17).

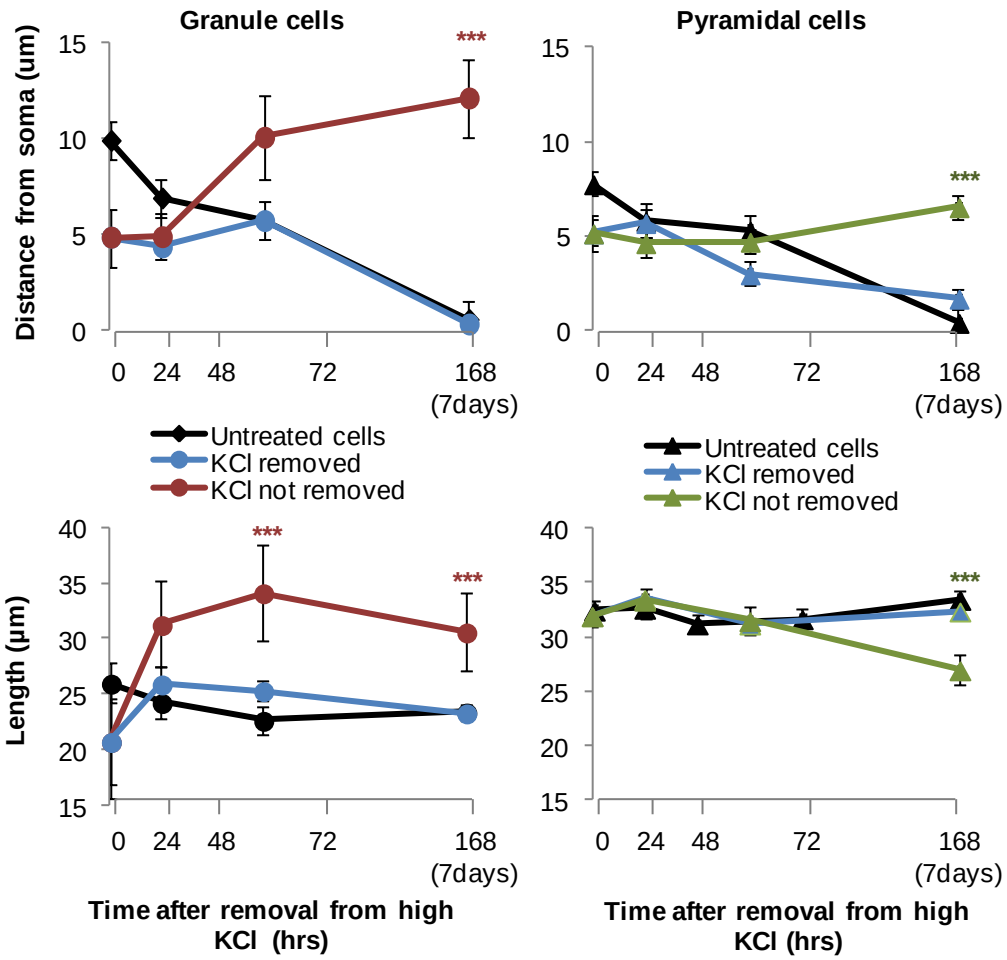

Figure 4.17 AIS properties recover to control levels within 24 hours of removal of KCl. Graphs showing AIS distance from the soma (top) and AIS length (bottom) in granule (left) and pyramidal (right) neurons at various times after the removal of KCl. Black line represents the AIS properties of control untreated neurons, red and green line, the AIS properties of granule (red) and pyramidal (green) cells in KCl and blue line the recovering cells, which had KCl removed after a 24 hour long depolarisation. Asterisks denote statistical significance between the untreated cells and the cells in continuous KCl (Mann-Whitney U-test, $P < 0.0001$).

4.15 Discussion

In this chapter I investigated the role of activity on axon initial segments of excitatory neurons in hippocampal cultures. In our culture system, AIS formation takes place in the first two weeks *in vitro*, when the majority of granule and pyramidal neurons form an AIS. Chronically depolarising the neurons at early stages of the AIS formation triggered a rapid (within 6 hours), long-lasting disassembly of the AIS. This decrease was observed mostly in young, developing neurons, between 4 and 7 DIV, and less so in older neurons (>DIV10), suggesting the existence of a developmental window for this activity-dependent AIS-disassembly. The effect was reversible upon removal of high potassium and was not linked to increased cell death. The loss of the AIS could also be rescued by blockage of L-type calcium channels with nifedipine (1µM), suggesting a role for calcium influx in this process. Surprisingly, inhibiting a calcium-dependent protease calpain, which has been previously implicated in AIS disassembly after neural injury, had no effect on the AIS numbers. Finally, chronic depolarisation also triggered rapid, reversible changes in AIS properties, leading to significant alterations in AIS length and position along the axon. Below I discuss these findings in more detail.

4.15.1 AIS development in excitatory cells in dissociated hippocampal cultures

In our culture system AISs were first detected at 2 DIV, when around 2% of granule and 13% of pyramidal neurons had a clearly-detectable AnkG immunostaining along their proximal axons. AIS formation was mostly complete by 13 DIV, at which time the majority of neurons had an AIS. The temporal characteristics of the AIS emergence in our culture system are consistent with other studies in dissociated hippocampal cultures (Boiko et al., 2007, Yang et al., 2007; Brechet et al., 2008, Martin et al., 2008, Galiano et al., 2012). The AIS typically forms shortly after the axon has been specified, however the rate of AIS formation may vary across and within different cell types and is highly dependent on the density of the hippocampal culture. High density cultures tend to initiate axogenesis and complete AIS formation faster than low density cultures (Boiko et al., 2007). For example, in a study using a high-density hippocampal culture (48,000 cells/cm^2, almost 3-times denser than our low-density culture of ~17,000 cells/cm^2), 14 ±3 % of neurons had an AIS at 1 DIV, 94 ± 2% at 7 DIV and 100% at 14 DIV, which is considerably faster than what was observed in our culture system (Boiko et al., 2007).

All previous studies into AIS development treat all hippocampal cells equally and no reports have been published that characterise AIS formation separately for granule and pyramidal cells. In this study, the rate of AIS emergence varied in these two populations of excitatory cells. In pyramidal cells, most of the AIS formation took place between 2 and 7 DIV, whereas in granule neurons the AIS formed over a longer period of time, between 3 and 13 DIV. This slower rate of AIS formation in granule cells was most likely due to a more immature state of these neurons in our culture system. In the intact hippocampus, granule cells are generated relatively late, after the majority of pyramidal neurons have already been born (Altman and Bayer, 1990; Danglot et al., 2006). Thus, at the time of culturing (E18), granule cells are less developed than pyramidal neurons, which then translates into marked differences in the time-course of AIS formation. In addition, not all neurons are at exactly the same developmental stage at E18. This intrinsic variability in the maturation state of neurons is inherent to all hippocampal neurons and may result in a highly variable time window for AIS formation, even when focusing on specific types of neurons. Although I have characterised the developmental profile of specific types of neurons at the population level, how long it takes for an individual neuron to form the AIS is yet to be explored.

Once formed, the AIS continues to develop and mature. In our culture system, the AIS properties changed significantly between 4 DIV and 14 DIV and followed different courses in the two classes of excitatory neurons. The AIS of immature pyramidal neurons at 4 DIV was shorter and located further away from the soma than the AIS of mature cells at 14 DIV. This course of AIS development is consistent with the 'distal boundary' hypothesis proposed for AIS development in cortical cells (Galiano et al., 2012). According to this hypothesis a distal axonal cytoskeleton functions as an intra-axonal boundary restricting AnkG to the proximal axon. The border of this boundary is delineated by ankyrin B, expressed all along the axon, from the tip of the growth cone to the distal end of the AIS. The expression pattern of ankyrin B does not overlap with ankyrin G, making them mutually exclusive. The AIS thus starts forming distally (where ankyrin B stops) and then gradually ‘fills in’ the proximal axon as the cell matures. Once the boundary is established, it remains there throughout the development of the AIS, anchoring the distal end of it in a fixed position. These dynamics of AIS maturation were clearly seen in pyramidal cells, however the presence of a fixed distal boundary was not observed in granule neurons. In these cells, the distal end of AnkG staining was progressively shifting closer to the soma as the cells matured, ruling out the existence of a fixed

cytoskeletal boundary at the distal end of the AIS. Taken together, these findings suggest the presence of distinct AIS maturation programmes in the two classes of excitatory neurons that need to be explored in more detail. For example, what happens to ankyrin B expression in granule cells during development? Does the ankyrin B/ankyrin G boundary move synchronously to a more proximal location or is there a gap between the two ankyrin domains? Although the latter is unlikely, a stain for ankyrin B should be performed in developing granule cells in order to better understand this mechanism.

Apart from changes in length and position of the AIS, I also observed significant developmental changes in AnkG levels as measured by immunofluorescence intensity. In both granule and pyramidal cells the intensity of AnkG staining progressively increased between 4 and 7-9 DIV, suggesting an ongoing addition of this protein to an already existing AnkG matrix. This is consistent with results from other studies, which show that the AIS still develops and matures after it has been formed (Boiko et al., 2007; Yang et al., 2007). AnkG is the 'master organiser' of the AIS, which is known to recruit other proteins to the AIS (Zhou et al., 1998; Jenkins and Bennett, 2001; Garrido et al., 2003; Pan et al., 2003; Hedstrom et al., 2007; Yang et al., 2007). Increasing levels of this protein should thus reflect a proportional increase in the levels of other components of the AIS that rely on AnkG binding, such as voltage-gated ion channels and a variety of cell adhesion molecules and cytoskeletal scaffolds. Immobilisation of proteins binding to AnkG at the AIS is a first step in the assembly of the diffusion barrier that separates the axonal and somatodendritic compartments (Brachet et al., 2010). In hippocampal neurons, the AIS-mediated diffusion barrier is not immediately formed after the AIS emerges but only when a specific density of the structure is achieved (around 7-10 DIV). Thus, the developmental increase in the levels of AnkG protein may reflect a changing molecular composition of the AIS as it matures and becomes fully functional.

4.15.2 Loss of AISs in response to depolarisation

Chronic depolarisation of 4-10 DIV hippocampal cultures with high levels of extracellular KCl resulted in decrease in a number of cells containing an AIS. This effect could arise from a number of reasons: (1) selective cell death of AIS-positive neurons, (2) a block in AIS formation, or (3) an active disassembly of existing AISs. The first possibility is unlikely as there was no detectable increase in cell death after the KCl treatment. Cell density was also not affected by the treatment and no new neurons are known to be born in our culture system (Evans et al., 2013), which

rules out an activity-dependent increase in young neurons without an AIS. Moreover, the decrease in AIS-positive neurons was reversible upon removal of KCl, which shows that chronically depolarised neurons were viable. The second possibility, a depolarisation-induced block of AIS formation, is also an unlikely candidate. There are two reasons for this. The first, is that the reduction in AIS-positive neurons was relatively rapid, within 3 hours, a time period over which there was no significant increase in the AIS-positive neurons in control conditions. In other words, the rate of AIS loss was much faster than that of AIS formation. The second reason is that new AISs were able to form in depolarised cultures after long treatments. Although this evidence is less conclusive, it does suggest that even during periods of depolarisation AISs can continue to assemble. I cannot, however, preclude a potential activity-induced delay in AIS formation, as removing KCl from depolarised cells led to a quicker AIS recovery than when the cells were left in depolarised conditions. Together, these findings strongly suggest that a decrease in AIS assembly cannot account for the dramatic and rapid decrease AIS-positive neurons. The results are best explained by a model in which AISs are dismantled in response to membrane depolarisation and can reform once the neurons are brought back to normal activity levels.

Molecular mechanisms of AIS disassembly

Activity-dependent AIS disassembly was a rapid, cell-autonomous event occurring within the first few hours of the onset of depolarisation. A clear, population-wide effect was noticeable after 3 hours in KCl, suggesting that a subset of cells initiated and completed AIS disassembly within that time frame. Therefore, a quick detection system must be in place to spot changes in activity levels and transduce them to relevant executive centres of the cell. In this chapter I showed that L-type calcium channels act as sensors for such a system, as blocking them with nifedipine abolished AIS disassembly in response to KCl treatment. The same channels also formed part of the detection system in activity-dependent AIS remodelling seen in mature hippocampal neurons (Grubb and Burrone, 2010). Recently, Evans et al. (2013) explored signalling pathways downstream of L-type channels and demonstrated that activity-dependent AIS relocation was dependent on calcium/calmodulin-activated phosphatase calcineurin. It would be interesting to establish whether calcineurin activation is also required for the AIS disassembly observed in young hippocampal excitatory neurons.

Depolarisation-induced AIS disassembly occurred within a similar timescale to the changes seen after ischaemic injury, where the whole AIS structure is proteolysed within two hours (Schafer et al., 2009). The protein responsible for AIS proteolysis in response to neural injury was the Ca^{2+}-dependent protease calpain, as blocking proteolysis with calpain inhibitor MDL28130 prevented AIS removal independently of ongoing cell death. Treating our cultures with MDL28130, however, did not block AIS disassembly, indicating that calpain is not involved in the activity-dependent AIS disassembly described in this chapter. Similarly, calpain was not required for AIS relocation in older hippocampal neurons (Evans et al., 2013). Therefore there must be a distinct mechanism for depolarisation-induced AIS disassembly in hippocampal excitatory neurons, which relies on Ca^{2+} influx through L-type Ca^{2+} channels but is independent of calpain-mediated proteolysis. Additional experiments are required to elucidate specific cascades downstream of the Ca^{2+} signal.

One possible target for AIS disassembly is the membrane cytoskeleton, which has unique organisation at the AIS. Actin filaments are arranged in periodic rings spanning the whole axon (Xu et al., 2012), whereas microtubules are fasciculated and run parallel to each (Kosaka et al., 1980). Previous studies showed that interfering with the stability of the microtubule network has profound consequences on the structure of the AIS. For example, a knock-down of casein kinase (CK2), a kinase essential for regulating microtubule stability, leads to a reduction of AnkG and Na_v channel immunofluorescence and a decrease in the number of cells with an AIS. Similar phenotypes are observed when silencing HDAC6, a tubulin deacetylase important for controlling microtubule growth (Tapia et al., 2013). Furthermore, addition of microtubule-stabilising drug, taxol, leads to the opposite phenotype, in which neurons begin to generate multiple axons (Witte, 2008) each with its own AIS (Evans and Grubb, unpublished observation). Together, these results suggest that microtubule stability could be a potential target for activity-dependent AIS plasticity in hippocampal neurons.

Bidirectional nature of AIS plasticity

After the initial period of disassembly, depolarised neurons eventually recover and begin to form new AISs. This loss of sensitivity to KCl occurs progressively, starting from around 8 DIV onwards, suggesting the existence of a critical window for this type of plasticity. It is not clear what developmental changes underlie this loss of sensitivity in hippocampal cultures. Several processes take place that coincide with the end of the critical window. One of them is the formation of a meshwork of

extracellular matrix (ECM) molecules around the AIS. The ECM surrounding the AIS has a unique composition showing a preferential enrichment in brevican, a chondroitin sulphate proteoglycan (Bruckner et al., 2006; John et al., 2006; Hedstrom et al., 2007). Previous work in the visual cortex showed that chondroitin sulphate proteoglycans (CSPGs) play a role in ocular dominance plasticity in the visual cortex (Mataga et al., 2002). CSPGs form dense perineuronal nets which strongly inhibit structural plasticity in adult animals, thus introducing a developmental window and limiting ocular dominance plasticity to earlier stages of development. However, an *in vivo* digestion of the ECM could reactivate structural plasticity beyond the critical period (Berardi et al., 2004). In hippocampal neurons, ensheathing the proximal axon by the ECM could act as an inhibitor of activity-dependent structural AIS plasticity. The ECM meshwork might stabilise the AIS structure to the extent when it becomes insensitive to activity-induced disassembly. Therefore it would be interesting to investigate whether enzymatic removal of the ECM would extend the critical window for activity-dependent AIS disassembly.

Yet another cause for the loss of sensitivity to KCl may be internal crosslinking at the AIS that is coincident with the formation of the diffusion barrier. Increasing levels of AnkG early in development leads to progressive recruitment and accumulation of a dense network of other AIS proteins, which may stabilise the whole structure and make the AIS less susceptible to activity-dependent disassembly. As the cell matures, the composition of voltage gated ion channels, especially Ca^{2+} channels, may also be altered. It has previously been shown that expression of voltage-gated Ca^{2+} channels, especially the L-type, is downregulated in later development in CA3 neurons (Morton et al., 2013). Perhaps similar changes also take place in granule and CA1 pyramidal cells, leading to a decrease in sensitivity to these early forms of plasticity. It is therefore also important to test the effects of KCl in neurons of different developmental stages. Specifically, it would be important to establish Ca^{2+} responses elicited by the KCl treatment. It is possible that at different developmental stages the levels of depolarisation required to activate AIS disassembly vary. In this chapter I kept the stimulus condition fixed for all developmental stages and showed a clear critical period of AIS plasticity. The next set of experiments would be to modify the stimulus and establish whether similar forms of plasticity can be triggered at other periods (eg. in more mature neurons).

There is considerable variability within and across different cell types in hippocampal cultures, highly influenced by the maturation state of the cells and their

direct extracellular environment. Therefore, to reduce variability inherent in a population of diverse cells, it would be necessary to perform the experiments described in this chapter at the level of a single neuron. This could be achieved with long-term live imaging of AIS-labelled neurons. The AIS could be live-labelled with an antibody against the extracellular domain of neurofascin-186, which is one of the major components of the AIS (Hedstrom et al., 2007; Zonta et al., 2011). Using this approach would allow me to follow structural changes at the AIS with more precision and determine spatiotemporal characteristics of AIS disassembly and re-assembly in response to addition and later removal of high extracellular KCl. It has previously been shown that axotomised hippocampal neurons tend to reform their axons directly opposite to the site of injury (Mattson et al., 1990; Gomis-Ruth et al. 2008). Do similar dynamics occur in activity-dependent AIS disassembly? Do the AISs that had been disassembled reform on the same axon or, perhaps, another neurite becomes respecified as axon? Imaging of AIS plasticity on a single neuron would help to answer these questions. This technique will also be helpful in elucidating the time-course of AIS development in control cultures.

4.15.3 Changes in AIS properties in response to depolarisation

Although a large number of AISs were removed after chronic depolarisation, the AISs that were left behind showed altered structural properties. There was a significant change in AIS length and position, the exact magnitude and direction of which depended on when the treatment was applied. Chronic depolarisation of young neurons, between 3-4 and 6-7 DIV, resulted in shorter and more proximal AISs, an effect observed in both types of excitatory neurons examined. As the results presented in this chapter are taken from a population of neurons rather than a single cell, it is unclear whether the changes in AIS properties reflect (1) a plastic remodelling of the AISs or (2) a selective removal of AISs with specific properties. For example, a proximal AIS location in 16-hr-depolarised cultures (at 7 DIV) may be a result of (1) a proximal movement of the AIS along the axon or (2) selective removal distally-located AISs, leaving the proximal AISs intact. If depolarisation induced a selective removal of distal AISs, the proximal shift in AIS position should coincide with the time of maximal AIS disassembly. In pyramidal neurons, the peak AIS disassembly was observed after 48 hours of depolarisation. However, this was not paralleled by a change in AIS position and thus suggests that AISs were disassembled irrespective of their position along the axon. In granule cells, however, the period of the most intense AIS disassembly coincided with the largest

proximal shift in AIS position. Longer, distally located AISs typically belong to more immature granule cells, which are perhaps the first targets for AIS disassembly.

The data presented in this chapter also showed that prolonging the duration of depolarisation did not lead to complete elimination of all AISs in the culture; instead, it resulted in a further change in AIS properties but in a different direction. Prolonging depolarisation from 8 to 14 DIV, resulted in structural AIS changes reminiscent of the activity-dependent changes previously described for hippocampal neurons (Grubb et al., 2010). In agreement with previous results, there was a significant distal shift in AIS position in both granule and pyramidal cells. Interestingly, however, prolonged depolarisation induced a significant elongation of the AIS in granule cells but a shortening in pyramidal neurons. As after 8 DIV the cells were largely insensitive to depolarisation-induced AIS disassembly, it can be assumed that the structural changes observed here were due to active AIS remodelling rather than selective removal of the AIS. The exact mechanism behind the distal AIS shift in response to chronic depolarisation is currently unknown (Grubb and Burrone, 2010). The data gathered here might provide some insight into how this may occur. As a change in AIS length always seems to precede the change in AIS position, the AIS remodelling may take place in two stages: (1) AIS assembly at the distal end of the existing structure followed by (2) a selective dismantling of the proximal part. However this would have to be confirmed by further experiments carried out at the level of a single cell.

Strikingly, the AIS properties of chronically (8 days; 14 DIV) depolarised cells resembled the AIS properties of young immature neurons (at 4 DIV). This may be due to ongoing AIS formation in neurons that had their AIS removed in response to KCl treatment. If new AISs, in turn, begin to form ‘from scratch’ and recapitulate all stages of the AIS development programme observed in immature cells, AIS properties of depolarised cells at 14 DIV should resemble the properties of young AISs for as long as AIS formation is detectable in the culture. This, however, was not the case, as removal of KCl from the culture media resulted in a rapid recovery of AIS properties to control levels before the formation of new AISs was complete. Therefore, formation of new AISs cannot explain the change in AIS properties observed after chronic depolarisation. In fact, new AISs that are formed in recovering cultures appear to match the properties of AISs of that developmental stage, rather than AIS properties of immature neurons. Perhaps, KCl treatment and associated Ca^{2+} currents revert the cells to early developmental expression patterns

that would alter AIS properties (Ben-Ari and Spitzer, 2010). Hippocampal neurons tend to be more depolarised early in development and subjecting the cultures to higher levels of depolarisation may thus act as a signal of an earlier developmental stage. The cells then respond by remodelling their AISs according to the specific developmental stage induced by increased levels of extracellular KCl.

A variation in AIS properties, seen both in development and after chronic depolarisation, may reflect different levels of neuronal excitability across and within different cells in the hippocampal culture. A cell can regulate its own excitability by modulating the length of the AIS or its distance from the cell body (Grubb and Burrone, 2010; Kuba et al., 2010). A distal shift in the AIS position leaves a larger, non-excitable region between the AIS and the cell body, resulting in a lower excitability of the cell. Changes in AIS length, on the other hand, may correlate with a changing number and density of Na_v channels that are necessary for initiation and propagation of the action potential. Longer AISs would typically recruit more sodium channels than shorter AISs. For example, in the auditory system of the chick, longer AISs exhibit higher Na^+ current density and lower spike threshold (Kuba et al. 2010). A variety of studies have shown a clear link between AIS properties and functional output of the cell. In the hippocampus, neurons with more distal AISs are less excitable, as they require larger current injections in order to fire an action potential (Grubb and Burrone, 2010). In the avian nucleus magnocellularis (NM) and nucleus laminaris (NL) the length of the AIS varies with the tuning frequency of neurons (Konishi, 2003). The AIS is shorter in neurons with a higher tuning frequency in the NM and shorter and more distal in neurons with a higher tuning frequency in NL (Kuba et al.,2006; Kuba and Ohmori, 2009). AIS length and position also varies in different types of retinal ganglion cells with different visual properties (Fried et al., 2009). Together these observations suggest that AIS position and length appears to be tuned to and determined by ongoing levels of neuronal activity.

4.14.4 A novel form of activity-dependent AIS plasticity

The results presented in this chapter demonstrate the existence of a novel form of activity-dependent AIS plasticity in the developing hippocampus, where altered activity leads to dismantling of the entire AIS. This type of plasticity appears to operate only in young immature neurons, indicating a presence of a developmental window beyond which no activity-induced AIS disassembly takes place. Instead, the neurons activate a different form of plasticity, where the AIS is structurally remodelled rather than being completely removed. Structural remodelling of the AIS

has been linked to changed excitability of a neuron (Grubb and Burrone, 2010), in line with a homeostatic adjustment of intrinsic excitability (Turrigiano and Nelson, 2004). According to this model, when a change in excitability occurs in one direction, the neuron will respond with an excitability change in the opposite direction, in an attempt to preserve an overall balance of activity. Complete AIS loss may thus function as a homeostatic mechanism that compensates for the increased activity levels by completely removing the structure responsible for generation of action potentials and thus ultimately activity itself. This seemingly drastic change may be necessary at earlier times in development when neurons may be especially vulnerable to activity-induced cytotoxicity. Complete removal of the AIS may prevent over-excitation of young neurons in developing networks. In the next chapter, I will address the functional significance of the AIS removal for the excitability of the cell.

Chapter 5

The consequences of AIS disassembly on neuronal excitability

5.1 Introduction

In the previous chapter I showed that chronically depolarising excitatory neurons with either high levels of KCl or optogenetics results in the reversible disassembly of the entire AIS. This effect was observed predominantly in young, 4-7 DIV, neurons and was dependent on Ca^{2+} influx through L-type voltage-gated calcium channels. In an attempt to explain the functional significance of these structural changes, I proposed the existence of a novel form of activity-dependent AIS plasticity in young hippocampal neurons. In this form of plasticity, a removal of an entire AIS may serve as a homeostatic mechanism of dealing with elevated levels of activity in developing neuronal networks. As the AIS is the primary site of action potential initiation and modulation (Kress et al., 2008; Winkels et al., 2009), its complete elimination should have profound consequences on the intrinsic excitability of the cell. In this chapter I test this possibility and explore the consequences of AIS absence on neuronal excitability.

Alterations in AIS length or position along the axon have been previously shown to affect the intrinsic excitability of neurons (Grubb and Burrone, 2010; Kuba et al., 2010; Kaphzan et al., 2011), however little is known about the effect of AIS removal on firing capabilities of cultured hippocampal neurons. The consequences of AnkG elimination on neuronal excitability have been examined primarily in cerebellar Purkinje cells. In cerebellum-specific AnkG knockout mice, AIS-negative Purkinje cells lack functional Na_v channels, and display higher threshold for action potential initiation and impaired firing of action potentials in response to somatic current injection (Zhou et al., 1998; Jenkins and Bennet, 2001; Sobotzik et al., 2009). In hippocampal neurons, the consequences of AIS absence on neuronal excitability have not yet been fully explored. One study, however, addressed this question indirectly. Tapia et al. (2013) investigated the role of GSK3 (glycogen synthase kinase 3) at the AIS in cultured hippocampal and cortical neurons. Pharmacological inhibition of GSK3 or the knockdown of its substrate, β-catenin, diminished the

levels of AnkG and voltage-gated sodium channels at the AIS, which also correlated with a lower amplitude of sodium currents and decreased the excitability of treated cells. Yet it is not clear whether this was the consequence of the pharmacological treatment or the result of specific disassembly of the AnkG scaffold, and therefore it needs to be explored in more depth.

In this chapter I explore functional consequences of absence of the AIS in cultured hippocampal neurons at 7 DIV. Specifically, I focus on how the absence of an AIS affects the firing capabilities of neurons. I attempt to answer this by comparing the firing properties of AIS-positive and AIS-negative neurons, both in control condition and after chronic depolarisation with KCl (20mM). Are cells without an AIS less excitable? Do the cells that have lost an AIS retain the ability to fire action potentials? If so, are the properties of these action potentials different in any way? Is there any change in the input-output curves after the AIS loss? To answer these questions, I use two functional measures of neuronal output, both in conjunction with a live-label of the AIS. First, I investigate calcium responses of AIS-positive and AIS-negative neurons in response to whole-field electrical stimulation. Secondly, I examine electrophysiological responses of the neurons to somatic current and voltage injections and characterise their firing properties in more detail.

5.2 Calcium imaging

Measurements of somatic calcium influx is a good correlate of neuronal activity (Neher and Sakaba, 2008; Tian et al., 2012). Whenever a neuron fires an action potential it is accompanied by a large and rapid influx of Ca^{2+} through voltage-gated $Ca^{2+}{}_v$ channels. Elevations in intracellular Ca^{2+} can be measured using a variety of organic fluorescent calcium indicators (Rudolf et al., 2003). Here, I used a cell-permeable calcium dye Oregon Green BAPTA-1 AM (OGB-1) to examine Ca^{2+} dynamics in 7 DIV cultured hippocampal neurons. OGB-1 is a non-ratiometric Ca^{2+} indicator which exhibits increases in fluorescence emission upon binding of Ca^{2+} ions, without a shift in its excitation spectra. OGB-1 is a highly sensitive calcium indicator (K_d = 240 nM) and has been consistently used in the field to measure rapid changes in Ca^{2+} levels that coincide with neuronal activity (Jackson et al., 2003; Manita and Ross, 2009). As the AM-ester version of the dye permeates all cells in culture, this approach allows wide-field imaging of many cells at once, thus providing a gross overview of neuronal activity in a large population of cells. An example image of OGB-1-loaded hippocampal neurons is shown in Figure 5.1a.

Prior to imaging, the AIS was labelled using a primary antibody against the extracellular domain of neurofascin-186 (NF-186), an AIS-specific cell adhesion molecule that directly interacts with AnkG through its cytoplasmic domain (Dzhashiashvilli et al., 2007). In hippocampal neurons NF-186 is not required for the assembly or maintenance of the AIS, but it appears to play a role in targeting the extracellular matrix (ECM) protein brevican and neural cell adhesion molecule (NrCAM) to the AIS. In addition, it is also important for forming and stabilising GABAergic connections from chandelier cells to the AIS of pyramidal neurons (Ango et al., 2004). NF-186 clustering at the AIS is highly dependent on AnkG binding and it typically co-localises with AnkG as detected by immunohistochemical methods (Figure 5.1b). Knocking down AnkG expression in either developing or mature hippocampal neurons disrupts targeting of NF-186 to the AIS (Hedstrom et al., 2007, 2008). Its strong dependence on AnkG binding and highly accessible extracellular domain makes NF-186 an excellent marker of the AIS in live neurons.

In order to understand how the absence of an AIS affects neuronal excitability and compare these responses to neurons that have already acquired an AIS, NF-186 stained neurons (from a 7 DIV culture) were loaded with OGB-1 and subjected to electrical field stimulation using two parallel platinum electrodes (Figure 2.2 in the Methods section). The cultures were stimulated with 10Hz bursts of 5, 10, 15 and 20 action potentials (APs; Figure 5.1c) delivered sequentially with a one-minute interval between the trains. AP-driven Ca^{2+}-responses were measured at the soma for all cells in the field of view. Specifically, I concentrated on two properties of the Ca^{2+} response: its peak change in fluorescence (maximum $\Delta F/F_0$) and the rate of decay of the fluorescence signal (Figure 5.1d). The first measure estimates the maximum amplitude of activity-evoked Ca^{2+} current, whereas the second approximates the dynamics of Ca^{2+} clearance from the cytoplasm of the stimulated cell.

Ca^{2+} responses were measured in NF-186-stained cultures that were either chronically (16-24 hrs) treated with 20mM KCl or left untreated (controls). As seen from the previous chapter, chronically depolarised neurons tend to dismantle their AIS, so that KCl-treated cultures will have a mixed population of AIS-negative cells: (1) the cells that have not yet formed an AIS and (2) the cells that originally had an AIS but lost it in response to increased activity (this last group is not present in control cultures). In this study I had no means of distinguishing between these two populations, and hence treated them as a single group. Any large differences

between control and KCl-treated cells, however, would indicate that these two subpopulations of cells are functionally distinct and require separate examination.

5.2.1 AIS-negative neurons are less likely to respond to electrical field stimulation

To investigate the functional consequences of the AIS absence, I began by examining what proportion of AIS-negative neurons responded to electrical field stimulation in comparison to AIS-positive cells. A responding cell was defined as a cell with responses above a carefully-defined threshold, which was empirically set from histograms showing a clear non-responding peak (data not shown). The value from the intersection of these peaks was taken as the threshold value used to differentiate the responding neurons from the pool of non-responsive cells. The threshold obtained in this way reliably matched the thresholds set by visual inspection of the traces.

First, I measured the percentage of responding cells in control and KCl-treated 7-DIV cultures. KCl was added at 6 DIV, left in the culture media for 16 – 24 hrs and removed before the cells were stimulated with different bursts of activity. It is important to note that all experiments were carried out in the presence of postsynaptic glutamate and GABA receptor blockers (APV, CNQX and gabazine) so that the field stimulation was not influenced by any fast synaptic transmission. To determine whether the strength of the stimulus affected the likelihood of observing a Ca^{2+} response, I plotted the percentage of responding cells as a function of the number of APs (Figure 5.2a). In both conditions, there was a clear increase in responding cells with increased duration of AP burst, reaching a plateau at 15 APs. This indicates the existence of a variable threshold for AP-evoked Ca^{2+} influx in different cells, whereby longer stimulation is required to trigger Ca^{2+} flux in a subset of high-threshold neurons. Next, I compared the percentage of responding cells in control and KCl conditions and, as expected, there were consistently fewer cells displaying Ca^{2+} transients in KCl-treated cultures, as compared to control cells. The differences, however, were statistically significant only in response to 10 APs ($P = 0.038$, unpaired t test; $n_{Control} = 3$ coverslips, $n_{KCl} = 4$ coverslips. A total of 159 control and 148 high-KCl-treated cells; Figure 5.2a).

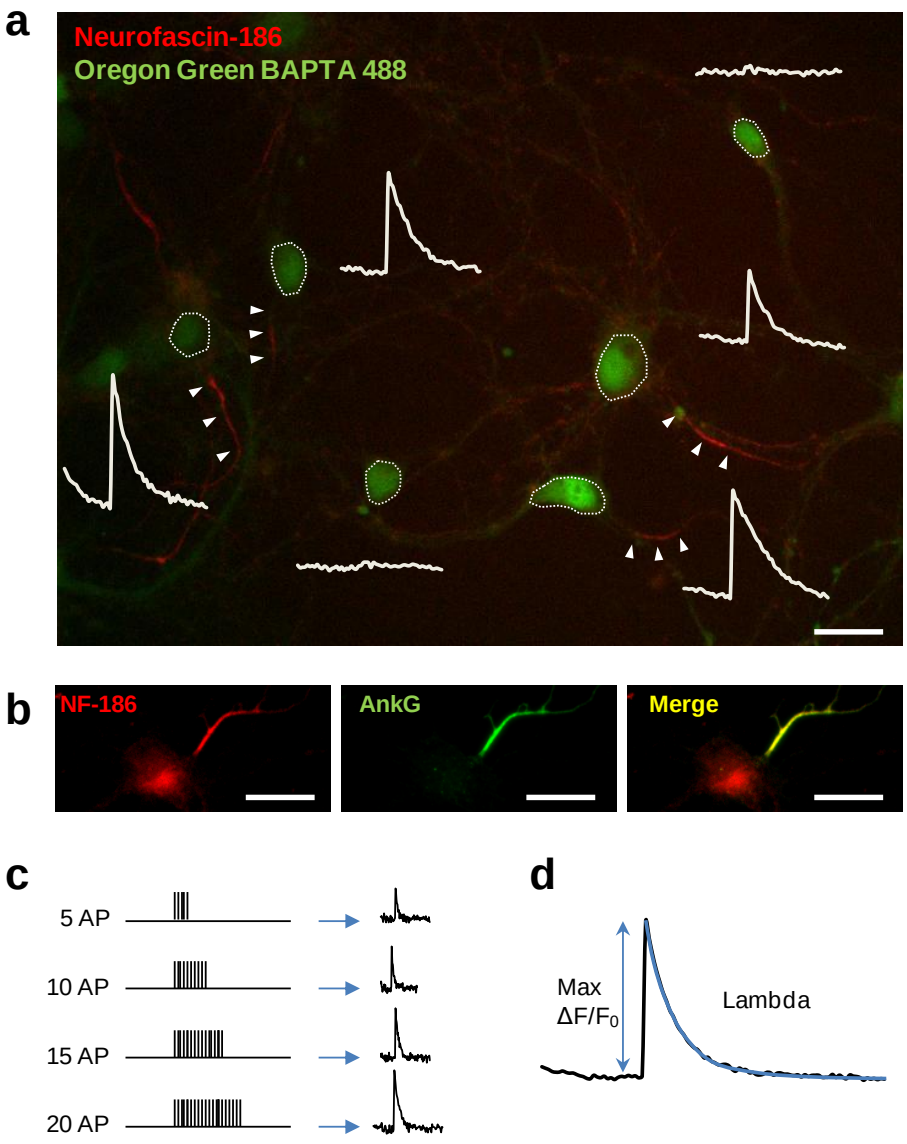

Figure 5.1 Calcium imaging in hippocampal cultures live-labelled for the AIS. (a) A single imaging frame showing neurons loaded with Oregon Green BAPTA -1 (OGB-1; green) and live-labelled for the AIS with neurofascin-186 (NF-186, red, arrowheads). Dotted lines delineate cell bodies of OGB-1-loaded neurons. Calcium flux was measured following field stimulation of the whole culture. White traces indicate the fluorescence change of individual OGB-1-loaded neurons, illustrating the dynamics of Ca^{2+} influx in response to electrical stimulation. (b) NF-186 immunostaining (red) perfectly overlaps with AnkG immunoreactivity in hippocampal cells. (c) Experimental design. The cultures were stimulated with 5, 10, 15 and 20 action potentials (1ms pulse, 10Hz) whilst recording Ca^{2+} responses. (d). The parameters measured were maximal change in fluorescence (Max $\Delta F/F_0$) and the time-constant for exponential decay of the signal, lambda. Scale bar, 20µm.

I have previously shown that KCl treatment triggers a decrease in AIS-positive neurons, defined as cells with clear AnkG immunoreactivity along the proximal axon. Here, I examined whether this decrease is still detectable with NF-186 as an AIS marker. In agreement with previous results, I detected significantly fewer AIS-positive cells in KCl than in control conditions ($p = 0.0342$, unpaired t test, $n_{Control} = 3$ coverslips, $n_{KCl} = 4$ coverslips), indicating that NF-186 is a suitable marker for depolarisation-induced AIS disassembly (Figure 5.2b). The most plausible explanation for the decrease in responding cells following KCl treatment is a decrease in neurons containing an AIS. To investigate this further, I quantified the percentage of responding cells separately for AIS-positive and AIS-negative neurons (pooled from control and KCl-treated cultures). As predicted, there was a striking dependence between the presence of AIS and the ability of the cell to respond to electrical stimulation. A significantly larger proportion of AIS-positive neurons responded to electrical stimulation compared to AIS-negative cells (AIS-positive: 5 AP, 52% ± 3.6%; 10 AP, 55.2 ± 3.7%; 1 5AP, 62.8 ± 2.9%; 20 AP, 61.9 ± 3.5%. AIS-negative: 5 AP, 1.2 ± 1.2%; 10 AP, 1.5 ± 1.2%; 15 AP, 1.5 ± 1.5%; 20 AP, 2.1 ± 1.4%; $P < 0.001$, unpaired t test; $n_{Control} = 3$ coverslips, $n_{KCl} = 4$ coverslips).

To determine whether KCl treatment itself had an effect on the ratio of responding neurons, I sub-divided the AIS-positive and AIS-negative neurons according to experimental condition (control and KCl) and calculated the proportion of responding cells for each group separately (Figure 5.2d). No statistically significant differences were detected in either of the conditions tested. Interestingly, there was a clear non-significant trend towards a lower percentage of responding cells in KCl-treated AIS-positive group, suggesting that KCl treatment may had an impact on the responsiveness of cells to electrical stimulation. AIS-negative neurons were affected by the KCl treatment to a lesser extent than AIS-positive cells, showing a non-significant trend in the opposite direction from what was observed for AIS-positive neurons. KCl-treated AIS-negative neurons more readily responded to electrical stimulation than the control cells lacking an AIS. This small difference may be explained by the presence of a functionally distinct population of AIS-negative neurons in the KCl condition, namely the cells that had formed an AIS but had it removed in response to prolonged KCl treatment. This idea is explored in more detail using whole-cell patch clamp recordings in section 5.3.

Overall, there was a strong link between the responsiveness of the cells to AP-evoked activity and the presence of the AIS. AIS-negative neurons were less likely

display Ca^{2+} transients in response to electrical field stimulation than AIS-positive neurons, strongly underlining the importance of the AIS in the regulation of neuronal excitability.

5.2.2 AIS-negative neurons have smaller Ca^{2+} response than AIS-positive neurons

In the previous section I showed that neurons lacking an AIS are less likely to respond to electrical field stimulation than cells containing an AIS. Here, I focus solely on responding cells and investigate whether the absence of an AIS affects the properties of the Ca^{2+} response. Specifically, I examined two properties of the Ca^{2+} response: (1) the peak amplitude of the Ca^{2+} transient, as estimated by the maximal $\Delta F/F_0$ value; and (2) the rate of Ca^{2+} extrusion, estimated from the exponential decay back to baseline after the end of the stimulus (Figure 5.1d).

First, I examined the differences in peak Ca^{2+} responses for control and KCl-treated neurons (Figure 5.3a). KCl-treated neurons had consistently lower values of maximal $\Delta F/F_{0,}$ although this difference was small and not statistically significant. On the contrary, separating the cells according to the presence or absence of the AIS, revealed a marked difference in Ca^{2+} response. Cells lacking an AIS had significantly lower amplitudes of Ca^{2+} influx compared to cells with an AIS ($P < 0.05$, unpaired t test, $n_{AIS+} = 105$ cells, $n_{AIS-} = 8$ cells; Figure 5.3b). To determine how KCl treatment affected the Ca^{2+} responses, I subdivided AIS-positive and AIS-negative neurons according to experimental condition. As there was only 1 responding AIS-negative cell in control condition, it was not included in the analysis. Consistent with previous observations, the Ca^{2+} response of AIS-positive neurons was consistently lower in KCl than in the control condition; however these differences were not statistically significant ($P > 0.05$, unpaired t test, $n_{AIS+} = 105$ cells, $n_{AIS-} = 8$ cells Figure 5.3c).

The decay constant of Ca^{2+} influx was not affected by either KCl treatment or the absence of the AIS (Figure 5.3c-e). No significant differences in lambda values were detected in either of the experimental groups examined.

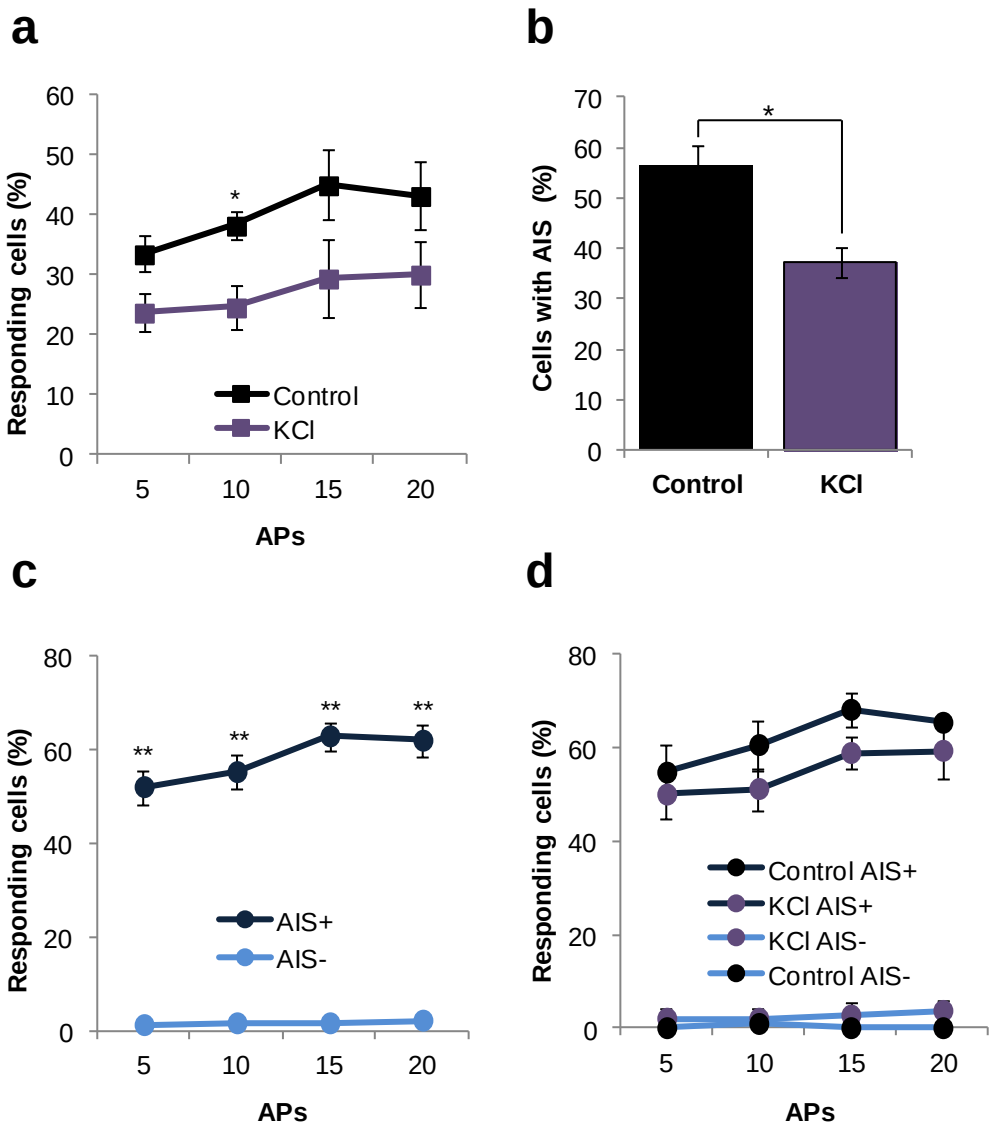

Figure 5.2 Cells lacking an AIS are less likely to respond to electrical field stimulation. (a) Percentage of responding cells in control (black line) and high-KCl-treated cells (purple line). (b) Percentage of cells with NF-186-labelled AISs in control (black) and KCl conditions (purple). *, p = 0.038; unpaired t test; $n_{Control}$ = 3 coverslips, n_{KCl} = 4 coverslips. A total of 159 control and 148 high-KCl-treated cells. (c) Percentage of AIS-positive (dark blue) and AIS-negative (light blue) responding cells. **, P < 0.01, unpaired t test, $n_{Control}$ = 3 coverslips, n_{KCl} = 4 coverslips (from 3 independent experiments). (d) Percentage of AIS-positive (dark blue line) and AIS-negative (light blue line) neurons in control (black data points) and KCl (purple date points) conditions. Error bars, SEM.

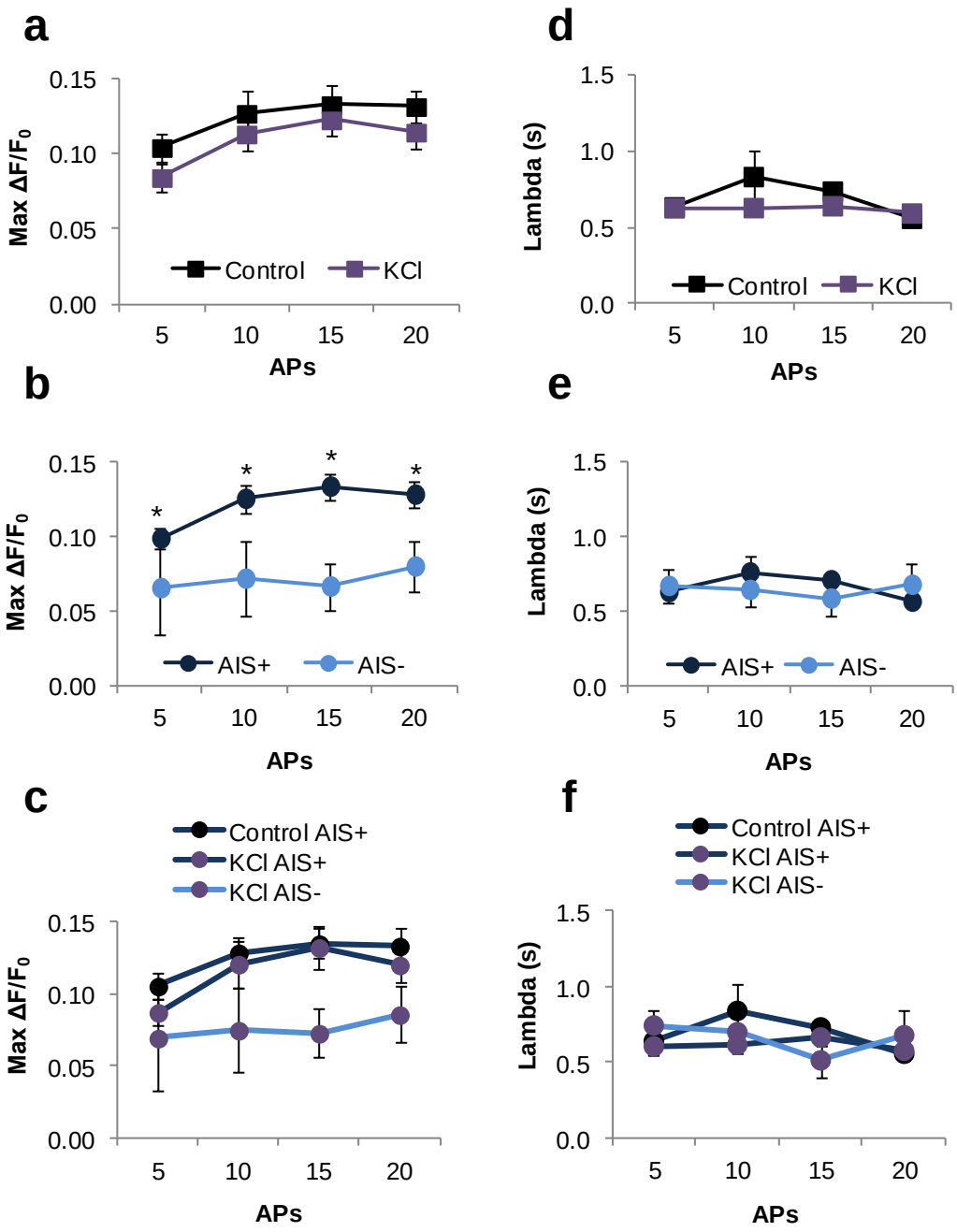

Figure 5.3 Cells lacking an AIS display smaller Ca^{2+} transients than cells with an AIS. Graphs showing mean values of max $\Delta F/F_0$ (a-c) and lambda (d-e) in cells that exhibited Ca^{2+} events in response to electrical field stimulation. All responding cells were split according to the presence or absence of the AIS (a and d; n_{AIS+} = 105, n_{AIS-} = 8), condition (control vs KCl, n = 68 and n = 45, respectively; b and e), and a combined effect of the presence/absence of the AIS and condition (c and f. $n_{Control\ AIS+}$ = 65, $n_{KCl\ AIS+}$ = 38, $n_{KCl\ AIS-}$ = 7, $n_{Control\ AIS-}$ = 1). Black lines indicate control cells, whereas blue lines, high-KCl-treated cells. *, P < 0.05. Error bars, SEM.

Taken together, the data presented in this section illustrates far-reaching consequences of chronic depolarisation on neuronal excitability. Chronic depolarisation leads to removal of the AIS from susceptible cells, decreasing their excitability levels. AIS-negative neurons were less likely to display Ca^{2+} transients in response to electrical field stimulation, suggesting an impaired ability of these cells to fire an action potential and/or to activate voltage-gated Ca^{2+}channels. Next, I explore the effect of the absence of the AIS on neuronal excitability in more detail, using whole-cell patch clamp electrophysiology.

5.3 Measuring the intrinsic excitability of hippocampal neurons

In this section I examine the resting and active membrane properties of neurons with and without the AIS. The AIS, as in the previous section, was labelled using an antibody against NF-186. A subset of cells was pre-treated with 20mM KCl (18-24 hours) as described earlier. AIS-labelled cells were first imaged and then patched in the whole-cell configuration. Patched neurons were analysed under both current clamp (-60mV holding voltage) and voltage clamp conditions. Specifically, I performed three protocols: (1) current clamp recordings of voltage traces in response to 10ms current injection - to examine the properties of single APs, (2) current clamp recordings of voltage traces in response to 500ms current injection – to investigate the characteristics of AP trains and (3) voltage-clamp recordings of macroscopic currents in response to increasing voltage steps – to characterise voltage-gated ionic conductances.

Figure 5.4 shows typical current and voltage traces from a control AIS-positive and AIS-negative neuron. The cells with a clear AIS stain reliably fired single action potentials in response to short (10ms) current injections, and trains of action potentials in response to longer (500ms) current pulses. In addition, AIS positive-neurons displayed large ionic conductances (Na^+ and K^+) evoked by gradually-increasing membrane depolarisation. In contrast, cells lacking an AIS exhibited characteristics of electrically silent immature neurons. These neurons generally did not fire action potentials in response to either 10ms or 500ms current injections. As these cells tended to be morphologically compact, having a small soma and short dendrites, incremental current injections induced considerable depolarisation, which however did not trigger sustained action potential firing. Moreover, there were no detectable active inward ion conductances and only small outward K^+ current in response to step-wise voltage depolarisations.

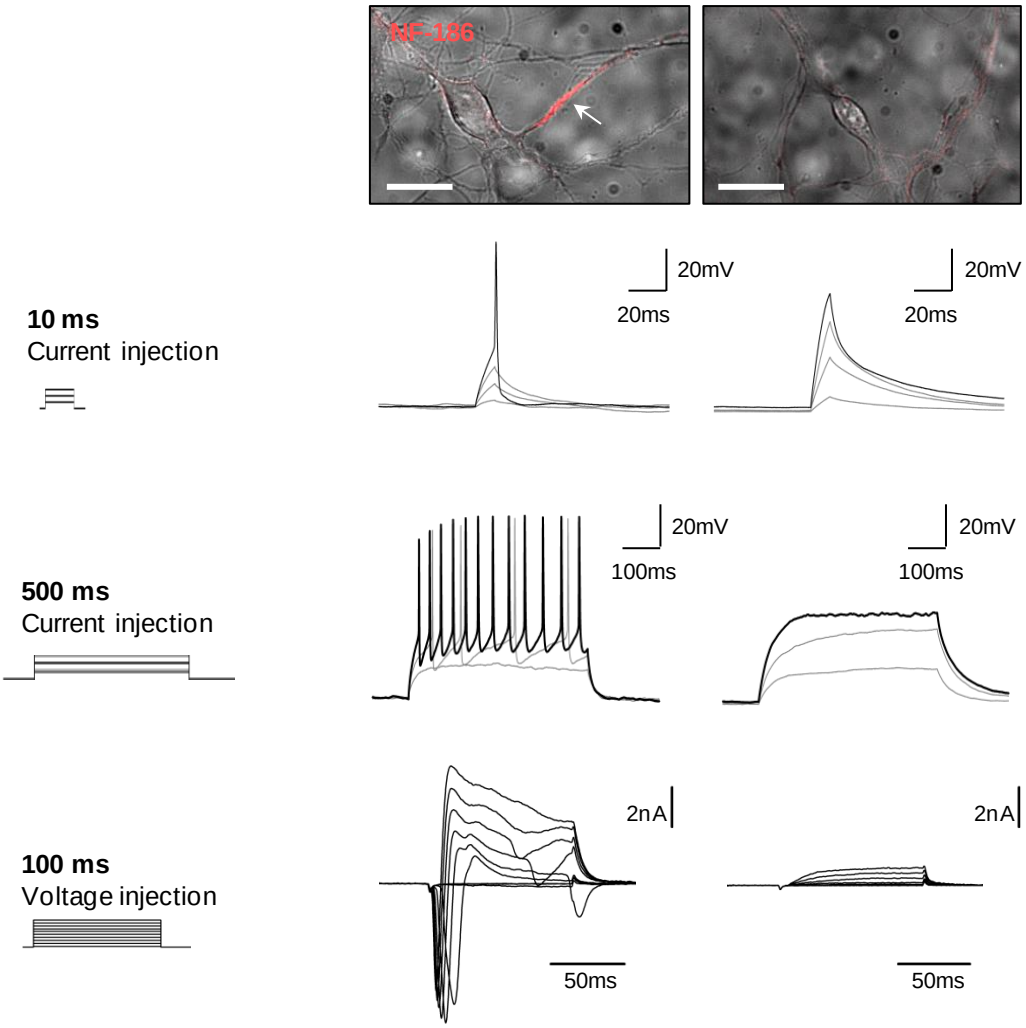

Figure 5.4 Representative electrophysiological recordings from 7 DIV control neurons live-stained for the AIS with NF-186. The top panel shows bright-field images of the NF-186-labelled neurons. Arrow indicates the AIS. The traces below each image show individual responses of the cells to current (10ms and 500ms) and voltage injections. Note the absence of action potentials and active ionic conductances in the AIS-negative neuron (right). Scale bar, 20µm**.**

Electrophysiological traces from KCl treated neurons show slightly different dynamic (Figure 5.5). Namely, both AIS-positive and AIS-negative neurons were capable of firing action potentials to short (10ms) current injection, regardless of the presence or absence of the AIS. The waveform of the action potential, however, was markedly different between these two conditions, as shown in the two example cells in figure 5.5. The cell lacking the AIS fired broader action potentials of smaller amplitude, whereas the cell containing the AIS fired narrow, tall spikes. Despite its apparent ability to fire action potentials, the cell lacking the AIS was unable to undergo repetitive firing in response to long (500ms) current injection. The AIS-positive cell, on the other hand, was able to initiate repetitive firing but displayed progressive attenuation, a feature not observed in control AIS-positive cells (Figure 5.4).

5.3.1 AIS-negative cells have decreased ability to fire action potentials

To determine how the absence of an AIS affects the ability of neurons to fire action potentials, I examined what proportion of AIS-positive and AIS-negative cells (pooled from control and KCl condition) was able to initiate a single action potential (defined as a fast-rising voltage increase that crossed the 0 mV line) in response to 10 ms somatic current injection. In agreement with the Ca^{2+} imaging data, AIS-negative neurons were much less likely to fire a singleaction potential than the AIS-positive cells (AIS-negative: 42% cells fired; 6 out of 14 cells. AIS-positive: 96% cells fired; 25 out of 26 cells) (Figure 5.6a). Interestingly, a considerable number of cells was able to initiate an AP despite the absence of an AIS.

A more careful examination of the data showed that most of the AIS-negative neurons that were capable of firing action potentials belonged to the KCl-treated group (Figure 5.6b). In control condition, only 1 out of 9 AIS-negative neurons was able to initiate a single action potential, in sharp contrast to AIS-positive cells, in which all cells (17 out 17) fired an AP. This clear-cut relation, however, was altered in high-KCl-treated cultures, where most cells spiked irrespective of the presence or absence of the AIS (5 out 5 AIS-negative cells and 8 out of 9 AIS-positive neurons). At first glance, this puzzling result may appear to contradict the Ca^{2+} imaging data shown in Figure 5.2. However, the data obtained from the longer current injections (described below), provide an interesting hypothesis that may reveal a possible mechanism for the AIS disassembly.

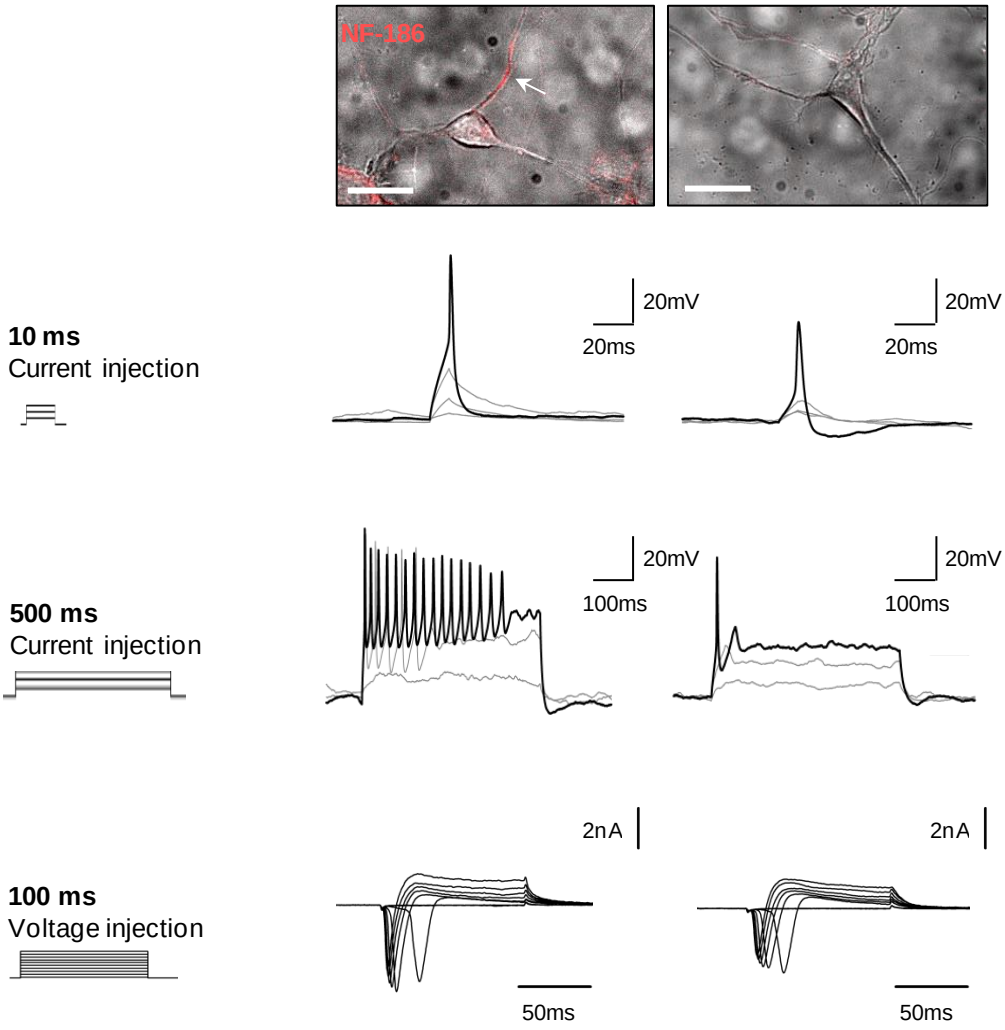

Figure 5.5 Representative electrophysiological recordings from 7 DIV high-KCl-treated neurons live-stained for the AIS with NF-186. The top panel shows bright-field images of the NF-186-labelled neurons. Arrow indicates an AIS. The traces below each image show individual responses of the cells to current (10ms and 500ms) and voltage injections. Note the altered waveform of an action potential and lack of repetitive firing in the AIS-negative neuron (right). Scale bar, 20µm.

To evoke action-potential trains I somatically injected 500ms-long current pulses of increasing amplitudes. Figure 5.6c shows a typical input-output curve, that plots the number of action potentials as a function of the amount of injected current. In AIS-positive neurons, increasing amounts of current elicited multiple action potentials of increasing frequency until the cell reached its maximal firing rate and plateaued. AIS-negative neurons, on the other hand, were largely incapable of initiating multiple action potentials at any current input densities. The maximal number of spikes in AIS-negative neurons was on average significantly smaller (1.8 ± 0.7) than in AIS-positive neurons (20.3 ± 3.1, two-tailed t test, $p = 0.0082$, $n_{Control} = 25$ $n_{KCl} = 6$) (Figure 5.6e). There was no significant difference between KCl-treated and control AIS-negative neurons, as neither of them was able to elicit sustained trains of action potentials, regardless of the amount of current injected. AIS-positive neurons, on the other hand, fired more spikes after KCl treatment than in control condition (28.8 ± 6.9 and 16.4 ± 2.9, respectively, mean ± SEM; Figure 5.6d and f). This difference, however, was not statistically significant ($p = 0.064$, unpaired t test, $n_{Control} = 17$, $n_{KCl} = 8$).

Taken together, these results show that, in control conditions, the presence or absence of the AIS determines the firing capabilities of the cell. In control conditions, the presence of the AIS was sufficient for the neuron to fire an action potential, whereas the absence of an AIS significantly reduced the chances of a cell to initiate an action potential or sustain repetitive firing. This dependence was not as clear in KCl treated cultures, where most cells were able to fire an action potential, regardless of the presence or absence of the AIS. This may suggest the existence of a distinct pool AIS-negative neurons in the KCl-treated group, most likely neurons that had their AIS removed in response to chronic depolarisation, but still retained sufficient number of Na^+ channels to initiate a single action potential, but not high frequency trains. This interesting possibility suggests that although the AIS is disassembled in response to membrane depolarisation, Na^+ channels are still present in the cell. Disruption of the AIS scaffolding, however, may have led to their redistribution along the axon, which significantly affected the firing properties of the cells.

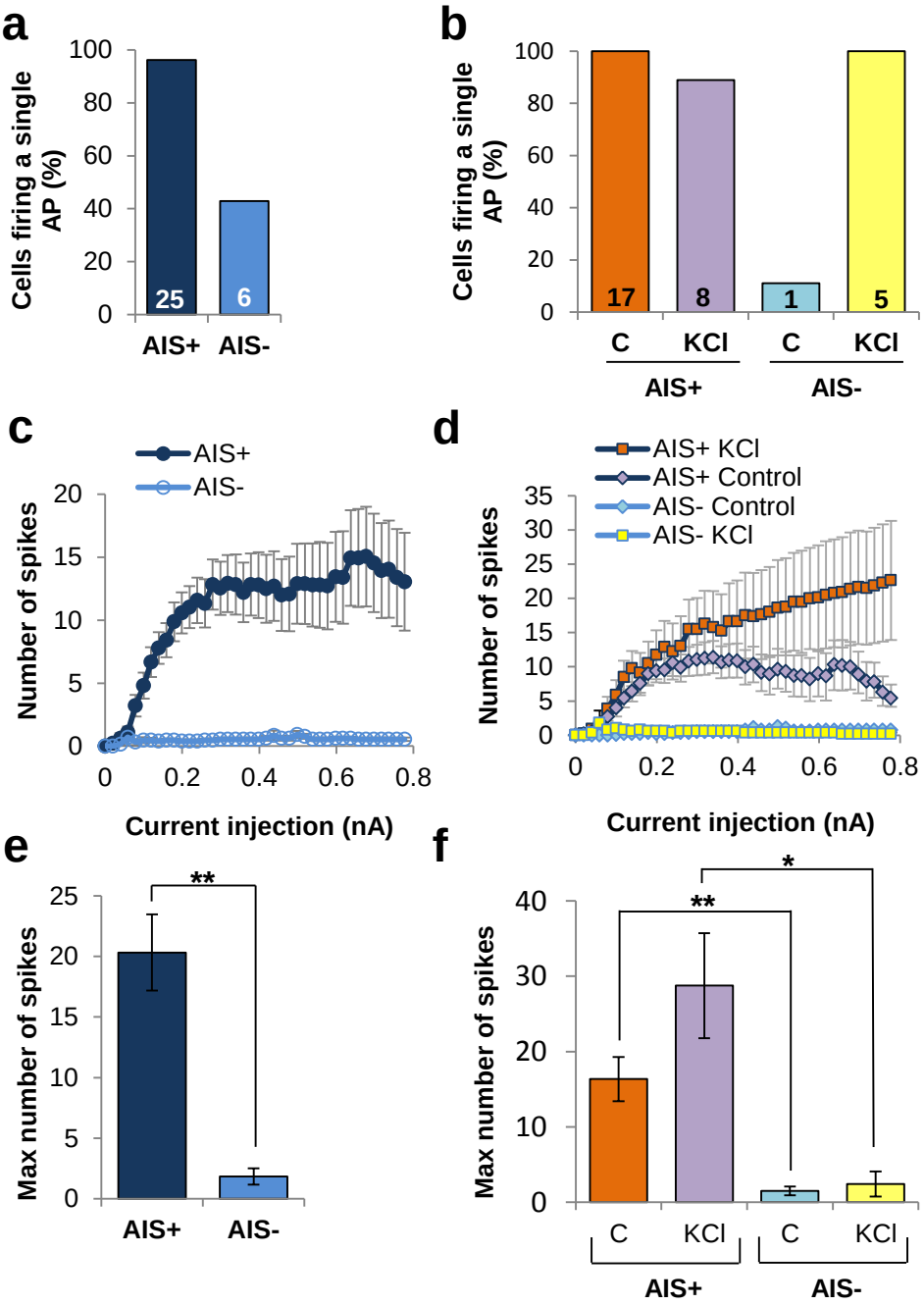

Figure 5.6 Neurons lacking an AIS have impaired ability to fire action potentials. (a) Graph showing a proportion of AIS-positive (AIS+, dark blue) and AIS-negative (AIS-, light blue) neurons firing an action potential in response to 10ms somatic current injection. (b) A proportion of AIS+ (orange and purple) and AIS- (light blue and yellow) neurons in control and KCl conditions. (c, d) Number of spikes elicited in AIS+ (dark blue line) and AIS-negative (light blue line) in control (orange and light blue data points) and KCl (purple and yellow data points) conditions, as a function of increasing amount of injected current. Note that in all AIS- cells the firing rate was consistently reduced at all input intensities. (e) Maximal number of spikes in AIS+ (dark blue) and AIS- (light blue) neurons. (f) Maximal number of spikes in AIS+ (orange and purple) and AIS- (light blue and yellow) neurons in control and KCl conditions. Numbers within bars indicate number of spiking cells within each condition. *, $P < 0.05$, **, $P < 0.01$, unpaired t test, $n_{Control} = 25$ $n_{KCl} = 6$. Error bars, SEM.

5.3.2 Neurons lacking an AIS have distinct passive membrane properties

In the previous section I have shown that control neurons lacking an AIS were mostly incapable of firing an action potential evoked by somatic current injection (only 1 out of 9 cells spiked), in contrast to AIS-positive cells, all of which were able to fire action potentials (17 out of 17cells spiked). This difference in firing efficacy between AIS-positive and AIS-negative cells may be explained by their distinct electrophysiological characteristics. In this section, I examine one of these characteristics, the passive membrane properties of AIS-positive and AIS-negative neurons in control and KCl conditions.

The membrane properties measured here were membrane capacitance, membrane resistance and resting membrane voltage. Membrane capacitance (C_m) is directly proportional to the membrane area and thus the overall size of the cell. Therefore it is often used as a reliable indicator of a cell's surface area as well as to normalise other electrophysiological measures for variability in cell size (Taylor et al., 2011). Membrane resistance (R_m) is an estimation of neuronal conductance at rest, which is directly proportional to the total number of open channels along the membrane. The resting membrane potential (V_m) describes the difference in voltage between interior and exterior of the cell. In hippocampal cells, this value changes in development, from more depolarised in young neurons (~40 mV) to more hyperpolarised in older cells (~60 mV) (Liu et al., 1996; Holter et al., 2007). The passive membrane properties of the cell can therefore strongly influence neuronal excitability, mostly by influencing the current threshold for action potential initiation.

First, I examined R_m, C_m and V_m of AIS-positive and AIS-negative neurons from control condition (Figure 5.7 a-c). Control AIS-negative cells had significantly higher R_m values (2.05 ± 0.79 nΩ) than AIS-positive neurons (0.58 ± 0.05 nΩ; p = 0.013, unpaired t test, n_{AIS+}= 17 cells, n_{AIS-} = 9 cells). Higher R_m of AIS-negative cells was mirrored by their significantly lower capacitance (17.92 ± 1.42 pF), as compared to AIS-positive cells (29.54 ± 1.81 pF; P < 0.0001, unpaired t test, n_{AIS+}= 17 cells, n_{AIS-} = 9 cells). High R_m and low C_m values of AIS-negative neurons indicate that they are, on average, smaller than the AIS-positive cells. The V_m values of AIS-positive and AIS-negative neurons were not significantly different (p = 0.59, unpaired t test), even though there was a clear trend towards a more depolarised V_m in AIS-negative neurons (Figure 5.7c).

Similar differences in membrane properties were observed in high-KCl-treated cells. Here, cells lacking an AIS had significantly higher values of R_m (1.39 ± 0.31 nΩ) and

lower values of C_m (17.66 ± 1.31pF) than neurons with an AIS (0.62 ± 0.06 nΩ and 26.36 ± 1.93 pF; p = 0.001 and p = 0.007 for R_m and C_m, respectively; unpaired t test, n_{AIS+}= 9 cells, n_{AIS-} = 5 cells; Figure 5.7d,e). There was no significant difference in V_m values in these two groups of cells, even though the general trend was towards a more depolarised resting potential in AIS-negative neurons (Figure 5.7f). These results indicate that in both control and KCl conditions, cells lacking an AIS are smaller and perhaps belong to a more immature group of cells.

5.3.3 KCl-treated AIS-negative cells show immature action potential properties

I have previously shown that KCl treatment increases the proportion of AIS-negative cells that fire an action potential. This puzzling result poses an obvious question: are the properties of individual spikes in these cells any different?

To answer this question I examined a number of parameters that characterise the action potential, such as current and voltage threshold for initiation, maximal voltage and the width at half-height(Figure 5.8a). Current and voltage threshold are direct measures of neuronal membrane excitability. The former represents the amount of current needed to fire an action potential, whereas the latter denotes the membrane voltage at which suffiecient number of voltage-gated Na^+ channels opens, leading to Na^+ influx and initiating the regenerative response. The maximal voltage and width at half-height describe the shape and height of the action potential.

First, I examined the values of current threshold density (current per area) in AIS-positive and AIS-negative neurons. AIS-negative neurons had higher current thresholds (13.10 ± 3.09 $pApF^{-1}$) than AIS-positive neurons from either control (9.89 ± 0.82 $pApF^{-1}$) or KCl-treated cultures (10.17 ± 1.04 $pApF^{-1}$) (Figure 5.8b). In addition, KCl-treated AIS-negative cells had on average a more depolarised voltage threshold (-18.66 ± 4.50 mV) than AIS-positive neurons (-25.76 ± 2.05 mV and -24.45 ± 4.27 mV in control and KCl-treated cultures, respectively; Figure 5.8c). These differences, however, were not statistically significant, possibly due to low number of recordings in each case. A significant difference, however, was detected in the waveform of the action potential. AIS-negative cells had significantly wider

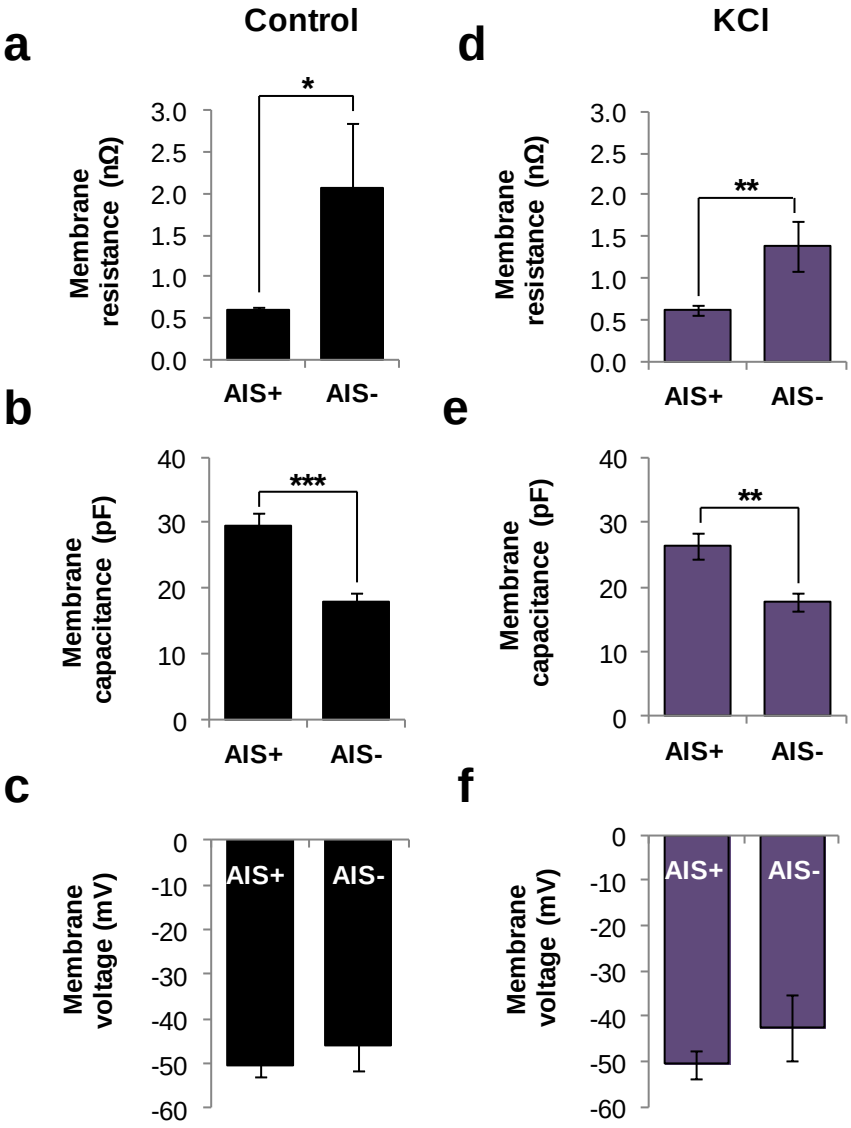

Figure 5.7 Neurons lacking an AIS have distinct passive membrane properties. Graphs showing the values of membrane resistance, R_m, membrane capacitance, C_m and resting membrane voltage, V_m in control (a-c) and high-KCl-treated neurons (d-e) . *, P < 0.05; **, P < 0.01; ***, P < 0.001, unpaired t test, Control: n_{AIS+} = 17 cells, n_{AIS-} = 9 cells; KCl: n_{AIS+} = 9 cells, n_{AIS-} = 5 cells. Error bars, SEM.

spikes, as measured by the value of width at half-height (2.09 ± 0.26 ms) than the AIS-positive cells (1.58 ± 0.10 and 1.28 ± 0.16 ms for control and KCl-treated

cultures respectively) which fired narrow, sharp spikes (P = 0.047, control and P = 0.009, KCl; unpaired t test, $n_{AIS-} = 5$; $n_{AIS+} = 16$, control; $n_{AIS+} = 7$, KCl; Figure 5.8d). The height of the spikes, as measured by the peak voltage (V_{max}) of the action potential, was not significantly different. Nonetheless, there was a clear trend towards lower V_{max} in AIS-negative neurons (19.92 ± 2.45mV) when compared to high-KCl treated AIS-positive cells (27.53 ± 4.31 mV), but not when compared to AIS-positive control neurons (17.93 ± 3.50 mV; Figure 5.8e).

Together, these results indicate that KCl-treated AIS-negative neurons exhibit firing characteristics that are characteristic of young immature neurons. They are capable of firing rudimentary spikes but they cannot initiate and sustain repetitive firing. Moreover, the electrophysiological characteristics of action potentials are significantly altered, so that although KCl-treated AIS-negative cells were able to generate single action potentials, they did so less efficiently than the cells containing the AIS. The ability of these cells to initiate single action potentials despite the absence of NF-186 immunoreactivity may indicate that AIS disassembly affected only the anchorage of spike-initiating Na_v channels, rather than led to their complete elimination from the axon. In the next section, I compare the amplitudes of Na^+ current in treated and untreated AIS-positive and AIS-negative neurons.

5.3.4 The amplitude of Na^+ current determines the firing properties of a neuron

Voltage-gated sodium (Na_v) channels are highly enriched at the AIS of cultured hippocampal neurons (Yang et al., 2007, Hedstrom et al., 2008). It has been estimated that there are 3 to 50 times more Na_v channels at the AIS than in the soma and proximal dendrites (Kole et al., 2008, Kress e tal. 2010, Tapia et al., 2013, Figure 5.8a). Sodium channels are recruited to the AIS through a direct interaction with AnkG (Garrido et al., 2003; Gasser et al., 2012) and are further stabilised by cross-linking with other scaffolding proteins, especially β-spectrins (Jenkins and Van Bennett, 2001). There are two major Na_v channel subtypes at the AIS of pyramidal hippocampal neurons: the high-threshold $Na_v1.2$ in the proximal AIS and the distally-expressed low-threshold $Na_v1.6$ (Kress et al., 2010). Different combinatorial arrangement of these channels, their density and gating properties have been shown to influence intrinsic excitability of the cell (Colbert and Pan, 2002; Kole et al., 2008; Kress et al., 2010).

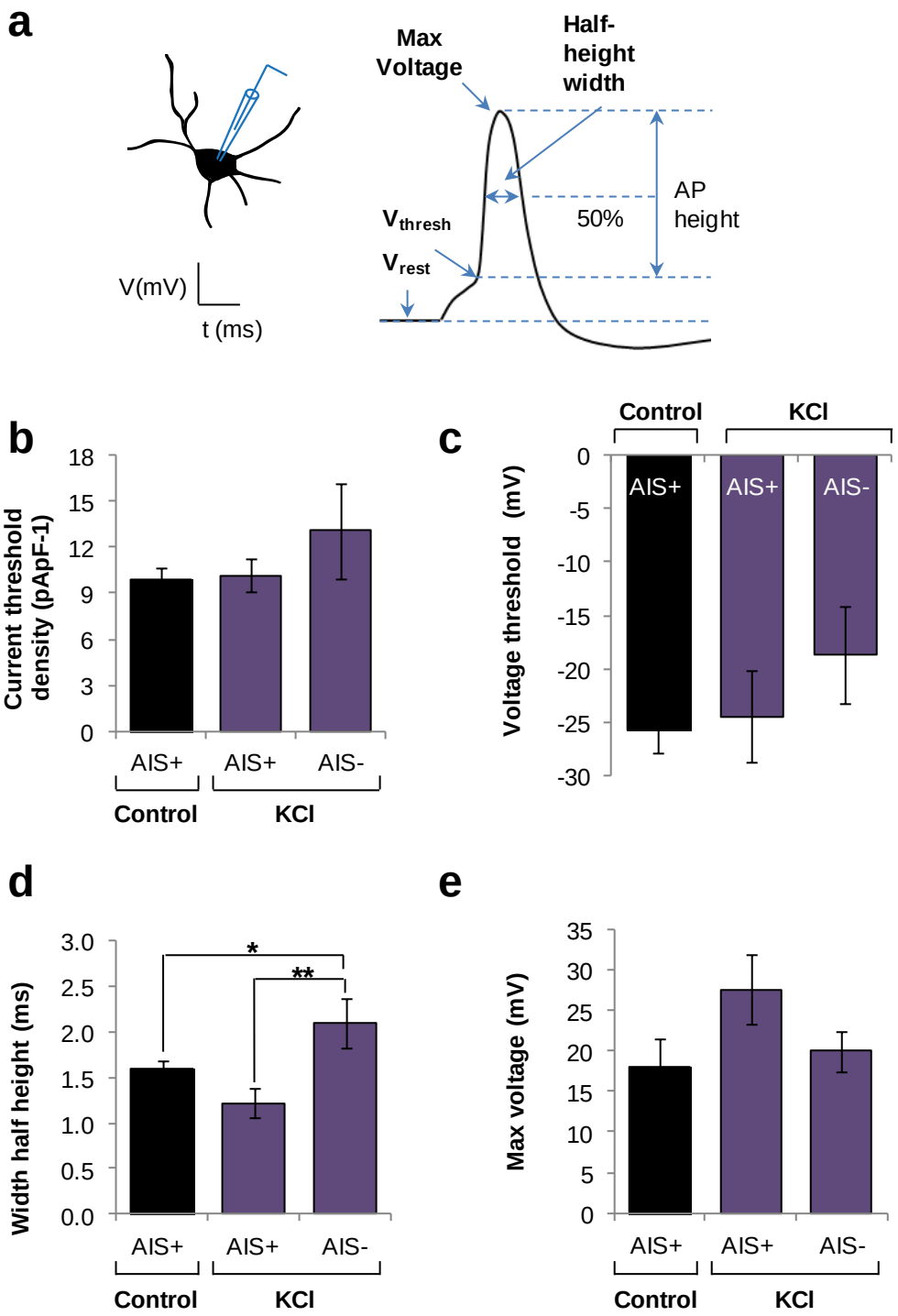

Figure 5.8 KCl-treated AIS-negative cells have impaired action potential properties (a) A schematic depicting the properties of an action potential (evoked by a somatic current injection) measured. V_{thresh}, voltage threshold; V_{rest}, resting membrane voltage (resting membrane potential). (b-e) Graphs showing the values of current threshold density (b), voltage threshold (c), width at half-height (d) and the maximal voltage of an action potential (e) in AIS-negative (AIS-) high-KCl treated neurons compared to AIS-positive (AIS+) neurons from control (black) and high-KCl (purple) cultures. Cells were recorded in the presence of AMPA/kainate, NMDA and $GABA_A$-R blockers. *, P < 0.05; **, P < 0.01; ***, P < 0.001, unpaired t test, Control: n_{AIS+} = 16 cells, n_{AIS-} = 9 cells; KCl: n_{AIS+}= 8 cells, n_{AIS-} = 5 cells. Error bars, SEM.

Here, I measured Na_v currents in AIS-positive and AIS-negative hippocampal neurons. Typically, whole-cell Na_v currents are investigated under a voltage clamp setting where other ionic currents (mostly K^+ and Ca^{2+}) are pharmacologically blocked. Because K^+ and Ca^{2+} currents are important for action potential firing, I could not record an action potential and measure Na^+ currents in the same cell. Therefore, I chose to perform current-voltage relations of all ionic conductances in voltage clamp, without pharmacologically blocking either K^+ or Ca^{2+} currents.

Figure 5.9b shows an example of current traces in response to increasing steps of membrane depolarization. The currents recorded at the soma showed that active conductances appeared beyond ~40 mV and were composed of a fast-rising but quickly inactivating inward current followed by a slower persistent outward current. The inward current corresponds to a mixture of Ca^{2+} and $^+$ currents whereas the outward current consists mainly of a K^+current. Although the inactivating inward current is a combination of the two conductances, the Na^+ currents are more than an order of magnitude larger than Ca^{2+} currents in cultured hippocampal neurons, when recorded at the soma. As a result, peak inward currents were taken to reflect mainly Na^+ currents (I_{Na}). Another issue with the measurement of fast inward Na^+ currents is a space clamp problem. This is apparent in Figure 5.4 (current trace, bottom left) where repetitive Na^+ current events were measured during a voltage step. In these traces the maximum current was achieved at low voltages, around the threshold for Na^+ channel activation, instead of gradually growing as membrane depolarisation is increased. Lack of proper space clamp makes the measurements of Na^+ currents problematic, nevertheless, the peak inward current can still give some estimate, even if imperfect, of the total number of Na^+ channels in a cell. In fact, this measure turns out to be one of the best predictors for the firing capabilities of neurons (Figure 5.9).

To estimate the magnitude of Na^+ currents, I measured the maximal amplitude of the inward conductance from the voltage-clamp recording (Figure 5.8b). The peak Na^+ current was strongly correlated with the majority of measures of neuronal excitability, including voltage threshold, current threshold, amplitude and width at half-height of the action potential and the maximum number of spikes. The higher the value of Na^+ current (I_{Na}), the lower the values of voltage threshold ($r = 0.405$, $p = 0.014$, $n = 36$, Figure 5.9c), current threshold density ($r = 0.539$, $P < 0.0001$, $n = 38$, Figure 5.9d) and width at half-height ($r = 0.569$, $P < 0.0001$, $n = 36$; Figure

5.9e), indicating that neurons with a high I_{Na} can initiate fast action potentials at less depolarised voltage with smaller amounts of input current, and thus are more excitable, than the cells with low values of $I_{Na.}$ The peak magnitude of Na^+ current was also strongly positively correlated with the maximal voltage(V_{max}) of an action potential ($r = 0.661$, $P < 0.0001$, $n = 36$, Figure 5.8f) and the maximal number of spikes a neuron was capable of firing ($r = 0.654$, $P < 0.001$, Pearson's r test, $n = 38$; Figure 5.8g). These results show that I_{Na} is a great predictor of the firing characteristics of a neuron. In the next section I explore whether the magnitude of I_{Na} can explain distinct firing properties observed in AIS-positive and AIS-negative neurons.

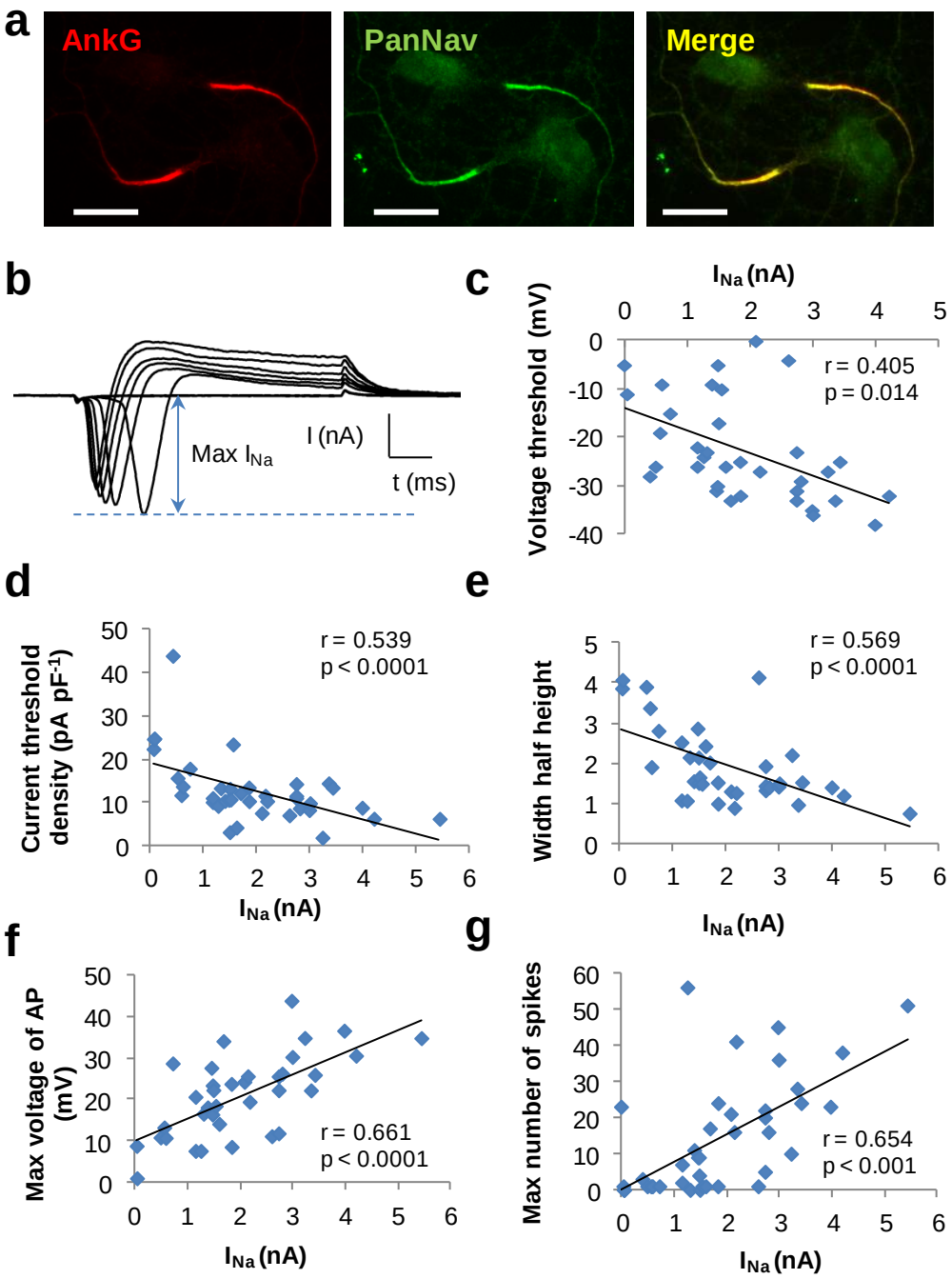

Figure 5.9 Sodium current as an indicator of firing properties of the cell. Voltage-gated sodium channels co-localise with AnkG at the AIS of 7 DIV neurons. (b) A sample trace of ionic conductances evoked by increasing voltage pulses. The inward current corresponds to sodium-mediated conductance (I_{Na}). The magnitude of voltage-evoked I_{Na} was estimated by taking the peak current as the measure of Na^+ conductance. (c-g) The peak value of I_{Na} correlated with passive and active properties of neurons, such as voltage threshold (c), current threshold density (d), width at half height (e), maximal voltage of an action potential (f) and a maximal number of spikes a cell could fire. Scale bar, 20µm.

5.3.5 AIS-negative cells display lower Na^+ currents

In order to visualise Na^+ currents in AIS-positive and AIS-negative cells, I plotted current-voltage relations for I_{Na} (Figure 5.10a-b). In both control and high-KCl treated cultures, the average I_{Na} trace of AIS-negative neurons was considerably distinct from the I_{Na} of AIS-positive neurons. Overall, it was clear that the values of I_{Na} were much lower in neurons lacking an AIS, irrespective of the condition.

To quantify the differences seen, I first compared the peak values of I_{Na} in all (control and KCl-treated) AIS-positive and AIS-negative neurons grouped together (Figure 5.10c). As predicted, the average peak I_{Na} value was significantly lower in AIS-negative (-1.22 ± 0.31 nA) than in AIS-positive neurons (- 2.34 ± 0.22 n, p = 0.005, unpaired t test, n_{AIS+} = 24 and n_{AIS-} = 14; Figure 5.9c). Next, I examined any differences in peak Na_v currents, separately for control and KCl-treated cells. In control cells, the peak I_{Na} amplitude was significantly higher (-2.13 ± 0.24 pA) in AIS-positive than in AIS-negative neurons (-1.03 ± 0.48 pA, p = 0.033, unpaired t test, n_{AIS+} = 16 and n_{AIS-} = 9). Similarly, in KCl condition, the peak Na_v current was significantly lower in neurons lacking the AIS(-1.55 ± 0.09pA) than in cells with the AIS (-2.79 ± 0.45 pA, P = 0.05, two-tailed t test, n_{AIS+} = 8 - and n_{AIS-}= 5 cells). Thus in spite of seemingly similar abilities of KCl-treated AIS-positive and AIS-negative neurons to initiate an action potential, the Na_v currents underlying neuronal excitability were considerably different and may account for distinct action potential properties seen in KCl-treated AIS-negative cells

Together, these results show that different magnitudes of Na_v current in AIS-positive and AIS-negative neurons can explain the distinct electrophysiological characteristic of these two groups of cells. In general, the larger the Na_v current, the more likely it was for the cell to respond to depolarising current injection by generating an action potential. There was a clear dependence between the maximal value of I_{Na} and the ability of a cell to fire multiple spikes, which was considerably impaired in AIS-negative neurons. In addition, the height and width of the action potential could be predicted by the magnitude of the Na^+ current, as low I_{Na} AIS-negative neurons tended to generate wider spikes of lower amplitude than the high I_{Na} AIS-positive cells.

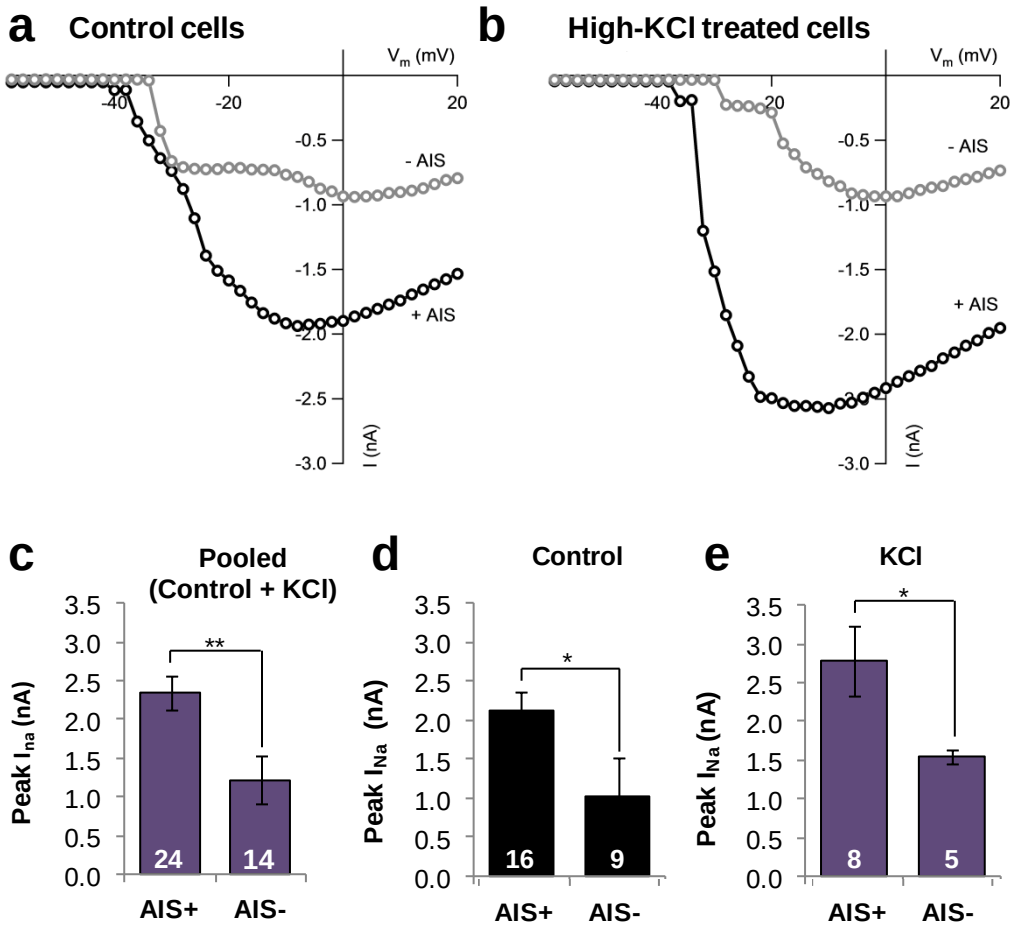

Figure 5.10 AIS-negative cells have lower sodium current than AIS-positive neurons. (a-b) Graphs showing averaged amplitudes of the Na^+ currents (I_{Na}) as a function of injected voltage in control (a) and high-KCl-treated neurons. (c) Peak I_{Na} in AIS-positive (AIS+) and AIS-negative (AIS-) cells pooled from control and KCl conditions. (d,e) Peak I_{Na} in AIS-positive and AIS-negative cells in control (d) and KCl conditions (e). Numbers within the bars indicate the number of cells within a condition. *, P < 0.05. **, P < 0.01. Error bars, SEM

5.4 Discussion

In this chapter I investigated the electrical properties of neurons with and without an AIS in cultured hippocampal neurons at 7 DIV. Neuronal excitability was examined by means of Ca^{2+} imaging and whole-cell patch-clamp techniques, in both control and KCl-treated neurons. Both methods revealed that neurons without an AIS showed impaired firing. The Ca^{2+} imaging experiments showed that cells lacking an AIS were less likely to display a Ca^{2+} transient in response to whole-field electrical stimulation than cells containing an AIS. In addition, the AIS-negative neurons that did respond, showed a significantly lower amplitude Ca^{2+} signal than AIS-positive cells. In agreement with this, the data obtained from patch-clamp experiments showed that neurons lacking the AIS were less likely to fire single action potentials and had severly impaired ability to generate multiple spikes in response to somatic current injection than the cells containing the AIS. In addition, AIS-negative cells displayed smaller somatic Na_vcurrents, confirming that the absence of the AIS impacts severely on the levels of neuronal excitability.

The two techniques used in this chapter were complementary, but did not show a complete agreement. The electrophysiological recordings detected a noticeably larger proportion of neurons that was able to fire action potentials than did the Ca^{2+} imaging experiments. This apparent discrepancy between the techniques is probably due to the higher sensitivity of the patch-clamp method compared to Ca^{2+} imaging. Ca^{2+} dyes cannot always resolve single action potentials, especially in immature neurons, so that a significant portion of firing cells may have gone undetected in the Ca^{2+} imaging experiments. Whole-cell patch-clamp techniques, on the other hand, can detect even the smallest spikes with high sensitivity, thus markedly decreasing the number of false negatives.

The magnitude of the input activity required to trigger a neuronal spike depends on the specific composition of the AIS, especially the density and types of voltage-gated Na^+ channels (Bean et al., 2007; Kole and Stuart, 2012). Interestingly, KCl treatment altered this seemingly clear-cut relationship between the presence of the AIS and the ability of a cell to fire an action potential. In KCl treated cultures, a vast majority of neurons (13 out of 14) was capable of firing a single action potential, irrespective of the presence or absence of the AIS. The absence of the AIS, however, severely affected the ability of the cells to generate repetitive firing. None of the AIS-negative neurons was able to fire multiple spikes, in either control or KCl-

treated conditions. Therefore, in developing neurons, a fully functional AIS appears to be necessary for repetitive firing, but not for the generation of single action potentials.

The ability of KCl-treated, AIS-negative cells to fire single action potentials indicates that they are functionally distinct from the control cells. Although it is unclear why these neurons are able to fire, I would like to suggest two possibilities. First, this group may represent the neurons that originally had an AIS but lost it after KCl treatment. As a result, these cells would have originally expressed Na_v channels and have had the ability to fire spikes. Upon disassembly of the AIS scaffold, the Na_v channels remained on the plasma membrane, but lost their clustering to the AIS and redistributed along the axon. The presence of Na_v channels at the plasma membrane allowed the neurons to fire action potentials, however less efficiently than the cells containing the AIS. This idea is bolstered by the fact that KCl-treated AIS-negative neurons still showed prominent Na_v currents (although smaller than AIS-positive neurons) and also fired action potentials. The second possibility is that KCl-treatment may have caused a change in membrane excitability, for example through upregulation of Na_v channels. In agreement with this idea, KCl-treated AIS-negative neurons had on average larger Na^+ currents than control AIS-negative cells, however, probably due to low n numbers, this difference was not statistically significant. In addition, KCl-treated AIS-negative neurons displayed passive electrical properties that are characteristic of immature neurons (low C_m and high R_m), suggesting they may belong to the set of neurons that did not have an AIS at the onset of the treatment. It is therefore possible that immature neurons, which did not previously have an AIS, could now change their excitability by adding new channels to their membrane, while retaining their immature morphological characteristics.

The excitability profile of AIS-negative neurons chronically treated with KCl is consistent with other studies where different components of the AIS have been either knocked down or inhibited. For example, in mice that lack cerebellar AnkG, the AIS does not assemble during development (Zhou et al., 1998; Jenkins and Bennett, 2001). Cerebellar Purkinje cells from these mice are impaired in their ability to fire action potentials in response to somatic current injection. In general, they fire less efficiently, have higher current thresholds and have a slower rate of maximal firing. Similarly, conditional knockouts in cerebellar neurons of another component of the AIS, NF-186, causes dismantling of the AIS in adult mice and impairment of

normal action potential initiation. As above, Purkinje neurons had a higher current threshold, and fired smaller and wider spikes than wild-type neurons. One outcome from the loss of the AIS was the absence of any spontaneous activity in Purkinje neurons, normally ongoing in the wild-type mice (Zonta et al., 2013). Thus, in agreement with the current data, an intact AIS is not necessary for the generation of action potentials (thought to occur somatically in these examples), however it significantly modifies the dynamics and shape of the spikes, as well as their input-output curve.

Even though the AIS is considered the primary region of spike initiation (Palmer and Stuart, 2006; Kress et al., 2008; Hi et al. 2009, Winkels et al., 2009), action potentials can initiate beyond the AIS (Colbert and Johnston, 1996). Neuronal spikes may be initiated within the soma or even dendrites (Stuart et al., 1997). The threshold for the initiation of an action potential depends on the density, availability and biophysical properties of ion channels on the membrane (Bean, 2007). Thus any high-density 'hot-spots' of voltage-gated ion channels may act as the initiation site for generation of single spikes (Kosaka et al., 2008). The AIS is the preferred spot for action potential generation precisely because of its high concentration of voltage-gated ion channels. It has been estimated that Na_v channel density at the AIS is around three times higher than at the soma in dentate granule cells, and up to 50 times higher in cortical pyramidal neurons (Colbert and Pan, 2002; Kole et al., 2008; Schmidt-Hieber and Bischofberger, 2010). The high-density of Na_v channels is maintained by the tight anchoring to the AIS scaffolds, through proteins such as AnkG and βIV-spectrin (Garrido et al., 2003; Pan et al., 2003; Dzhashiashvili et al., 2007). Removing AnkG or βIV-spectrin expression in hippocampal neurons has been shown to block clustering of Na_v channels and impair the firing ability of the cells. For example, βIV-spectrin-deficient 'quivering' mice have reduced Na_v channels densities and reduced excitability in granule cells of the dentate gyrus, leading to decreases in network activity (Yang et al., 2004; Winkels et al., 2009).

An inability to initiate repetitive firing in AIS-negative neurons may have been specifically caused by a low expression of $Na_v1.6$ channels. Distally-located $Na_v1.6$ channels have lower thresholds of activation and display less inactivation than proximally-located $Na_v1.2$ channels (Kole et al., 2008; Hu et al., 2009). These properties make $Na_v1.6$ channels vital for high-frequency firing (Boiko et al., 2003; Blackenbury et al. 2009). The expression of $Na_v1.6$ is developmentally regulated; their clustering at the AIS occurs later in development, after the expression of

$Na_v1.2$ channels. This developmental transition to $Na_v1.6$ expression improves firing reliability during sustained depolarisation and may account for the more efficient repetitive firing observed in mature neurons (Osorio et al., 2010). The localisation of $Na_v1.6$ at the AIS is regulated by its β1subunit (encoded by the *Scn1b* gene) and cerebellar-specific Scn1b null mice show a reduced proportion of AnkG-positive AISs expressing $Na_v1.6$, leading toa decreased excitability of the neurons (Blackenbury et al., 2009).

Deficiency in repetitive firing may also be explained by altered properties of K_v currents in AIS-negative-neurons. The characteristics of K_v conductance is determined by the number, distribution and specific isotype of K_v channels expressed. For example, K_v1 channels delay the onset of action potential firing (Storm et al., 1988) and influence action potential threshold, interspike interval and its width at half-height (Bekkers and Delaney, 2001; Goldberg et al., 2008; Kole et al., 2007). K_v7 channels, on the other hand influence spike-frequency adaptation and spontaneous action potential firing (Peters et al., 2005; Hu et al., 2007; Shah et al., 2007; Yue and Yaari, 2004). Narrow, fast spikes may be crucial for enabling rapid recovery of Na_v channels from depolarisation-induced inactivation. By regulating axonal action potential half-width, K_v1 channels can determine the duration of axonal action potentials and thereby indirectly affect transmitter release. K_v1 channels have been previously shown to be regulated by neuronal activity. For example, chronic silencing of neuronal activity (with TTX or blocking synaptic transmission) inhibits the expression of K_v1 in cultured hippocampal neurons (Grosse et al., 2000).

Lastly, activity may regulate the expression of Na_v and K_v channels through posttranslational modifications, such as phosphorylation of certain residues that may affect their interactions with the AIS scaffold. For example, Na_v channel expression at the AIS can be regulated by phosphorylation with GSK3 (glycogen synthase kinase 3), as pharmacological inhibition of GSK3 or knockdown of its substrate β-catenin decreases the levels of Na_v channels at the AIS (Tapia et al. 2013). Similarly, phosphorylation of $Na_v1.2$ channel by CK2 (casein kinase2) increases the affinity of $Na_v1.2$ to AnkG and causes accumulation of $Na_v1.2$ at the AIS of hippocampal neurons (Brechet et al., 2008). Both GSK3 and CK2 are enriched at the AIS, where they may regulate the interactions between different components of the AIS. The expression of K_v channels, on the other hand, is

regulated by the kinase Cdk5 (cyclin-dependent kinase 5), which promotes their targeting to the axonal membrane (Vacher et al., 2011).

To summarise, I have shown that lack of the AIS has profound functional consequences on intrinsic excitability of hippocampal neurons at 7 DIV. In control conditions, AIS-negative neurons were largely incapable of initiating action potentials, regardless of the amount of depolarising current injected. KCl-treated neurons could fire single action potentials but not multiple spikes. In contrast, AIS-positive neurons in either condition efficiently fired single and multiple action potentials. The difference between firing properties of AIS-positive and AIS-negative neurons can be accounted for by their distinct Na_v currents, which strongly correlated with the majority of passive and active membrane properties of the cell. Cells lacking the AIS displayed lower currents than the cells containing the AIS, suggesting that an altered density, kinetics and isoforms of Na_v may underlie the differences between AIS-positive and AIS-negative neurons.

Activity-dependent AIS disassembly as a model of homeostatic regulation of intrinsic excitability

The most striking finding of this thesis is the activity-dependent AIS disassembly.The reversibility of this change and its profound influence on neuronal excitability is consistent with a homeostatic model of intrinsic excitability. According to this model, neurons can regulate their own excitability in response to activity oscillations, whereby, in an attempt to preserve an overall balance of activity, a change of activity in one direction is counterbalanced with an excitability change in the opposite direction (Nelson and Turrigiano, 2004). Homeostatic control of network activity can occur via a number of mechanisms. One of them is 'synaptic scaling' (Turrigiano et al., 1999) in which activity deprivation leads to the up-regulation of excitatory and down-regulation of inhibitory synaptic inputs (Turrigiano and Nelson, 2004). Yet another, non-synaptic mechanism of homeostatic control can occur at the level of a single cell, whereby neurons regulate their own excitability in an activity-dependent manner (Grubb and Burrone, 2010; Kuba et al., 2009).

Intrinsic electrical properties of neurons are key for their function, as they determine how the cell integrates synaptic inputs and determines its characteristic firing. Activity perturbations are relatively common in the nervous system, especially during development, where new synapses are continuously formed and eliminated, and the strength of these connections are also constantly changing. Indeed, it is easy to imagine situations where, for example, neurons receive too many (and/or too strong) inputs that can drive the neuron, and ultimately the network, to hyperactivity. The converse, a loss of inputs, is also possible. Neurons therefore have the task of remaining stable whilst allowing for on-going synaptic plasticity to happen as circuits wire up. In order to maintain stability within the network, neurons have to be able to regulate their own excitability to counteract any extreme activity-perturbations. Activity-dependent AIS disassembly may be one such mechanism.

How does activity lead to AIS disassembly and ensuing decrease in neuronal excitability? The exact mechanism is not yet known, however the data presented in this thesis suggests that this may occur through several steps. First, elevated activity triggers Ca^{2+} influx though L-type voltage gated channels, which in turn, through unknown signalling pathways, trigger the dismantling of the AIS scaffold. Second, AIS disassembly causes the loss of membrane anchorage of voltage-gated ion channels, which may become redistributed along the axon and the soma. Lack

of AIS anchorage may also induce selective endocytosis of specific channels and alter gating properties of the remaining channels. Finally, changes in the distribution, density and biophysical properties of ion channels can in turn alter firing properties of the neuron, leading to decreased excitability (Figure 5.11).

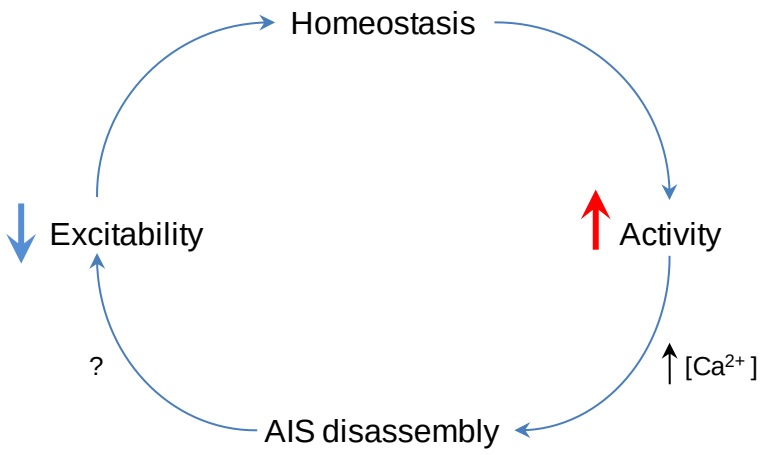

Figure 5.11 AIS disassembly mediates decreased excitability and promotes network homeostasis. Increase in activity (red arrow) triggers increase in intracellular ([Ca^{2+}]) leading to AIS disassembly. AIS disassembly results in a compensatory decrease in neuronal excitability (blue arrow) and restoration of homeostasis.

Chapter 6

Summary

In this thesis I explored the role of activity in early development of hippocampal neurons *in vitro*. Specifically, I investigated the effect of early membrane depolarisation on three distinct compartments of the cells: dendrites, axons and the axon initial segments.

In chapter 3 I examined the effect of chronic (16hr) depolarisation on development of dendritic and axonal arborisations in prox1-positive (dentate granule cells) and prox1-negative (consisting mostly of pyramidal cells and GABAergic interneurons) cells. Activity was induced by either global cell depolarisation with elevated levels of KCl or by a spatiotemporally-controlled optogenetic photostimulation of ChR-2 expressing neurons. Either of the above methods induced a modest decrease in the size of dendritic arbours in dentate granule cells, without significantly affecting their shape and/or the length of the axon. In the remainder of the hippocampal neurons, chronic depolarisation led to two different effects, depending on which method of activity modulation was used. The cells depolarised with elevated [KCl] showed a marked decrease in total axonal lengths, but not in the total lengths of their dendritic arbours. The neurons depolarised with optogenetic photostimulation, on the other hand, displayed a significant decrease in both dendritic and axonal lengths, even though the latter was observed in only one stimulation condition. The shape of the dendritic tree was largely unaffected by either of the two methods of membrane depolarisation.

In chapter 4 I explored the effects of membrane depolarisation on early development of the axon initial segment (AIS) in dentate granule cells and pyramidal hippocampal neurons. First, I characterised the timecourse of AIS formation in these two groups of neurons. In our culture system, first AISs emerge around 2 DIV, after which progressively larger numbers of cells begin forming an AIS, reaching a plateau at 7 DIV for pyramidal cells and around 13 DIV for granule neurons. By the end of the second week *in vitro*, a majority of neurons have an AIS. Next, I characterised how the properties of the AIS change in development. In both groups of neurons, AIS shifts closer to the soma as the cells mature. In pyramidal cells, a proximal AIS shift is accompanied by an increase in the AIS length. In

granule cells, on the other hand the AIS becomes more proximal and shorter as the development progresses. In addition, I observed a gradual increase in the intensity of AnkG immunofluorescence, suggesting progressive accumulation of AnkG protein during AIS development and maturation.

Having established the timeline of AIS formation, I then proceeded to examine whether young (4 – 7 DIV) granule and pyramidal cells display any form of AIS plasticity in response to chronic membrane depolarisation. Strikingly, chronic membrane depolarisation with either elevated levels of KCl or optogenetic stimulation led to rapid (within 6 hours), cell-death independent, AIS disassembly in a subset of granule and pyramidal neurons. This effect required Ca^{2+} influx though L-type voltage-gated Ca^{2+} channels, but surprisingly, did not depend on calpain-mediated proteolysis. AIS disassembly was observed primarily in young, 4-7 DIV, neurons suggesting the existence of a developmental window for this type of plasticity. In addition, activity-induced AIS disassembly was bidirectional, and could be reversed by the removal of KCl from the culture media. Extending the duration of depolarisation led to a progressive desensitisation of neurons to KCl treatment, which is also consistent with a developmental restriction of activity-induced AIS disassembly to exclusively early stages of development. Perhaps due to their more immature state, granule cells were more susceptible to AIS disassembly than pyramidal neurons.

Next, I examined the properties of the AISs that were not disassembled in response to elevated activity. Interestingly, KCl treatment induced a rapid (within 6 hours) change in AIS properties, the magnitude and direction of which was dependent on the specific developmental stage at which the KCl treatment was administered. In young immature neurons (< 8 DIV), chronic depolarisation caused a proximal shift of the AIS, accompanied by a small decrease in AIS length. In older cells, on the other hand, enhanced activity induced a distal shift of the AIS coupled to an altered AIS length: longer AIS in granule and shorter AIS in pyramidal neurons. Strikingly, the AISs of chronically (1 week) depolarised 14DIV neurons resembled the AISs of young immature cells at 4 DIV. Similar to activity-induced AIS-disassembly, the change in AIS properties was reversible upon removal of the source of depolarisation.

In chapter 5 I examined the functional consequences of the AIS absence on the excitability of 7 DIV neurons using Ca^{2+} imaging and patch-clamp electrophysiology. In Ca^{2+} imaging experiments I showed that neurons lacking an AIS are less likely to

display a Ca^{2+} transient in response to electrical field stimulation. In addition, the maximal amplitude of Ca^{2+} flux was significantly lower in AIS-negative neurons than in AIS-positive cells, indicating a lower excitability of neurons lacking an AIS. In agreement with the Ca^{2+} imaging data, electrophysiological recordings from AIS-positive and AIS-negative neurons revealed an impaired ability of cells without an AIS to fire single and multiple action potentials. Interestingly, AIS-negative neurons that were pre-treated (16 – 24 hours) with KCl were capable of firing single action potentials, but could not sustain repetitive firing. Careful examination of action potential properties, however, showed that KCl-treated AIS negative neurons had altered action potential waveform, characterised primarily by broadening of the spike. In addition, AIS-negative neurons had passive membrane properties (membrane capacitance and resistance) characteristic of young immature neurons, in contrast to AIS-positive cells, which displayed more mature membrane properties. Distinct electrophysiological properties of neurons strongly correlated with the amplitude of Na^{+} currents evoked by incremental voltage injections. The larger the maximal Na^{+} current, the more likely it was for the cell to respond to depolarising current injection by generating an action potential. Cells lacking an AIS had significantly smaller Na^{+} currents, further emphasising the importance of intact AnkG/NF-186 scaffold for clustering of Na_v channels at the AIS.

Bibliography

Alarcon, M., Abrahams, B.S., Stone, J.L., Duvall, J.A., Perederiy, J.V., Bomar, J.M., Sebat, J., Wigler, M., Martin, C.L., Ledbetter, D.H., Nelson, S.F., Cantor, R.M. & Geschwind, D.H. 2008, "Linkage, association, and gene-expression analyses identify CNTNAP2 as an autism-susceptibility gene", *American Journal of Human Genetics,* vol. 82, no. 1, pp. 150-159.

Altman, J. & Bayer, S.A. 1990, "Migration and distribution of two populations of hippocampal granule cell precursors during the perinatal and postnatal periods", *The Journal of comparative neurology,* vol. 301, no. 3, pp. 365-381.

Amaral, D.G. 1978, "A Golgi study of cell types in the hilar region of the hippocampus in the rat", *The Journal of comparative neurology,* vol. 182, no. 4 Pt 2, pp. 851-914.

Amaral, D.G., Scharfman, H.E. & Lavenex, P. 2007, "The dentate gyrus: fundamental neuroanatomical organization (dentate gyrus for dummies)", *Progress in brain research,* vol. 163, pp. 3-22.

Ango, F., di Cristo, G., Higashiyama, H., Bennett, V., Wu, P. & Huang, Z.J. 2004, "Ankyrin-based subcellular gradient of neurofascin, an immunoglobulin family protein, directs GABAergic innervation at purkinje axon initial segment", *Cell,* vol. 119, no. 2, pp. 257-272.

Barker, J.L., Behar, T., Li, Y.X., Liu, Q.Y., Ma, W., Maric, D., Maric, I., Schaffner, A.E., Serafini, R., Smith, S.V., Somogyi, R., Vautrin, J.Y., Wen, X.L. & Xian, H. 1998, "GABAergic cells and signals in CNS development", *Perspectives on developmental neurobiology,* vol. 5, no. 2-3, pp. 305-322.

Bean, B.P. 2007, "The action potential in mammalian central neurons", *Nature reviews. Neuroscience,* vol. 8, no. 6, pp. 451-465.

Bekkers, J.M. & Delaney, A.J. 2001, "Modulation of excitability by alpha-dendrotoxin-sensitive potassium channels in neocortical pyramidal neurons", *The Journal of neuroscience : the official journal of the Society for Neuroscience,* vol. 21, no. 17, pp. 6553-6560.

Ben-Ari, Y., Cherubini, E., Corradetti, R. & Gaiarsa, J.L. 1989, "Giant synaptic potentials in immature rat CA3 hippocampal neurones", *The Journal of physiology,* vol. 416, pp. 303-325.

Ben-Ari, Y. & Spitzer, N.C. 2010, "Phenotypic checkpoints regulate neuronal development", *Trends in neurosciences,* vol. 33, no. 11, pp. 485-492.

Bender, K.J., Ford, C.P. & Trussell, L.O. 2010, "Dopaminergic modulation of axon initial segment calcium channels regulates action potential initiation", *Neuron,* vol. 68, no. 3, pp. 500-511.

Bender, K.J. & Trussell, L.O. 2012, "The physiology of the axon initial segment", *Annual Review of Neuroscience,* vol. 35, pp. 249-265.

Bender, K.J. & Trussell, L.O. 2009, "Axon initial segment Ca2+ channels influence action potential generation and timing", *Neuron,* vol. 61, no. 2, pp. 259-271.

Bender, K.J., Uebele, V.N., Renger, J.J. & Trussell, L.O. 2012, "Control of firing patterns through modulation of axon initial segment T-type calcium channels", *The Journal of physiology,* vol. 590, no. Pt 1, pp. 109-118.

Bender, R.A., Galindo, R., Mameli, M., Gonzalez-Vega, R., Valenzuela, C.F. & Baram, T.Z. 2005, "Synchronized network activity in developing rat hippocampus involves regional hyperpolarization-activated cyclic nucleotide-gated (HCN) channel function", *The European journal of neuroscience,* vol. 22, no. 10, pp. 2669-2674.

Bennett, V. & Lambert, S. 1999, "Physiological roles of axonal ankyrins in survival of premyelinated axons and localization of voltage-gated sodium channels", *Journal of neurocytology,* vol. 28, no. 4-5, pp. 303-318.

Benson, D.L., Watkins, F.H., Steward, O. & Banker, G. 1994, "Characterization of GABAergic neurons in hippocampal cell cultures", *Journal of neurocytology,* vol. 23, no. 5, pp. 279-295.

Berardi, N., Pizzorusso, T. & Maffei, L. 2004, "Extracellular matrix and visual cortical plasticity: freeing the synapse", *Neuron,* vol. 44, no. 6, pp. 905-908.

Berkefeld, H., Fakler, B. & Schulte, U. 2010, "Ca2+-activated K+ channels: from protein complexes to function", *Physiological Reviews,* vol. 90, no. 4, pp. 1437-1459.

Blankenship, A.G. & Feller, M.B. 2010, "Mechanisms underlying spontaneous patterned activity in developing neural circuits", *Nature reviews.Neuroscience,* vol. 11, no. 1, pp. 18-29.

Boiko, T., Rasband, M.N., Levinson, S.R., Caldwell, J.H., Mandel, G., Trimmer, J.S. & Matthews, G. 2001, "Compact myelin dictates the differential targeting of two sodium channel isoforms in the same axon", *Neuron,* vol. 30, no. 1, pp. 91-104.

Boiko, T., Vakulenko, M., Ewers, H., Yap, C.C., Norden, C. & Winckler, B. 2007, "Ankyrin-dependent and -independent mechanisms orchestrate axonal compartmentalization of L1 family members neurofascin and L1/neuron-glia cell adhesion molecule", *The Journal of neuroscience : the official journal of the Society for Neuroscience,* vol. 27, no. 3, pp. 590-603.

Boiko, T., Van Wart, A., Caldwell, J.H., Levinson, S.R., Trimmer, J.S. & Matthews, G. 2003, "Functional specialization of the axon initial segment by isoform-specific sodium channel targeting", *The Journal of neuroscience : the official journal of the Society for Neuroscience,* vol. 23, no. 6, pp. 2306-2313.

Bouchard, J.F., Horn, K.E., Stroh, T. & Kennedy, T.E. 2008, "Depolarization recruits DCC to the plasma membrane of embryonic cortical neurons and enhances axon extension in response to netrin-1", *Journal of neurochemistry,* vol. 107, no. 2, pp. 398-417.

Brachet, A., Leterrier, C., Irondelle, M., Fache, M.P., Racine, V., Sibarita, J.B., Choquet, D. & Dargent, B. 2010, "Ankyrin G restricts ion channel diffusion at the axonal initial segment before the establishment of the diffusion barrier", *The Journal of cell biology,* vol. 191, no. 2, pp. 383-395.

Brackenbury, W.J., Calhoun, J.D., Chen, C., Miyazaki, H., Nukina, N., Oyama, F., Ranscht, B. & Isom, L.L. 2010, "Functional reciprocity between Na+ channel Nav1.6 and beta1 subunits in the coordinated regulation of excitability and neurite outgrowth", *Proceedings of the National Academy of Sciences of the United States of America,* vol. 107, no. 5, pp. 2283-2288.

Brakebusch, C., Seidenbecher, C.I., Asztely, F., Rauch, U., Matthies, H., Meyer, H., Krug, M., Bockers, T.M., Zhou, X., Kreutz, M.R., Montag, D., Gundelfinger, E.D. & Fassler, R. 2002, "Brevican-deficient mice display impaired hippocampal CA1 long-term potentiation but show no obvious deficits in learning and memory", *Molecular and cellular biology,* vol. 22, no. 21, pp. 7417-7427.

Bray, J.G. & Mynlieff, M. 2011, "Involvement of protein kinase C and protein kinase A in the enhancement of L-type calcium current by GABAB receptor activation in neonatal hippocampus", *Neuroscience,* vol. 179, pp. 62-72.

Brechet, A., Fache, M.P., Brachet, A., Ferracci, G., Baude, A., Irondelle, M., Pereira, S., Leterrier, C. & Dargent, B. 2008, "Protein kinase CK2 contributes to the organization of sodium channels in axonal membranes by regulating their interactions with ankyrin G", *The Journal of cell biology,* vol. 183, no. 6, pp. 1101-1114.

Brown, D.A. & Passmore, G.M. 2009, "Neural KCNQ (Kv7) channels", *British journal of pharmacology,* vol. 156, no. 8, pp. 1185-1195.

Bruckner, G., Grosche, J., Schmidt, S., Hartig, W., Margolis, R.U., Delpech, B., Seidenbecher, C.I., Czaniera, R. & Schachner, M. 2000, "Postnatal development of perineuronal nets in wild-type mice and in a mutant deficient in tenascin-R", *The Journal of comparative neurology,* vol. 428, no. 4, pp. 616-629.

Bruckner, G., Szeoke, S., Pavlica, S., Grosche, J. & Kacza, J. 2006, "Axon initial segment ensheathed by extracellular matrix in perineuronal nets", *Neuroscience,* vol. 138, no. 2, pp. 365-375.

Brunig, I., Suter, A., Knuesel, I., Luscher, B. & Fritschy, J.M. 2002, "GABAergic terminals are required for postsynaptic clustering of dystrophin but not of GABA(A) receptors and gephyrin", *The Journal of neuroscience : the official journal of the Society for Neuroscience,* vol. 22, no. 12, pp. 4805-4813.

Burgoyne, R.D. 2007, "Neuronal calcium sensor proteins: generating diversity in neuronal Ca2+ signalling", *Nature reviews.Neuroscience,* vol. 8, no. 3, pp. 182-193.

Burkarth, N., Kriebel, M., Kranz, E.U. & Volkmer, H. 2007, "Neurofascin regulates the formation of gephyrin clusters and their subsequent translocation to the axon hillock of hippocampal neurons", *Molecular and cellular neurosciences,* vol. 36, no. 1, pp. 59-70.

Burrone, J., Li, Z. & Murthy, V.N. 2006, "Studying vesicle cycling in presynaptic terminals using the genetically encoded probe synaptopHluorin", *Nature protocols,* vol. 1, no. 6, pp. 2970-2978.

Callewaert, G., Eilers, J. & Konnerth, A. 1996, "Axonal calcium entry during fast 'sodium' action potentials in rat cerebellar Purkinje neurones", *The Journal of physiology,* vol. 495 (Pt 3), no. Pt 3, pp. 641-647.

Canepari, M., Willadt, S., Zecevic, D. & Vogt, K.E. 2010, "Imaging inhibitory synaptic potentials using voltage sensitive dyes", *Biophysical journal,* vol. 98, no. 9, pp. 2032-2040.

Ceglia, I., Kim, Y., Nairn, A.C. & Greengard, P. 2010, "Signaling pathways controlling the phosphorylation state of WAVE1, a regulator of actin polymerization", *Journal of neurochemistry,* vol. 114, no. 1, pp. 182-190.

Chang, K.T. & Berg, D.K. 2001, "Voltage-gated channels block nicotinic regulation of CREB phosphorylation and gene expression in neurons", *Neuron,* vol. 32, no. 5, pp. 855-865.

Chang, S. & De Camilli, P. 2001, "Glutamate regulates actin-based motility in axonal filopodia", *Nature neuroscience,* vol. 4, no. 8, pp. 787-793.

Colbert, C.M. & Pan, E. 2002, "Ion channel properties underlying axonal action potential initiation in pyramidal neurons", *Nature neuroscience,* vol. 5, no. 6, pp. 533-538.

Coleman, P.D. & Riesen, A.H. 1968, "Evironmental effects on cortical dendritic fields. I. Rearing in the dark", *Journal of anatomy,* vol. 102, no. Pt 3, pp. 363-374.

Crepel, V., Aronov, D., Jorquera, I., Represa, A., Ben-Ari, Y. & Cossart, R. 2007, "A parturition-associated nonsynaptic coherent activity pattern in the developing hippocampus", *Neuron,* vol. 54, no. 1, pp. 105-120.

Crisp, S.J., Evers, J.F. & Bate, M. 2011, "Endogenous patterns of activity are required for the maturation of a motor network", *The Journal of neuroscience : the official journal of the Society for Neuroscience,* vol. 31, no. 29, pp. 10445-10450.

Danglot, L., Triller, A. & Marty, S. 2006, "The development of hippocampal interneurons in rodents", *Hippocampus,* vol. 16, no. 12, pp. 1032-1060.

Davis, J.Q. & Bennett, V. 1994, "Ankyrin binding activity shared by the neurofascin/L1/NrCAM family of nervous system cell adhesion molecules", *The Journal of biological chemistry,* vol. 269, no. 44, pp. 27163-27166.

Deisseroth, K. 2011, "Optogenetics", *Nature methods,* vol. 8, no. 1, pp. 26-29.

Devaux, J.J., Kleopa, K.A., Cooper, E.C. & Scherer, S.S. 2004, "KCNQ2 is a nodal K+ channel", *The Journal of neuroscience : the official journal of the Society for Neuroscience,* vol. 24, no. 5, pp. 1236-1244.

Diefenbach, T.J., Guthrie, P.B. & Kater, S.B. 2000, "Stimulus history alters behavioral responses of neuronal growth cones", *The Journal of neuroscience : the official journal of the Society for Neuroscience,* vol. 20, no. 4, pp. 1484-1494.

Duflocq, A., Le Bras, B., Bullier, E., Couraud, F. & Davenne, M. 2008, "Nav1.1 is predominantly expressed in nodes of Ranvier and axon initial segments", *Molecular and cellular neurosciences,* vol. 39, no. 2, pp. 180-192.

Dulla, C.G. & Huguenard, J.R. 2009, "Who let the spikes out?", *Nature neuroscience,* vol. 12, no. 8, pp. 959-960.

Dzhashiashvili, Y., Zhang, Y., Galinska, J., Lam, I., Grumet, M. & Salzer, J.L. 2007, "Nodes of Ranvier and axon initial segments are ankyrin G-dependent domains that assemble by distinct mechanisms", *The Journal of cell biology,* vol. 177, no. 5, pp. 857-870.

Enes, J., Langwieser, N., Ruschel, J., Carballosa-Gonzalez, M.M., Klug, A., Traut, M.H., Ylera, B., Tahirovic, S., Hofmann, F., Stein, V., Moosmang, S., Hentall, I.D. & Bradke, F. 2010, "Electrical activity suppresses axon growth through Ca(v)1.2 channels in adult primary sensory neurons", *Current biology : CB,* vol. 20, no. 13, pp. 1154-1164.

Evans, M.D. and Grubb, M.S. 2011, ‘’Mechanisms of activity-dependent plasticity at the

axon initial segment’’, *Society for Neuroscience Abstracts*, 37:874.04Evans, M.D., Sammons, R.P., Lebron, S., Dumitrescu, A.S., Watkins, T.B., Uebele, V.N., Renger, J.J. & Grubb, M.S. 2013, "Calcineurin signaling mediates activity-dependent relocation of the axon initial segment", *The Journal of neuroscience : the official journal of the Society for Neuroscience,* vol. 33, no. 16, pp. 6950-6963.

Eyraud, D., Richard, O., Borie, D.C., Schaup, B., Carayon, A., Vezinet, C., Movschin, M., Vaillant, J.C., Coriat, P. & Hannoun, L. 2002, "Hemodynamic and hormonal responses to the sudden interruption of caval flow: insights from a prospective study of hepatic vascular exclusion during major liver resections", *Anesthesia and Analgesia,* vol. 95, no. 5, pp. 1173-8, table of contents.

Faherty, C.J., Kerley, D. & Smeyne, R.J. 2003, "A Golgi-Cox morphological analysis of neuronal changes induced by environmental enrichment", *Brain research.Developmental brain research,* vol. 141, no. 1-2, pp. 55-61.

Faul, C., Donnelly, M., Merscher-Gomez, S., Chang, Y.H., Franz, S., Delfgaauw, J., Chang, J.M., Choi, H.Y., Campbell, K.N., Kim, K., Reiser, J. & Mundel, P. 2008, "The actin cytoskeleton of kidney podocytes is a direct target of the antiproteinuric effect of cyclosporine A", *Nature medicine,* vol. 14, no. 9, pp. 931-938. Feinberg, K., Eshed-Eisenbach, Y., Frechter, S., Amor, V., Salomon, D., Sabanay, H., Dupree, J.L., Grumet, M., Brophy, P.J., Shrager, P. & Peles, E. 2010, "A glial signal consisting of gliomedin and NrCAM clusters axonal Na+ channels during the formation of nodes of Ranvier", *Neuron,* vol. 65, no. 4, pp. 490-502.

Feldmeyer, D., Kask, K., Brusa, R., Kornau, H.C., Kolhekar, R., Rozov, A., Burnashev, N., Jensen, V., Hvalby, O., Sprengel, R. & Seeburg, P.H. 1999, "Neurological dysfunctions in mice expressing different levels of the Q/R site-unedited AMPAR subunit GluR-B", *Nature neuroscience,* vol. 2, no. 1, pp. 57-64.

Ferreira, A., Kincaid, R. & Kosik, K.S. 1993, "Calcineurin is associated with the cytoskeleton of cultured neurons and has a role in the acquisition of polarity", *Molecular biology of the cell,* vol. 4, no. 12, pp. 1225-1238. Fields, R.D., Neale, E.A. & Nelson, P.G. 1990, "Effects of patterned electrical activity on neurite outgrowth from mouse sensory neurons", *The Journal of neuroscience : the official journal of the Society for Neuroscience,* vol. 10, no. 9, pp. 2950-2964.

Fleidervish, I.A., Lasser-Ross, N., Gutnick, M.J. & Ross, W.N. 2010, "Na+ imaging reveals little difference in action potential-evoked Na+ influx between axon and soma", *Nature neuroscience,* vol. 13, no. 7, pp. 852-860.

Fletcher, T.L., De Camilli, P. & Banker, G. 1994, "Synaptogenesis in hippocampal cultures: evidence indicating that axons and dendrites become competent to form synapses at different stages of neuronal development", *The Journal of neuroscience : the official journal of the Society for Neuroscience,* vol. 14, no. 11 Pt 1, pp. 6695-6706.

Friedman, J.I., Vrijenhoek, T., Markx, S., Janssen, I.M., van der Vliet, W.A., Faas, B.H., Knoers, N.V., Cahn, W., Kahn, R.S., Edelmann, L., Davis, K.L., Silverman, J.M., Brunner, H.G., van Kessel, A.G., Wijmenga, C., Ophoff, R.A. & Veltman, J.A. 2008, "CNTNAP2 gene dosage variation is associated with schizophrenia and epilepsy", *Molecular psychiatry,* vol. 13, no. 3, pp. 261-266.

Galiano, M.R., Jha, S., Ho, T.S., Zhang, C., Ogawa, Y., Chang, K.J., Stankewich, M.C., Mohler, P.J. & Rasband, M.N. 2012, "A distal axonal cytoskeleton forms an intra-axonal boundary that controls axon initial segment assembly", *Cell,* vol. 149, no. 5, pp. 1125-1139.

Garrido, J.J., Giraud, P., Carlier, E., Fernandes, F., Moussif, A., Fache, M.P., Debanne, D. & Dargent, B. 2003, "A targeting motif involved in sodium channel clustering at the axonal initial segment", *Science (New York, N.Y.),* vol. 300, no. 5628, pp. 2091-2094.

Gasser, A., Ho, T.S., Cheng, X., Chang, K.J., Waxman, S.G., Rasband, M.N. & Dib-Hajj, S.D. 2012, "An ankyrinG-binding motif is necessary and sufficient for targeting Nav1.6 sodium channels to axon initial segments and nodes of Ranvier", *The Journal of*

neuroscience : the official journal of the Society for Neuroscience, vol. 32, no. 21, pp. 7232-7243.

Gaudilliere, B., Konishi, Y., de la Iglesia, N., Yao, G. & Bonni, A. 2004, "A CaMKII-NeuroD signaling pathway specifies dendritic morphogenesis", *Neuron,* vol. 41, no. 2, pp. 229-241.

Giamanco, K.A., Morawski, M. & Matthews, R.T. 2010, "Perineuronal net formation and structure in aggrecan knockout mice", *Neuroscience,* vol. 170, no. 4, pp. 1314-1327.

Glickfeld, L.L., Roberts, J.D., Somogyi, P. & Scanziani, M. 2009, "Interneurons hyperpolarize pyramidal cells along their entire somatodendritic axis", *Nature neuroscience,* vol. 12, no. 1, pp. 21-23.

Goldberg, E.M., Clark, B.D., Zagha, E., Nahmani, M., Erisir, A. & Rudy, B. 2008, "K+ channels at the axon initial segment dampen near-threshold excitability of neocortical fast-spiking GABAergic interneurons", *Neuron,* vol. 58, no. 3, pp. 387-400.

Goldberg, J.L., Espinosa, J.S., Xu, Y., Davidson, N., Kovacs, G.T. & Barres, B.A. 2002, "Retinal ganglion cells do not extend axons by default: promotion by neurotrophic signaling and electrical activity", *Neuron,* vol. 33, no. 5, pp. 689-702.

Gomez, T.M. & Zheng, J.Q. 2006, "The molecular basis for calcium-dependent axon pathfinding", *Nature reviews.Neuroscience,* vol. 7, no. 2, pp. 115-125.

Gomis-Ruth, S., Wierenga, C.J. & Bradke, F. 2008, "Plasticity of polarization: changing dendrites into axons in neurons integrated in neuronal circuits", *Current biology : CB,* vol. 18, no. 13, pp. 992-1000.

Gong, C.X., Grundke-Iqbal, I., Damuni, Z. & Iqbal, K. 1994, "Dephosphorylation of microtubule-associated protein tau by protein phosphatase-1 and -2C and its implication in Alzheimer disease", *FEBS letters,* vol. 341, no. 1, pp. 94-98.

Goslin, K., Schreyer, D.J., Skene, J.H. & Banker, G. 1988, "Development of neuronal polarity: GAP-43 distinguishes axonal from dendritic growth cones", *Nature,* vol. 336, no. 6200, pp. 672-674.

Goto, S., Yamamoto, H., Fukunaga, K., Iwasa, T., Matsukado, Y. & Miyamoto, E. 1985, "Dephosphorylation of microtubule-associated protein 2, tau factor, and tubulin by calcineurin", *Journal of neurochemistry,* vol. 45, no. 1, pp. 276-283.

Grubb, M.S. & Burrone, J. 2010, "Activity-dependent relocation of the axon initial segment fine-tunes neuronal excitability", *Nature,* vol. 465, no. 7301, pp. 1070-1074.

Grubb, M.S. & Burrone, J. 2010, "Building and maintaining the axon initial segment", *Current opinion in neurobiology,* vol. 20, no. 4, pp. 481-488.

Grubb, M.S., Shu, Y., Kuba, H., Rasband, M.N., Wimmer, V.C. & Bender, K.J. 2011, "Short- and long-term plasticity at the axon initial segment", *The Journal of neuroscience : the official journal of the Society for Neuroscience,* vol. 31, no. 45, pp. 16049-16055.

Hanson, M.G. & Landmesser, L.T. 2004, "Normal patterns of spontaneous activity are required for correct motor axon guidance and the expression of specific guidance molecules", *Neuron,* vol. 43, no. 5, pp. 687-701.

Hausser, M. & Smith, S.L. 2007, "Neuroscience: controlling neural circuits with light", *Nature,* vol. 446, no. 7136, pp. 617-619.

Hedstrom, K.L., Ogawa, Y. & Rasband, M.N. 2008, "AnkyrinG is required for maintenance of the axon initial segment and neuronal polarity", *The Journal of cell biology,* vol. 183, no. 4, pp. 635-640.

Hedstrom, K.L., Xu, X., Ogawa, Y., Frischknecht, R., Seidenbecher, C.I., Shrager, P. & Rasband, M.N. 2007, "Neurofascin assembles a specialized extracellular matrix at the axon initial segment", *The Journal of cell biology,* vol. 178, no. 5, pp. 875-886.

Henley, J.R., Huang, K.H., Wang, D. & Poo, M.M. 2004, "Calcium mediates bidirectional growth cone turning induced by myelin-associated glycoprotein", *Neuron,* vol. 44, no. 6, pp. 909-916.

Hinman, J.D., Rasband, M.N. & Carmichael, S.T. 2013, "Remodeling of the axon initial segment after focal cortical and white matter stroke", *Stroke; a journal of cerebral circulation,* vol. 44, no. 1, pp. 182-189.

Hodgkin, A.L. & Huxley, A.F. 1952, "A quantitative description of membrane current and its application to conduction and excitation in nerve", *The Journal of physiology,* vol. 117, no. 4, pp. 500-544.

Hu, W., Tian, C., Li, T., Yang, M., Hou, H. & Shu, Y. 2009, "Distinct contributions of Na(v)1.6 and Na(v)1.2 in action potential initiation and backpropagation", *Nature neuroscience,* vol. 12, no. 8, pp. 996-1002.

Hubel, D.H. & Wiesel, T.N. 1970, "The period of susceptibility to the physiological effects of unilateral eye closure in kittens", *The Journal of physiology,* vol. 206, no. 2, pp. 419-436.

Ibarretxe, G., Perrais, D., Jaskolski, F., Vimeney, A. & Mulle, C. 2007, "Fast regulation of axonal growth cone motility by electrical activity", *The Journal of neuroscience : the official journal of the Society for Neuroscience,* vol. 27, no. 29, pp. 7684-7695.

Inda, M.C., DeFelipe, J. & Munoz, A. 2006, "Voltage-gated ion channels in the axon initial segment of human cortical pyramidal cells and their relationship with chandelier cells", *Proceedings of the National Academy of Sciences of the United States of America,* vol. 103, no. 8, pp. 2920-2925.

Itoh, K., Ozaki, M., Stevens, B. & Fields, R.D. 1997, "Activity-dependent regulation of N-cadherin in DRG neurons: differential regulation of N-cadherin, NCAM, and L1 by distinct patterns of action potentials", *Journal of neurobiology,* vol. 33, no. 6, pp. 735-748.

Iwano, T., Masuda, A., Kiyonari, H., Enomoto, H. & Matsuzaki, F. 2012, "Prox1 postmitotically defines dentate gyrus cells by specifying granule cell identity over CA3 pyramidal cell fate in the hippocampus", *Development (Cambridge, England),* vol. 139, no. 16, pp. 3051-3062.

Jenkins, S.M. & Bennett, V. 2001, "Ankyrin-G coordinates assembly of the spectrin-based membrane skeleton, voltage-gated sodium channels, and L1 CAMs at Purkinje neuron initial segments", *The Journal of cell biology,* vol. 155, no. 5, pp. 739-746.

John, N., Krugel, H., Frischknecht, R., Smalla, K.H., Schultz, C., Kreutz, M.R., Gundelfinger, E.D. & Seidenbecher, C.I. 2006, "Brevican-containing perineuronal nets of extracellular matrix in dissociated hippocampal primary cultures", *Molecular and cellular neurosciences,* vol. 31, no. 4, pp. 774-784.

Kastanenka, K.V. & Landmesser, L.T. 2010, "In vivo activation of channelrhodopsin-2 reveals that normal patterns of spontaneous activity are required for motoneuron guidance and maintenance of guidance molecules", *The Journal of neuroscience : the official journal of the Society for Neuroscience,* vol. 30, no. 31, pp. 10575-10585.

Kayyali, U.S., Zhang, W., Yee, A.G., Seidman, J.G. & Potter, H. 1997, "Cytoskeletal changes in the brains of mice lacking calcineurin A alpha", *Journal of neurochemistry,* vol. 68, no. 4, pp. 1668-1678. Khalilov, I., Esclapez, M., Medina, I., Aggoun, D., Lamsa, K., Leinekugel, X., Khazipov, R. & Ben-Ari, Y. 1997, "A novel in vitro preparation: the intact hippocampal formation", *Neuron,* vol. 19, no. 4, pp. 743-749.

Khirug, S., Yamada, J., Afzalov, R., Voipio, J., Khiroug, L. & Kaila, K. 2008, "GABAergic depolarization of the axon initial segment in cortical principal neurons is caused by the Na-K-2Cl cotransporter NKCC1", *The Journal of neuroscience : the official journal of the Society for Neuroscience,* vol. 28, no. 18, pp. 4635-4639.

Kobayashi, T., Storrie, B., Simons, K. & Dotti, C.G. 1992, "A functional barrier to movement of lipids in polarized neurons", *Nature,* vol. 359, no. 6396, pp. 647-650.

Kole, M.H., Ilschner, S.U., Kampa, B.M., Williams, S.R., Ruben, P.C. & Stuart, G.J. 2008, "Action potential generation requires a high sodium channel density in the axon initial segment", *Nature neuroscience,* vol. 11, no. 2, pp. 178-186.

Kole, M.H., Letzkus, J.J. & Stuart, G.J. 2007, "Axon initial segment Kv1 channels control axonal action potential waveform and synaptic efficacy", *Neuron,* vol. 55, no. 4, pp. 633-647.

Kole, M.H. & Stuart, G.J. 2012, "Signal processing in the axon initial segment", *Neuron,* vol. 73, no. 2, pp. 235-247.

Konishi, M. 2003, "Coding of auditory space", *Annual Review of Neuroscience,* vol. 26, pp. 31-55.

Konishi, Y. & Setou, M. 2009, "Tubulin tyrosination navigates the kinesin-1 motor domain to axons", *Nature neuroscience,* vol. 12, no. 5, pp. 559-567.

Kordeli, E., Lambert, S. & Bennett, V. 1995, "AnkyrinG. A new ankyrin gene with neural-specific isoforms localized at the axonal initial segment and node of Ranvier", *The Journal of biological chemistry,* vol. 270, no. 5, pp. 2352-2359.

Kosaka, T. 1980, "The axon initial segment as a synaptic site: ultrastructure and synaptology of the initial segment of the pyramidal cell in the rat hippocampus (CA3 region)", *Journal of neurocytology,* vol. 9, no. 6, pp. 861-882.

Kramer, A.A., Ingraham, N.E., Sharpe, E.J. & Mynlieff, M. 2012, "Levels of Ca(V)1.2 L-Type Ca(2+) Channels Peak in the First Two Weeks in Rat Hippocampus Whereas Ca(V)1.3 Channels Steadily Increase through Development", *Journal of signal transduction,* vol. 2012, pp. 597214.

Krichmar, J.L., Nasuto, S.J., Scorcioni, R., Washington, S.D. & Ascoli, G.A. 2002, "Effects of dendritic morphology on CA3 pyramidal cell electrophysiology: a simulation study", *Brain research,* vol. 941, no. 1-2, pp. 11-28.

Kuba, H. 2012, "Structural tuning and plasticity of the axon initial segment in auditory neurons", *The Journal of physiology,* vol. 590, no. Pt 22, pp. 5571-5579.

Kuba, H., Ishii, T.M. & Ohmori, H. 2006, "Axonal site of spike initiation enhances auditory coincidence detection", *Nature,* vol. 444, no. 7122, pp. 1069-1072.

Kuba, H. & Ohmori, H. 2009, "Roles of axonal sodium channels in precise auditory time coding at nucleus magnocellularis of the chick", *The Journal of physiology,* vol. 587, no. Pt 1, pp. 87-100.

Kuba, H., Oichi, Y. & Ohmori, H. 2010, "Presynaptic activity regulates Na(+) channel distribution at the axon initial segment", *Nature,* vol. 465, no. 7301, pp. 1075-1078.

Leinekugel, X., Khalilov, I., Ben-Ari, Y. & Khazipov, R. 1998, "Giant depolarizing potentials: the septal pole of the hippocampus paces the activity of the developing intact septohippocampal complex in vitro", *The Journal of neuroscience : the official journal of the Society for Neuroscience,* vol. 18, no. 16, pp. 6349-6357.

Leinekugel, X., Khazipov, R., Cannon, R., Hirase, H., Ben-Ari, Y. & Buzsaki, G. 2002, "Correlated bursts of activity in the neonatal hippocampus in vivo", *Science (New York, N.Y.),* vol. 296, no. 5575, pp. 2049-2052.

Liu, Y.B., Lio, P.A., Pasternak, J.F. & Trommer, B.L. 1996, "Developmental changes in membrane properties and postsynaptic currents of granule cells in rat dentate gyrus", *Journal of neurophysiology,* vol. 76, no. 2, pp. 1074-1088.

Lopez-Bendito, G. & Molnar, Z. 2003, "Thalamocortical development: how are we going to get there?", *Nature reviews.Neuroscience,* vol. 4, no. 4, pp. 276-289.

Lorincz, A. & Nusser, Z. 2010, "Molecular identity of dendritic voltage-gated sodium channels", *Science (New York, N.Y.),* vol. 328, no. 5980, pp. 906-909.

Lorincz, A. & Nusser, Z. 2008, "Cell-type-dependent molecular composition of the axon initial segment", *The Journal of neuroscience : the official journal of the Society for Neuroscience,* vol. 28, no. 53, pp. 14329-14340.

Ma, L., Greenwood, J.A. & Schachner, M. 2011, "CRP1, a protein localized in filopodia of growth cones, is involved in dendritic growth", *The Journal of neuroscience : the official journal of the Society for Neuroscience,* vol. 31, no. 46, pp. 16781-16791.

Martin, P.M., Carnaud, M., Garcia del Cano, G., Irondelle, M., Irinopoulou, T., Girault, J.A., Dargent, B. & Goutebroze, L. 2008, "Schwannomin-interacting protein-1 isoform IQCJ-SCHIP-1 is a late component of nodes of Ranvier and axon initial segments", *The Journal of neuroscience : the official journal of the Society for Neuroscience,* vol. 28, no. 24, pp. 6111-6117.

Mataga, N., Nagai, N. & Hensch, T.K. 2002, "Permissive proteolytic activity for visual cortical plasticity", *Proceedings of the National Academy of Sciences of the United States of America,* vol. 99, no. 11, pp. 7717-7721.

Mattson, M.P., Dou, P. & Kater, S.B. 1988, "Outgrowth-regulating actions of glutamate in isolated hippocampal pyramidal neurons", *The Journal of neuroscience : the official journal of the Society for Neuroscience,* vol. 8, no. 6, pp. 2087-2100.

Mattson, M.P., Taylor-Hunter, A. & Kater, S.B. 1988, "Neurite outgrowth in individual neurons of a neuronal population is differentially regulated by calcium and cyclic AMP", *The Journal of neuroscience : the official journal of the Society for Neuroscience,* vol. 8, no. 5, pp. 1704-1711.

McAllister, A.K., Katz, L.C. & Lo, D.C. 1996, "Neurotrophin regulation of cortical dendritic growth requires activity", *Neuron,* vol. 17, no. 6, pp. 1057-1064.

Menendez de la Prida, L., Bolea, S. & Sanchez-Andres, J.V. 1998, "Origin of the synchronized network activity in the rabbit developing hippocampus", *The European journal of neuroscience,* vol. 10, no. 3, pp. 899-906.

Ming, G., Henley, J., Tessier-Lavigne, M., Song, H. & Poo, M. 2001, "Electrical activity modulates growth cone guidance by diffusible factors", *Neuron,* vol. 29, no. 2, pp. 441-452.

Mire, E., Mezzera, C., Leyva-Diaz, E., Paternain, A.V., Squarzoni, P., Bluy, L., Castillo-Paterna, M., Lopez, M.J., Peregrin, S., Tessier-Lavigne, M., Garel, S., Galceran, J., Lerma, J. & Lopez-Bendito, G. 2012, "Spontaneous activity regulates Robo1 transcription to mediate a switch in thalamocortical axon growth", *Nature neuroscience,* vol. 15, no. 8, pp. 1134-1143.

Mizuno, H., Hirano, T. & Tagawa, Y. 2007, "Evidence for activity-dependent cortical wiring: formation of interhemispheric connections in neonatal mouse visual cortex requires projection neuron activity", *The Journal of neuroscience : the official journal of the Society for Neuroscience,* vol. 27, no. 25, pp. 6760-6770.

Mobley, A.S., Miller, A.M., Araneda, R.C., Maurer, L.R., Muller, F. & Greer, C.A. 2010, "Hyperpolarization-activated cyclic nucleotide-gated channels in olfactory sensory neurons regulate axon extension and glomerular formation", *The Journal of neuroscience : the official journal of the Society for Neuroscience,* vol. 30, no. 49, pp. 16498-16508.

Moody, W.J. & Bosma, M.M. 2005, "Ion channel development, spontaneous activity, and activity-dependent development in nerve and muscle cells", *Physiological Reviews,* vol. 85, no. 3, pp. 883-941.

Morton, R.A., Norlin, M.S., Vollmer, C.C. & Valenzuela, C.F. 2013, "Characterization of L-type voltage-gated Ca(2+) channel expression and function in developing CA3 pyramidal neurons", *Neuroscience,* vol. 238, pp. 59-70.

Nagel, G., Szellas, T., Huhn, W., Kateriya, S., Adeishvili, N., Berthold, P., Ollig, D., Hegemann, P. & Bamberg, E. 2003, "Channelrhodopsin-2, a directly light-gated cation-selective membrane channel", *Proceedings of the National Academy of Sciences of the United States of America,* vol. 100, no. 24, pp. 13940-13945.

Nakada, C., Ritchie, K., Oba, Y., Nakamura, M., Hotta, Y., Iino, R., Kasai, R.S., Yamaguchi, K., Fujiwara, T. & Kusumi, A. 2003, "Accumulation of anchored proteins forms membrane diffusion barriers during neuronal polarization", *Nature cell biology,* vol. 5, no. 7, pp. 626-632.

Nielsen, J., Gotfryd, K., Li, S., Kulahin, N., Soroka, V., Rasmussen, K.K., Bock, E. & Berezin, V. 2009, "Role of glial cell line-derived neurotrophic factor (GDNF)-neural cell adhesion molecule (NCAM) interactions in induction of neurite outgrowth and identification of a binding site for NCAM in the heel region of GDNF", *The Journal of neuroscience : the official journal of the Society for Neuroscience,* vol. 29, no. 36, pp. 11360-11376.

Nishimura, K., Akiyama, H., Komada, M. & Kamiguchi, H. 2007, "betaIV-spectrin forms a diffusion barrier against L1CAM at the axon initial segment", *Molecular and cellular neurosciences,* vol. 34, no. 3, pp. 422-430.

Nishiyama, M., von Schimmelmann, M.J., Togashi, K., Findley, W.M. & Hong, K. 2008, "Membrane potential shifts caused by diffusible guidance signals direct growth-cone turning", *Nature neuroscience,* vol. 11, no. 7, pp. 762-771.

Obermair, G.J., Szabo, Z., Bourinet, E. & Flucher, B.E. 2004, "Differential targeting of the L-type Ca2+ channel alpha 1C (CaV1.2) to synaptic and extrasynaptic compartments in hippocampal neurons", *The European journal of neuroscience,* vol. 19, no. 8, pp. 2109-2122.

Ogawa, Y. & Rasband, M.N. 2008, "The functional organization and assembly of the axon initial segment", *Current opinion in neurobiology,* vol. 18, no. 3, pp. 307-313.

Ogiwara, I., Miyamoto, H., Morita, N., Atapour, N., Mazaki, E., Inoue, I., Takeuchi, T., Itohara, S., Yanagawa, Y., Obata, K., Furuichi, T., Hensch, T.K. & Yamakawa, K. 2007, "Nav1.1 localizes to axons of parvalbumin-positive inhibitory interneurons: a circuit basis for epileptic seizures in mice carrying an Scn1a gene mutation", *The Journal of neuroscience : the official journal of the Society for Neuroscience,* vol. 27, no. 22, pp. 5903-5914.

Osorio, N., Cathala, L., Meisler, M.H., Crest, M., Magistretti, J. & Delmas, P. 2010, "Persistent Nav1.6 current at axon initial segments tunes spike timing of cerebellar granule cells", *The Journal of physiology,* vol. 588, no. Pt 4, pp. 651-670.

Palay, S.L., Sotelo, C., Peters, A. & Orkand, P.M. 1968, "The axon hillock and the initial segment", *The Journal of cell biology,* vol. 38, no. 1, pp. 193-201.

Palmer, L.M. & Stuart, G.J. 2006, "Site of action potential initiation in layer 5 pyramidal neurons", *The Journal of neuroscience : the official journal of the Society for Neuroscience,* vol. 26, no. 6, pp. 1854-1863.

Pan, Z., Kao, T., Horvath, Z., Lemos, J., Sul, J.Y., Cranstoun, S.D., Bennett, V., Scherer, S.S. & Cooper, E.C. 2006, "A common ankyrin-G-based mechanism retains KCNQ and NaV channels at electrically active domains of the axon", *The Journal of neuroscience : the official journal of the Society for Neuroscience,* vol. 26, no. 10, pp. 2599-2613.

Peters, A., Proskauer, C.C. & Kaiserman-Abramof, I.R. 1968, "The small pyramidal neuron of the rat cerebral cortex. The axon hillock and initial segment", *The Journal of cell biology,* vol. 39, no. 3, pp. 604-619.

Rasband, M.N. 2010, "The axon initial segment and the maintenance of neuronal polarity", *Nature reviews.Neuroscience,* vol. 11, no. 8, pp. 552-562.

Rasmussen, H.B., Frokjaer-Jensen, C., Jensen, C.S., Jensen, H.S., Jorgensen, N.K., Misonou, H., Trimmer, J.S., Olesen, S.P. & Schmitt, N. 2007, "Requirement of subunit co-assembly and ankyrin-G for M-channel localization at the axon initial segment", *Journal of cell science,* vol. 120, no. Pt 6, pp. 953-963.

Redmond, L., Kashani, A.H. & Ghosh, A. 2002, "Calcium regulation of dendritic growth via CaM kinase IV and CREB-mediated transcription", *Neuron,* vol. 34, no. 6, pp. 999-1010.

Roberts, M.T., Bender, K.J. & Trussell, L.O. 2008, "Fidelity of complex spike-mediated synaptic transmission between inhibitory interneurons", *The Journal of neuroscience : the official journal of the Society for Neuroscience,* vol. 28, no. 38, pp. 9440-9450.

Rush, A.M., Dib-Hajj, S.D. & Waxman, S.G. 2005, "Electrophysiological properties of two axonal sodium channels, Nav1.2 and Nav1.6, expressed in mouse spinal sensory neurones", *The Journal of physiology,* vol. 564, no. Pt 3, pp. 803-815.

Schafer, D.P., Jha, S., Liu, F., Akella, T., McCullough, L.D. & Rasband, M.N. 2009, "Disruption of the axon initial segment cytoskeleton is a new mechanism for neuronal injury", *The Journal of neuroscience : the official journal of the Society for Neuroscience,* vol. 29, no. 42, pp. 13242-13254.

Schmidt-Hieber, C. & Bischofberger, J. 2010, "Fast sodium channel gating supports localized and efficient axonal action potential initiation", *The Journal of neuroscience : the official journal of the Society for Neuroscience,* vol. 30, no. 30, pp. 10233-10242.

Scorcioni, R., Lazarewicz, M.T. & Ascoli, G.A. 2004, "Quantitative morphometry of hippocampal pyramidal cells: differences between anatomical classes and reconstructing laboratories", *The Journal of comparative neurology,* vol. 473, no. 2, pp. 177-193.

Shah, M., Mistry, M., Marsh, S.J., Brown, D.A. & Delmas, P. 2002, "Molecular correlates of the M-current in cultured rat hippocampal neurons", *The Journal of physiology,* vol. 544, no. Pt 1, pp. 29-37.

Shah, M.M., Migliore, M., Valencia, I., Cooper, E.C. & Brown, D.A. 2008, "Functional significance of axonal Kv7 channels in hippocampal pyramidal neurons", *Proceedings of the National Academy of Sciences of the United States of America,* vol. 105, no. 22, pp. 7869-7874.

Sin, W.C., Haas, K., Ruthazer, E.S. & Cline, H.T. 2002, "Dendrite growth increased by visual activity requires NMDA receptor and Rho GTPases", *Nature,* vol. 419, no. 6906, pp. 475-480.

Singh, K.K. & Miller, F.D. 2005, "Activity regulates positive and negative neurotrophin-derived signals to determine axon competition", *Neuron,* vol. 45, no. 6, pp. 837-845.

Sit, S.Y., Xie, K., Jacutin-Porte, S., Taber, M.T., Gulwadi, A.G., Korpinen, C.D., Burris, K.D., Molski, T.F., Ryan, E., Xu, C., Wong, H., Zhu, J., Krishnananthan, S., Gao, Q., Verdoorn, T. & Johnson, G. 2002, "(+)-Dinapsoline: an efficient synthesis and pharmacological profile of a novel dopamine agonist", *Journal of medicinal chemistry,* vol. 45, no. 17, pp. 3660-3668.

Smith, Z.D., Gray, L. & Rubel, E.W. 1983, "Afferent influences on brainstem auditory nuclei of the chicken: n. laminaris dendritic length following monaural conductive hearing loss", *The Journal of comparative neurology,* vol. 220, no. 2, pp. 199-205.

Smith-Swintosky, V.L., Gozes, I., Brenneman, D.E., D'Andrea, M.R. & Plata-Salaman, C.R. 2005, "Activity-dependent neurotrophic factor-9 and NAP promote neurite outgrowth in rat hippocampal and cortical cultures", *Journal of molecular neuroscience : MN,* vol. 25, no. 3, pp. 225-238.

Sobotzik, J.M., Sie, J.M., Politi, C., Del Turco, D., Bennett, V., Deller, T. & Schultz, C. 2009, "AnkyrinG is required to maintain axo-dendritic polarity in vivo", *Proceedings of the National Academy of Sciences of the United States of America,* vol. 106, no. 41, pp. 17564-17569.

Song, A.H., Wang, D., Chen, G., Li, Y., Luo, J., Duan, S. & Poo, M.M. 2009, "A selective filter for cytoplasmic transport at the axon initial segment", *Cell,* vol. 136, no. 6, pp. 1148-1160.

Spitzer, N.C. 2006, "Electrical activity in early neuronal development", *Nature,* vol. 444, no. 7120, pp. 707-712.

Storm, J.F. 1988, "Temporal integration by a slowly inactivating K+ current in hippocampal neurons", *Nature,* vol. 336, no. 6197, pp. 379-381.

Sur, M., Angelucci, A. & Sharma, J. 1999, "Rewiring cortex: the role of patterned activity in development and plasticity of neocortical circuits", *Journal of neurobiology,* vol. 41, no. 1, pp. 33-43.

Szabadics, J., Varga, C., Molnar, G., Olah, S., Barzo, P. & Tamas, G. 2006, "Excitatory effect of GABAergic axo-axonic cells in cortical microcircuits", *Science (New York, N.Y.),* vol. 311, no. 5758, pp. 233-235.

Tan, Z.J., Peng, Y., Song, H.L., Zheng, J.J. & Yu, X. 2010, "N-cadherin-dependent neuron-neuron interaction is required for the maintenance of activity-induced dendrite growth", *Proceedings of the National Academy of Sciences of the United States of America,* vol. 107, no. 21, pp. 9873-9878.

Tashiro, A., Dunaevsky, A., Blazeski, R., Mason, C.A. & Yuste, R. 2003, "Bidirectional regulation of hippocampal mossy fiber filopodial motility by kainate receptors: a two-step model of synaptogenesis", *Neuron,* vol. 38, no. 5, pp. 773-784.

Tian, L., Hires, S.A. & Looger, L.L. 2012, "Imaging neuronal activity with genetically encoded calcium indicators", *Cold Spring Harbor protocols,* vol. 2012, no. 6, pp. 647-656.

Turrigiano, G.G. & Nelson, S.B. 2004, "Homeostatic plasticity in the developing nervous system", *Nature reviews.Neuroscience,* vol. 5, no. 2, pp. 97-107.

Vacher, H. & Trimmer, J.S. 2011, "Diverse roles for auxiliary subunits in phosphorylation-dependent regulation of mammalian brain voltage-gated potassium channels", *Pflugers Archiv : European journal of physiology,* vol. 462, no. 5, pp. 631-643.

Vaillant, A.R., Zanassi, P., Walsh, G.S., Aumont, A., Alonso, A. & Miller, F.D. 2002, "Signaling mechanisms underlying reversible, activity-dependent dendrite formation", *Neuron,* vol. 34, no. 6, pp. 985-998.

Valentijn, S.A., van Hooren, S.A., Bosma, H., Touw, D.M., Jolles, J., van Boxtel, M.P. & Ponds, R.W. 2005, "The effect of two types of memory training on subjective and objective memory performance in healthy individuals aged 55 years and older: a randomized controlled trial", *Patient education and counseling,* vol. 57, no. 1, pp. 106-114.

van Hooren, S.A., Anteunis, L.J., Valentijn, S.A., Bosma, H., Ponds, R.W., Jolles, J. & van Boxtel, M.P. 2005, "Does cognitive function in older adults with hearing impairment improve by hearing aid use?", *International journal of audiology,* vol. 44, no. 5, pp. 265-271.

van Ooyen, A., Duijnhouwer, J., Remme, M.W. & van Pelt, J. 2002, "The effect of dendritic topology on firing patterns in model neurons", *Network (Bristol, England),* vol. 13, no. 3, pp. 311-325.

Van Wart, A., Trimmer, J.S. & Matthews, G. 2007, "Polarized distribution of ion channels within microdomains of the axon initial segment", *The Journal of comparative neurology,* vol. 500, no. 2, pp. 339-352.

Wang, C.L., Zhang, L., Zhou, Y., Zhou, J., Yang, X.J., Duan, S.M., Xiong, Z.Q. & Ding, Y.Q. 2007, "Activity-dependent development of callosal projections in the somatosensory cortex", *The Journal of neuroscience : the official journal of the Society for Neuroscience,* vol. 27, no. 42, pp. 11334-11342.

Wang, G.X. & Poo, M.M. 2005, "Requirement of TRPC channels in netrin-1-induced chemotropic turning of nerve growth cones", *Nature,* vol. 434, no. 7035, pp. 898-904.

Watanabe, K., Al-Bassam, S., Miyazaki, Y., Wandless, T.J., Webster, P. & Arnold, D.B. 2012, "Networks of polarized actin filaments in the axon initial segment provide a mechanism for sorting axonal and dendritic proteins", *Cell reports,* vol. 2, no. 6, pp. 1546-1553.

Wayman, G.A., Impey, S., Marks, D., Saneyoshi, T., Grant, W.F., Derkach, V. & Soderling, T.R. 2006, "Activity-dependent dendritic arborization mediated by CaM-kinase I activation and enhanced CREB-dependent transcription of Wnt-2", *Neuron,* vol. 50, no. 6, pp. 897-909.

WIESEL, T.N. & HUBEL, D.H. 1963, "Effects of Visual Deprivation on Morphology and Physiology of Cells in the Cats Lateral Geniculate Body", *Journal of neurophysiology,* vol. 26, pp. 978-993.

Williams, M.E., Wilke, S.A., Daggett, A., Davis, E., Otto, S., Ravi, D., Ripley, B., Bushong, E.A., Ellisman, M.H., Klein, G. & Ghosh, A. 2011, "Cadherin-9 regulates synapse-specific differentiation in the developing hippocampus", *Neuron,* vol. 71, no. 4, pp. 640-655.

Wimmer, V.C., Reid, C.A., So, E.Y., Berkovic, S.F. & Petrou, S. 2010, "Axon initial segment dysfunction in epilepsy", *The Journal of physiology,* vol. 588, no. Pt 11, pp. 1829-1840.

Winckler, B., Forscher, P. & Mellman, I. 1999, "A diffusion barrier maintains distribution of membrane proteins in polarized neurons", *Nature,* vol. 397, no. 6721, pp. 698-701.

Winkels, R., Jedlicka, P., Weise, F.K., Schultz, C., Deller, T. & Schwarzacher, S.W. 2009, "Reduced excitability in the dentate gyrus network of betaIV-spectrin mutant mice in vivo", *Hippocampus,* vol. 19, no. 7, pp. 677-686.

Witte, H., Neukirchen, D. & Bradke, F. 2008, "Microtubule stabilization specifies initial neuronal polarization", *The Journal of cell biology,* vol. 180, no. 3, pp. 619-632.

Wollner, D.A. & Catterall, W.A. 1986, "Localization of sodium channels in axon hillocks and initial segments of retinal ganglion cells", *Proceedings of the National Academy of Sciences of the United States of America,* vol. 83, no. 21, pp. 8424-8428.

Wong, A.W., Ghosh, N., McKinnon, K.P., Reed, W., Piskurich, J.F., Wright, K.L. & Ting, J.P. 2002, "Regulation and specificity of MHC2TA promoter usage in human primary T lymphocytes and cell line", *Journal of immunology (Baltimore, Md.: 1950),* vol. 169, no. 6, pp. 3112-3119.

Wong, R.O. & Ghosh, A. 2002, "Activity-dependent regulation of dendritic growth and patterning", *Nature reviews.Neuroscience,* vol. 3, no. 10, pp. 803-812.

Wong, W.T., Sanes, J.R. & Wong, R.O. 1998, "Developmentally regulated spontaneous activity in the embryonic chick retina", *The Journal of neuroscience : the official journal of the Society for Neuroscience,* vol. 18, no. 21, pp. 8839-8852.

Woodruff, A.R., Monyer, H. & Sah, P. 2006, "GABAergic excitation in the basolateral amygdala", *The Journal of neuroscience : the official journal of the Society for Neuroscience,* vol. 26, no. 46, pp. 11881-11887.

Xu, K., Zhong, G. & Zhuang, X. 2013, "Actin, spectrin, and associated proteins form a periodic cytoskeletal structure in axons", *Science (New York, N.Y.),* vol. 339, no. 6118, pp. 452-456.

Yamada, R.X., Sasaki, T., Ichikawa, J., Koyama, R., Matsuki, N. & Ikegaya, Y. 2008, "Long-range axonal calcium sweep induces axon retraction", *The Journal of neuroscience : the official journal of the Society for Neuroscience,* vol. 28, no. 18, pp. 4613-4618.

Yamamoto, N. & Lopez-Bendito, G. 2012, "Shaping brain connections through spontaneous neural activity", *The European journal of neuroscience,* vol. 35, no. 10, pp. 1595-1604.

Yang, Y., Ogawa, Y., Hedstrom, K.L. & Rasband, M.N. 2007, "betaIV spectrin is recruited to axon initial segments and nodes of Ranvier by ankyrinG", *The Journal of cell biology,* vol. 176, no. 4, pp. 509-519.

Yu, X. & Malenka, R.C. 2003, "Beta-catenin is critical for dendritic morphogenesis", *Nature neuroscience,* vol. 6, no. 11, pp. 1169-1177.

Yu, Y., Maureira, C., Liu, X. & McCormick, D. 2010, "P/Q and N channels control baseline and spike-triggered calcium levels in neocortical axons and synaptic boutons", *The Journal of neuroscience : the official journal of the Society for Neuroscience,* vol. 30, no. 35, pp. 11858-11869.

Zheng, J.Q. 2000, "Turning of nerve growth cones induced by localized increases in intracellular calcium ions", *Nature,* vol. 403, no. 6765, pp. 89-93.

Zhou, D., Lambert, S., Malen, P.L., Carpenter, S., Boland, L.M. & Bennett, V. 1998, "AnkyrinG is required for clustering of voltage-gated Na channels at axon initial segments and for normal action potential firing", *The Journal of cell biology,* vol. 143, no. 5, pp. 1295-1304.

Zhou, W. & Goldin, A.L. 2004, "Use-dependent potentiation of the Nav1.6 sodium channel", *Biophysical journal,* vol. 87, no. 6, pp. 3862-3872.

Zonta, B., Desmazieres, A., Rinaldi, A., Tait, S., Sherman, D.L., Nolan, M.F. & Brophy, P.J. 2011, "A critical role for Neurofascin in regulating action potential initiation through maintenance of the axon initial segment", *Neuron,* vol. 69, no. 5, pp. 945-956.